Tumour-suppressive Effects of Pannexin 1 and its Mechanism of Action and Regulation in Rhabdomyosarcoma

XIAO XIANG

Thesis submitted to the University of Ottawa

in partial fulfillment of the requirements for the degree of

DOCTOR OF PHILOSOPHY

Department of Cellular and Molecular Medicine

University of Ottawa

Ottawa, Ontario, Canada

ABSTRACT

Rhabdomyosarcoma (RMS) is a paediatric neoplasm of skeletal muscle in dire need of novel therapeutic strategies. We explored the role of pannexin 1 (PANX1), an emerging regulator of skeletal muscle differentiation, in the two major histological subtypes of RMS: embryonal RMS (eRMS) and alveolar RMS (aRMS).

We found that PANX1 levels are down-regulated in eRMS and aRMS tissue specimens and patient-derived cell lines. While *PANX1* transcripts were expressed in RMS, we showed that the majority lacked the putative 5' untranslated region (5'UTR) and the first ATG start codon, which contributed to low PANX1 expression. Re-introduction of PANX1 in eRMS and aRMS patient-derived cell lines induced their partial differentiation and suppressed their malignant properties *in vitro* and *in vivo*. Notably, our data suggest that the PANX1-mediated tumour-inhibitory function in RMS does not depend on its canonical channel function.

Furthermore, our genome-wide transcriptomic study found that PANX1 over-expression in RMS cells induced changes in expression of genes in various cellular processes and signaling pathways involved in tumour-suppression including connexin 43 (Cx43), which was previously shown to induce RMS cell differentiation. At the protein level, we showed that the PANX1 interactome in RMS cells involved plasma membrane and cytoskeleton associated proteins including the neuroblast differentiation-associated protein AHNAK, also known as desmoyokin. We demonstrated that PANX1-mediated tumour-suppression in RMS cells depended on its interaction with AHNAK. We further constructed the first searchable PANX1 transcriptome and interactome databases and made them available for the scientific community.

We then searched for a means by which to increase PANX1 levels as a new therapeutic approach for RMS. We found quercetin, a clinical approved natural flavonoid, as a PANX1 up-regulator in RMS cells. This induction of PANX1 expression involved alternative transcription of a *PANX1* mRNA variant containing a translationally active 5'UTR, which depended, in part, on binding of the transcription factor ETV4 (ETS Variant Transcription Factor 4) in the *PANX1* promoter. Moreover, quercetin treatment induced RMS cell differentiation, inhibited tumour spheroid growth, and induced regression of established tumour spheroids.

Collectively, we demonstrate down-regulation of PANX1 in RMS and the dramatic tumour-inhibitory effects of restoring PANX1 expression in this malignancy. We show that PANX1-induced tumour-suppression does not rely on its canonical channel function but rather by signaling transduction via interaction with AHNAK. We reveal that PANX1 expression can be regulated at the translational level by the 5'UTR of its mRNA via quercetin-induced alternative transcription. We further demonstrate quercetin as a potential therapeutic agent for RMS by showing its tumour-suppressive effects in RMS. These studies not only substantiate our current understanding of PANX1, but also establish PANX1 as a therapeutic target in RMS and provide potential therapeutic options for its treatment.

ACKNOWLEDGEMENT

First and foremost, I wish to express my most sincere gratitude to my supervisor, Dr. Kyle N. Cowan, for his continuous guidance, support, and friendship. Over the years, he has given me the academic freedom to explore my research interests but also patiently led me back on track when I lose my way. I would also like to extend my deepest appreciation to our research associate, Dr. Stéphanie Langlois, who has been there at every step of the way during my academic training to offer her never-ending patience, ingenious advice, and most importantly, heartfelt caring. Under their mentorship, not only have I learned everything I know to become a better researcher and a critical thinker, but also a better communicator of scientific knowledge.

I wish to thank my thesis advisory committee members, Dr. Bernard Jasmin, Dr. Martin Holcik, and Dr. Steffany Bennett for their constructive criticism, guidance, and encouragement which are instrumental towards the completion of this thesis.

I would like to thank Dr. Tommy Alain for giving me the opportunity to collaborate with his laboratory. He has provided me with the necessary resources, expertise, and feedback needed to reach my research goals.

I want to give my special thanks to Dr. Bruno Fonseca, Dr. Tyson Graber, Dr. Stephen Baird, and Dr. Stephanie Fowler for their scientific advice as well as for coaching me through various techniques. Special thanks also go to all the past and current lab members who have always been there to keep me company and offer me help when it is needed.

I want to thank all my friends and colleagues at the CHEO Research Institute, especially our lab manager, Lynn Kyte, who have made it a wonderful place to work at.

Finally, I would like to express my whole-hearted gratitude to my parents Xiaodi Xiang and Ji Zhao for their unconditional love, care, and support over these years which allowed me to pursue my academic development abroad. I am forever grateful to my dearest grandparents, Yang Xiang, Yunfen Liu, Guanzhen Zhao, and Yunbi Yan, for their wisdom and constant reminder to be responsible, kind, and selfless.

To Yang Xiang and Guanzhen Zhao

TABLE OF CONTENTS

LIST OF TABLES

LIST OF FIGURES

LIST OF ABBREVIATIONS

3D	3-dimensional
5'UTR	5' untranslated region
7AAD	7-Aminoactinomycin D
ACTB	Beta actin
AHNAK	Neuroblast differentiation-associated protein AHNAK
ANOVA	Analysis of variance
APOBEC2	Apolipoprotein B mRNA-editing enzyme catalytic subunit 2
aRMS	Alveolar RMS
Arp3	Actin-related protein 3
ASC	Apoptosis-associated speck-like protein containing a CARD
ATP	Adenosine triphosphate
bHLH	Basic helix-loop-helix
BioID	Biotin Identification
BP	Biological process
BrdU	Bromodeoxyuridine
CBX	Carbenoxolone
CDKNIC	Cyclin dependent kinase inhibitor
co-IP	Co-immunoprecipitation
COPII	Coat protein complex II
CREB	cAMP response element-binding protein
Crmp2	Collapsin response mediator protein 2

Cryo-EM	Cryo-electron microscopy
Cx43	Connexin 43
DAVID	Database for annotation, visualization, and integrated discovery
DE	Differential expression
DHPR	Dihydropyridine receptor
DMD	Duchene muscular dystrophy
DMSO	Dimethyl sulfoxide
EDTA	Ethylenediaminetetraacetic acid
EGFR	Epidermal growth factor receptor
ER	Endoplasmic reticulum
eRMS	Embryonal RMS
ETV4	ETS variant transcription factor 4
FDR	False discovery rate
FFS	Event-free survival
FN	Fusion-negative
FOXO1	Forkhead box O1
FP	Fusion-positive
GAPDH	Glyceraldehyde 3-phosphate dehydrogenase
GEO	Gene expression omnibus
GFP	Green fluorescent protein
GMP	Guanosine monophosphate
GO	Gene ontology

GSK3β	Glycogen synthase kinase 3 β
HIV	Human deficiency viruse
HPLC-ESI-MS/MS	High-performance liquid chromatography/electrospray ionization tandem mass spectrometry
HSMM	Human skeletal muscle myoblast
IGF2	Insulin growth factor 2
IL-1β	Interleukin 1β
IL-6RE-BP	IL-6 receptor binding protein
IM	Intramuscular
KD	Knockdown
KO	Knockout
LOH	Loss-of-heterozygosity
MAPK	Mitogen-activated protein kinase
MARCKS	Myristoylated alanine rich C-kinase substrate
MHC	Myosin heavy chain
MIF	Mean image fluorescence
MMP2	Matrix metalloprotease 2
MRF	Myogenic regulatory factor
MRF4	Myogenic regulatory factor 4
Myf5	Myogenic factor 5
MyoD/MYOD	Myoblast determination protein
MyoG/MYOG	Myogenin
NF-κB	Nuclear factor kappa-light-chain-enhancer of activated B cell

NHLH1	Helix-loop-helix protein 1
NLRP	Nod-like receptor protein
NTC	Non-targeting control
OD	Optical density
P2XR	P2X receptor
P2YR	P2Y receptor
PANX	Pannexin
PAX3/Pax3	Paired-homeobox transcription factor 3
PAX7/Pax7	Paired-homeobox transcription factor 7
PKC	Protein kinase C
PLC-β	Phospholipase C-β
pRMS	Pleomorphic rhabdomyosarcoma
RMS	Rhabdomyosarcoma
RNA-seq	RNA sequencing
RyR	Ryanodine receptor
SDS-PAGE	Sodium dodecyl sulphate–polyacrylamide gel electrophoresis
SFK	Src family kinase
shRNA	Short-hairpin RNA
siRNA	Small interfering RNA
spRMS	Spindle cell rhabdomyosarcoma
TF	Transcription factor
TIS	Translation initiation site
TNFα	Tumour necrosis factor α

TRAF2	TNF receptor-associated factor 2
TSS	Transcription start site
T-tubule	Transverse-tubule
ORF	Open reading frame
uORF	Upstream open reading frame
UTRN	Utrophin
VAC	Vincristine, actinomycin D, and cyclophosphamide
VSMC	Vascular smooth muscle cell
XIAP	X-linked inhibitor of apoptosis
YFP	Yellow fluorescent protein
α1DR	α1D-adrenergic receptor

1. CHAPTER ONE: GENERAL INTRODUCTION

Rhabdomyosarcoma (RMS) is a cancer reminiscent of undifferentiated skeletal muscle tissue. Based on prior work from our laboratory establishing pannexin 1 (PANX1), the major channel for adenosine triphosphate (ATP) release in mammals, as a novel regulator of skeletal muscle differentiation, we conducted a series of studies exploring the role of PANX1 in RMS in attempt to uncover novel therapeutic targets for this disease.

By assessing both patient-derived cell lines and paediatric tumour specimens, we showed that PANX1 levels in embryonal RMS (eRMS) and alveolar RMS (aRMS) resembled that seen in undifferentiated human skeletal muscle cells and tissue, which was low compared to differentiated myoblasts and adult skeletal muscle tissue specimens, respectively. While qPCR showed low *PANX1* mRNA levels, RNA-sequencing (RNA-seq) detected considerable *PANX1* transcripts in RMS. However, alignment analysis of RNA-seq reads showed that most *PANX1* mRNAs lacked the putative 5' untranslated region (5'UTR) and were truncated beyond the start codon, thus leading to reduced PANX1 protein expression.

Since PANX1 was down-regulated in RMS, we re-introduced it in eRMS and aRMS cell lines using both transient expression by transfection and a cumate-inducible lentivirus-based stable expression system. While PANX1 expression did not induce terminal myogenic differentiation of eRMS and aRMS cells, it dramatically reduced their proliferation and migration, inhibited their 3-dimensional (3D) tumour spheroid formation, and induced the regression of established spheroids by apoptosis. Further *in vivo* studies using orthotopic eRMS and aRMS mouse models also showed significant tumour-suppression by PANX1 expression alone. As our initial mechanistic studies indicated that the tumour-inhibitor

function of PANX1 was not mediated by its channel activity, we then used unbiased transcriptomic and proteomic studies to delineate its mechanism of action. Bioinformatical analysis of RNA-seq data showed a significant change in expression of genes related to various cellular processes, such as migration and apoptosis, and signaling pathways linked to tumour-suppression. We further validated our RNA-seq data by demonstrating a PANX1-mediated change in the expression of several gene targets including the up-regulation of connexin 43 (Cx43), a previously known inducer of RMS differentiation. Using BioID (proximity-dependent biotin identification) and co-immunoprecipitation using PANX1-enriched fractions coupled with mass spectrometry, we identified the neuroblast differentiation associated protein AHNAK as a novel interactor of PANX1, which was subsequently shown to participate in the PANX1-mediated tumour-inhibitory mechanism.

Having established up-regulation of PANX1 as a potential therapeutic approach, we next explored means by which to increase its expression in RMS. Quercetin, a naturally occurring polyphenol, was found in a recent genome-wide transcriptome profiling of murine cerebrocortical cells to up-regulate *Panx1* mRNA. Thus, it provided us with a potential pharmacological tool to modulate PANX1 levels and study its regulation in RMS. After demonstrating up-regulation of PANX1 at protein levels in RMS, we discovered that quercetin induced the transcription of a translationally functional 5'Leader-containing *PANX1* mRNA variant by enhancing the binding of the transcription factor ETV4 (ETS Variant Transcription Factor 4) to the *PANX1* promoter. Finally, we showed that quercetin treatment in RMS cells dramatically reduced their malignant properties by inducing their myogenic differentiation, inhibiting tumour spheroid growth, and promoting regression of established tumour spheroids.

These results suggest that PANX1 expression can be regulated at the translational level and that quercetin may constitute a potential new therapeutic agent for treatment of RMS.

In order to familiarize readers with the material pertinent to this thesis, the Introduction will be divided into two major sections; in the first section, the clinical features, histological subtypes, diagnosis, pathogenesis, and current therapeutic management of RMS will be reviewed; the second section will be dedicated to PANX1, in which its discovery, structural characteristics and channel function will first be reviewed, followed by its links to human cancers, currently known interactors, and transcriptional and translational regulation.

1.1 RHABDOMYOSARCOMA

1.1.1 A Brief Historical Overview

In a study published in 1854, C.O. Weber, a German physician, described a localized recurrent tissue mass consisted of striated muscle from all stages of differentiation (Weber and Virchow, 1854). Many tumours with such features were described in the subsequent years, however, it was not until 1942 that they were collectively recognized by A.P. Stout as rhabdomyosarcomas (RMS), tumours derived from skeletal muscle (Stout, 1946). From the limited 121 cases that were available at the time, A.P. Stout described RMS as a cancer of very variable gross characteristics, growth rate and appearances, and that inflicted people of both sexes and from all age groups (Stout, 1946). However, due to the rare and variable nature of RMS, little progress was made in regard to its clinical management (Newton et al., 1999; Stout, 1946). This challenge was finally overcome following the foundation of the Intergroup Rhabdomyosarcoma Study Group (IRSG) in 1972, which was a collaborative effort to facilitate resource-pooling and clinical data-sharing across multiple independent

institutions in an attempt to investigate the biology and therapeutic options of RMS (Newton et al., 1999; Raney et al., 2001). In subsequent years, four major clinical RMS patient (IRS-I to IRS-IV) studies were completed, which have fundamentally shaped our understanding of RMS and led to dramatical improvement in its clinical outcome (Malempati and Hawkins, 2012; Newton et al., 1999; Raney et al., 2001).

1.1.2 Epidemiology

Today, RMS is recognized as the most common soft tissue sarcoma in children, accounting for 3 – 4% of all childhood malignancies (Dasgupta et al., 2016). Annually, approximately 4.5 cases of RMS are reported per million individuals younger than 20 years of age (Chen et al., 2019; Shern et al., 2014), and this translates to about 350 newly diagnosed patients per year in the United States (Ognjanovic et al., 2009) and 25 patients per year in Canada (Canadian Cancer Statistics Advisory Committee, 2019). More than 50% of cases of RMS are diagnosed in the first decade of life with a slight male predominance, and the frequency of their onset decreases with age (Ognjanovic et al., 2009). RMS can originate from any anatomic site that contains a muscle bed as well as regions that lack skeletal muscle (Crist et al., 1995; Maurer et al., 1993; Wang, 2012). The most prominent sites of origin include the genito-urinary tract (~31%), head and neck region (~25%), and extremities (~13%) (Crist et al., 1995; Maurer et al., 1993; Wang, 2012). However, the incidence of RMS and its anatomic site of origination may depend on the histologic subtype (refer to section 1.1.4 for detailed discussion) (De Giovanni et al., 2009). RMS typically arise sporadically, and their genetic risk factors are largely unknown to date (Skapek et al., 2019). Nevertheless, certain genetic disorders have been linked to the development of RMS, such as Li-Fraumeni Syndrome

(Diller et al., 1995; Trahair et al., 2007), neurofibromatosis type I (Crucis et al., 2015; Ferrari et al., 2007), Costello syndrome (Kratz et al., 2011), Noonan syndrome (Moschovi et al., 2007), Beckwith-Wiedemann syndrome (DeBaun and Tucker, 1998; Samuel et al., 1999) and DICER1 syndrome (Dehner et al., 2012; Doros et al., 2012).

1.1.3 Histological Subtypes

Historically, RMS was divided into two major histological subtypes: embryonal and alveolar RMS (Dagher and Helman, 1999). However, spindle cell/sclerosing and pleomorphic RMS have been recognized as the third and fourth histological subtypes, respectively, according to the current World Health Organization (WHO) classification (Fletcher et al., 2013).

Embryonal Rhabdomyosarcoma

Embryonal RMS (eRMS) are named after the appearance of embryonic myogenesis in their tumour histology, which often consist of tumour cells at various stages of myogenic differentiation (Parham and Barr, 2013). Botryoid and anaplastic eRMS are two variants of classical eRMS, and collectively, they represent approximately 70% of all RMS (Fletcher et al., 2013; Parham and Ellison, 2006; Qualman et al., 2008). eRMS predominantly affects children less than 5 years of age and are rarely reported in adolescents (Ognjanovic et al., 2009). While eRMS are most often found in the head and neck region or in the urinary tract, the botryoid variant manifests itself under the mucosal layer of bladder, nasopharynx, and vaginal or biliary tract (Fletcher et al., 2013). Despite being the most common histologic subtype, eRMS are largely associated with a favourable prognosis with a 5-year event-free survival

(EFS) of 87% for localised tumours (Meza et al., 2006). While the botryoid variant predicts a favourable prognosis, the presence of anaplasia negatively influences the clinical outcome (Meza et al., 2006). However, the prognosis for eRMS with distal metastasis is still poor with a 5-year EFS of 43% (Meza et al., 2006).

At the molecular level, eRMS display a wide range of genetic alterations including chromosomal copy-number variations and somatic or germline mutations (Shern et al., 2014). More than half of eRMS cases show loss-of-heterozygosity (LOH) at chromosome 11p15.5 (Shern et al., 2014), which houses a large cluster of imprinted genes important for regulation of cellular growth such as insulin growth factor 2 (*IGF2*) and cyclin dependent kinase inhibitor (*CDKN1C*) (Smith et al., 2007). In addition, mutations in genes involved in the RAS pathway that regulates cell cycle and proliferation such as *NRAS, KRAS,* and *HRAS* have been reported in one third of cases (Shern et al., 2014). Loss of function mutations in *TP53* are commonly seen in eRMS with features of anaplasia (Hettmer et al., 2014). Therefore, transformation of eRMS is believed to be a result from additive mutational burden instead of a single driver mutation (Leiner and Le Loarer, 2020).

Alveolar Rhabdomyosarcoma

Alveolar RMS (aRMS) histologically resembles the fetal alveoli of the lungs with undifferentiated round cells with hyperchromatic nuclei (Leiner and Le Loarer, 2020; Parham and Barr, 2013). There is also a solid variant of aRMS that is defined by densely packed cells without discernible alveolar arrangement (Newton et al., 1995; Parham and Barr, 2013). However, the solid variant is often difficult to diagnose by histocytology alone as its characteristic dense aggregation of cells is also seen in some

cases of eRMS (Leiner and Le Loarer, 2020; Parham and Barr, 2013). Epidemiologically, the aRMS subtype makes up approximately 30% of all RMS cases with a predilection in adolescents and young adults and tends to arise from the extremities, trunk, and perineum/perianal region (Parham and Ellison, 2006). Nevertheless, aRMS are an aggressive subtype of RMS with approximately 50% of them presenting with metastatic invasion into either the nearby or distal lymph nodes or organs such as lungs and bone marrow (Leiner and Le Loarer, 2020; Parham and Ellison, 2006; Williamson et al., 2010). Patients diagnosed with metastatic aRMS generally have poor prognosis with an estimated overall 5-year EFS rate of only 31% (Meza et al., 2006).

Approximately 80% of aRMS tumours are associated with a hallmark recurrent chromosomal translation that fuses either the q35 arm on chromosome 2 or the p36 arm on chromosome 1 to the q14 arm on chromosome 13 (Malempati and Hawkins, 2012). This results in chimeric transcription factors (TF) by joining the N-terminal DNA binding domain of PAX3 or PAX7 to the C-terminal transactivation domain of FOXO1, respectively (Malempati and Hawkins, 2012). Fusion of *PAX3-FOXO1* is more common and occurs in about 60% of aRMS cases whereas the fusion of *PAX7-FOXO1* is observed in about 20% of cases (Barr et al., 2006; Chen et al., 2019). Together, these aRMS are termed fusion-positive (FP) aRMS thus making the remaining aRMS tumours fusion-negative (FN) aRMS. The PAX3- or PAX7-FOXO1 are potent transcriptional activators, which drive aberrant gene expression leading to its tumourigenic transformation (Chen et al., 2019; Fredericks et al., 1995). On the other hand, FN aRMS resembles eRMS molecularly with LOH at chromosome

11p15.5 and point mutations with *RAS* family genes at a higher rate than FP aRMS (Shern et al., 2014; Williamson et al., 2010). Clinically, patients with FN aRMS are associated with favourable prognosis with comparable 5-year overall survival to those diagnosed with eRMS, while FP aRMS is more invasive and leads to poorer overall clinical outcome (Williamson et al., 2010).

Other Histological Subtypes

Other histological subtypes of RMS occur with much lower frequency than those of eRMS or aRMS, together making up less than 5% of all RMS (Fletcher et al., 2013). Spindle cell RMS (spRMS), which used to be considered a variant of eRMS, is now classified as a separate histologic subtype (Fletcher et al., 2013). The spRMS subtype represents approximately 3% of all RMS diagnoses and includes a sclerosing variant characterized by abundant hyalinization of stromal tissue (Fletcher et al., 2013). This subtype of RMS is predominantly found in young children with a predilection for infants, and can arise from any anatomic site with soft tissue (Cavazzana et al., 1992; Leuschner et al., 1993). While spRMS in infants are often associated with gene fusion of *VGLL2* (vestigial-like 2) and *NCOA2* (nuclear receptor co-activator 2) and local recurrence, spRMS in older children generally show mutation in *MYOD1* gene and exhibit a worse clinical outcome (Alaggio et al., 2016). Pleomorphic RMS (pRMS) is an extremely rare subtype of RMS which accounts for only 1% of all RMS cases (Carvalho et al., 2019). It is almost exclusively found in adults older than 60 years of age with lower extremity locations as the most common anatomic site of onset. (Carvalho et al., 2019). Although little is known about the mutational landscape of pRMS tumours, immunohistochemistry and electron microscopy studies have shown

features of scant skeletal muscle differentiation (Furlong et al., 2001). Despite their rarity, pRMS tumours have a relapse rate of 53.8% and more than 80% metastasize within 5 years resulting in a high mortality rate of 70% (Carvalho et al., 2019; Furlong et al., 2001).

Collectively, RMS are diverse in histology and underlying molecular profiles, which both are key prognostic factors (Skapek et al., 2019). Overall, the spindle cell/sclerosing subtype shows the most favourable clinical outcome while the alveolar subtype performs the most poorly clinically, which is further exacerbated by the presence of fusion genes, *PAX-FOXO1* (Sultan et al., 2009). Moreover, adolescents and adults tend to develop the alveolar and pleomorphic subtypes leading to poorer prognosis with a 5-year overall survival rate of 27% compared with 61% in children, who are more likely to have the embryonal and spindle cell/sclerosing subtypes (Sultan et al., 2009).

1.1.4 Pathogenic Origin

Soft tissue sarcomas are malignant neoplasms that arise from mesenchymal cells (Hoang et al., 2018). These pluripotent cells originate from the mesoderm and have the propensity to differentiate into bone, cartilage, fat, nerves, fibrous tissue, as well as cardiac, smooth, and skeletal muscles (Uccelli et al., 2008). RMS are a group of soft tissue sarcomas with histologic features reminiscent of skeletal muscle (Skapek et al., 2019).

The formation of skeletal muscle involves a series of intricately regulated steps in which mononucleated skeletal muscle precursors, myoblasts, undergo irreversible

cell cycle arrest and sequential differentiation along the myogenic lineage to form multinucleated myotubes that ultimately become contractile skeletal muscle fibres (Bentzinger et al., 2012; Burattini et al., 2004; Chal and Pourquié, 2017) (Fig. 1.1). During this process, a pool of myogenic progenitors escape terminal myogenic differentiation and become satellite cells that reside in the periphery of the skeletal muscle fibres under the basal lamina (Bentzinger et al., 2012; Chal and Pourquié, 2017). These cells are usually quiescent but can be stimulated to re-enter the myogenic differentiation program such as during skeletal muscle regeneration following injury (Bentzinger et al., 2012; Chal and Pourquié, 2017).

Myogenic differentiation is carefully orchestrated by two main families of transcription factors which are the paired-homeobox transcription factors 3 (PAX3) and 7 (PAX7), belonging to the basic helix-loop-helix (bHLH) family, and myogenic regulatory factors (MRF), including myoblast determination protein 1 (MyoD1), Myogenic factor 5 (Myf5), myogenic regulatory factor 4 (MRF4), and myogenin (MyoG) (Bentzinger et al., 2012; Chal and Pourquié, 2017). PAX3/7 are typically found in uncommitted embryonic progenitors and satellite cells while MRFs are expressed in more differentiated cells in the skeletal muscle lineage (Bentzinger et al., 2012). These transcription factors are temporally activated and deactivated during myogenic differentiation and control the expression of skeletal muscle specific genes required for early lineage specification, commitment of myogenic differentiation, myocyte fusion and formation of myotubes (Bentzinger et al., 2012) (Fig. 1.1).

One prevailing hypothesis indicates that RMS arise from uncontrolled proliferation of cells in the skeletal muscle lineage that fail to complete the myogenic

differentiation program (Keller and Guttridge, 2013; Yu and Guttridge, 2018) (Fig. 1.1). This is supported by their aberrant expression of PAX3/7, MRFs and skeletal muscle-specific proteins, histological resemblance of immature skeletal muscle, and typical onset in or near skeletal muscle beds (Parham and Barr, 2013; Shern et al., 2014, 2015; Wang, 2012). Consistent with this hypothesis is also the observation of the overrepresented population of satellite cell-like precursors in eRMS tumours from *in vivo* animal models suggesting their involvement during tumourigenesis (Langenau et al., 2007; Wagers and Conboy, 2005). Moreover, recapitulation of the hallmark mutations found in RMS in both adult human skeletal myoblasts and in mature skeletal muscle tissue in mouse models have both led to the development of eRMS (Linardic et al., 2005) and aRMS (Keller and Capecchi, 2005), respectively. These experiments also demonstrate the skeletal muscle lineage-dependency of RMS tumourigensis (Hettmer and Wagers, 2010; Lav et al., 2015), which may explain the heterogeneity of phenotypes of RMS tumours observed clinically. Notably, RMS tumours often become more differentiated following chemotherapy (Marchal et al., 1997), which further supports the notion that RMS arises from skeletal muscle progenitors.

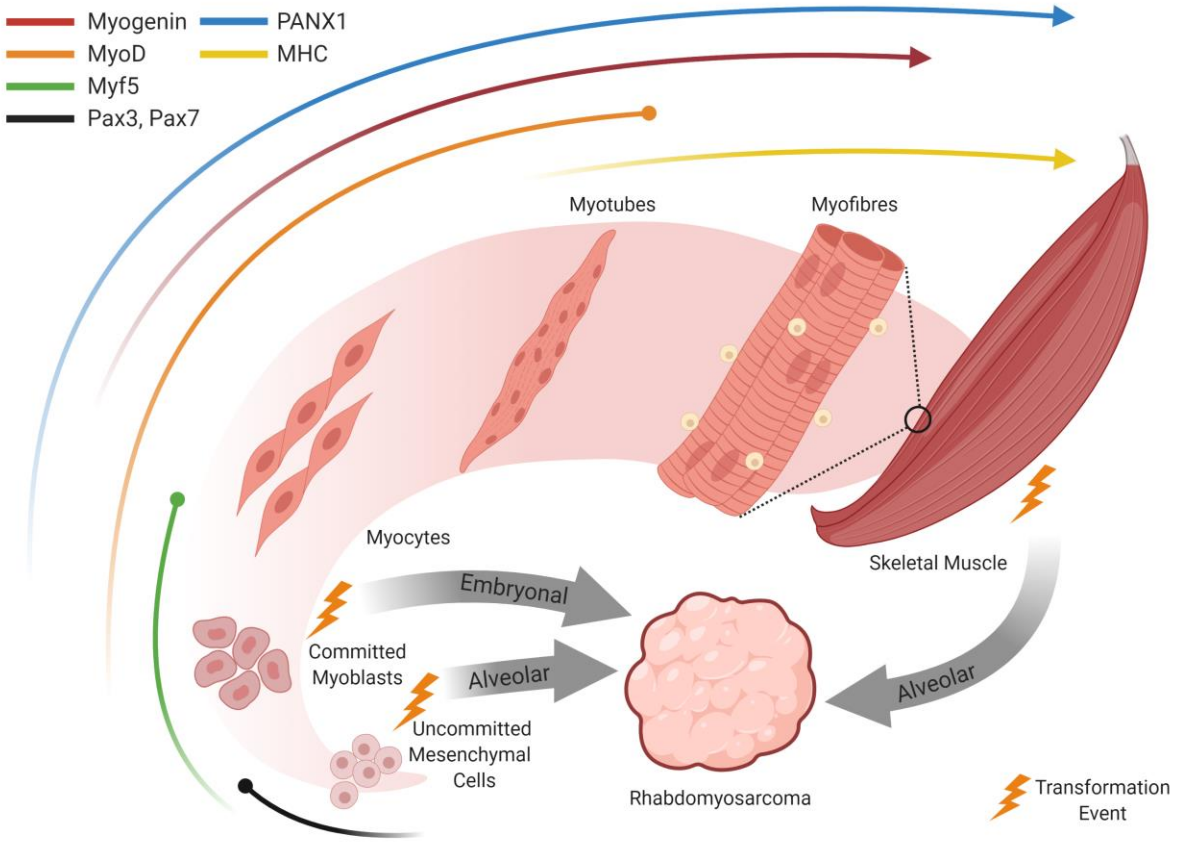
Myogenin
MyoD
Myf5
Pax3, Pax7
PANX1
MHC
Myotubes
Myofibres
Myocytes
Skeletal Muscle
Embryonal
Committed
Myoblasts
Alveolar
Uncommitted
Mesenchymal
Cells
Rhabdomyosarcoma
Alveolar
Transformation
Event

Figure 1.1 Myogenic Differentiation and the Pathological Origin of RMS.

The cellular stages of myogenic differentiation as described in the text. Coloured lines represent the expression of the corresponding myogenic factors or skeletal muscle-related proteins in their respective cellular differentiation stages. Dotheads indicate the down-regulation or termination of the expression while arrowheads indicated the continued expression as detected at the protein level beyond the cellular differentiation stage. Myosin heavy chain (MHC) is a structural protein found in maturing and functional skeletal muscle which is a commonly used molecular marker for late-stage myogenic differentiation (Langlois et al., 2014). Pannexin 1 (PANX1) is an important regulator of myogenic differentiation which will be discussed in detail in the following section. Shaded dark arrows present the proposed cellular stage that can give rise to the indicated histologic subtype of RMS as described in the following section.

However, RMS tumours can also arise from anatomic sites devoid of skeletal muscle such as the bladder, genito-urinary and biliary tracts, and bone marrow (Parham and Barr, 2013; Wang, 2012). This has led to an alternative hypothesis that RMS arises from primitive mesenchymal cells or cells of non-skeletal muscle lineage (Charytonowicz et al., 2009) (Fig. 1.1). In accordance with this conjecture, mesenchymal stem cells bearing PAX-FOXO1 fusion oncoproteins have also been shown to initiate neoplastic transformation into aRMS-like tumours (Ren et al., 2008). Furthermore, ectopic expression of MRFs alone have been shown to convert several non-myogenic cell types into the skeletal muscle lineage (Ludolph and Konieczny, 1995), thus expression of skeletal muscle-related proteins in RMS may simply be a result of their tumourigenic transformation (Hettmer and Wagers, 2010).

Currently, RMS is generally considered to be a neoplasm of skeletal muscle, however, no consensus has been reached regarding its exact origin.

1.1.5 Diagnosis

Clinically, RMS typically manifests itself as a localized tissue mass. It can be either asymptomatic if present in the orbital region or it can be associated with symptoms related to tumour size or presence of metastatic invasion into distal organs (Egas-Bejar and Huh, 2014). Although imaging studies such as computed tomography (CT) scans or magnetic resonance imaging can reveal the size and location of RMS, its diagnosis is based on its immunohistochemical profile and histological appearance (Dziuba et al., 2018; Egas-Bejar and Huh, 2014). The sine quo non of RMS is the presence of embryonic myogenesis in the tumour tissue (Dziuba et al., 2018; Parham and Barr, 2013). Thus, the immunochemical diagnosis of RMS involves identification

of muscle specific proteins, such as desmin, myosin or muscle-specific actin, and MRFs, such as MyoD1 and myogenin (Parham and Barr, 2013). Under light microscopy, RMS appears as atypical rhabdomyoblasts with various stages of embryonic differentiation, from highly differentiated tadpole- or ribbon-shaped cells with cross-striation to poorly differentiated primitive round cells (Dziuba et al., 2018). Histological identification of these developing immature cells of skeletal muscle lineage is also key to the diagnosis of RMS (Dziuba et al., 2018).

1.1.6 Risk Stratification

RMS risk stratification is complex and involves a stepwise system of staging, clinical grouping, and assignment of risk groups (Dasgupta et al., 2016). The staging of RMS is based on the pre-treatment status of the tumour and TNM (T: site, N: regional nodes, M: metastasis) criteria (Dasgupta et al., 2016). The TNM criteria include the anatomic site and size of the primary tumour, involvement of the regional lymph nodes and the presence of distal metastasis (Dasgupta et al., 2016). The assignment of clinical group determines the pathological status after surgical resection but precedes the start of chemo- or radiotherapy (Dasgupta et al., 2016). Patients are assigned to a clinical group according to the condition of the residual disease, which assesses the completeness of surgical resection and dissemination of tumour to lymph nodes or distal organs (Dasgupta et al., 2016). The determinants of risk group assignment encompass all previous criteria and further include histology, molecular profiling, and fusion status. Based on these criteria, patients are ultimately assigned into low-, intermediate-, and high-risk groups for further optimization of the therapeutic intensity (Dasgupta et al., 2016). This comprehensive risk stratification

system has been shown to accurately reflect the clinical outcome (Dasgupta et al., 2016).

1.1.7 Therapeutic Strategies

The past five decades of intergroup clinical studies have dramatically increased the overall survival of paediatric patients from 25% in the 1970s to 70% today (Crist et al., 1995; Darwish et al., 2020; Maurer et al., 1993). This is owing to the development of multi-disciplinary approaches involving surgery, radiation therapy and chemotherapy (Chen et al., 2019; Miwa et al., 2020). Surgery is mainly reserved for localized primary RMS tumours where complete resection can be achieved, however, pre-treatment surgery and late re-excision can both be performed to reduce the burden of chemotherapy (Dasgupta et al., 2016). The residual disease is then further managed by multi-agent chemotherapy using vincristine, actinomycin D, and cyclophosphamide (known as VAC) with or without radiation therapy (Raney et al., 2011). Methods to further improve this multi-modal therapy are continuously explored and implemented in the present day. For instance, patients in the low-risk group, especially those with localized onset of eRMS, generally have excellent prognosis, thus efforts have been made to alleviate the intensity of chemotherapy by shortening the duration and lowering the dosages used while still maintaining 3-year EFS and overall survival rates of 89% and 98%, respectively (Walterhouse et al., 2014). In the intermediate- and high-risk groups, a recent clinical study has shown an improvement in the 5-year EFS from 69.8% to 77.6% with addition of metronomic maintenance chemotherapy when compared to standard intensive treatment alone (Bisogno et al., 2019).

However, the clinical management of patients with metastatic and relapsed RMS remains a major clinical challenge to date (Chen et al., 2019; Hettmer et al., 2014; Yohe et al., 2019). Indeed, despite these advanced treatment modalities, more than 70% of patients diagnosed with metastatic or relapsed RMS eventually succumb to the disease (Oberlin et al., 2008; Sultan et al., 2009). Those fortunate enough to survive the malignancy are plagued with life-long functional and cosmetic defects due to invasive therapies (Punyko et al., 2005). More importantly, the overall cure rate of patients in the high-risk group has remained below 30% since 1990s suggesting that the VAC chemotherapy backbone to treatment has reached its efficacy plateau (Egas-Bejar and Huh, 2014), underscoring the need for novel therapeutic strategies (Chen et al., 2019; Miwa et al., 2020; Yohe et al., 2019).

1.2 PANNEXINS

Pannexins are single membrane channel proteins that consist of three family members which are denoted as PANX1, PANX2, and PANX3 (or Panx1, Panx2, and Panx3 in rodents) (Penuela et al., 2013). PANX1/Panx1 is ubiquitously expressed and can be detected as heterogeneously glycosylated species across various tissues or organs such as brain, spleen, skin, lung, kidney, as well as cardiac and skeletal muscle (Baranova et al., 2004; Celetti et al., 2010; Cowan et al., 2012; Dolmatova et al., 2012; Langlois et al., 2014; Penuela et al., 2007; Riquelme et al., 2013). However, the tissue expression of the other two family members is less diverse, with Panx3 limited to skin, bone, cartilage, and skeletal muscle (Penuela et al., 2007), and Panx2 restricted to the brain (Baranova et al., 2004). While sharing no or limited sequence homology to connexins or innexins, respectively, Panxs are topologically similar to gap junction proteins each having four α-helical transmembrane domains, two extracellular loops, one intracellular loop, and cytoplasmic amino (N-) and carboxyl (C-) termini (Baranova et al., 2004; Panchina et al., 2000; Penuela et al., 2007). Panx1 and Panx3 are similar to each other and share ~60% sequence homology but are significantly different from Panx2, which has a much larger C-terminal domain that may convey unique functionalities (Penuela et al., 2007; Yen and Saier, 2007).

1.2.1 An Overview of Pannexin 1

PANX1/Panx1 contains four evolutionarily conserved cysteine residues, two in each extracellular loop (Baranova et al., 2004; Panchina et al., 2000), which are required for the formation of functional channels as replacing any of these cysteine residues to serine residue by site-directed mutagenesis will abolish channel activity (Bunse et al., 2011; Wang and Dahl, 2010). Using chemical cross-linkers and electron

microscopy, Panx1 protomers are shown to oligomerize into homohexameric channels (Ambrosi et al., 2010; Boassa et al., 2007). However, recent studies using single-particle cryo-electron microscopy (cryo-EM) have for the first time determined the structure of human PANX1 channel, which supports the previous notion of four-transmembrane topology but indicates a homoheptameric assembly of seven identical PANX1 protomers (Deng et al., 2020; Jin et al., 2020; Michalski et al., 2020; Qu et al., 2020; Ruan et al., 2020; Syrjanen et al., 2020). The PANX1 protomers are linked by disulfide bonds between the cysteine residues in the extracellular loops around a central symmetry axis to form the channel (Deng et al., 2020; Jin et al., 2020; Michalski et al., 2020; Qu et al., 2020; Ruan et al., 2020; Syrjanen et al., 2020). The pore of the PANX1 channel is lined by a ring of seven tryptophan residues in the N-terminus which are speculated to act as a molecular filter that defines the size of permeable molecules (Deng et al., 2020; Ruan et al., 2020).

As a polytopic integral membrane protein, Panx1 is presumed to follow the classic endoplasmic reticulum (ER)-Golgi apparatus-plasma membrane transportation pathway that is common to integral proteins (Penuela and Laird, 2012). Initial modification of Panx1 takes place in the ER where sugar moieties are added to the asparagine residue at position 254 (N254) in the extracellular loop that consists of high-mannose chains (Penuela and Laird, 2012; Penuela et al., 2009). Modified Panx1 carrying high-mannose chains is then delivered to the Golgi apparatus by Sar1-dependent coat protein complex II (COPII) vesicles for additional processing into complex glycoproteins before being targeted to the plasma membrane (Bhalla-Gehi et al., 2010). For this reason, Panx1 can be resolved as three distinct glycosylation species

in sodium dodecyl sulphate–polyacrylamide gel electrophoresis (SDS-PAGE) that represents the basic (Gly0), high-mannose (Gly1), and complex (Gly2) glycosylation (Penuela et al., 2007). It has been suggested that the complex sugar moieties in the extracellular loop of Panx1 prevent the docking of the opposing channels to form gap junctions by steric hindrance (Penuela et al., 2007; Sosinsky et al., 2011). Moreover, glycosylation has also been shown to regulate trafficking of Panx1 to the plasma membrane as blocking N-glycosylation by site-directed mutagenesis or pharmacological agents significantly reduce Panx1 levels at the cell surface (Boassa et al., 2007; Penuela et al., 2007, 2009). In addition to glycosylation, Panx1 is shown to be phosphorylated by Scr family kinases (SFK) at tyrosine position 308 (Y308) leading to channel activation (Weilinger et al., 2012). Phosphorylation of plasma membrane-bound PANX1 occurs at Y198, which is important for the ATP release regulating vascular smooth muscle vasoconstriction (DeLalio et al., 2019). S-nitrosylation constitutes another post-translational modification (PTM) of Panx1 where covalently attaching NO groups to cysteines at positions 40 and 346 can impede Panx1 channel activities (Lohman et al., 2012; Penuela et al., 2014a). Other PTMs such as sialylation or O-glycosylation have not been observed in PANX1 (Penuela et al., 2014a).

Panx1 channels form voltage sensitive pores in the plasma membrane that have very low opening probability at negative resting potentials, thus remaining closed under normal physiological conditions (Bruzzone et al., 2003). Aside from being activated by positive membrane potentials that can be achieved in excitable cells types such as neurons and myocytes (Bond and Naus, 2014), Panx1 channels can be opened by mechanical forces such as physical stretching of plasma membrane (Furlow et al.,

2015; Xia et al., 2012), membrane swelling under hypotonic stress (Li et al., 2012, 2011a; Locovei et al., 2006a; Xia et al., 2012), and fluid shear stress (Penuela et al., 2007, 2009; Verschuren et al., 2020); proteolytic cleavage of the C-terminal tail by caspase 3 or 7 at Asp-Val-Val-Asp (DVVD) consensus site between positions 376 – 379 (Chekeni et al., 2010); increasing extracellular K^+ concentrations to ≥ 10 mM (Silverman et al., 2009); and rise of intracellular Ca^{2+} concentrations, such as following the activation of ionotropic P2X or metabotropic P2Y purinergic receptors (Locovei et al., 2006b; Pelegrin and Surprenant, 2006). Once opened, Panx1 channels in the plasma membrane at the cell surface are permeable to various inorganic ions including Na^+, $Ca2^+$, K^+, and Cl^- (Ma et al., 2012; Wang and Dahl, 2018), and small molecules up to 1.5 kDa in size including metabolites such as creatine, spermidine, guanosine monophosphate (GMP) and adenosine triphosphate (ATP) (Bao et al., 2004; Medina et al., 2020). While it is not completely understood, current evidence suggests that two different open-channel conformations exist for Panx1 channels depending on the mode of activation (Dahl, 2018; Wang et al., 2014). When opened by membrane depolarization, ATP, caspase cleavage, or intracellular Ca^{2+}in the presence of high extracellular K^+ concentration (> 50 mM) or P2X receptors, Panx1 channels exhibit poor selectivity and allow passage of molecules ⩾ than 0.5 kDa such as ATP (Dahl, 2018; Wang et al., 2014). However, activation of Panx1 channels by the aforementioned stimuli in the absence of extracellular K^+ ions creates a highly selective pore for Cl^- ions that inhibits the passage of ATP and other molecules similar in size (Dahl, 2018; Wang et al., 2014). Activated Panx1 channels can be suppressed by a growing list of pharmacological compounds including the clinically approved drugs

probenecid and carbenoxolone (Bruzzone et al., 2005; Silverman et al., 2008; Willebrords et al., 2017). Probenecid is a well-established drug used to treat gout by facilitating the secretion of the disease-causing uric acid (Hainer et al., 2014). At therapeutic concentrations, probenecid has been shown to block Panx1-mediated currents with a half maximal inhibitory concentration of 150 μM without affecting connexin channels, thus making it a popular Panx1 channel inhibitor (Silverman et al., 2008). Carbenoxolone (CBX) is a derivative of glycyrrhetinic acid which has been used clinically to treat peptic, oral, and esophageal ulcers (Pinder et al., 1976). CBX has also been used as a reversible inhibitor of Cx channels at concentrations ≥ 100 μM (Davidson et al., 1986). However, Panx1 channels are more sensitive to CBX than Cx channels are and have been shown to be blocked at lower concentrations in the 10 – 30 μM range (Bruzzone et al., 2005), which are often used to help differentiate the two types of channels (Li et al., 2012; Ma et al., 2009a). Recently, cryo-EM structural analyses have revealed that CBX blocks the central pore of PANX1 channel by direct interaction with the W74 residue from each of the seven protomers (Michalski et al., 2020). Moreover, Panx1 channels can be specifically suppressed by mimetic peptides such as 10PANX1 (or 10Panx1), which is a 10-amino acid long sequence found in the first extracellular loop that directly blocks the channel pore (Pelegrin and Surprenant, 2006).

Despite being able to mediate the passage of diverse types of ions and molecules, Panx1 channels at the cell surface are best known as the major ATP conduits in mammalian cells which have important biological implications such as activation of the purinergic signaling pathways (Bao et al., 2004; Velasquez and

Eugenin, 2014). Indeed, the released ATP can activate P2X or P2Y receptors in the cell membrane via either autocrine or paracrine signaling that in turn mediate the intracellular release of Ca^{2+} (Velasquez and Eugenin, 2014). Thus far, Panx1 channels have been implicated in a plethora of cellular functions under physiological and pathological states. For instance, Panx1 channels have been proposed to mediate Ca^{2+} wave propagation in endothelial cells via purinergic signaling which regulates vasoconstriction under stress or hypotonicity (Begandt et al., 2017; Billaud et al., 2011; DeLalio et al., 2018); ATP released from Panx1 channels has also been shown to regulate the beating of cilia in air-way epithelial cells important for mucous clearance (Krick et al., 2016; Ransford et al., 2009; Seminario-Vidal et al., 2011); caspase-activated Panx1 channels in apoptotic cells release ATP as "find-me" signals to attract macrophages for phagocytosis (Chekeni et al., 2010) while other metabolites released, such as spermidine and GMP, can suppress inflammation of surrounding cells (Medina et al., 2020); SFK activation of Panx1 facilitates adhesion and emigration of leukocytes along the endothelial vascular wall during acute systemic inflammation (Lohman et al., 2015); Panx1 channels are important during development and are shown to regulate proliferation and differentiation of neurons (Wicki-Stordeur et al., 2012), keratinocytes (Celetti et al., 2010), skeletal muscle myoblasts (Langlois et al., 2014), and adipose stromal cells (Lee et al., 2018); human immunodeficiency viruses (HIV) hijack Panx1 channels to facilitate cell entry (Séror et al., 2011); activation of Panx1 channels contributes to ischemic neuronal death during stroke or neural degeneration after intracerebral hemorrhage (Bargiotas et al., 2011, 2012); Panx1 channels are increased in epileptic brain tissue and are considered a central signaling hub for development of seizures (Aquilino et al., 2019, 2020; Dossi et al., 2018; Thompson et al., 2008);

moreover, a subset of Panx1 channels can be found in the ER membrane and act as Ca^{2+} leak channels that have implications in maintaining Ca^{2+} homeostasis (Vanden Abeele et al., 2006).

1.2.2 Role of Pannexin 1 in Skeletal Muscle

As described earlier, myogenic differentiation is a well coordinated process of myogenic commitment, myocyte alignment, and fusion (Bentzinger et al., 2012). Panx1 channels play a critical role in the acquisition of myogenic commitment through the ATP-dependent activation of purinergic receptors which in turn lead to the rise of intracellular Ca^{2+} levels required for expression of Myf5 (Riquelme et al., 2015). Indeed, blocking purinergic receptors or knocking down Panx1 channels both inhibit this process (Riquelme et al., 2015). Our laboratory has found that PANX1 levels are low in initially undifferentiated human skeletal muscle myoblasts (HSMM) but rapidly increase upon myogenic differentiation and remain highly expressed in differentiated HSMM myotubes (Langlois et al., 2014). Ectopic introduction of PANX1 in undifferentiated HSMM promotes myogenic differentiation and fusion (Langlois et al., 2014). Accordingly, these processes were inhibited by probenecid or CBX, together identifying PANX1 channels as an important regulator of myogenic differentiation (Langlois et al., 2014). This increase in Panx1 levels was also observed during the development of mouse skeletal muscles (Pham et al., 2018). Specifically, Panx1 levels remain low from embryonic day 14.5 through postnatal day 1 where an initial small significant increase can be observed and then continue to increase and peak after 4 weeks (Pham et al., 2018). A similar increase in Panx1 levels was also seen during muscle regeneration *in vivo* (Pham et al., 2018).

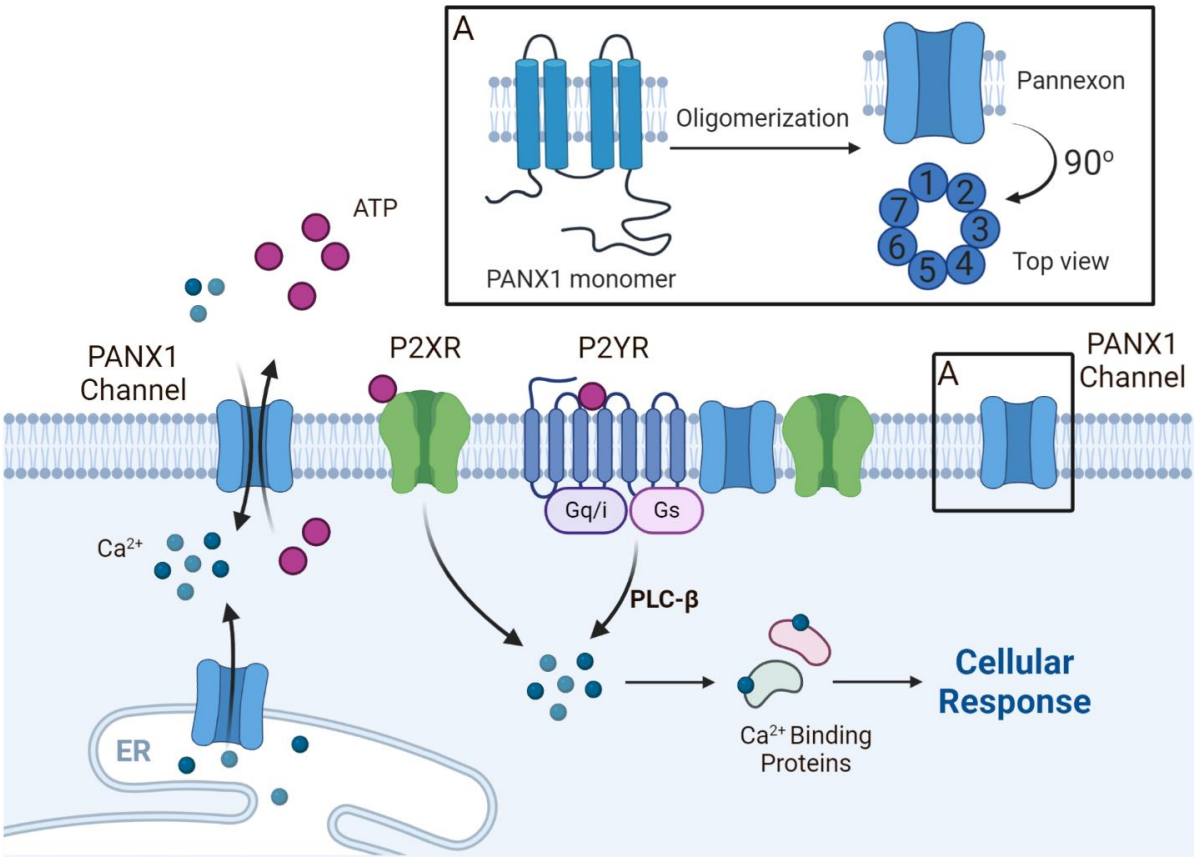
A
Oligomerization
Pannexon
90°
1
2
3
4
5
6
7
Top view
PANX1 monomer
ATP
PANX1
Channel
P2XR
P2YR
A
PANX1
Channel
Gq/i
Gs
Ca2+
PLC-β
ER
Ca2+ Binding
Proteins
Cellular
Response

Figure 1.2 Structure and Mechanism of Autocrine and Paracrine Signaling of PANX1 Channels.

The structure and function of PANX1 channels are as described in the text. Briefly, PANX1 channels are four-pass membrane proteins with intracellularly orientated amino (N-) and carboxyl termini (inset A). When oligomerized into a homoheptameric channel, PANX1 channels in the endoplasmic reticulum (ER) or at the plasma membrane can mediate the passage of ions and small metabolites such as Ca^{2+} and ATP. The released signaling molecules, such as ATP, can bind to P2X and P2Y receptors to induced direct influx of Ca^{2+} as in the case of P2XRs or release of Ca^{2+} from intracellular storages via phospholipase C-β (PLC-β) pathway as in the case of G protein-(Gs/Gq/Gi) coupled P2YRs (Burnstock, 2006). Intracellular Ca^{2+} can further induce PANX1 channel activation leading to signal amplification or binding to specific proteins for the mediation of cellular responses.

Panx1 is localized in the transverse-tubules (T-tubules) between the dihydropyridine (DHPR) and ryanodine receptors (RyR) of skeletal muscle (Riquelme et al., 2013). When muscle fibres are subjected to electric stimuli, Panx1 channels open and induce calcium transients through activation of P2Y receptors (Buvinic et al., 2009; Riquelme et al., 2013). This rise in intracellular Ca^{2+} levels can also enhance the contractile force of muscle fibres further implicating Panx1 channels in force potentiation (Riquelme et al., 2013) and regulating expression of skeletal muscle-specific genes (Arias-Calderón et al., 2016). Consistently, Panx1 channels become phosphorylated during potentiation which is suggestive of an open pore conformation (Riquelme et al., 2013). Under pathological conditions such as Duchene muscular dystrophy (DMD), which is characterized by progressive muscular atrophy due to impaired regeneration (Rodrigues et al., 2016), Panx1 levels are reduced, suggesting a possible role of Panx1 channels during skeletal muscle regeneration and in skeletal muscle disease (Cea et al., 2012; Pham et al., 2018).

1.2.3 Pannexin 1 in Cancer

Given its important implications in various diseases, it is perhaps not surprising that Panx1 channels are also involved in carcinogenesis. In fact, shortly after its discovery by Panchin et al. in 2000 (Panchina et al., 2000), several high-throughput sequencing-based studies revealed an association of *Panx1* transcript levels to the grade, metastatic spread, and oncogenesis of several cancer types (Litvin, 2006). These studies also suggest a paradoxical role of Panx1 during carcinogenesis (Litvin, 2006). For instance, highly metastatic mouse hepatocarcinoma cells tend to show more Panx1 expression compared to their less or non-metastatic counterparts (Song et al., 2005).

Similarly, high levels of Panx1 were found in multiple myeloma cell lines, where it was proposed to act as an oncoprotein during myelomagenesis (Largo et al., 2006). On the other hand, inhibition of serous carcinoma cell proliferation leads to reduced *PANX1* mRNA levels (Pohl et al., 2005). Notably, evidence of this paradoxical role of Panx1 continues to be documented even to date where Panx1 expression is found to be either beneficial or detrimental depending on the cell type from which the cancer originates (Jiang and Penuela, 2016). Thus, it has been suggested that Panx1 channel function may be modulated by the co-expression of other receptors which may ultimately alter the downstream signaling pathways leading to different cellular outcomes (Jiang and Penuela, 2016).

Down-regulation of Pannexin 1 during Cancer Progression

One of the first studies that implicated Panx1 in carcinogenesis came from work by Lai et al. using the C6 glioma murine cell line (Lai et al., 2007). The authors found that *Panx1* transcripts were detected in normal astrocytes but were absent in C6 glioma cells (Lai et al., 2007). Ectopic expression of green fluorescent protein (GFP)-tagged Panx1 in C6 cells induced a morphological change from a typical spindle shape to a flattened cell morphology (Lai et al., 2007). This morphological change in C6 cells was accompanied by a reduction in cell proliferation and migration, as well as a diminution in the number and size of 3-dimensional (3D) tumour spheroids (Lai et al., 2007), which was later attributed to the ability of Panx1 to enhance actin microfilament-mediated cellular compaction (Bao et al., 2012). Furthermore, Panx1 expression also inhibited C6 glioma growth *in vivo* (Lai et al., 2007). Thus, the authors suggested that Panx1 had tumour-suppressive effects in C6 glioma cells (Lai et al., 2007).

PANX1 levels are also found to be reduced in human tissue specimens of both basal and squamous cell carcinomas compared to normal epidermis (Cowan et al., 2012). Ectopic expression of Panx1 in rat epidermal keratinocytes lowered their cell proliferation and differentiation, leading to disruption of the organotypic epidermis architecture (Celetti et al., 2010). Thus, the reduced PANX1 levels have been speculated to have a protective role during transformation of these non-melanocytic skin cancers (Jiang and Penuela, 2016).

Although not studied in detail, ectopic expression of yellow fluorescent protein (YFP)-tagged PANX1 in human cervical cancer derived HeLa cells that lack endogenous PANX1 significantly reduced their proliferation (Schalper et al., 2014). In addition, it has been shown that PANX1 levels are reduced in human gallbladder adenocarcinoma tissue specimens compared to those of normal gallbladder (Schalper et al., 2014). This reduction of PANX1 levels was negatively correlated with Ki67 levels suggesting a possible role of PANX1 in growth suppression of gallbladder adenocarcinomas (Schalper et al., 2014; Weigel and Dowsett, 2010).

Up-regulation of Pannexin 1 during Cancer Progression

On the contrary, neoplasmic transformation can lead to increased Panx1 levels which promotes the progression of certain cancer types. Penuela et al. found that Panx1 is highly expressed in three isogenic mouse melanoma cell lines and that its levels are positively correlated with the metastatic potential of those cell lines (Penuela et al., 2012). Knockdown (KD) of Panx1 using short-hairpin RNA (shRNA) in the most aggressive melanoma cell line induced a phenotypical transformation that resembled that of normal melanocytes (Penuela et al., 2012). Reduction of Panx1 also inhibits

tumourigenesis of melanoma cells following transplantation onto chicken chorioallantoic membrane (Penuela et al., 2012). In a more recent study from the same group, they also found PANX1 to be highly expressed in primary human melanoma cells (Freeman et al., 2019). Their malignant properties could be suppressed by both shRNA mediated KD of PANX1 and pharmacological inhibition of PANX1 channels by probenecid or CBX (Freeman et al., 2019).

Similarly, Panx1 levels are up-regulated in the mouse testicular cancer cell line I-10 compared to normal Leydig cells (Liu et al., 2019). Pharmacological inhibition of Panx1 channels by probenecid and shRNA-mediated KD of Panx1 both led to reduced of migration and invasion of I-10 cells with concomitant reduction of vimentin, E-cadherin, and matrix-metalloproteinase 9 involved in extracellular matrix modification (Liu et al., 2019). Interestingly, increased expression of exogenous Panx1 in I-10 cells dramatically exacerbates their invasiveness, suggesting a positive correlation of Panx1 levels and testicular cancer aggressiveness (Liu et al., 2019).

A gain-of-function Panx1 mutant has been identified by whole-transcriptomic RNA sequencing (RNA-seq) of four murine isogenic breast cancer cell lines (Furlow et al., 2015). This nonsense single nucleotide mutation (C268T) changes the glutamine at position 90 to a premature stop codon, thus generating a N-terminal fragment denoted as $PANX1^{1-89}$ (Furlow et al., 2015). When ectopically expressed in breast cancer cells, $PANX1^{1-89}$ can physically interact with endogenous PANX1 to form hyperactive channels with increased ATP release, promoting metastasis (Furlow et al., 2015). Conversely, blocking PANX1 channels with CBX reduced breast cancer cell metastasis (Furlow et al., 2015). The authors proposed that this pool of released

extracellular ATP in the tumour microenvironment can activate autocrine and paracrine purinergic signaling pathways that leads to inhibition of intravascular cell death resulting in enhanced metastasis (Furlow et al., 2015). Alternatively, endogenous PANX1 channels at the plasma membrane can also be opened by mechanical stretching during metastasis as the tumour cells become deformed after entering the microvasculature (Furlow et al., 2015).

1.2.4 Known Pannexin 1 Interactors

The first evidence that prompted the subsequent investigation into PANX1/Panx1 interactors came from Bruzzone et al. (2005) who demonstrated physical interaction between Panx1 and Panx2. Intermixing between Panx1 and Panx2 leads to reduced Panx1 channel activity but enhanced plasma membrane targeting of Panx2 (Ambrosi et al., 2010; Penuela et al., 2009). This process likely takes place during the post-translational processing stage in the ER (Penuela et al., 2009). As Panx1 and Panx2 are abundantly expressed in the brain, it is the most likely place this intermixing may take place (Swayne et al., 2010; Wicki-Stordeur and Swayne, 2013; Wicki-Stordeur et al., 2012). However, the physiological role of this interaction remains unknown. Unglycoslyated mutant Panx1 and Panx3 can also intermix in an over-expression system, but it is currently unknown if this also occurs endogenously in physiological or pathological conditions and its implication needs to be further elucided (Penuela et al., 2009).

As the major ATP release channel, the functional relationship between Panx1 and ATP-gated P2 purinergic receptors has been well-implicated in various physiological and pathological conditions (Wicki-Stordeur and Swayne, 2014).

However, Panx1 also physically interacts with P2 receptors. Out of the seven known P2X receptors, Panx1 has been shown to co-immunoprecipitate (Co-IP) with $P2X_2$, $P2X_3$, $P2X_4$, and $P2X_7$ receptors (Hung et al., 2013; Li et al., 2011b; Pelegrin and Surprenant, 2006; Silverman et al., 2009). When over-expressed in macrophages, exogenous Panx1 interacts with $P2X_7R$ to form a large pore through which the pro-inflammatory cytokine interleukin 1β (IL-1β) is released (Pelegrin and Surprenant, 2006). Moreover, activation of this pore by prolonged ATP exposure leads to intracellular activation of caspase 1 and cell death (Pelegrin and Surprenant, 2006). Notably, the formation of this large pore requires the expression of Panx1, as expression of $P2X_7R$ alone only leads to a non-selective cation channel impermeable to ATP (Locovei et al., 2007). This interaction between Panx1 and $P2X_7R$ was later found to involve the proline residue at position 451 within the SH_3 domain in the C-terminus of $P2X_7R$ (Iglesias et al., 2008). This large pore complex was later discovered to be the inflammasome, which is a multi-protein structure that regulates innate immune response to microbial infection (Rathinam and Fitzgerald, 2016). While $P2X_7R$ is a known part of the inflammasome, Panx1 has also been shown to co-immunoprecipitate with many inflammasome components, such as Nod-like receptor proteins (NLRP1, 2, and 3), Apoptosis-associated speck-like protein containing a CARD (ASC), caspase 1, caspase 11, and X-linked inhibitor of apoptosis (XIAP) (Minkiewicz et al., 2013; Silverman et al., 2009; Wang et al., 2013). However, whether these proteins interact directly with Panx1 or through other adapter proteins remains to be investigated. When activated, the inflammasome induces a form of cell death termed pyroptosis (Frank and Vince, 2019), which requires the activation of Panx1 channels by caspase 11 cleavage (Yang et al., 2015). Interestingly, it has been shown using

Panx1 knockout (KO) mouse models that Panx1 is not needed for the assembly and release of pro-inflammatory cytokines, IL-1β and IL-18, but rather is required for induction of early apoptosis and ATP release (Chen et al., 2020; Qu et al., 2011; Wang et al., 2013). These conflicting findings have been proposed to have been derived due to the different types of macrophages used for these studies, and that the functional relationship between Panx1 and $P2X_7R$ in macrophages is state- or subset-dependent (Wicki-Stordeur and Swayne, 2014). In addition to the inflammasome, the interaction between Panx1 and $P2X_7R$ is also required during ATP-induced (> 200 μM) internalization of surface Panx1 channels (Boyce et al., 2015; Boyce et al., 2017; Swayne and Boyce 2017). This interaction involves W74, the pore-lining residue of the Panx1 channel (Boyce et al., 2017). Therefore, this previously known ATP-sensing residues not only activates Panx1 channels at low ATP levels (~5 μM) but also autoinhibit Panx1 channel activities by inducing their internalization when high ATP levels are detected (Qiu and Dhal 2009; Qiu et al., 2012; Boyce et al., 2015; Boyce et al., 2017).

The C-terminus of Panx1 has been shown to interact with actin microfilaments for trafficking to and stabilization in the plasma membrane (Bhalla-Gehi et al., 2010). Using Co-IP coupled with mass spectroscopy, Panx1 has been found to interact with many cytoskeletal proteins of which actin and actin-related protein 3 (Arp3) were further shown to co-immunoprecipitate with Panx1 in N2a neuroblastoma cells (Wicki-Stordeur and Swayne, 2013). Thus, Panx1 is likely to participate in the regulation of cellular actin remodeling, which is important for filopodia and lamellipodia formation (Dimchev et al., 2017; Leijnse et al., 2015; Mattila and Lappalainen, 2008), cell

migration (Gardel et al., 2010; Hervas-Raluy et al., 2019; Inagaki and Katsuno, 2017), and neurite outgrowth (Chia et al., 2016; Miller and Suter, 2018). As the C-terminus of Panx1 is involved in channel gating, the mechanosensitive activation of Panx1 channels has been proposed to involve the interaction between their C-termini with the actin microfilament cytoskeleton (Boyce et al., 2014). While the disruption of microtubules by nocodazole does not affect stabilization of Panx1 channels at the plasma membrane (Bhalla-Gehi et al., 2010), their C-termini have recently been shown to directly interact with the collapsing response mediator protein 2 (Crimp2), which is a stabilizer of microtubules (Xu et al., 2018). In that study, Panx1 was shown to sequester Crimp2 in N2a cells leading to the destabilization of microtubules. Treatment with probenecid interrupted this interaction (Xu et al., 2018). The released Crimp2 could then facilitate tubulin polymerization and microtubule stability, which have implications in neurite outgrowth (Xu et al., 2018).

In the vascular smooth muscle cells (VSMC) of resistance arteries, Panx1 was shown to co-immunoprecipitate with α1D-adrenergic receptors (α1DR) (Billaud et al., 2011). The release of ATP from Panx1 channels after phenylephrine-mediated activation of α1DR led to vasoconstriction likely through P2YRs (Billaud et al., 2011). In a subsequent study, the Panx1-α1DR complex was shown to be concentrated in caveolae of VSMC near areas of concentrated sympathetic nerve innervation, which is supported by co-localization and co-immunoprecipitation data of Panx1 with caveolin-1 (DeLalio et al., 2018). In rodent skeletal muscle tissue, Panx1 has been found to co-immunoprecipitate with DHPR, $P2Y_2R$, and dystrophin as a multiprotein complex involved in excitation-transcription coupling, suggesting a role of Panx1 in regulating

the expression of skeletal muscle-specific genes (Arias-Calderón et al., 2016; Jorquera et al., 2013).

1.2.5 Transcriptional and Translational Regulation of Pannexin 1

Human *PANX1* is located on chromosome 11q14.3 and consists of 5 exons with 4 intervening introns which are together flanked by a putative 5' untranslated region (UTR) of at least 335 nucleotides and a 1097 nucleotide-long 3' UTR (Baranova et al., 2004; Panchina et al., 2000). Two splice variants exist for *PANX1* due to the presence of two possible splice donor/acceptor sites that define the 5' border of exon 5, which result in a difference of a 4 amino acid (GMNI) insertion 22 amino acids upstream of the C-terminus (Baranova et al., 2004). The protein products of the two variants of *PANX1* are shown to both traffic to the plasma membrane and have identical channel characteristics when ectopically expressed in HEK293T cells (Ma et al., 2009b). Rodent *Panx1* shares the same gene organization than that of human *PANX1* (Baranova et al., 2004). However, rat *Panx1* in pituitary cells is expressed as two mRNA variants due to alternative splicing in exons 2 and 4, which results in two shorter Panx1 isoforms, one lacking the region from F108 to Q180 spanning the second transmembrane domain and a part of the intracellular loop and the other lacking the region from from V307 to C426 in the C-terminus (Li et al., 2011a). Both shorter Panx1 isoforms can intermix with the full length Panx1 and act as dominant-negative effectors to modulate Panx1 channel functions (Li et al., 2011a). A similar splice variant of *Panx1* missing the sequence corresponding to the second transmembrane domain was also identified in the rat epididymis, but whether it also leads to a functional Panx1 isoform is unknown (Turmel et al., 2011).

Developmental and Pathological Changes of Pannexin 1 Expression

Little is known about the underlying mechanism involved in the regulation of PANX1 expression, but there have been numerous reports of both human *PANX1* and rodent *Panx1*, as well as their encoding protein products, being dynamically expressed during development or under pathological states (Boyce et al., 2018; Jiang and Penuela, 2016; Penuela et al., 2014b; Schalper et al., 2014). These studies strongly suggest the notion that *PANX1* (or *Panx1*) is under tissue- or state-dependent transcriptional or translational control (Boyce et al., 2018).

In addition to being up-regulated during murine skeletal muscle development and human skeletal muscle myogenic differentiation described in the previous section (Langlois et al., 2014; Pham et al., 2018), Panx1 levels in primary adipose-derived stromal cells also become increased upon induction into an adipogenic lineage (Lee et al., 2018). On the contrary, rat *Panx1* in brain tissue is highly expressed between embryonic day 20.5 (E20.5) and post-natal day 3 (P3) but starts to gradually decease on P7 becoming undetectable by P72 (Vogt et al., 2005). Similarly, the expression of mouse *Panx1* in the brain and eye peaks on E18 but dramatically decreases upon birth, and continues to reduce into adulthood (Ray et al., 2005). In a recent study, *Panx1* has been shown to be expressed in the afferent ganglia of the cranial nerves and spinal cord as early as E9.5 and becomes transiently increased on E11.5 before returning to a lower level (Raslan et al., 2016). In developing murine skin, Panx1 expression is high upon birth but decreases during aging (Celetti et al., 2010). Moreover, Panx1 levels are also down-regulated during differentiation of ventricular zone-derived neurites and neural crest-like cells (Wicki-Stordeur et al., 2016).

Besides being perturbed during carcinogenesis (Jiang and Penuela, 2016; Penuela et al., 2014b; Schalper et al., 2014), Panx1 levels are also regulated in response to a variety of pathological conditions. For instance, in a rat stroke model *Panx1* mRNA levels become elevated after middle cerebral artery occlusion-induced cerebral infarction over 14 days with a peak on day 7 (Jiang et al., 2012). Sleep deprivation leads to induction of *Panx1* in the mouse cortex and is attributed to the diminished availability of glycogen in the brain, which has implications in migraine formation (Kilic et al., 2018; Kovalzon et al., 2016). Panx1 levels in rat epididymis increase after orchiectomy and can be suppressed by maintenance of exogeneous testosterone, suggesting epididymal Panx1 expression is susceptible to androgen-suppression (Dufresne and Cyr, 2014; Turmel et al., 2011).

Epigenetic, Transcriptional, and Translational Regulation of Pannexin 1

Some pathological conditions have been shown to affect Panx1 levels through epigenetic modifications. *Panx1* mRNA and protein levels in the rat dorsal root ganglion are both increased subsequent to nerve injury by spinal nerve ligation (Zhang et al., 2015). This is caused by the enrichment of H3K4me3 and H3K9ac activating and reduced binding of H3K9me2 and H3k27me3 repressing histone modifications around the transcription start site (TSS) in the *Panx1* promoter (Zhang et al., 2015). Parental vitamin D-depletion in rats induces hypermethylation of the *Panx1* promoter in the kidney tissue of the offspring leading to reduced transcript levels, which is speculated to play a role in vitamin-D induced susceptibility to hypertension (Meems et al., 2016).

A recent sequence alignment study confirmed that the *Panx1* promoter is evolutionarily conserved and is rich in CpG islands, which are sensitive to treatment by the demethylating reagent 5-azacytidine (Dufresne and Cyr, 2014). Moreover, Dufresne and Cyr have also found, through *in silico* sequence prediction, that the rat epididymal *Panx1* promoter has consensus elements for transcription factors (TF), cAMP response element-binding protein (CREB), ETS variant transcription factor 4 (ETV4), IL-6 receptor binding protein (IL-6RE-BP), and Helix-loop-helix protein 1 (NHLH1) near the TSS (Dufresne and Cyr, 2014). CREB and ETV4 are further shown to bind to their respective consensus sites in the *Panx1* promoter to induce Panx1 expression (Dufresne and Cyr, 2014). The authors have also demonstrated that the Panx1 increase in the epididymal tissue of orchidectomized rats is due to enriched binding of CREB and ETV4 to the *Panx1* promoter (Dufresne and Cyr, 2014). A recent study aimed at deciphering the role of PANX1 channels in inflammation has revealed a mechanism of *PANX1* mRNA and protein up-regulation by tumour necrosis factor α (TNFα) mediated activation of nuclear factor kappa-light-chain-enhancer of activated B cells (NF-κB) pathway via phosphorylation of NF-kB–p65 protein (Yang et al., 2020). Interestingly, up-regulation of PANX1 channels in the plasma membrane can lead to increase in intracellular Ca^{2+} concentration and further phosphorylation of NF-kB–p65 resulting in a feedforward loop to amplify IL-6 release during inflammation (Sanchez Arias et al., 2020; Yang et al., 2020).

Several studies have shown the presence of various *Panx1* transcripts with different 5’ UTR lengths (Vanden Abeele et al., 2006; Dufresne and Cyr, 2014; Kwon et al., 2014; Li et al., 2011a), which not only indicate multiple TSS but also suggest

possible translational regulation of *Panx1* by upstream open reading frames (uORFs) (Araujo et al., 2012; Barbosa et al., 2013; Chen and Tarn, 2019; Lin et al., 2019). However, there are currently no reports on *Panx1* translational control mechanisms.

1.3 RATIONALE AND HYPOTHESIS

Despite the past few decades of intensive research efforts, the overall cure rate for metastatic and recurrent RMS remains dismal, and the current therapies have reached their efficacy plateau. As RMS are widely thought to arise from skeletal muscle progenitors, inducing their cellular differentiation into a normal skeletal muscle phenotype, known as the differentiation therapy, has been proposed as a novel therapeutic strategy. Interestingly, we have reported that PANX1 levels are low in undifferentiated human primary skeletal muscle cells but are rapidly up-regulated upon myogenic differentiation to promote this process. Thus, I hypothesized that:

(1) **PANX1 levels are down-regulated in human RMS specimens and patient-derived RMS cell lines, and that re-introduction of PANX1 in RMS will alleviate their malignant properties.**

(2) **PANX1-mediated signal transduction suppresses RMS progression.**

(3) **Down-regulation of PANX1 expression in RMS results from a deregulation at the transcriptional and/or translational levels.**

1.4 OBJECTIVES

1. To assess the levels of *PANX1* mRNA and protein in human eRMS and aRMS tumour specimens and patient-derived cell lines, compared to skeletal muscle cells and tissue, and determine the effect of PANX1 re-introduction on the malignant properties of Rh18 (eRMS) and Rh30 (aRMS) cell lines *in vitro* and *in vivo*.

   The above objective will determine whether PANX1 is dysregulated in RMS and can be a potential therapeutic target for RMS.

2. Identify the mechanism of PANX1-induced RMS suppression by assessing its channel function and protein-protein interactions.

   This objective will further enhance our current understanding of PANX1 function in cancer.

3. Determine the mechanism of transcriptional and/or translational regulation of *PANX1* in the context of RMS by assessing its transcript integrity, promoter, and 5' leader sequence.

   Results from this objective will contribute to the current limited knowledge on *PANX1* expression regulation under pathological conditions.

1.5 REFERENCES

Vanden Abeele, F., Bidaux, G., Gordienko, D., Beck, B., Panchin, Y. V., Baranova, A. V., Ivanov, D. V., Skryma, R., and Prevarskaya, N. (2006). Functional implications of calcium permeability of the channel formed by pannexin 1. J. Cell Biol. *174*, 535–546.

Alaggio, R., Zhang, L., Sung, Y.S., Huang, S.C., Chen, C.L., Bisogno, G., Zin, A., Agaram, N.P., LaQuaglia, M.P., Wexler, L.H., et al. (2016). A molecular study of pediatric spindle and sclerosing rhabdomyosarcoma identification of novel and recurrent VGLL2-related fusions in infantile cases. Am. J. Surg. Pathol. *40*, 224–235.

Ambrosi, C., Gassmann, O., Pranskevich, J.N., Boassa, D., Smock, A., Wang, J., Dahl, G., Steinem, C., and Sosinsky, G.E. (2010). Pannexin1 and pannexin2 channels show quaternary similarities to connexons and different oligomerization numbers from each other. J. Biol. Chem. *285*, 24420–24431.

Aquilino, M.S., Whyte-Fagundes, P., Zoidl, G., and Carlen, P.L. (2019). Pannexin-1 channels in epilepsy. Neurosci. Lett. *695*, 71–75.

Aquilino, M.S., Whyte-fagundes, P., Lukewich, M.K., Zhang, L., Bardakjian, B.L., Zoidl, G.R., and Carlen, P.L. (2020). Pannexin-1 deficiency decreases epileptic activity in mice. Int. J. Mol. Sci. *21*, 1–14.

Araujo, P.R., Yoon, K., Ko, D., Smith, A.D., Qiao, M., Suresh, U., Burns, S.C., and Penalva, L.O.F. (2012). Before It Gets Started: Regulating Translation at the 5’ UTR. Comp. Funct. Genomics *2012*, 475731.

Arias-Calderón, M., Almarza, G., Díaz-Vegas, A., Contreras-Ferrat, A., Valladares, D., Casas, M., Toledo, H., Jaimovich, E., and Buvinic, S. (2016). Characterization of a multiprotein complex involved in excitation-transcription coupling of skeletal muscle. Skelet. Muscle *6*, 15.

Bao, B.A., Lai, C.P., Naus, C.C., and Morgan, J.R. (2012). Pannexin1 drives multicellular aggregate compaction via a signaling cascade that remodels the actin cytoskeleton. J. Biol. Chem. *287*, 8407–8416.

Bao, L., Locovei, S., and Dahl, G. (2004). Pannexin membrane channels are

mechanosensitive conduits for ATP. FEBS Lett. *572*, 65–68.

Baranova, A., Ivanov, D., Petrash, N., Pestova, A., Skoblov, M., Kelmanson, I., Shagin, D., Nazarenko, S., Geraymovych, E., Litvin, O., et al. (2004). The mammalian pannexin family is homologous to the invertebrate innexin gap junction proteins. Genomics *83*, 706–716.

Barbosa, C., Peixeiro, I., and Romão, L. (2013). Gene Expression Regulation by Upstream Open Reading Frames and Human Disease. PLoS Genet. *9*, 1–12.

Bargiotas, P., Krenz, A., Hormuzdi, S.G., Ridder, D.A., Herb, A., Barakat, W., Penuela, S., von Engelhardt, J., Monyer, H., and Schwaninger, M. (2011). Pannexins in ischemia-induced neurodegeneration. Proc. Natl. Acad. Sci. U. S. A. *108*, 20772–20777.

Bargiotas, P., Krenz, A., Monyer, H., and Schwaninger, M. (2012). Functional outcome of pannexin-deficient mice after cerebral ischemia. Channels *6*, 453–456.

Barr, F.G., Smith, L.M., Lynch, J.C., Strzelecki, D., Parham, D.M., Qualman, S.J., and Breitfeld, P.P. (2006). Examination of Gene Fusion Status in Archival Samples of Alveolar Rhabdomyosarcoma Entered on the Intergroup Rhabdomyosarcoma Study-III Trial. J. Mol. Diagnostics *8*, 202–208.

Begandt, D., Good, M.E., Keller, A.S., DeLalio, L.J., Rowley, C., Isakson, B.E., and Figueroa, X.F. (2017). Pannexin channel and connexin hemichannel expression in vascular function and inflammation. BMC Cell Biol. *18*, 2.

Bentzinger, C.F., Wang, Y.X., and Rudnicki, M.A. (2012). Building Muscle: Molecular Regulation of Myogenesis. Cold Spring Harb. Perspect. Biol. *4*, a008342–a008342.

Bhalla-Gehi, R., Penuela, S., Churko, J.M., Shao, Q., and Laird, D.W. (2010). Pannexin1 and pannexin3 delivery, cell surface dynamics, and cytoskeletal interactions. J. Biol. Chem. *285*, 9147–9160.

Billaud, M., Lohman, A.W., Straub, A.C., Looft-Wilson, R., Johnstone, S.R., Araj, C.A., Best, A.K., Chekeni, F.B., Ravichandran, K.S., Penuela, S., et al. (2011). Pannexin1 Regulates α1-Adrenergic Receptor-Mediated Vasoconstriction. Circ. Res. *109*, 80–85.

Bisogno, G., De Salvo, G.L., Bergeron, C., Gallego Melcón, S., Merks, J.H., Kelsey, A.,

Martelli, H., Minard-Colin, V., Orbach, D., Glosli, H., et al. (2019). Vinorelbine and continuous low-dose cyclophosphamide as maintenance chemotherapy in patients with high-risk rhabdomyosarcoma (RMS 2005): a multicentre, open-label, randomised, phase 3 trial. Lancet Oncol. *20*, 1566–1575.

Boassa, D., Ambrosi, C., Qiu, F., Dahl, G., Gaietta, G., and Sosinsky, G. (2007). Pannexin1 channels contain a glycosylation site that targets the hexamer to the plasma membrane. J. Biol. Chem. *282*, 31733–31743.

Bond, S.R., and Naus, C.C. (2014). The pannexins: past and present. Front. Physiol. *5*, 58.

Boyce, A.K.J., Wicki-Stordeur, L.E., and Swayne, L.A. (2014). Powerful partnership: crosstalk between pannexin 1 and the cytoskeleton. Front. Physiol. *5*, 27.

Boyce, A.K.J., Epp, A.L., Nagarajan, A., and Swayne, L.A. (2018). Transcriptional and post-translational regulation of pannexins. Biochim. Biophys. Acta - Biomembr. *1860*, 72–82.

Bruzzone, R., Hormuzdi, S.G., Barbe, M.T., Herb, A., and Monyer, H. (2003). Pannexins, a family of gap junction proteins expressed in brain. Proc. Natl. Acad. Sci. U. S. A. *100*, 13644–13649.

Bruzzone, R., Barbe, M.T., Jakob, N.J., and Monyer, H. (2005). Pharmacological properties of homomeric and heteromeric pannexin hemichannels expressed in Xenopus oocytes. J. Neurochem. *92*, 1033–1043.

Bunse, S., Schmidt, M., Hoffmann, S., Engelhardt, K., Zoidl, G., and Dermietzel, R. (2011). Single cysteines in the extracellular and transmembrane regions modulate Pannexin 1 channel function. J. Membr. Biol. *244*, 21–33.

Burattini, S., Ferri, R., Battistelli, M., Curci, R., Luchetti, F., and Falcieri, E. (2004). C2C12 murine myoblasts as a model of skeletal muscle development: Morpho-functional characterization. Eur. J. Histochem. *48*, 223–233.

Burnstock, G. (2006). Purinergic signalling. Br. J. Pharmacol. *147 Suppl*, S172-81.

Buvinic, S., Almarza, G., Bustamante, M., Casas, M., López, J., Riquelme, M., Sáez, J.C., Huidobro-Toro, J.P., and Jaimovich, E. (2009). ATP released by electrical stimuli elicits

calcium transients and gene expression in skeletal muscle. J. Biol. Chem. *284*, 34490–34505.

Canadian Cancer Statistics Advisory Committee (2019). Canadian Cancer Statistics (Toronto, NO.).

Carvalho, S.D., Pissaloux, D., Crombé, A., Coindre, J.M., and Le Loarer, F. (2019). Pleomorphic Sarcomas: The State of the Art. Surg. Pathol. Clin. *12*, 63–105.

Cavazzana, A.O., Schmidt, D., Ninfo, V., Harms, D., Tollot, M., Carli, M., Treuner, J., Betto, R., and Salviati, G. (1992). Spindle Cell Rhabdomyosarcoma. Am. J. Surg. Pathol. *16*, 229–235.

Cea, L. a, Riquelme, M. a, Cisterna, B. a, Puebla, C., Vega, J.L., Rovegno, M., and Sáez, J.C. (2012). Connexin- and pannexin-based channels in normal skeletal muscles and their possible role in muscle atrophy. J. Membr. Biol. *245*, 423–436.

Celetti, S.J., Cowan, K.N., Penuela, S., Shao, Q., Churko, J., and Laird, D.W. (2010). Implications of pannexin 1 and pannexin 3 for keratinocyte differentiation. J. Cell Sci. *123*, 1363–1372.

Chal, J., and Pourquié, O. (2017). Making muscle: Skeletal myogenesis in vivo and in vitro. Dev. *144*, 2104–2122.

Charytonowicz, E., Cordon-Cardo, C., Matushansky, I., and Ziman, M. (2009). Alveolar rhabdomyosarcoma: Is the cell of origin a mesenchymal stem cell? Cancer Lett. *279*, 126–136.

Chekeni, F.B., Elliott, M.R., Sandilos, J.K., Walk, S.F., Kinchen, J.M., Lazarowski, E.R., Armstrong, A.J., Penuela, S., Laird, D.W., Salvesen, G.S., et al. (2010). Pannexin 1 channels mediate 'find-me' signal release and membrane permeability during apoptosis. Nature *467*, 863–867.

Chen, H.-H., and Tarn, W.-Y. (2019). uORF-mediated translational control: recently elucidated mechanisms and implications in cancer. RNA Biol. *16*, 1327–1338.

Chen, C., Dorado Garcia, H., Scheer, M., and Henssen, A.G. (2019). Current and Future Treatment Strategies for Rhabdomyosarcoma. Front. Oncol. *9*, 1–18.

Chen, K.W., Demarco, B., and Broz, P. (2020). Pannexin-1 promotes NLRP3 activation during apoptosis but is dispensable for canonical or noncanonical inflammasome activation. Eur. J. Immunol. *50*, 170–177.

Chia, J.X., Efimova, N., and Svitkina, T.M. (2016). Neurite outgrowth is driven by actin polymerization even in the presence of actin polymerization inhibitors. Mol. Biol. Cell *27*, 3695–3704.

Cowan, K.N., Langlois, S., Penuela, S., Cowan, B.J., and Laird, D.W. (2012). Pannexin1 and Pannexin3 exhibit distinct localization patterns in human skin appendages and are regulated during keratinocyte differentiation and carcinogenesis. Cell Commun. Adhes. *19*, 45–53.

Crist, W., Gehan, E.A., Ragab, A.H., Dickman, P.S., Donaldson, S.S., Fryer, C., Hammond, D., Hays, D.M., Herrmann, J., Heyn, R., et al. (1995). The Third Intergroup Rhabdomyosarcoma Study. J. Clin. Oncol. *13*, 610–630.

Crucis, A., Richer, W., Brugières, L., Bergeron, C., Marie-Cardine, A., Stephan, J.L., Girard, P., Corradini, N., Munzer, M., Lacour, B., et al. (2015). Rhabdomyosarcomas in children with neurofibromatosis type I: A national historical cohort. Pediatr. Blood Cancer *62*, 1733–1738.

Dagher, R., and Helman, L. (1999). Rhabdomyosarcoma : An Overview. Oncologist *4*, 34–44.

Dahl, G. (2018). The Pannexin1 membrane channel: distinct conformations and functions. FEBS Lett. *592*, 3201–3209.

Darwish, C., Shim, T., Sparks, A.D., Chillakuru, Y., Strum, D., Benito, D.A., and Monfared, A. (2020). Pediatric Head and Neck Rhabdomyosarcoma: An Analysis of Treatment and Survival in the United States (1975-2016). Int. J. Pediatr. Otorhinolaryngol. *139*, 110403.

Dasgupta, R., Fuchs, J., and Rodeberg, D. (2016). Rhabdomyosarcoma. Semin. Pediatr. Surg. *25*, 276–283.

Davidson, J.S., Baumgarten, I.M., and Harley, E.H. (1986). Reversible inhibition of intercellular junctional communication by glycyrrhetinic acid. Biochem. Biophys. Res. Commun. *134*, 29–36.

DeBaun, M.R., and Tucker, M.A. (1998). Risk of cancer during the first four years of life in children with The Beckwith-Wiedemann Syndrome Registry. J. Pediatr. *132*, 398–400.

Dehner, L.P., Jarzembowski, J.A., and Hill, D.A. (2012). Embryonal rhabdomyosarcoma of the uterine cervix: A report of 14 cases and a discussion of its unusual clinicopathological associations. Mod. Pathol. *25*, 602–614.

DeLalio, L.J., Keller, A.S., Chen, J., Boyce, A.K.J., Artamonov, M. V., Askew-Page, H.R., Stevenson Keller, T.C., Johnstone, S.R., Weaver, R.B., Good, M.E., et al. (2018). Interaction between pannexin 1 and caveolin-1 in smooth muscle can regulate blood pressure. Arterioscler. Thromb. Vasc. Biol. *38*, 2065–2078.

DeLalio, L.J., Billaud, M., Ruddiman, C.A., Johnstone, S.R., Butcher, J.T., Wolpe, A.G., Jin, X., Keller, T.C.C.S.S.C.S., Keller, A.S., Rivière, T., et al. (2019). Constitutive SRC-mediated phosphorylation of pannexin 1 at tyrosine 198 occurs at the plasma membrane. J. Biol. Chem. *294*, 6940–6956.

Deng, Z., He, Z., Maksaev, G., Bitter, R.M., Rau, M., Fitzpatrick, J.A.J., and Yuan, P. (2020). Cryo-EM structures of the ATP release channel pannexin 1. Nat. Struct. Mol. Biol. *27*, 373–381.

Diller, L., Sexsmith, E., Gottlieb, A., Li, F.P., and Malkin, D. (1995). Germline p53 mutations are frequently detected in young children with rhabdomyosarcoma. J. Clin. Invest. *95*, 1606–1611.

Dimchev, G., Steffen, A., Kage, F., Dimchev, V., Pernier, J., Carlier, M.-F., and Rottner, K. (2017). Efficiency of lamellipodia protrusion is determined by the extent of cytosolic actin assembly. Mol. Biol. Cell *28*, 1311–1325.

Dolmatova, E., Spagnol, G., Boassa, D., Baum, J.R., Keith, K., Ambrosi, C., Kontaridis, M.I., Sorgen, P.L., Sosinsky, G.E., and Duffy, H.S. (2012). Cardiomyocyte ATP release through pannexin 1 aids in early fibroblast activation. Am. J. Physiol. Heart Circ. Physiol. *303*, H1208-18.

Doros, L., Yang, J., Dehner, L., Rossi, C.T., Skiver, K., Jarzembowski, J.A., Messinger, Y., Schultz, K.A., Williams, G., André, N., et al. (2012). DICER1 Mutations in embryonal

rhabdomyosarcomas from children with and without familial PPB-tumor predisposition syndrome. Pediatr. Blood Cancer *59*, 558–560.

Dossi, E., Blauwblomme, T., Moulard, J., Chever, O., Vasile, F., Guinard, E., Le Bert, M., Couillin, I., Pallud, J., Capelle, L., et al. (2018). Pannexin-1 channels contribute to seizure generation in human epileptic brain tissue and in a mouse model of epilepsy. Sci. Transl. Med. *10*, 1–14.

Dufresne, J., and Cyr, D.G. (2014). Regulation of the Pannexin-1 Promoter in the Rat Epididymis. Biol. Reprod. *91*, 143–143.

Dziuba, I., Kurzawa, P., Dopierała, M., Larque, A.B., and Januszkiewicz-Lewandowska, D. (2018). Rhabdomyosarcoma in children – Current pathologic and molecular classification. Polish J. Pathol. *69*, 20–32.

Egas-Bejar, D., and Huh, W.W. (2014). Rhabdomyosarcoma in adolescent and young adult patients: current perspectives. Adolesc. Health. Med. Ther. *5*, 115–125.

Ferrari, A., Bisogno, G., Macaluso, A., Casanova, M., D'Angelo, P., Pierani, P., Zanetti, I., Alaggio, R., Cecchetto, G., and Carli, M. (2007). Soft-tissue sarcomas in children and adolescents with neurofibromatosis type 1. Cancer *109*, 1406–1412.

Fletcher, C.D.M., Hogendoorn, P., Mertens, F., and Bridge, J. (2013). WHO Classification of Tumours of Soft Tissue and Bone (Lyon, France: IARC Press).

Frank, D., and Vince, J.E. (2019). Pyroptosis versus necroptosis: similarities, differences, and crosstalk. Cell Death Differ. *26*, 99–114.

Fredericks, W.J., Galili, N., Mukhopadhyay, S., Rovera, G., Bennicelli, J., Barr, F.G., and Rauscher, F.J. (1995). The PAX3-FKHR fusion protein created by the t(2;13) translocation in alveolar rhabdomyosarcomas is a more potent transcriptional activator than PAX3. Mol. Cell. Biol. *15*, 1522–1535.

Freeman, T.J., Sayedyahossein, S., Johnston, D., Sanchez-Pupo, R.E., O'Donnell, B., Huang, K., Lakhani, Z., Nouri-Nejad, D., Barr, K.J., Harland, L., et al. (2019). Inhibition of pannexin 1 reduces the tumorigenic properties of human melanoma cells. Cancers (Basel). *11*, 1–24.

Furlong, M.A., Mentzel, T., and Fanburg-Smith, J.C. (2001). Pleomorphic rhabdomyosarcoma in adults: A clinicopathologic study of 38 cases with emphasis on morphologic variants and recent skeletal muscle-specific markers. Mod. Pathol. *14*, 595–603.

Furlow, P.W., Zhang, S., Soong, T.D., Halberg, N., Goodarzi, H., Mangrum, C., Wu, Y.G., Elemento, O., and Tavazoie, S.F. (2015). Mechanosensitive pannexin-1 channels mediate microvascular metastatic cell survival. Nat. Cell Biol. *7*, 943–952.

Gardel, M.L., Schneider, I.C., Aratyn-Schaus, Y., and Waterman, C.M. (2010). Mechanical Integration of Actin and Adhesion Dynamics in Cell Migration. Annu. Rev. Cell Dev. Biol. *26*, 315–333.

De Giovanni, C., Landuzzi, L., Nicoletti, G., Lollini, P.L., and Nanni, P. (2009). Molecular and cellular biology of rhabdomyosarcoma. Futur. Oncol *5*, 1449–1475.

Hainer, B.L., Matheson, E., and Travis Wilkes, R. (2014). Diagnosis, treatment, and prevention of gout. Am. Fam. Physician *90*, 831–836.

Hervas-Raluy, S., Garcia-Aznar, J.M., and Gomez-Benito, M.J. (2019). Modelling actin polymerization: the effect on confined cell migration. Biomech. Model. Mechanobiol. *18*, 1177–1187.

Hettmer, S., and Wagers, A.J. (2010). Muscling in: Uncovering the origins of rhabdomyosarcoma. Nat. Med. *16*, 171–173.

Hettmer, S., Li, Z., Billin, A.N., Barr, F.G., Cornelison, D.D.W., Ehrlich, A.R., Guttridge, D.C., Hayes-Jordan, A., Helman, L.J., Houghton, P.J., et al. (2014). Rhabdomyosarcoma: Current Challenges and Their Implications for Developing Therapies. Cold Spring Harb. Perspect. Med. *4*, a025650.

Hoang, N.T., Acevedo, L.A., Mann, M.J., and Tolani, B. (2018). A review of soft-tissue sarcomas: Translation of biological advances into treatment measures. Cancer Manag. Res. *10*, 1089–1114.

Hung, S.-C., Choi, C.H., Said-Sadier, N., Johnson, L., Atanasova, K.R., Sellami, H., Yilmaz, Ö., and Ojcius, D.M. (2013). P2X4 Assembles with P2X7 and Pannexin-1 in Gingival Epithelial Cells and Modulates ATP-induced Reactive Oxygen Species Production and

Inflammasome Activation. PLoS One *8*, e70210.

Iglesias, R., Locovei, S., Roque, a, Alberto, a P., Dahl, G., Spray, D.C., and Scemes, E. (2008). P2X7 receptor-Pannexin1 complex: pharmacology and signaling. Am. J. Physiol. Cell Physiol. *295*, C752-60.

Inagaki, N., and Katsuno, H. (2017). Actin Waves: Origin of Cell Polarization and Migration? Trends Cell Biol. *27*, 515–526.

Jiang, J.X., and Penuela, S. (2016). Connexin and pannexin channels in cancer. BMC Cell Biol. *17*, 12.

Jiang, T., Xu, R.X., Zhang, A.W., Di, W., Xiao, Z.J., Miao, J.Y., Luo, N., and Fang, Y.N. (2012). Effects of transcranial direct current stimulation on hemichannel pannexin-1 and neural plasticity in rat model of cerebral infarction. Neuroscience *226*, 421–426.

Jin, Q., Zhang, B., Zheng, X., Li, N., Xu, L., Xie, Y., Song, F., Bhat, E.A., Chen, Y., Gao, N., et al. (2020). Cryo-EM structures of human pannexin 1 channel. Cell Res. *30*, 449–451.

Jorquera, G., Altamirano, F., Contreras-Ferrat, A., Almarza, G., Buvinic, S., Jacquemond, V., Jaimovich, E., and Casas, M. (2013). Cav1.1 controls frequency-dependent events regulating adult skeletal muscle plasticity. J. Cell Sci. *126*, 1189–1198.

Keller, C., and Capecchi, M.R. (2005). New genetic tactics to model alveolar rhabdomyosarcoma in the mouse. Cancer Res. *65*, 7530–7532.

Keller, C., and Guttridge, D.C. (2013). Mechanisms of impaired differentiation in rhabdomyosarcoma. FEBS J. *280*, 4323–4334.

Kilic, K., Karatas, H., Dönmez-Demir, B., Eren-Kocak, E., Gursoy-Ozdemir, Y., Can, A., Petit, J.M., Magistretti, P.J., and Dalkara, T. (2018). Inadequate brain glycogen or sleep increases spreading depression susceptibility. Ann. Neurol. *83*, 61–73.

Kovalzon, V.M., Moiseenko, L.S., Ambaryan, A. V, Kurtenbach, S., Shestopalov, V.I., and Panchin, Y. V (2016). Sleep-wakefulness cycle and behavior in pannexin1 knockout mice. Behav. Brain Res. *318*, 24–27.

Kratz, C.P., Rapisuwon, S., Reed, H., Hasle, H., and Rosenberg, P.S. (2011). Cancer in

Noonan, Costello, cardiofaciocutaneous and LEOPARD syndromes. Am. J. Med. Genet. Part C Semin. Med. Genet. *157*, 83–89.

Krick, S., Wang, J., St-Pierre, M., Gonzalez, C., Dahl, G., and Salathe, M. (2016). Dual Oxidase 2 (Duox2) Regulates Pannexin 1-mediated ATP Release in Primary Human Airway Epithelial Cells via Changes in Intracellular pH and Not H 2 O 2 Production. J. Biol. Chem. *291*, 6423–6432.

Kwon, T.-J., Kim, D.-B., Bae, J.W., Sagong, B., Choi, S.-Y., Cho, H.-J., Kim, U.-K., and Lee, K.-Y. (2014). Molecular cloning, characterization, and expression of pannexin genes in chicken. Poult. Sci. *93*, 2253–2261.

Lai, C.P.K., Bechberger, J.F., Thompson, R.J., MacVicar, B.A., Bruzzone, R., and Naus, C.C. (2007). Tumor-suppressive effects of pannexin 1 in C6 glioma cells. Cancer Res. *67*, 1545–1554.

Langenau, D.M., Keefe, M.D., Storer, N.Y., Guyon, J.R., Kutok, J.L., Le, X., Goessling, W., Neuberg, D.S., Kunkel, L.M., and Zon, L.I. (2007). Effects of RAS on the genesis of embryonal rhabdomyosarcoma. Genes Dev. *21*, 1382–1395.

Langlois, S., Xiang, X., Young, K., Cowan, B.J., Penuela, S., and Cowan, K.N. (2014). Pannexin 1 and pannexin 3 channels regulate skeletal muscle myoblast proliferation and differentiation. J. Biol. Chem. *289*, 30717–30731.

Largo, C., Alvarez, S., Saez, B., Blesa, D., Martin-Subero, J.I., González-García, I., Brieva, J.A., Dopazo, J., Siebert, R., Calasanz, M.J., et al. (2006). Identification of overexpressed genes in frequently gained/amplified chromosome regions in multiple myeloma. Haematologica *91*, 184–191.

Lav, R., Heera, R., and Cherian, L.M. (2015). Decoding the ‘embryonic’ nature of embryonal rhabdomyosarcoma. J. Dev. Orig. Health Dis. 1–6.

Lee, V., Barr, K., Kelly, J., Johnston, D., Brown, C., Robb, K., Gros, R., Flynn, L., and Penuela, S. (2018). Pannexin 1 regulates adipose stromal cell differentiation and fat accumulation. Sci. Rep. 1–14.

Leijnse, N., Oddershede, L.B., and Bendix, P.M. (2015). An updated look at actin dynamics

in filopodia. Cytoskeleton *72*, 71–79.

Leiner, J., and Le Loarer, F. (2020). The current landscape of rhabdomyosarcomas: an update. Virchows Arch. *476*, 97–108.

Leuschner, I., Newton, W.A., Schmidt, D., Sachs, N., Asmar, L., Hamoudi, A., Harms, D., and Maurer, H.M. (1993). Spindle Cell Variants of Embryonal Rhabdomyosarcoma in the Paratesticular Region. Am. J. Surg. Pathol. *17*, 221–230.

Li, A., Leung, C.T., Peterson-Yantorno, K., Stamer, W.D., Mitchell, C.H., and Civan, M.M. (2012). Mechanisms of ATP release by human trabecular meshwork cells, the enabling step in purinergic regulation of aqueous humor outflow. J. Cell. Physiol. *227*, 172–182.

Li, S., Tomić, M., and Stojilkovic, S.S. (2011a). Characterization of novel Pannexin 1 isoforms from rat pituitary cells and their association with ATP-gated P2X channels. Gen. Comp. Endocrinol. *174*, 202–210.

Li, S., Bjelobaba, I., Yan, Z., Kucka, M., Tomić, M., and Stojilkovic, S.S. (2011b). Expression and roles of pannexins in ATP release in the pituitary gland. Endocrinology *152*, 2342–2352.

Lin, Y., May, G.E., Kready, H., Nazzaro, L., Mao, M., Spealman, P., Creeger, Y., and McManus, C.J. (2019). Impacts of uORF codon identity and position on translation regulation. Nucleic Acids Res. *47*, 9358–9367.

Linardic, C., Downie, D., and Qualman, S. (2005). Genetic modeling of human rhabdomyosarcoma. Cancer Res. 4490–4495.

Litvin, O. (2006). What is hidden in the pannexin treasure trove: the sneak peek and the guesswork. J. Cell. Mol. Med. *10*.

Liu, H., Yuan, M., Yao, Y., Wu, D., Dong, S., and Tong, X. (2019). In vitro effect of Pannexin 1 channel on the invasion and migration of I-10 testicular cancer cells via ERK1/2 signaling pathway. Biomed. Pharmacother. *117*, 109090.

Locovei, S., Bao, L., and Dahl, G. (2006a). Pannexin 1 in erythrocytes: function without a gap. Proc. Natl. Acad. Sci. U. S. A. *103*, 7655–7659.

Locovei, S., Wang, J., and Dahl, G. (2006b). Activation of pannexin 1 channels by ATP through P2Y receptors and by cytoplasmic calcium. FEBS Lett. *580*, 239–244.

Locovei, S., Scemes, E., Qiu, F., Spray, D.C., and Dahl, G. (2007). Pannexin1 is part of the pore forming unit of the P2X7 receptor death complex. FEBS Lett. *581*, 483–488.

Lohman, A.W., Weaver, J.L., Billaud, M., Sandilos, J.K., Griffiths, R., Straub, A.C., Penuela, S., Leitinger, N., Laird, D.W., Bayliss, D.A., et al. (2012). S-Nitrosylation Inhibits Pannexin 1 Channel Function. J. Biol. Chem. *287*, 39602–39612.

Lohman, A.W., Leskov, I.L., Butcher, J.T., Johnstone, S.R., Stokes, T.A., Begandt, D., DeLalio, L.J., Best, A.K., Penuela, S., Leitinger, N., et al. (2015). Pannexin 1 channels regulate leukocyte emigration through the venous endothelium during acute inflammation. Nat. Commun. *6*, 7965.

Ludolph, D.C., and Konieczny, S.F. (1995). Transcription factor families: muscling in on the myogenic program. FASEB J. *9*, 1595–1604.

Ma, W., Hui, H., Pelegrin, P., and Surprenant, A. (2009a). Pharmacological characterization of pannexin-1 currents expressed in mammalian cells. J. Pharmacol. Exp. Ther. *328*, 409–418.

Ma, W., Hui, H., Hui, H., Pelegrin, P., Pelegrin, P., Surprenant, A., and Surprenant, A. (2009b). Pharmacological Characterization of Pannexin-1 Currents. Pharmacology *5*.

Ma, W., Compan, V., Zheng, W., Martin, E., North, R.A., Verkhratsky, A., and Surprenant, A. (2012). Pannexin 1 forms an anion-selective channel. Pflugers Arch. Eur. J. Physiol. *463*, 585–592.

Malempati, S., and Hawkins, D.S. (2012). Rhabdomyosarcoma: Review of the Children's Oncology Group (COG) soft-tissue Sarcoma committee experience and rationale for current COG studies. Pediatr. Blood Cancer *59*, 5–10.

Marchal, J.A., Prados, J., Melguizo, C., Fernández, J.E., Vélez, C., Alvarez, L., and Aránega, A. (1997). Actinomycin D treatment leads to differentiation and inhibits proliferation in rhabdomyosarcoma cells. J. Lab. Clin. Med. *130*, 42–50.

Mattila, P.K., and Lappalainen, P. (2008). Filopodia: molecular architecture and cellular functions. Nat. Rev. Mol. Cell Biol. *9*, 446–454.

Maurer, H.M., Gehan, E.A., Beltangady, M., Crist, W., Dickman, P.S., Donaldson, S.S., Fryer, C., Hammond, D., Hays, D.M., Herrmann, J., et al. (1993). The intergroup rhabdomyosarcoma study-II. Cancer *71*, 1904–1922.

Medina, C.B., Mehrotra, P., Arandjelovic, S., Perry, J.S.A., Guo, Y., Morioka, S., Barron, B., Walk, S.F., Ghesquière, B., Krupnick, A.S., et al. (2020). Metabolites released from apoptotic cells act as tissue messengers. Nature *580*, 130–135.

Meems, L.M.G., Mahmud, H., Buikema, H., Tost, J., Michel, S., Takens, J., Verkaik-Schakel, R.N., Vreeswijk-Baudoin, I., Mateo-Leach, I. V., Plosch, T., et al. (2016). Parental vitamin D deficiency during pregnancy is associated with increased blood pressure in offspring via Panx1 hypermethylation. Am. J. Physiol. - Hear. Circ. Physiol. ajpheart.00141.2016.

Meza, J.L., Anderson, J., Pappo, A.S., and Meyer, W.H. (2006). Analysis of prognostic factors in patients with nonmetastatic rhabdomyosarcoma treated on intergroup rhabdomyosarcoma studies III and IV: The children's oncology group. J. Clin. Oncol. *24*, 3844–3851.

Michalski, K., Syrjanen, J.L., Henze, E., Kumpf, J., Furukawa, H., and Kawate, T. (2020). The Cryo-EM structure of a pannexin 1 reveals unique motifs for ion selection and inhibition. Elife *9*, 9–11.

Miller, K.E., and Suter, D.M. (2018). An Integrated Cytoskeletal Model of Neurite Outgrowth. Front. Cell. Neurosci. *12*.

Minkiewicz, J., de Rivero Vaccari, J.P., and Keane, R.W. (2013). Human astrocytes express a novel NLRP2 inflammasome. Glia *61*, 1113–1121.

Miwa, S., Yamamoto, N., Hayashi, K., Takeuchi, A., Igarashi, K., and Tsuchiya, H. (2020). Recent advances and challenges in the treatment of rhabdomyosarcoma. Cancers (Basel). *12*, 1–18.

Moschovi, M., Vassiliki, T., and Anna, P. (2007). Erratum: Rhabdomyosarcoma in a patient

with Noonan syndrome phenotype and review of the literature (Journal of Pediatric Hematology/Oncology (2007) 29, (341-344)). J. Pediatr. Hematol. Oncol. *29*, 512.

Newton, W.A., Gehan, E.A., Webber, B.L., Marsden, H.B., van Unnik, A.J.M., Hamoudi, A.B., Tsokos, M.C., Shimada, H., Harms, D., Schmidt, D., et al. (1995). Classification of rhabdomyosarcomas and related sarcomas. Pathologic aspects and proposal for a new classification-an intergroup rhabdomyosarcoma study. Cancer *76*, 1073–1085.

Newton, W.A., Webber, B., Hamoudi, A.B., Gehan, E.A., and Maurer, H.M. (1999). Early history of pathology studies by the intergroup rhabdomyosarcoma study group. Pediatr. Dev. Pathol. *2*, 275–285.

Oberlin, O., Rey, A., Lyden, E., Bisogno, G., Stevens, M.C.G.G., Meyer, W.H., Carli, M., and Anderson, J.R. (2008). Prognostic factors in metastatic rhabdomyosarcomas: results of a pooled analysis from United States and European cooperative groups. J. Clin. Oncol. *26*, 2384–2389.

Ognjanovic, S., Linabery, A.M., Charbonneau, B., and Ross, J.A. (2009). Trends in childhood rhabdomyosarcoma incidence and survival in the United States, 1975-2005. Cancer *115*, 4218–4226.

Panchina, Y., Kelmanson, I., Matz, M., Lukyanov, K., Usman, N., and Lukyanov, S. (2000). A ubiquitous family of putative gap junction molecules. Curr. Biol. *10*, R473–R474.

Parham, D.M., and Barr, F.G. (2013). Classification of rhabdomyosarcoma and its molecular basis. Adv. Anat. Pathol. *20*, 387–397.

Parham, D.M., and Ellison, D.A. (2006). Rhabdomyosarcomas in adults and children: An update. Arch. Pathol. Lab. Med. *130*, 1454–1465.

Pelegrin, P., and Surprenant, A. (2006). Pannexin-1 mediates large pore formation and interleukin-1β release by the ATP-gated P2X7 receptor. EMBO J. *25*, 5071–5082.

Penuela, S., and Laird, D.W. (2012). The cellular life of pannexins. Wiley Interdiscip. Rev. Membr. Transp. Signal. *1*, 621–632.

Penuela, S., Bhalla, R., Gong, X.Q., Cowan, K.N., Celetti, S.J., Cowan, B.J., Bai, D., Shao,

Q., and Laird, D.W. (2007). Pannexin 1 and pannexin 3 are glycoproteins that exhibit many distinct characteristics from the connexin family of gap junction proteins. J. Cell Sci. *120*, 3772–3783.

Penuela, S., Bhalla, R., Nag, K., and Laird, D.W. (2009). Glycosylation regulates pannexin intermixing and cellular localization. Mol. Biol. Cell *20*, 4313–4323.

Penuela, S., Gyenis, L., Ablack, A., Churko, J.M., Berger, A.C., Litchfield, D.W., Lewis, J.D., and Laird, D.W. (2012). Loss of pannexin 1 attenuates melanoma progression by reversion to a melanocytic phenotype. J. Biol. Chem. *287*, 29184–29193.

Penuela, S., Gehi, R., and Laird, D.W. (2013). The biochemistry and function of pannexin channels. Biochim. Biophys. Acta - Biomembr. *1828*, 15–22.

Penuela, S., Simek, J., and Thompson, R.J. (2014a). Regulation of pannexin channels by post-translational modifications. FEBS Lett. *588*, 1411–1415.

Penuela, S., Harland, L., Simek, J., and Laird, D.W. (2014b). Pannexin channels and their links to human disease. Biochem. J. *461*, 371–381.

Pham, T. Le, St-Pierre, M.E., Ravel-Chapuis, A., Parks, T.E.C., Langlois, S., Penuela, S., Jasmin, B.J., and Cowan, K.N. (2018). Expression of Pannexin 1 and Pannexin 3 during skeletal muscle development, regeneration, and Duchenne muscular dystrophy. J. Cell. Physiol. *233*, 7057–7070.

Pinder, R.M., Brogden, R.N., Sawyer, P.R., Speight, T.M., Spencer, R., and Avery, G.S. (1976). Carbenoxolone: a review of its pharmacological properties and therapeutic efficacy in peptic ulcer disease. Drugs *11*, 245–307.

Pohl, G., Ho, C.L., Kurman, R.J., Bristow, R., Wang, T.L., and Shih, I.M. (2005). Inactivation of the mitogen-activated protein kinase pathway as a potential target-based therapy in ovarian serous tumors with KRAS or BRAF mutations. Cancer Res. *65*, 1994–2000.

Punyko, J. a, Mertens, A.C., Gurney, J.G., Yasui, Y., Donaldson, S.S., Rodeberg, D. a, Raney, R.B., Stovall, M., Sklar, C. a, Robison, L.L., et al. (2005). Long-term medical effects of childhood and adolescent rhabdomyosarcoma: a report from the childhood cancer survivor

study. Pediatr. Blood Cancer *44*, 643–653.

Qu, R., Dong, L., Zhang, J., Yu, X., Wang, L., and Zhu, S. (2020). Cryo-EM structure of human heptameric Pannexin 1 channel. Cell Res. *30*, 446–448.

Qu, Y., Misaghi, S., Newton, K., Gilmour, L.L., Louie, S., Cupp, J.E., Dubyak, G.R., Hackos, D., and Dixit, V.M. (2011). Pannexin-1 is required for ATP release during apoptosis but not for inflammasome activation. J. Immunol. *186*, 6553–6561.

Qualman, S., Lynch, J., Bridge, J., Parham, D., Teot, L., Meyer, W., and Pappo, A. (2008). Prevalence and clinical impact of anaplasia in childhood rhabdomyosarcoma: A report from the Soft Tissue Sarcoma Committee of the Children's Oncology Group. Cancer *113*, 3242–3247.

Raney, R.B., Maurer, H.M., Anderson, J.R., Andrassy, R.J., Donaldson, S.S., Qualman, S.J., Wharam, M.D., Wiener, E.S., and Crist, W.M. (2001). The Intergroup Rhabdomyosarcoma Study Group (IRSG): Major lessons from the IRS-I through IRS-IV studies as background for the current IRS-V treatment protocols. Sarcoma *5*, 9–15.

Raney, R.B., Walterhouse, D.O., Meza, J.L., Andrassy, R.J., Breneman, J.C., Crist, W.M., Maurer, H.M., Meyer, W.H., Parham, D.M., and Anderson, J.R. (2011). Results of the Intergroup Rhabdomyosarcoma Study Group D9602 protocol, using vincristine and dactinomycin with or without cyclophosphamide and radiation therapy, for newly diagnosed patients with low-risk embryonal rhabdomyosarcoma: A report from the soft. J. Clin. Oncol. *29*, 1312–1318.

Ransford, G. a, Fregien, N., Qiu, F., Dahl, G., Conner, G.E., and Salathe, M. (2009). Pannexin 1 contributes to ATP release in airway epithelia. Am. J. Respir. Cell Mol. Biol. *41*, 525–534.

Raslan, A., Hainz, N., Beckmann, A., Tschernig, T., and Meier, C. (2016). Pannexin-1 expression in developing mouse nervous system: new evidence for expression in sensory ganglia. Cell Tissue Res. *364*, 29–41.

Rathinam, V.A.K., and Fitzgerald, K.A. (2016). Inflammasome Complexes: Emerging Mechanisms and Effector Functions. Cell *165*, 792–800.

Ray, A., Zoidl, G., Weickert, S., Wahle, P., and Dermietzel, R. (2005). Site-specific and developmental expression of pannexin1 in the mouse nervous system. Eur. J. Neurosci. *21*, 3277–3290.

Ren, Y.X., Finckenstein, F.G., Abdueva, D. a., Shahbazian, V., Chung, B., Weinberg, K.I., Triche, T.J., Shimada, H., and Anderson, M.J. (2008). Mouse mesenchymal stem cells expressing PAX-FKHR form alveolar rhabdomyosarcomas by cooperating with secondary mutations. Cancer Res. *68*, 6587–6597.

Riquelme, M. a, Cea, L. a, Vega, J.L., Boric, M.P., Monyer, H., Bennett, M.V.L., Frank, M., Willecke, K., and Sáez, J.C. (2013). The ATP required for potentiation of skeletal muscle contraction is released via pannexin hemichannels. Neuropharmacology *75*, 594–603.

Riquelme, M.A., Cea, L.A., Vega, J.L., Puebla, C., Vargas, A.A., Shoji, K.F., Subiabre, M., and Sáez, J.C. (2015). Pannexin channels mediate the acquisition of myogenic commitment in C2C12 reserve cells promoted by P2 receptor activation. Front. Cell Dev. Biol. *3*, 25.

Rodrigues, M., Echigoya, Y., Fukada, S.I., and Yokota, T. (2016). Current Translational Research and Murine Models for Duchenne Muscular Dystrophy. J. Neuromuscul. Dis. *3*, 29–48.

Ruan, Z., Orozco, I.J., Du, J., and Lü, W. (2020). Structures of human pannexin 1 reveal ion pathways and mechanism of gating. Nature.

Samuel, D.P., Tsokos, M., and DeBaun, M.R. (1999). Hemihypertrophy and a poorly differentiated embryonal rhabdomyosarcoma of the pelvis. Med. Pediatr. Oncol. *32*, 38–43.

Sanchez Arias, J.C., Wicki-Stordeur, L.E., Candlish, R.C., van der Slagt, E., Paci, I., Rao, P.P.N., MacVicar, B.A., and Swayne, L.A. (2020). PANX1 in inflammation heats up: New mechanistic insights with implications for injury and infection. Cell Calcium *90*, 102253.

Schalper, K.A., Carvajal-Hausdorf, D., and Oyarzo, M.P. (2014). Possible role of hemichannels in cancer. Front. Physiol. *5 JUN*, 1–18.

Seminario-Vidal, L., Okada, S.F., Sesma, J.I., Kreda, S.M., van Heusden, C.A., Zhu, Y., Jones, L.C., O'Neal, W.K., Penuela, S., Laird, D.W., et al. (2011). Rho signaling regulates pannexin 1-mediated ATP release from airway epithelia. J. Biol. Chem. *286*, 26277–26286.

Séror, C., Melki, M.-T., Subra, F., Raza, S.Q., Bras, M., Saïdi, H., Nardacci, R., Voisin, L., Paoletti, A., Law, F., et al. (2011). Extracellular ATP acts on P2Y2 purinergic receptors to facilitate HIV-1 infection. J. Exp. Med. *208*, 1823–1834.

Shern, J.F., Chen, L., Chmielecki, J., Wei, J.S., Patidar, R., Rosenberg, M., Ambrogio, L., Auclair, D., Wang, J., Song, Y.K., et al. (2014). Comprehensive genomic analysis of rhabdomyosarcoma reveals a landscape of alterations affecting a common genetic axis in fusion-positive and fusion-negative tumors. Cancer Discov. *4*, 216–231.

Shern, J.F., Yohe, M.E., and Khan, J. (2015). Pediatric Rhabdomyosarcoma. Crit. Rev. Oncog. *20*, 227–243.

Silverman, W., Locovei, S., and Dahl, G. (2008). Probenecid, a gout remedy, inhibits pannexin 1 channels. Am. J. … *33101*, 761–767.

Silverman, W.R., de Rivero Vaccari, J.P., Locovei, S., Qiu, F., Carlsson, S.K., Scemes, E., Keane, R.W., and Dahl, G. (2009). The pannexin 1 channel activates the inflammasome in neurons and astrocytes. J. Biol. Chem. *284*, 18143–18151.

Skapek, S.X., Ferrari, A., Gupta, A.A., Lupo, P.J., Butler, E., Shipley, J., Barr, F.G., and Hawkins, D.S. (2019). Rhabdomyosarcoma. Nat. Rev. Dis. Prim. *5*, 14–16.

Smith, A.C., Choufani, S., Ferreira, J.C., and Weksberg, R. (2007). Growth regulation, imprinted genes, and chromosome 11p15.5. Pediatr. Res. *61*, 43–47.

Song, B., Tang, J.W., Wang, B., Cui, X.N., Hou, L., Sun, L., Mao, L.M., Zhou, C.H., Du, Y., Wang, L.H., et al. (2005). Identify lymphatic metastasis-associated genes in mouse hepatocarcinoma cell lines using gene chip. World J. Gastroenterol. *11*, 1463–1472.

Sosinsky, G.E., Boassa, D., Dermietzel, R., Duffy, H.S., Laird, D.W., MacVicar, B., Naus, C.C., Penuela, S.S., Scemes, E., Spray, D.C., et al. (2011). Pannexin channels are not gap junction hemichannels. Channels *5*, 193–197.

Stout, A.P. (1946). Rhabdomyosarcoma of the skeletal muscles. Ann. Surg. *123*, 447–472.

Sultan, I., Qaddoumi, I., Yaser, S., Rodriguez-Galindo, C., and Ferrari, A. (2009). Comparing adult and pediatric rhabdomyosarcoma in the surveillance, epidemiology and end

results program, 1973 to 2005: An analysis of 2,600 patients. J. Clin. Oncol. *27*, 3391–3397.

Swayne, L.A., Sorbara, C.D., and Bennett, S. a L. (2010). Pannexin 2 is expressed by postnatal hippocampal neural progenitors and modulates neuronal commitment. J. Biol. Chem. *285*, 24977–24986.

Syrjanen, J.L., Michalski, K., Chou, T.H., Grant, T., Rao, S., Simorowski, N., Tucker, S.J., Grigorieff, N., and Furukawa, H. (2020). Structure and assembly of calcium homeostasis modulator proteins. Nat. Struct. Mol. Biol.

Thompson, R.J., Jackson, M.F., Olah, M.E., Rungta, R.L., Hines, D.J., Beazely, M. a, MacDonald, J.F., and Macvicar, B. a (2008). Activation of pannexin-1 hemichannels augments aberrant bursting in the hippocampus. Science (80-.). *322*, 1555–1559.

Trahair, T., Andrews, L., and Cohn, R.J. (2007). Recognition of Li Fraumeni syndrome at diagnosis of a locally advanced extremity rhabdomyosarcoma. Pediatr. Blood Cancer *48*, 345–348.

Turmel, P., Dufresne, J., Hermo, L., Smith, C.E., Penuela, S., Laird, D.W., and Cyr, D.G. (2011). Characterization of pannexin1 and pannexin3 and their regulation by androgens in the male reproductive tract of the adult rat. Mol. Reprod. Dev. *78*, 124–138.

Uccelli, A., Moretta, L., and Pistoia, V. (2008). Mesenchymal stem cells in health and disease. Nat. Rev. Immunol. *8*, 726–736.

Velasquez, S., and Eugenin, E. a (2014). Role of Pannexin-1 hemichannels and purinergic receptors in the pathogenesis of human diseases. Front. Physiol. *5*, 96.

Verschuren, E.H.J., Rigalli, J.P., Castenmiller, C., Rohrbach, M.U., Bindels, R.J.M., Peters, D.J.M., Arjona, F.J., and Hoenderop, J.G.J. (2020). Pannexin-1 mediates fluid shear stress-sensitive purinergic signaling and cyst growth in polycystic kidney disease. FASEB J. *34*, 6382–6398.

Vogt, A., Hormuzdi, S.G., and Monyer, H. (2005). Pannexin1 and Pannexin2 expression in the developing and mature rat brain. Mol. Brain Res. *141*, 113–120.

Wagers, A.J., and Conboy, I.M. (2005). Cellular and molecular signatures of muscle

regeneration: Current concepts and controversies in adult myogenesis. Cell *122*, 659–667.

Walterhouse, D.O., Pappo, A.S., Meza, J.L., Breneman, J.C., Hayes-Jordan, A.A., Parham, D.M., Cripe, T.P., Anderson, J.R., Meyer, W.H., and Hawkins, D.S. (2014). Shorter-duration therapy using vincristine, dactinomycin, and lower-dose cyclophosphamide with or without radiotherapy for patients with newly diagnosed low-risk rhabdomyosarcoma: A report from the soft tissue sarcoma committee of the Children's Oncology . J. Clin. Oncol. *32*, 3547–3552.

Wang, C. (2012). Childhood rhabdomyosarcoma: Recent advances and prospective views. J. Dent. Res. *91*, 341–350.

Wang, J., and Dahl, G. (2010). SCAM analysis of Panx1 suggests a peculiar pore structure. J. Gen. Physiol. *136*, 515–527.

Wang, J., and Dahl, G. (2018). Pannexin1: A multifunction and multiconductance and/or permeability membrane channel. Am. J. Physiol. - Cell Physiol. *315*, C290–C299.

Wang, H., Xing, Y., Mao, L., Luo, Y., Kang, L., and Meng, G. (2013). Pannexin-1 influences peritoneal cavity cell population but is not involved in NLRP3 inflammasome activation. Protein Cell *4*, 259–265.

Wang, J., Ambrosi, C., Qiu, F., Jackson, D.G., Sosinsky, G., and Dahl, G. (2014). The membrane protein Pannexin1 forms two open-channel conformations depending on the mode of activation. Sci. Signal. *7*, ra69.

Weber, C.O., and Virchow, R. (1854). Anatomische Untersuchung einer hypertrophischen Zunge nebst Bemerkungen über die Neubildung quergestreifter Muskelfasern. Arch. Für Pathol. Anat. Und Physiol. Und Für Klin. Med. *7*, 115–125.

Weigel, M.T., and Dowsett, M. (2010). Current and emerging biomarkers in breast cancer: prognosis and prediction. Endocr. Relat. Cancer *17*, R245–R262.

Weilinger, N.L., Tang, P.L., and Thompson, R.J. (2012). Anoxia-induced NMDA receptor activation opens Pannexin channels via Src family kinases. J. Neurosci. *32*, 12579–12588.

Wicki-Stordeur, L.E., and Swayne, L.A. (2013). Panx1 regulates neural stem and progenitor

cell behaviours associated with cytoskeletal dynamics and interacts with multiple cytoskeletal elements. Cell Commun. Signal. *11*, 1–8.

Wicki-Stordeur, L.E., and Swayne, L.A. (2014). The emerging Pannexin 1 signalome: a new nexus revealed? Front. Cell. Neurosci. *7*, 287.

Wicki-Stordeur, L.E., Dzugalo, A.D., Swansburg, R.M., Suits, J.M., and Swayne, L.A. (2012). Pannexin 1 regulates postnatal neural stem and progenitor cell proliferation. Neural Dev. *7*, 11.

Wicki-Stordeur, L.E., Sanchez-Arias, J.C., Dhaliwal, J., Carmona-Wagner, E.O., Shestopalov, V.I., Lagace, D.C., and Swayne, L.A. (2016). Pannexin 1 Differentially Affects Neural Precursor Cell Maintenance in the Ventricular Zone and Peri-Infarct Cortex. J. Neurosci. *36*, 1203–1210.

Willebrords, J., Maes, M., Crespo Yanguas, S., and Vinken, M. (2017). Inhibitors of connexin and pannexin channels as potential therapeutics. Pharmacol. Ther.

Williamson, D., Missiaglia, E., De Reyniès, A., Pierron, G., Thuille, B., Palenzuela, G., Thway, K., Orbach, D., Laé, M., Fréneaux, P., et al. (2010). Fusion gene-negative alveolar rhabdomyosarcoma is clinically and molecularly indistinguishable from embryonal rhabdomyosarcoma. J. Clin. Oncol. *28*, 2151–2158.

Xia, J., Lim, J.C., Lu, W., Beckel, J.M., Macarak, E.J., Laties, A.M., and Mitchell, C.H. (2012). Neurons respond directly to mechanical deformation with pannexin-mediated ATP release and autostimulation of P2X 7 receptors. J. Physiol. *590*, 2285–2304.

Xu, X., Wicki-stordeur, L.E., Sanchez-arias, J.C., and Liu, M. (2018). Probenecid Disrupts a Novel Pannexin 1-Collapsin Response Mediator Protein 2 Interaction and Increases Microtubule Stability. Front. Cell. Neurosci. *12*, 1–13.

Yang, D., He, Y., Muñoz-Planillo, R., Liu, Q., and Núñez, G. (2015). Caspase-11 Requires the Pannexin-1 Channel and the Purinergic P2X7 Pore to Mediate Pyroptosis and Endotoxic Shock. Immunity 1–10.

Yang, Y., Delalio, L.J., Best, A.K., Macal, E., Milstein, J., Donnelly, I., Miller, A.M., McBride, M., Shu, X., Koval, M., et al. (2020). Endothelial Pannexin 1 Channels Control

Inflammation by Regulating Intracellular Calcium. J. Immunol. *204*, 2995–3007.

Yen, M.R., and Saier, M.H. (2007). Gap junctional proteins of animals: The innexin/pannexin superfamily. Prog. Biophys. Mol. Biol. *94*, 5–14.

Yohe, M.E., Heske, C.M., Stewart, E., Adamson, P.C., Ahmed, N., Antonescu, C.R., Chen, E., Collins, N., Ehrlich, A., Galindo, R.L., et al. (2019). Insights into pediatric rhabdomyosarcoma research: Challenges and goals. Pediatr. Blood Cancer 1–10.

Yu, P.Y., and Guttridge, D.C. (2018). Dysregulated Myogenesis in Rhabdomyosarcoma (Elsevier Inc.).

Zhang, Y., Laumet, G., Chen, S.-R., Hittelman, W.N., and Pan, H.-L. (2015). Pannexin-1 Up-regulation in the Dorsal Root Ganglion Contributes to Neuropathic Pain Development. J. Biol. Chem. *290*, 14647–14655.

2. CHAPTER TWO: PANNEXIN 1 INHIBITS RHABDOMYOSARCOMA PROGRESSION THROUGH A MECHANISM INDEPENDENT OF ITS CANONICAL CHANNEL FUNCTION

Authors: Xiao Xiang, Stéphanie Langlois, Marie-Eve St-Pierre, Jessica Barré, David Grynspan, Bibianna Purgina, and Kyle N. Cowan

Status: Published

Oncogenesis

2018 Nov 21;7(11):89. doi: 10.1038/s41389-018-0100-4.

2.1 ACKNOWLEDGEMENTS

The majority of the experiments in this manuscript were performed by me under the supervision of Kyle N. Cowan. Stéphanie Langlois performed the Western blot presented in Figure 2.1 and the dye uptake assays. Marie-Eve St-Pierre performed the Western blot presented in Figure 2.3 and helped me with injections when performing the *in vivo* studies. Jessica Barré helped me perform the immunohistochemistry of human tissue specimens in Figure 2.1. The human tissue specimens were collected and kindly provided by David Grynspan and Bibianna Purgina. This manuscript was written and revised by me with editorial help from Stéphanie Langlois and Kyle N. Cowan.

2.2 ABSTRACT

Rhabdomyosarcoma (RMS) is an aggressive soft tissue sarcoma of childhood thought to arise from impaired differentiation of skeletal muscle progenitors. We have recently identified Pannexin 1 (PANX1) channels as a novel regulator of skeletal myogenesis. In the present study, we determined that PANX1 transcript and protein levels are down-regulated in embryonal (eRMS) and alveolar RMS (aRMS) patient-derived cell lines and primary tumor specimens as compared to differentiated skeletal muscle myoblasts and tissue, respectively. While not sufficient to overcome the inability of RMS to reach terminal differentiation, ectopic expression of PANX1 in eRMS (Rh18) and aRMS (Rh30) cells significantly decreased their proliferative and migratory potential. Furthermore, ectopic PANX1 abolished 3D spheroid formation in eRMS and aRMS cells and induced regression of established spheroids through induction of apoptosis. Notably, PANX1 expression also significantly reduced the growth of human eRMS and aRMS tumor xenografts *in vivo*. Interestingly, PANX1 does not form active channels when expressed in eRMS (Rh18) and aRMS (Rh30) cells and the addition of PANX1 channel inhibitors did not alter or reverse the PANX1-mediated reduction of cell proliferation and migration. Moreover, expression of channel-defective PANX1 mutants not only disrupted eRMS and aRMS 3D spheroids, but also inhibited *in vivo* RMS tumor growth. Altogether our findings suggest that PANX1 alleviates RMS malignant properties *in vitro* and *in vivo* through a process that is independent from its canonical channel function.

Keywords: Apoptosis; Cancer; Channel; Pannexin; Rhabdomyosarcoma

2.3 INTRODUCTION

Rhabdomyosarcoma (RMS) is the most common soft tissue sarcoma of childhood (Egas-Bejar and Huh, 2014). Histopathological classification includes two major subtypes: embryonal (eRMS) and alveolar (aRMS) (Rudzinski et al., 2013). eRMS is more frequent, genetically heterogeneous, and associated with a better prognosis (Dobson et al., 2016; Parham and Barr, 2013). On the other hand, aRMS is less common and more aggressive, with a worse outcome (Dobson et al., 2016; Parham and Barr, 2013). RMS cells are positive for myogenic markers and resemble normal muscle progenitors but are unable to complete the multistep process leading to terminal differentiation (Keller and Guttridge, 2013; Tapscott et al., 1993). Despite invasive treatments such as surgery, radiotherapy, and chemotherapy, the prognosis of children with metastatic RMS has not improved and the 5 year survival rate remains less than 30% (Malempati and Hawkins, 2012), underscoring the need to identify novel therapeutic strategies. Targeting the molecular players involved in the dysregulated myogenic pathways in RMS to promote its differentiation towards skeletal muscle tissue is thought to be a possible new strategy to alleviate RMS malignancy (Hettmer et al., 2014).

Interestingly, we have recently identified Pannexin1 (PANX1) as a novel regulator of myogenic differentiation (Langlois et al., 2014). PANX1 (known as Panx1 in rodents) levels are very low in undifferentiated human skeletal muscle myoblasts, but are up-regulated during their differentiation to promote this process through a mechanism that involves its channel activity (Langlois et al., 2014). Pannexins are a family of single membrane channel proteins (Panx1, Panx2, and Panx3) that are differentially expressed amongst various cells, tissues, and organs (Langlois and Cowan, 2017). Panx1 channels at the cell surface act as the major conduit for ATP release (Bao et al., 2004) and have been implicated in many physiologic and

pathologic processes including calcium wave propagation (Locovei et al., 2006a), vasodilatation (Locovei et al., 2006b), inflammatory responses (Pelegrin and Surprenant, 2006; Silverman et al., 2009), apoptosis (Chekeni et al., 2010; Sandilos et al., 2012; Yang et al., 2015), epilepsy (Thompson et al., 2008), and human immunodeficiency virus infection (Orellana et al., 2013; Paoletti et al., 2013; Séror et al., 2011).

Only recently, however, has Panx1 been studied in the context of cancer. Initial reports showed that Panx1 levels are low in glioma cell lines and that Panx1 over-expression suppresses rat C6 glioma tumor formation (Lai et al., 2007). It was then reported that Panx1 levels are up-regulated in murine melanoma cell lines and correlated with their aggressiveness (Penuela et al., 2012). Loss of Panx1 attenuated melanoma progression through reversion to a melanocytic phenotype (Penuela et al., 2012). In human cancer, PANX1 levels were shown to be down-regulated in keratinocyte tumors (Cowan et al., 2012). On the other hand, high *PANX1* mRNA expression is correlated with poor overall survival in breast cancer patients (Stewart et al., 2016). Furthermore, a mutation encoding a truncated form of PANX1 is recurrently enriched in highly metastatic breast cancer cells (Furlow et al., 2015). This truncated version permits metastatic cell survival in the vasculature by enhancing PANX1 channel activity. Importantly, PANX1 channel blockade reduced breast cancer metastasis efficiency *in vivo* (Furlow et al., 2015). Altogether these studies indicate that Panx1/PANX1 expression and/or channel activity are altered in some forms of cancer, may be correlated with their aggressiveness, and that restoration of its levels and/or activity alleviate tumor malignant characteristics. Here, we show that PANX1 is down-regulated in human eRMS and aRMS primary tumor specimens and patient-derived cell lines, when compared to normal differentiated skeletal muscle cells and tissue. Once expressed in eRMS (Rh18) and aRMS (Rh30) cells, PANX1 did not overcome the inability of RMS to reach terminal differentiation but rather significantly decreased their

malignant properties *in vitro* and *in vivo*. Based on the current knowledge of PANX1 channels, our data obtained from dye uptake assays, utilization of PANX1 channel inhibitors, and expression of PANX1 mutants deficient in channel activity, altogether indicate that PANX1 tumor suppressive roles in RMS do not require its canonical channel activity suggesting the existence of novel PANX1 functions.

2.4 MATERIALS AND METHODS

Human Tissue Samples and Cell Lines

Human samples (7 normal; 7 eRMS; 6 aRMS), collected following informed consent, were obtained from the Department of Pathology and Laboratory Medicine, Children's Hospital of Eastern Ontario and the Ottawa Hospital, Ottawa, Ontario, Canada, after institutional ethics board approval. Rh18, Rh36, Rh28, Rh30 and Rh41 cell lines were from Dr. P. Houghton (St. Jude Children's Hospital, Memphis, TN, USA). RD and HEK293T cell lines were from American Type Culture Collection. HSMM were from Lonza and differentiated as previously described (Langlois et al., 2014). Cells were mycoplasma-negative.

Plasmid Construction, Transfections, and Stable Cell Lines Generation

PANX1 cDNA (Origene, Rockville, MD, USA) was subcloned into pCDH-CuO-MCS-EF1-GFP lentiviral vector (System Biosciences, Palo Alto, CA, USA). PANX1 constructs encoding change from cysteine to serine at position 66, 84, or 265 were generated using the QuickChange site-directed mutagenesis kit (Agilent Technologies, Santa Clara, CA, USA) and verified by sequencing.

Transfections used Lipofectamine 2000 Reagent (Thermo Scientific, Waltham, MA, USA). Stable cell lines were generated using the SparQ Cumate Switch Inducible System (System Bioscience). Cells stably expressing CymR repressor (pCDH-EF1-CymR-T2A-Neo lentivector) were transduced with pCDH-CuO-MCS-EF1-GFP, pCDH-CuO-PANX1-EF1-GFP (PANX1), pCDH-CuO-C66S-EF1-GFP (C66S), pCDH-CuO-C84S-EF1-GFP (C84S) or pCDH-CuO-C265S-EF1-GFP (C265S) lentivectors and selected. PANX1 expression was induced with 30 µg/mL cumate.

RNA Extraction, Reverse Transcription, and Quantitative PCR Analysis

Total RNA was extracted using RNeasy Mini Kit (Qiagen, Germantown, MD, USA) and reverse transcription was performed using High-Capacity cDNA Reverse Transcription Kit (Thermo Scientific). The synthesized cDNA was used as template for quantitative PCR using iQ™ SYBR® Green Supermix kit (Bio-Rad, Hercules, CA, USA) on Mastercycler ep *realplex* (Eppendorf, Hamburg, Germany) real-time PCR system with specific primers for *PANX1* (forward 5'-CGGAGTACGTGTTCTCGGATT-3'; reverse 5'-CCTGACGCCAGGAGAAAGAA-3') and Glyceraldehyde 3-phosphate dehydrogenase (GAPDH) (forward 5'-CAAGACCTTGGGCTGGGAC-3', reverse 5'-AGGCTGCGGGCTCAATTTAT-3'). Relative expression was determined using the comparative Ct method.

Antibodies

Primary antibodies: PANX1 (Sigma-Aldrich, St-Louis, MO, USA; HPA0169300), MHC (R&D Systems, Minneapolis, MN, USA; MAB4470), MyoD (Santa Cruz, Dallas, TX, USA; sc-760), myogenin (Santa Cruz; sc-12732), tubulin (Santa Cruz; sc-8035), GAPDH (Advanced ImmunoChemical, Long Beach, CA, USA; 2RGM2), EGFR (Santa Cruz; sc-03-G), GM130 (Abcam, Cambridge, MA, USA; ab169276), calnexin (Santa Cruz; sc-46669), BrdU (Thermo Scientific; 03-3900). Secondary antibodies conjugated to Alexa Fluor 405, 488, or 594 (Thermo Scientific; A-31553, A-11001, or A-11012), and Alexa 680- (Thermo Scientific; A21109) or infrared fluorescent-labeled secondary antibodies IRDye 800 (VWR, Radnor, PA, USA; CA610-132-121).

Immunofluorescence Microscopy

Human tissue sections were labeled as previously described (Cowan et al., 2012). Olympus Fluoview FV-1000 Laser Confocal Microscope image acquisition was performed sequentially with the microscope settings kept constant (Cowan et al., 2012). Quantification used accompanying analysis software. Positive labeling in skeletal muscle optimized cut-offs for positive labeling (Cowan et al., 2012). Relative densitometric units were quantified within a constant fixed area.

Cells were immunolabeled as previously described (Langlois et al., 2014). For comparison of myogenic factor expression, images of 15 random fields (20X objective) were counted.

Western Blotting

Cell lysates were obtained and analyzed as previously described (Cowan et al., 2012; Langlois et al., 2014).

Proliferation Assay

Cells were transfected with the empty vector or PANX1. Twenty-four hours post-transfection, cells were incubated with 10 µM BrdU (Sigma-Aldrich) for 3 hours (Rh18) or 1 hour (Rh30) and processed for immunohistochemistry (Langlois et al., 2014).

Stable cell lines were incubated with 100 µM CBX (or DMSO) or 200 µM 10PANX (or scramble (Scr) peptide) for 48 hours in the presence of cumate. The assay was performed according to the manufacturer's protocol (BrdU colorimetric kit, Roche Applied Sciences, Penzberg, Germany).

Migration Assay

A 96-well WoundMaker device (Essen Bioscience, Ann Arbor, MI, USA) created a uniform scratch in cells monolayer. CBX (or DMSO) or 10PANX (or scramble (Scr) peptide) were added at 100 µM and 200 µM, respectively. Migration was measured by IncuCyte ZOOM Live Cell Imaging System (Essen Bioscience).

3D Spheroid Formation and Regression Assays

Cumate pre-treated cells were seeded in Ultra Low Adhesion plates. In regression experiments, cumate treatment began only once spheroids had formed (48 hours post-seeding). Mean Image Fluorescence was measured using IncuCyte ZOOM Live Cell Imaging System.

Viability Assay and Flow Cytometry

Viable cells seeded on agar (BD Biosciences, San Jose, CA, USA) (Wolf et al., 2011) were counted by Trypan Blue (Thermo Scientific) dye exclusion. For flow cytometry, cells were washed in cold PBS, re-suspended, stained with Pacific Blue conjugated Annexin V and 7-Aminoactinomycin D (7-AAD) (BD Biosciences), and analyzed using the LSRFortessa X-20 (BD Biosciences) cell analyzer and FACSDiva software (Draganov et al., 2015).

Dye Uptake Assay

Sulforhodamine B dye uptake assay was performed as previously described, and normalized to PANX1 levels (Celetti et al., 2010; Penuela et al., 2007, 2009).

Cell Surface Biotinylation Assay

Cell surface biotinylation assay was performed as previously described (Langlois et al., 2008).

Xenograft Studies

Experiments were approved by the Animal Care Committee at the University of Ottawa and conducted per the Canadian Council of Animal Care guidelines. Two million cumate-treated cells were injected into the gastrocnemius muscle of 4- to 6-week-old female SCID mice (Charles River Laboratories, Wilmington, MA, USA). PANX1 (3 mice for eRMS; 10 for aRMS) or C265S (6 mice) mutant expressing cells were injected into the right leg, while the empty vector cells were injected into the left leg (Petricoin et al., 2007). Mice were intraperitoneally injected every 3 days with 50 µL cumate (600 µg/mL) and sacrificed when tumors reached 2000 mm^3 ($V = L \times W \times H \times \pi/6$ (L: length; W: width; H: height of tumor)) (Aslam et al., 2014).

Statistics

For all *in vitro* assays, cells in each group were plated in triplicates, and each experiment was performed three times (n=3). Statistical significance was determined using unpaired two-tailed Student's *t*-tests and analysis of variance (ANOVA) followed by Tukey's, Bonferroni, or Dunnett's post hoc tests. Results are given as mean ± s.d. Results with $P<0.05$ were considered significant.

2.5 RESULTS

PANX1 is Down-Regulated in RMS

Quantitative real-time PCR, immunofluorescence microscopy, and Western blotting were performed to examine PANX1 expression in a panel of patient-derived aRMS (Rh28, Rh30, Rh41) and eRMS (Rh18, Rh36, RD) cell lines compared to those of undifferentiated and differentiated human skeletal muscle myoblasts (HSMM). *PANX1* expression was significantly increased in differentiated HSMM compared to undifferentiated cells (Fig. 2.1A). *PANX1* transcript levels were low in all RMS cell lines tested and were comparable to that of undifferentiated HSMM (Fig. 2.1A). In keeping with these data, immunolabeling (Fig. 2.1B) and Western blot (Fig. 2.1C) analysis revealed that PANX1 is highly expressed in differentiated HSMM, while PANX1 levels are very low or below detectable levels in all RMS cell lines as well as in undifferentiated HSMM.

To confirm the pertinence of these findings, we examined PANX1 levels in RMS tumor specimens. PANX1 was immunolabeled in 13 pediatric RMS tumors (7 eRMS and 6 aRMS) as well as in 7 pediatric normal skeletal muscle samples. As expected (Langlois et al., 2014), PANX1 was detected as a punctate labeling in normal muscle tissue (Fig. 2.1D). While PANX1 was also detected as punctate structures in RMS tumors (Fig. 2.1D), its levels were strikingly lower in both RMS subtypes compared to normal skeletal muscle tissue (Fig. 2.1E). Altogether these results indicate that PANX1 expression is down-regulated in aRMS and eRMS.

PANX1 Expression Impedes RMS Cell Proliferation and Migration

Next, we wanted to assess whether restoration of PANX1 expression can reduce RMS malignant properties. A representative cell line for each RMS subtype, Rh18 for eRMS and Rh30 for aRMS, have been used. PANX1 was detected as multiple bands (~38–50 kDa) by Western blot (Fig. 2.2A) reflecting its various glycosylation degrees (Boassa et al., 2007; Langlois et al., 2014; Penuela et al., 2007, 2009). eRMS and aRMS cells expressing PANX1 were submitted to a BrdU incorporation assay along with their respective control GFP-expressing cells. PANX1 expression reduced the proliferation of eRMS (Fig. 2.2B) and aRMS (Fig. 2.2C) cells by ~50-60%. Based on these promising results, we generated stable Rh18 and Rh30 cell lines using a cumate-inducible gene expression system to regulate PANX1 expression. These cell lines show a significant induction of PANX1 levels only in cumate-treated PANX1-transductants (Fig. 2.2D and E). Using these stable cell lines, a scratch wound migration assay showed a reduction of migration by PANX1-expressing eRMS (Fig. 2.2F) and aRMS (Fig. 2.2G) cells. Collectively, these results reveal that introduction of PANX1 in RMS reduces their growth and migratory potential *in vitro*.

PANX1 Expression does not Trigger RMS Terminal Differentiation

Having previously shown that PANX1 expression promotes HSMM fusion and differentiation (Langlois et al., 2014), we wanted to examine whether PANX1 could induce RMS differentiation. First, eRMS (Rh18) and RMS (Rh30) cells were transfected with GFP or PANX1, immunolabeled for PANX1, and nuclei were counted in transfected cells. About 20% of aRMS cells expressing PANX1 contained 2 or more nuclei (Fig. 2.3A, arrows; Fig. 2.3B, quantification) while the majority of control cells were mononucleated. This was not observed in eRMS cells, as 7-8% of both control and PANX1-expressing cells were multinucleated (Fig. 2.3A-B). In order to determine whether the change in phenotype observed

in PANX1-expressing aRMS cells was associated with myogenic differentiation, the levels of several myogenic factors were examined over a period of 10 days. MyoD and myogenin levels were relatively unchanged in both control and PANX1-expressing aRMS cells while myosin heavy chain (MHC) remained below detectable limits (Fig. 2.3C). As multinucleated cells constituted only a small proportion of the cells culture, myogenic factor expression was then specifically examined in mono- and multinucleated cells by immunofluorescence (Fig. 2.3D). While the proportion of MyoD-positive cells remained unchanged despite the nucleation status of PANX1-expressing cells, more multinucleated PANX1-expressing aRMS cells were myogenin-positive compared to their mononucleated counterparts. MHC was again not detected in PANX1-expressing cells indicating that terminal differentiation had not been reached. These results suggest that although an early fusion stage of myogenesis may have been attained in aRMS cells, PANX1 expression was not sufficient to trigger their differentiation.

PANX1 Expression Prevents 3D RMS Spheroid Formation and Induces their Regression by Apoptosis

To examine the role of PANX1 in tumor formation, we first utilized 3D spheroid cultures as this model more closely resembles *in vivo* tumors (Ma et al., 2012). Aggregation and compaction in GFP control and PANX1-expressing eRMS (Rh18) and aRMS (Rh30) cells were first observed 48 hours after seeding on agar (Fig. 2.4A-B). While the growth of control spheroids continued to increase over time, PANX1 expression prevented the formation of eRMS (Fig. 2.4A and C) and aRMS (Fig. 2.4B and D) spheroids. Only loose aggregates were formed by PANX1-expressing cells, which gradually lost their constitutive GFP fluorescence possibly due to cell death.

To test this possibility, the viability of eRMS and aRMS spheroids was determined over a period of 10 days. As expected, control cells showed a continuous increase in viable cell number. By contrast, PANX1-expressing eRMS (Fig. 2.4E, left panel) and aRMS (Fig. 2.4F, left panel) cells displayed a significant reduction in viability compared to control cells with the overall number of live PANX1-expressing aRMS cells remaining unchanged for 10 days. To examine whether these effects were due to apoptosis, flow cytometry was performed using Annexin V and 7-AAD (Ciarapica et al., 2014). In order to capture early apoptotic events, cells were examined after being in suspension for 4 days. The percentage of early apoptotic cells was significantly higher amongst PANX1-expressing eRMS cells compared to control cells (Fig. 2.4E, right panel), while both early and late apoptotic populations were increased in PANX1-expressing aRMS cells (Fig. 2.4F, right panel).

Of particular relevance in terms of therapeutic intervention for RMS treatment, we next examined whether PANX1 was able to trigger RMS spheroid regression. As Rh18 (eRMS) and Rh30 (aRMS) cells formed sizable spheroids 48 hours after being in suspension, cumate treatment was initiated at that time point to induce PANX1 expression. While control spheroids displayed an ongoing growth, there was a continuous decrease of fluorescence in PANX1-expressing eRMS and aRMS spheroids after initiation of cumate treatment eventually reaching a level that was similar to that of cells in suspension prior to spheroid formation (Fig. 2.4G-H). Taken together, our data demonstrate that PANX1 expression prevents RMS spheroid formation and triggers their regression through the induction of apoptosis.

PANX1 Expression Decreases RMS Tumor Growth In Vivo

The numerous tumor-suppressive effects of PANX1 in RMS cells *in vitro* prompted us to explore its impact on tumor growth *in vivo*. Cumate-treated eRMS (Rh18) and aRMS (Rh30)

cells expressing the empty vector (GFP) or PANX1 were injected into the gastrocnemius muscle of mice and kept under cumate treatment. Control eRMS and aRMS cells formed rapidly growing tumors reaching the ethical endpoint of ~2000 mm^3 after 45 days and 36 days, respectively (Fig. 2.5A-B). Conversely, tumors formed by PANX1-expressing eRMS and aRMS cells grew significantly slower (Fig. 2.5A-B), which was clearly depicted by a reduction of approximately 50% in their tumor weight at the endpoint (Fig. 2.5C-D). Induction of PANX1 expression in all eRMS and aRMS xenografts was confirmed by Western blotting (Fig. 2.5E-F). Overall, these results revealed that PANX1 expression reduces RMS tumor growth *in vivo*.

PANX1-Mediated Tumor Suppressive Properties are not Abrogated by PANX1 Channel Inhibition

In order to understand the mechanism by which PANX1 reduces RMS malignant properties, we assessed its channel function using dye uptake. As expected, differentiated HSMM, which express high PANX1 levels, showed a significant increase in dye uptake incidence compared to undifferentiated HSMM, which express only low levels of PANX1 (Fig. 2.6A). Similar to undifferentiated HSMM, eRMS and aRMS cells showed low dye uptake incidence. Surprisingly, PANX1 expression did not induce dye uptake in eRMS nor aRMS cells (Fig. 2.6A). As a control, the PANX1 construct used to generate the stable RMS cell lines was transfected into HEK293T cells, which have been utilized in many studies examining Panx1 channel activity (Penuela et al., 2007, 2009; Sandilos et al., 2012), and showed a significant elevation of dye uptake compared to GFP-expressing cells (Fig. 2.6A). In order to eliminate the possibility that the lack of dye uptake by PANX1 in RMS cells was due to an

absence of its localization at the plasma membrane, cell surface biotinylation assays were performed. Ectopic PANX1 was found at the cell surface of both eRMS and aRMS cells (Fig. 2.6B). Based on these findings, we hypothesized that the PANX1 tumor suppressive effects are independent of its channel function. eRMS and aRMS cells were thus subjected to a BrdU incorporation assay in the presence or absence of the PANX1 channel blocker carbenoxolone (CBX) and the specific mimetic peptide inhibitor of PANX1, 10PANX. Similar to our previous findings, the vehicle- or scramble (Scr) peptide-treated PANX1-expressing eRMS (Fig. 2.6C) and aRMS (Fig. 2.6D) exhibited significantly reduced cell proliferation compared to their respective control cells. However, this PANX1-mediated effect was not altered by CBX or 10PANX (Fig. 2.6C-D). Similarly, the significant reduction of cell migration mediated by PANX1 was not affected or reversed by the inhibitors in both eRMS (Fig. 2.6E) and aRMS (Fig. 2.6F) cells. Taken together, these data suggest that the PANX1-mediated tumor suppressive effects in RMS are independent from its canonical channel activity.

Characterization of Channel Deficient PANX1 Mutants

In order to confirm these data, we sought to generate PANX1 mutants that constitutively lack channel activity. Bunse and colleagues showed that substitution of a single cysteine residue with serine at amino acid positions 66, 84 and 264 resulted in complete loss of Panx1 channel function (Bunse et al., 2011). We thus mutated the corresponding cysteine residues at position 66, 84, and 265 of human PANX1 to generate the C66S, C84S, and C265S mutants, respectively. When expressed in HEK293T cells, similar to PANX1, all three mutants exhibit multiple bands by Western blot (Fig. 2.7A) known as the core unglycosylated protein (Gly0), a high mannose-glycosylated species associated with the ER (Gly1), and the extensively glycosylated species (Gly2) that is modified in the Golgi apparatus and then

traffics to the plasma membrane (Boassa et al., 2007; Penuela et al., 2007, 2009). The C66S, C84S, and C265S mutants displayed a slight enrichment in the Gly1 species expression when compared to PANX1. As opposed to wild-type PANX1, all three mutants exhibited dramatically reduced dye uptake incidence following mechanical stimulation when expressed in HEK293T cells (Fig. 2.7B). Similar results were obtained when high (50 mM) potassium medium was used to activate PANX1 channels (data not shown) (Silverman et al., 2009). In order to examine their localization, PANX1 and the C66S, C84S, and C265S mutants were co-labeled with Golgi apparatus and endoplasmic reticulum (ER) markers in HEK293T cells. As shown in Fig. 2.7C, there was no evident co-localization of PANX1, or the PANX1 mutants, with the Golgi apparatus marker GM130. However, a proportion of the intracellular pool of both PANX1 and the PANX1 mutants was found co-localized with the ER marker calnexin (Fig. 2.7C; arrows). In order to quantify PANX1 mutants at the cell surface of HEK293T cells and eliminate the possibility that the lack of dye uptake by PANX1 mutants was due to reduced or absence of localization at the plasma membrane, cell surface biotinylation assays were performed. As shown in Figure 2.7D-F, ectopic PANX1 and all three PANX1 mutants were found at the plasma membrane as approximately 3-5% of their total expression was detected at the cell surface (Fig. 2.7E). Their absolute levels at the plasma membrane were also similar (Fig. 2.7F). Together, our results suggest that similar to PANX1, all three PANX1 mutants are localized in the ER and at the cell surface of HEK293T cells. However, unlike PANX1, the C66S, C84S, and C265S mutants exhibit deficient channel function.

PANX1 Mutants Reduce RMS Malignant Properties despite being Deficient in Channel Function

After having established that the C66S, C84S, and C265S PANX1 mutants are deficient in channel function, we next wanted to utilize these constructs to assess their potential at alleviating RMS malignant properties. When expressed in eRMS (Fig. 2.8A) and aRMS (Fig. 2.8B) cells, all three mutants were similar to the wild-type protein as the Gly0, Gly1, and Gly2 species could be detected. However, Gly1 was the main species expressed for the PANX1 mutants likely reflecting intracellular localization in the ER. Similar to wild-type PANX1, all three mutants were incapable of dye uptake following mechanical stimulation in eRMS (Fig. 2.8A) and aRMS (Fig. 2.8B) cells. To determine whether these PANX1 mutants could reduce RMS malignant properties, stable Rh18 (eRMS) and Rh30 (aRMS) cell lines expressing the C66S, C84S, or C265S mutant under the cumate switch system were submitted to 3D spheroid assays. Remarkably, expression of C66S, C84S, and C265S mutants inhibited the formation of eRMS and aRMS spheroids (Fig. 2.8C) and induced their regression (Fig. 2.8D) to the same extent as wild-type PANX1, relative to controls. To strengthen our findings, cumate-treated Rh30 cells, representing the most aggressive RMS subtype, expressing the GFP vector or the C265S mutant were injected into mice gastrocnemius muscles and kept under cumate-inducing conditions. While the volume of control tumors increased rapidly, the C265S-expressing aRMS xenografts grew significantly slower (Fig. 2.8E). Similar to wild-type PANX1, expression of the C265S mutant lead to ~50% reduction in tumour volume at endpoint (Fig. 2.8F). Collectively, our findings indicate that PANX1 mutants reduce RMS malignant properties *in vitro* and *in vivo* despite being deficient in channel function.

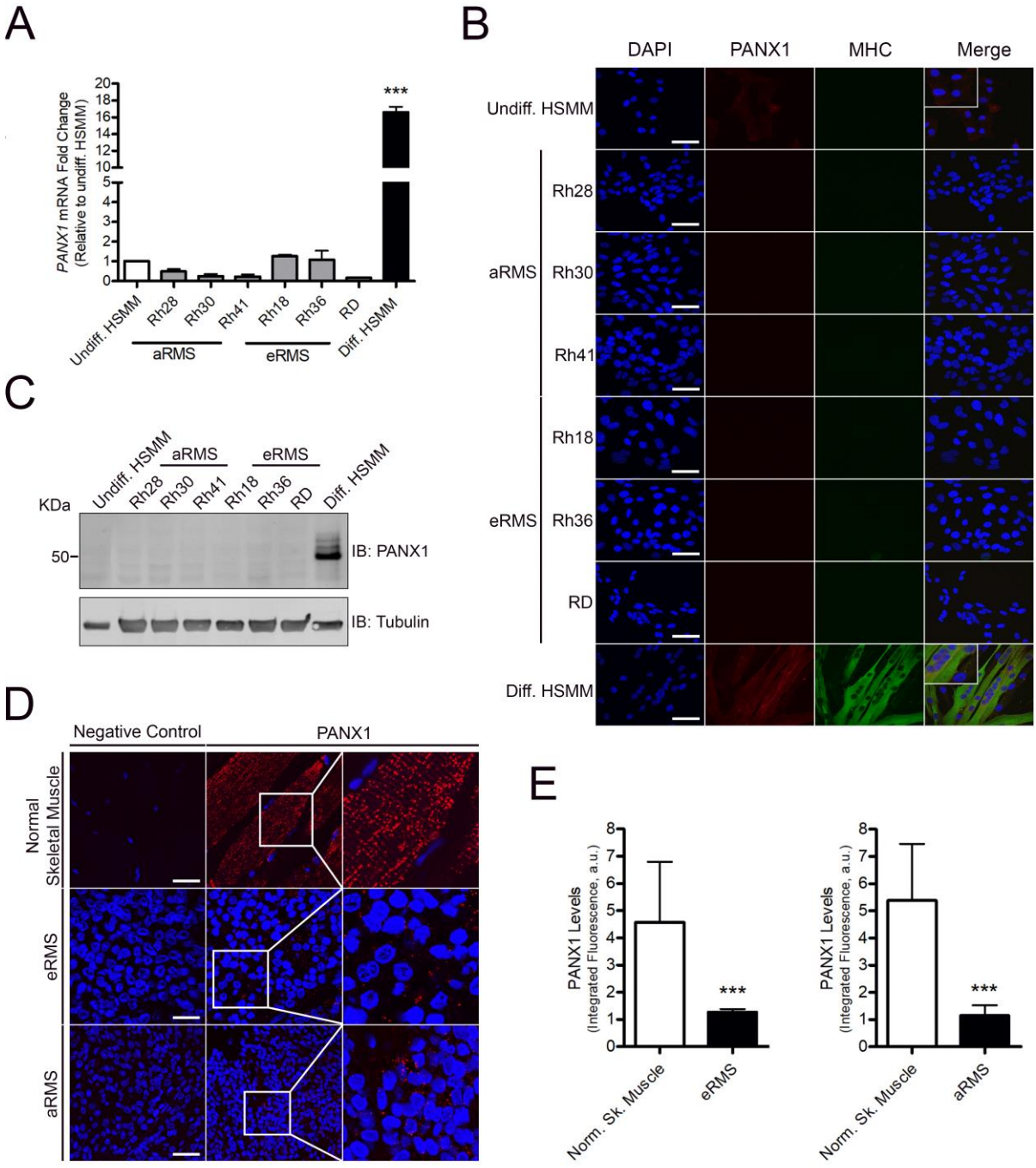
A
PANX1 mRNA Fold Change (Relative to undiff. HSMM)
***
Undiff. HSMM
Rh28
Rh30
Rh41
Rh18
Rh36
RD
Diff. HSMM
aRMS
eRMS
B
DAPI
PANX1
MHC
Merge
Undiff. HSMM
aRMS
eRMS
Rh28
Rh30
Rh41
Rh18
Rh36
RD
Diff. HSMM
C
KDa
50
IB: PANX1
IB: Tubulin
D
Negative Control
PANX1
Normal Skeletal Muscle
eRMS
aRMS
E
PANX1 Levels (Integrated Fluorescence, a.u.)
***
Norm. Sk. Muscle
eRMS
aRMS

Figure 2.1 PANX1 is Down-Regulated in Human eRMS and aRMS.

(A) RT-qPCR analysis, **(B)** immunofluorescent labeling (PANX1, red), and **(C)** Western blot of six patient-derived RMS cell lines (3 aRMS and 3 eRMS), undifferentiated (Undiff.) and differentiated (Diff.) human skeletal muscle myoblasts (HSMM) revealed that PANX1 transcript and protein levels are down-regulated when compared to differentiated HSMM. Myosin heavy chain (MHC, green) was used as a marker for myogenic differentiation. Tubulin was used as a loading control. *** $P<0.001$ compared to differentiated HSMM. Results are expressed as mean ± s.d. **(D)** Representative images of human RMS primary tumors and normal skeletal muscle from formalin-fixed, paraffin-embedded sections were immunolabeled for PANX1 (red), which was quantified in **(E)**. The negative control, without primary antibodies, confirmed labeling specificity. *** $P<0.001$ compared to normal skeletal muscle. Results are expressed as mean ± s.d. Blue = nuclei, Bars = 30 μm.

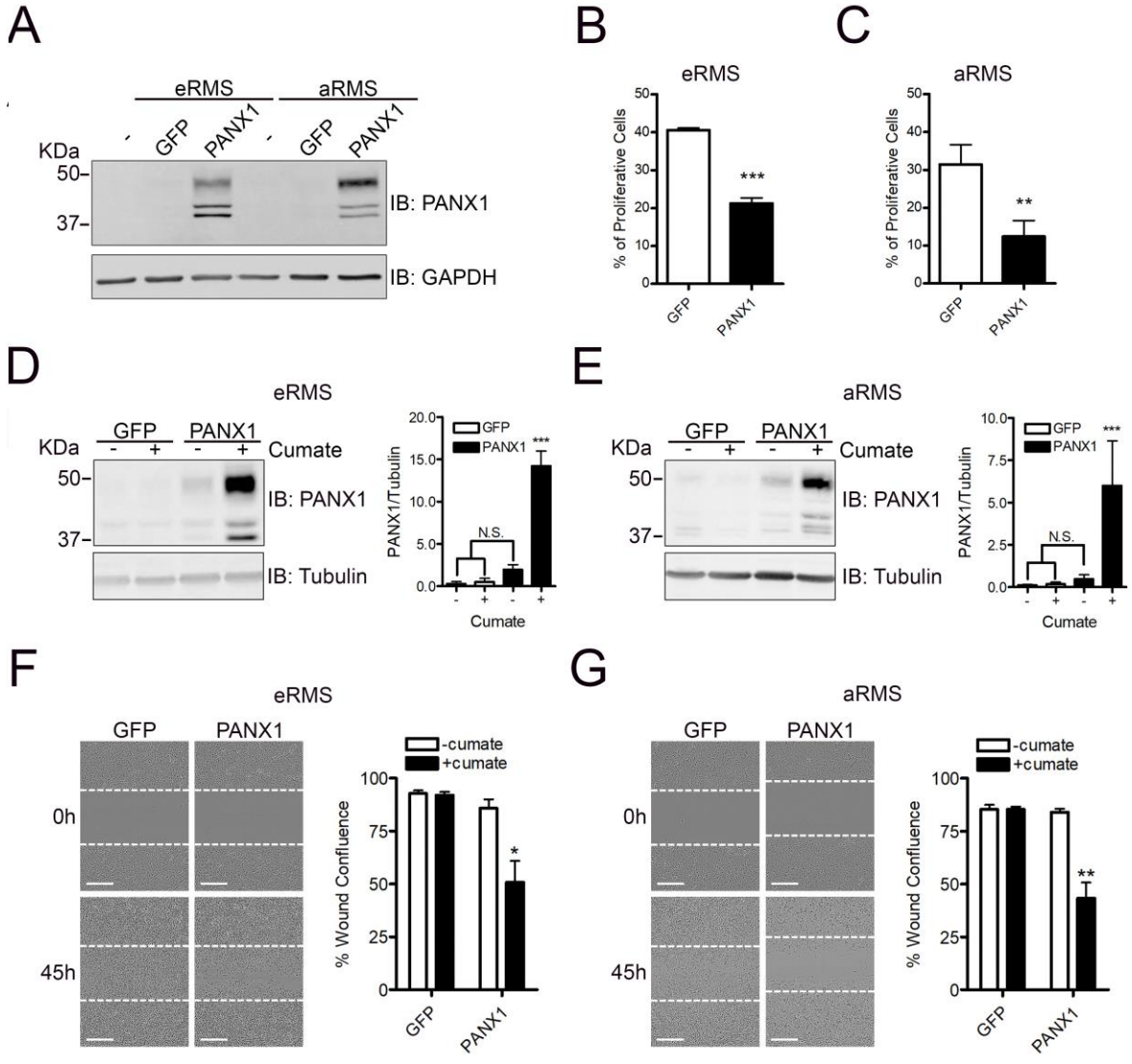
A
eRMS
aRMS
-
GFP
PANX1
-
GFP
PANX1
KDa
50
37
IB: PANX1
IB: GAPDH
B
eRMS
% of Proliferative Cells
***
GFP
PANX1
C
aRMS
% of Proliferative Cells
**
GFP
PANX1
D
eRMS
GFP
PANX1
KDa
Cumate
50
37
IB: PANX1
IB: Tubulin
PANX1/Tubulin
GFP
PANX1
***
N.S.
Cumate
E
aRMS
GFP
PANX1
KDa
Cumate
50
37
IB: PANX1
IB: Tubulin
PANX1/Tubulin
GFP
PANX1
***
N.S.
Cumate
F
eRMS
GFP
PANX1
0h
45h
-cumate
+cumate
% Wound Confluence
*
GFP
PANX1
G
aRMS
GFP
PANX1
0h
45h
-cumate
+cumate
% Wound Confluence
**
GFP
PANX1

Figure 2.2 PANX1 Expression Inhibits RMS Cell Proliferation and Migration.

eRMS (Rh18) and aRMS (Rh30) cells ectopically expressing PANX1 were analyzed by BrdU incorporation and scratch wound migration assays. **(A)** Representative Western blot of eRMS (Rh18) and aRMS (Rh30) cells transiently transfected with PANX1. GAPDH was used as a loading control. BrdU incorporation assay showed a significant reduction of proliferation in eRMS (Rh18) **(B)** and aRMS (Rh30) **(C)** cells over-expressing PANX1. *** $P<0.001$ and ** $P<0.01$ compared to GFP. Western blot analysis and quantification of eRMS (Rh18) **(D)** and aRMS (Rh30) **(E)** inducible stable cells over-expressing PANX1 after treatment with 30 µg/mL cumate for 24h. Tubulin was used as loading control. *** $P<0.001$ compared to GFP without cumate, GFP with cumate and PANX1 without cumate. N.S.: not significant. Representative pictures and quantification of stable eRMS (Rh18) **(F)** and aRMS (Rh30) **(G)** cells, treated with or without cumate to induce PANX1 over-expression, subjected to scratch wound assay for 45 hours. The dotted lines show cell boundaries after initial scratch. The confluence of the wound areas was quantified 45h post wounding, which showed a significant reduction in cumate-treated PANX1 over-expressing stable eRMS (Rh18) **(F)** and aRMS (Rh30) **(G)** compared to their respective controls. ** $P<0.01$, * $P<0.05$ compared to GFP without cumate, GFP with cumate, and PANX1 without cumate. Results are expressed as mean ± s.d. Bars = 300 µm.

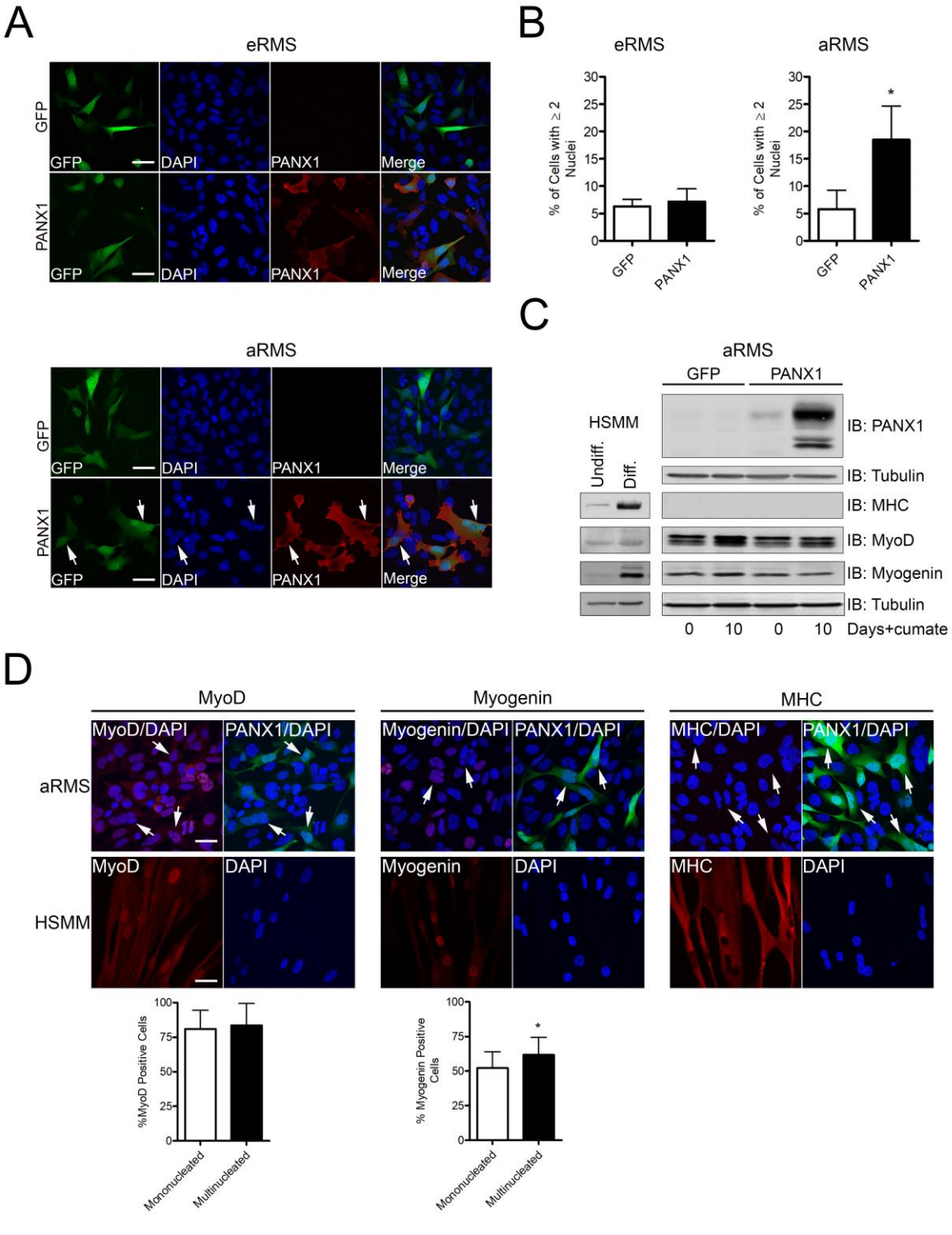
A
eRMS
GFP
PANX1
GFP
DAPI
PANX1
Merge
aRMS
B
eRMS
aRMS
% of Cells with ≥ 2 Nuclei
GFP
PANX1
C
aRMS
GFP
PANX1
HSMM
Undiff.
Diff.
IB: PANX1
IB: Tubulin
IB: MHC
IB: MyoD
IB: Myogenin
IB: Tubulin
0
10
0
10
Days+cumate
D
MyoD
Myogenin
MHC
aRMS
HSMM
MyoD/DAPI
PANX1/DAPI
Myogenin/DAPI
MHC/DAPI
MyoD
Myogenin
MHC
DAPI
%MyoD Positive Cells
% Myogenin Positive Cells
Mononucleated
Multinucleated

Figure 2.3 PANX1 Expression does not Trigger RMS Cell Terminal Differentiation.

(A) PANX1 (red) immunofluorescence labeling of eRMS (Rh18) and aRMS (Rh30) transfected with PANX1 or the control vector GFP. While no morphological changes were observed in eRMS cells, a population of PANX1 over-expressing aRMS cells was multinucleated (arrows). Blue = nuclei, Bars = 20 μm. **(B)** Quantification of multinucleation (% of cells with ≥ 2 nuclei) of aRMS (Rh30) cells showed a significant increase with PANX1 over-expression. * $P<0.05$ compared to GFP. **(C)** Cumate-inducible stable aRMS (Rh30) cells were cultured in growth media with 30 μg/mL cumate for 10 days, and analyzed for MHC, MyoD, and myogenin levels. Cells were collected for analysis immediately prior to cumate treatment on Day 0. Undifferentiated and differentiated HSMM were used as myogenic marker controls. Tubulin was used as a loading control. **(D)** Representative immunofluorescence images of aRMS (Rh30) cells transfected with PANX1 and labeled with MyoD, myogenin, or MHC (red). Cells transfected with PANX1 (GFP-positive) are shown in green. Differentiated HSMM were used as positive controls. The percentage of mono- and multinucleated (arrows) PANX1-expressing cells positive for MyoD, myogenin and MHC were quantified in a double-blinded manner. * $P<0.05$ compared to mononucleated cells. Bars = 20 μm. Results are expressed as mean ± s.d.

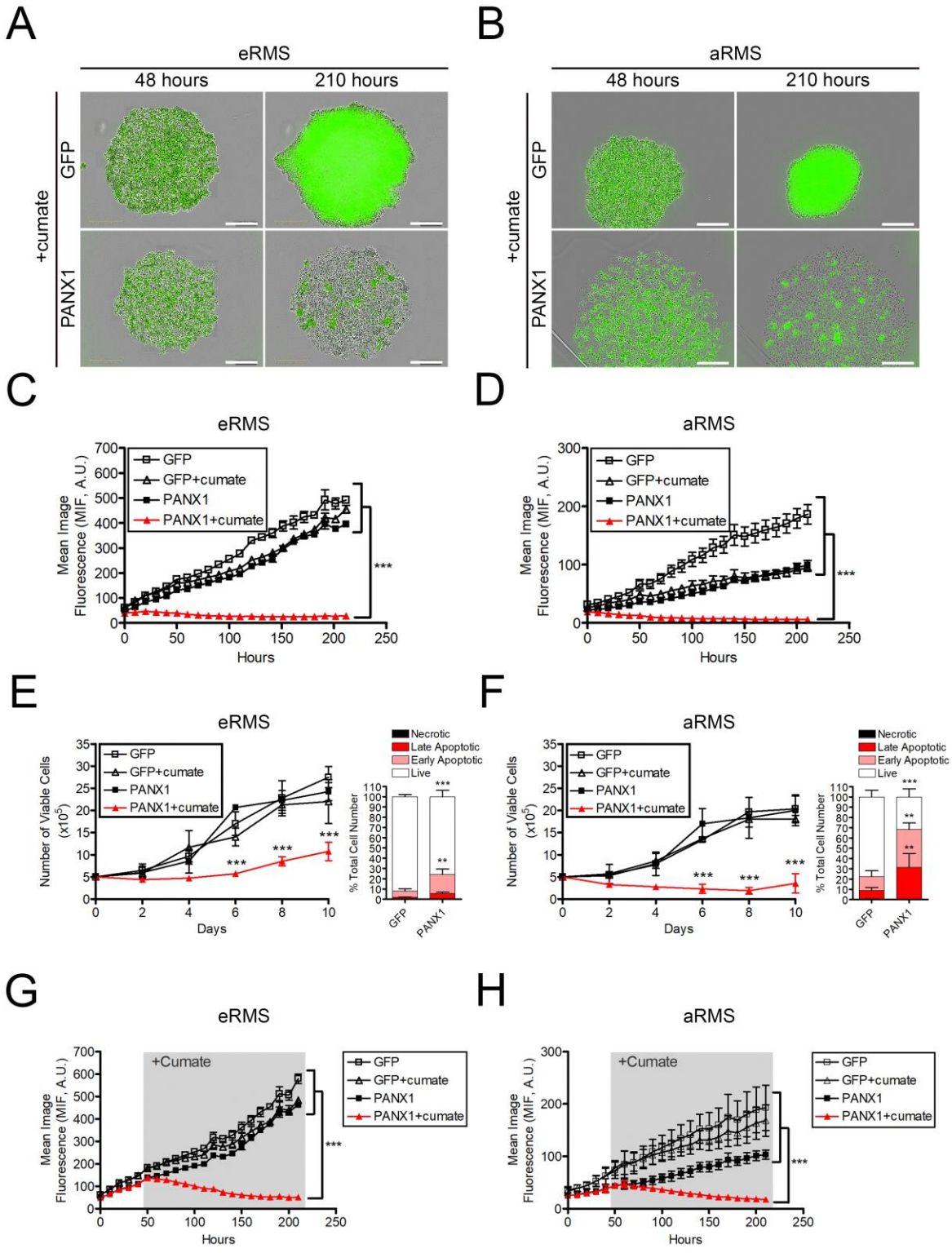
A
eRMS
48 hours
210 hours
+cumate
GFP
PANX1
B
aRMS
48 hours
210 hours
+cumate
GFP
PANX1
C
eRMS
Mean Image Fluorescence (MIF, A.U.)
GFP
GFP+cumate
PANX1
PANX1+cumate
***
Hours
D
aRMS
Mean Image Fluorescence (MIF, A.U.)
GFP
GFP+cumate
PANX1
PANX1+cumate
***
Hours
E
eRMS
Number of Viable Cells (x10^5)
GFP
GFP+cumate
PANX1
PANX1+cumate
***
Days
% Total Cell Number
Necrotic
Late Apoptotic
Early Apoptotic
Live
***
**
GFP
PANX1
F
aRMS
Number of Viable Cells (x10^5)
GFP
GFP+cumate
PANX1
PANX1+cumate
***
Days
% Total Cell Number
Necrotic
Late Apoptotic
Early Apoptotic
Live
***
**
GFP
PANX1
G
eRMS
Mean Image Fluorescence (MIF, A.U.)
+Cumate
GFP
GFP+cumate
PANX1
PANX1+cumate
***
Hours
H
aRMS
Mean Image Fluorescence (MIF, A.U.)
+Cumate
GFP
GFP+cumate
PANX1
PANX1+cumate
***
Hours

Figure 2.4 PANX1 Expression Blocked Formation and Induced Regression of 3D RMS Spheroids through Induction of Cell Apoptosis.

Stable eRMS (Rh18) and aRMS (Rh30) cells were pre-treated and maintained with 30 µg/mL cumate to induce PANX1 expression and 3D spheroid formation was monitored over 210 hours. Representative images taken at 48 and 210 hours clearly show that over-expression of PANX1 prevented eRMS (Rh18) **(A)** and aRMS (Rh30) **(B)** spheroid formation. Mean image fluorescence (MIF), a surrogate measurement for spheroid size, was measured over time for both eRMS (Rh18) **(C)** and aRMS (Rh30) **(D)** cells. A.U.: arbitrary units. Bars = 1000 µm. The viability of stable eRMS (Rh18) **(E; left panel)** and aRMS (Rh30) **(F; left panel)** cells grown in suspension on agar for 10 days in the absence or presence of cumate was assessed every 2 days. Viable cell counts showed a significantly reduced number of viable cells within cumate-induced PANX1 RMS spheroids. *** $P<0.001$ compared to untreated GFP cells, GFP cells treated with cumate, and untreated PANX1 cells. After being grown in suspension for 4 days, live (Annexin V-, 7-AAD-), early apoptotic (Annexin V+, 7-AAD-), late apoptotic (Annexin V+, 7-AAD+) and necrotic (Annexin V-, 7-AAD+) cell populations were quantified as percentages of the total cell population and revealed a significant increase in apoptotic cell populations within PANX1 over-expressing eRMS (Rh18) **(E; right panel)** and aRMS (Rh30) **(F; right panel)** spheroids. *** $P<0.001$, ** $P<0.01$ compared to respective control cells expressing GFP. Results are expressed as mean ± s.d. In the spheroid regression assay, stable eRMS (Rh18) and aRMS (Rh30) cells were first allowed to form spheroids for 48 hours before being treated with cumate to induce PANX1 expression. Spheroid growth was monitored for a total of 210 hours. While the mean image fluorescence (MIF) of control stable eRMS (Rh18) **(G)** and aRMS (Rh30) **(H)** spheroids progressively increased over time, a continuous and

significant decrease of MIF was measured upon PANX1 expression. *** P<0.001 compared to untreated GFP cells, GFP cells treated with cumate, and untreated PANX1 cells. Results are expressed as mean ± s.d. A.U.: arbitrary units. Bars = 1000 μm.

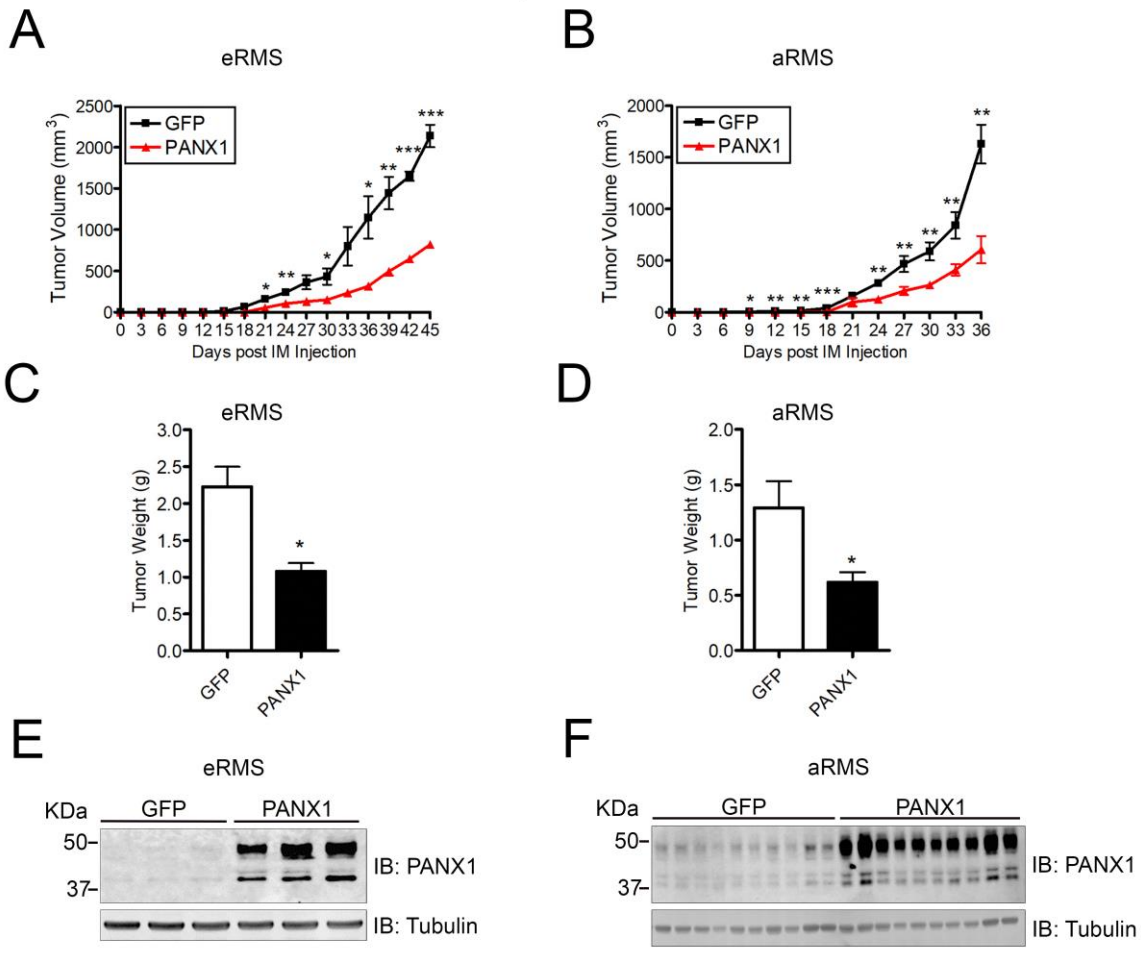
A
eRMS
Tumor Volume (mm3)
GFP
PANX1
Days post IM Injection
B
aRMS
Tumor Volume (mm3)
GFP
PANX1
Days post IM Injection
C
eRMS
Tumor Weight (g)
GFP
PANX1
D
aRMS
Tumor Weight (g)
GFP
PANX1
E
eRMS
KDa
GFP
PANX1
50–
37–
IB: PANX1
IB: Tubulin
F
aRMS
KDa
GFP
PANX1
50–
37–
IB: PANX1
IB: Tubulin

Figure 2.5 Expression of PANX1 Decreases RMS Tumor Growth *in vivo*.

Stable GFP control and PANX1 over-expressing eRMS (Rh18) and aRMS (Rh30) cells were injected orthotopically into the left and right gastrocnemius of the mice (mice randomly assigned, not a blinded method). PANX1 expression was maintained by intraperitoneal injection of cumate every 3 days. PANX1 over-expression in eRMS (Rh18) **(A)** and aRMS (Rh30) **(B)** cells led to a significantly reduced growth rate compared to their respective GFP controls. At endpoint, PANX1-expressing eRMS (Rh18) **(C)** and aRMS (Rh30) **(D)** xenografts weighted significantly less than the control tumors. Day 0 denotes the day of cell intramuscular (IM) injection. * $P<0.05$, ** $P<0.01$, *** $P<0.001$ compared to GFP. Results are expressed as mean ± s.d. Western blots of eRMS (Rh18) **(E)** and aRMS (Rh30) **(F)** xenografts demonstrate successful induction of PANX1 by cumate *in vivo*. Tubulin was used as loading control.

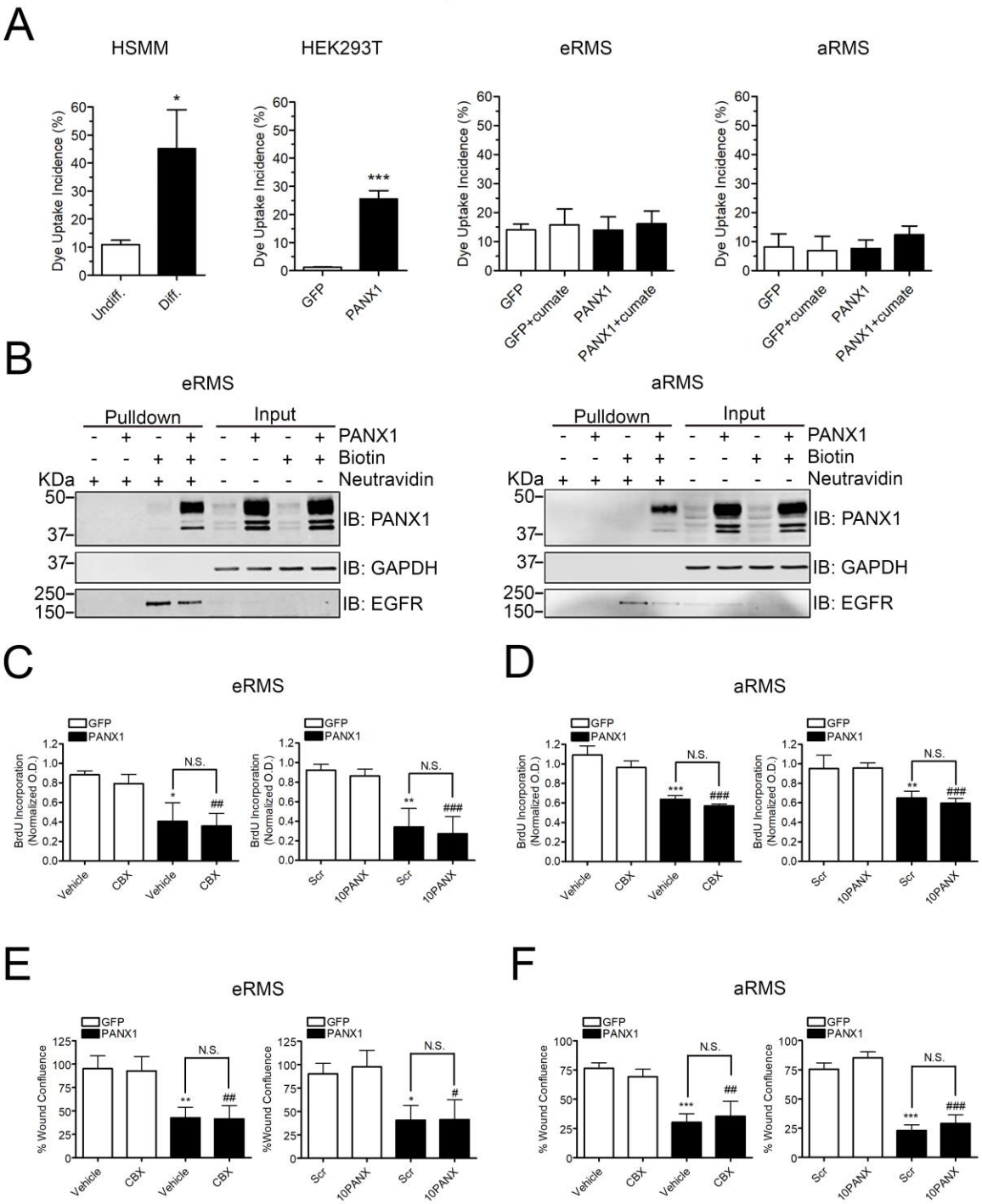
A
HSMM
HEK293T
eRMS
aRMS
Dye Uptake Incidence (%)
Undiff.
Diff.
GFP
PANX1
GFP+cumate
PANX1+cumate
B
eRMS
aRMS
Pulldown
Input
PANX1
Biotin
Neutravidin
KDa
IB: PANX1
IB: GAPDH
IB: EGFR
C
D
eRMS
aRMS
BrdU Incorporation (Normalized O.D.)
N.S.
Vehicle
CBX
Scr
10PANX
E
F
% Wound Confluence

Figure 2.6 PANX1 is Incapable of Dye Uptake in Rh18 and Rh30 Cells and its Tumor Suppressive Functions are not Reduced by PANX1 Channel Inhibitors.

(A) PANX1 expression did not augment dye uptake incidence in eRMS (Rh18) and aRMS (Rh30) cells following mechanical stimulation. By contrast, differentiated (Diff.) HSMM, which express high endogenous levels of PANX1 displayed a significant increase of dye uptake, as compared to undifferentiated (Undiff.) HSMM, which express low PANX1 levels. HEK293T cells were used as a positive control for ectopic PANX1 expression using the same construct that was utilized to engineer the stable eRMS (Rh18) and aRMS (Rh30) cell lines. HSMM: * $P<0.05$ compared to Undiff.; HEK293T: *** $P<0.001$ compared to GFP. Results are expressed as mean ± s.d. **(B)** Western blot analysis of cell surface biotinylation assays showing localization of PANX1 in the plasma membrane fraction of both eRMS (Rh18) and aRMS (Rh30) cells. GAPDH was used as a marker for cytosolic proteins, while EGFR (epidermal growth factor receptor) was used as a marker for plasma membrane proteins. eRMS (Rh18) and aRMS (Rh30) stable cells expressing PANX1 or control GFP vector were incubated for 48 hours with either CBX (100 μM) or 10PANX (200 μM) and subjected to BrdU assays. As shown earlier, PANX1 expression resulted in a significant reduction of eRMS **(C)** and aRMS **(D)** cell proliferation, which remained unchanged when treated by CBX and 10PANX compared to the vehicle DMSO control or the scramble (Scr) peptide. Normalized optical density (O.D.) was calculated compared to that of the respective untreated GFP control cells. eRMS (Rh18) and aRMS (Rh30) stable cells expressing PANX1 or control GFP vector were subjected to a scratch wound assay in the presence or absence of CBX (100 μM) and 10PANX (200 μM). The percent wound confluence was calculated 45 hours post-scratch using the IncuCyte Analysis System. The reduction of wound confluence induced by PANX1

expression was not altered by CBX nor 10PANX compared to their respective controls in both eRMS (Rh18) **(E)** and aRMS (Rh30) **(F)** cells. * P<0.05, ** P<0.01 and *** P<0.001 compared to GFP vehicle or GFP Scr controls. ##P<0.01 and ###P<0.001 compared to CBX- or 10PANX-treated GFP controls. N.S.: not significant. Results are expressed as mean ± s.d.

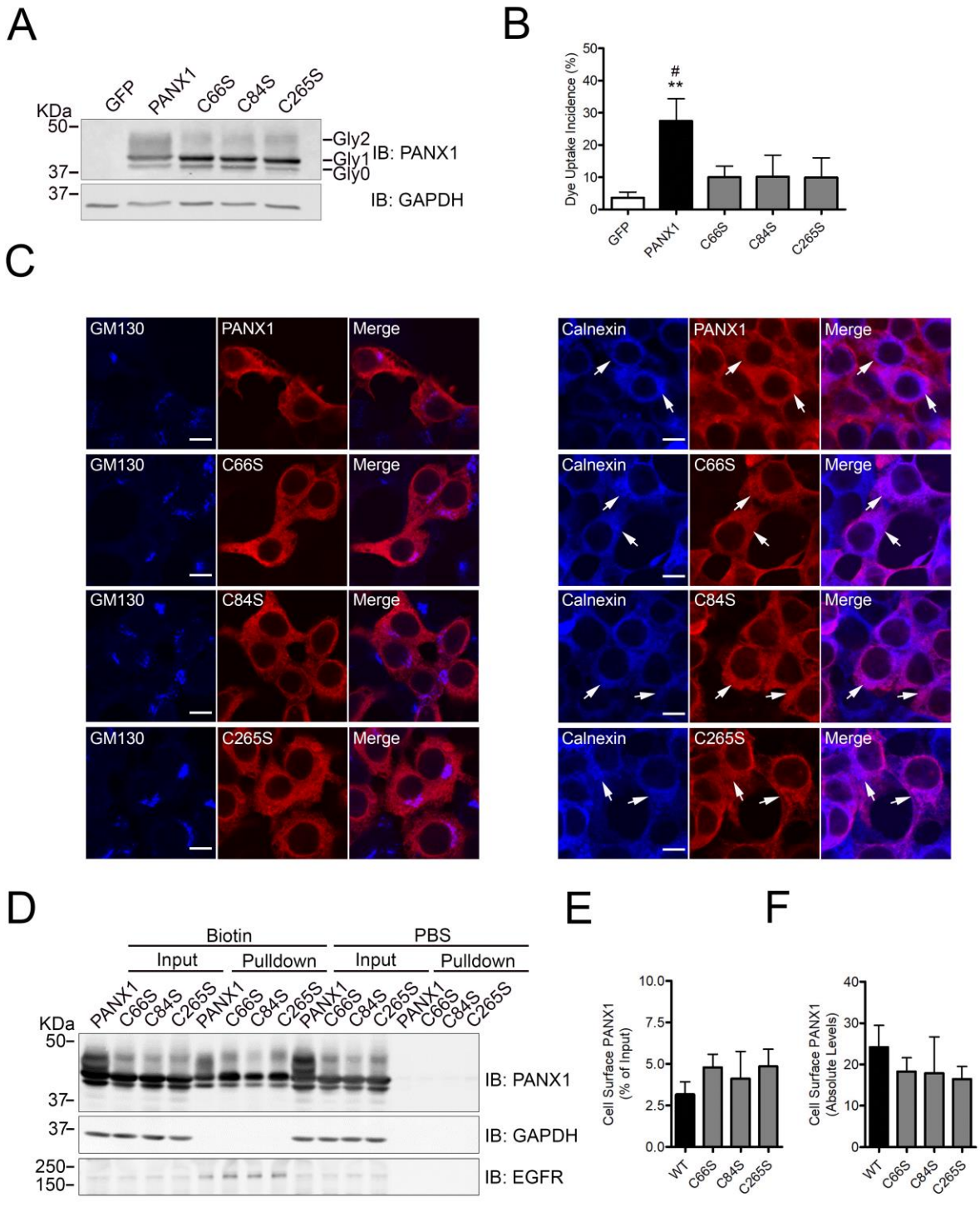
A
KDa
GFP
PANX1
C66S
C84S
C265S
50
37
37
Gly2
Gly1
Gly0
IB: PANX1
IB: GAPDH
B
Dye Uptake Incidence (%)
#
**
GFP
PANX1
C66S
C84S
C265S
C
GM130
PANX1
Merge
C66S
C84S
C265S
Calnexin
D
Biotin
PBS
Input
Pulldown
IB: PANX1
IB: GAPDH
IB: EGFR
250
150
E
Cell Surface PANX1 (% of Input)
F
Cell Surface PANX1 (Absolute Levels)
WT

Figure 2.7 C66S, C84S, and C265S PANX1 Mutants are Channel Deficient.

(A) Western blot of C66S, C84S, and C265S PANX1 mutants show banding patterns similar to wild-type PANX1 in HEK293T cells. The Gly0, Gly1, and Gly2 species of PANX1 are indicated. GAPDH was used as a loading control. **(B)** Expression of C66S, C84S, and C265S mutants in HEK293T cells did not increase dye uptake incidence, unlike wild-type PANX1 expressing cells. ** $P<0.001$ compared to GFP, # $P<0.01$ compared to C66S, C84S and C265S. **(C)** HEK293T cells were transfected with PANX1, C66S, C84S and C265S constructs. The cells were then co-labeled for PANX1 (red) together with GM130 (Golgi apparatus marker) or calnexin (ER marker) in blue. Representative images show some co-localization (arrows) of PANX1 and the three mutants with calnexin. Bars = 8 μm. **(D)** Cell surface biotinylation experiments demonstrate that PANX1, as well as all three PANX1 mutants are detected at the plasma membrane of HEK293T cells. GAPDH was used as a marker for cytosolic proteins, while EGFR was used as a marker for membrane proteins. Densitometric analysis and quantification of cell surface biotinylation experiments show that all three mutants are localized at the cell surface in the same amount as PANX1. Cell surface expression was calculated relative to the total protein in input lanes **(E)** and was also calculated as absolute protein levels in the pulldown lanes **(F)**.

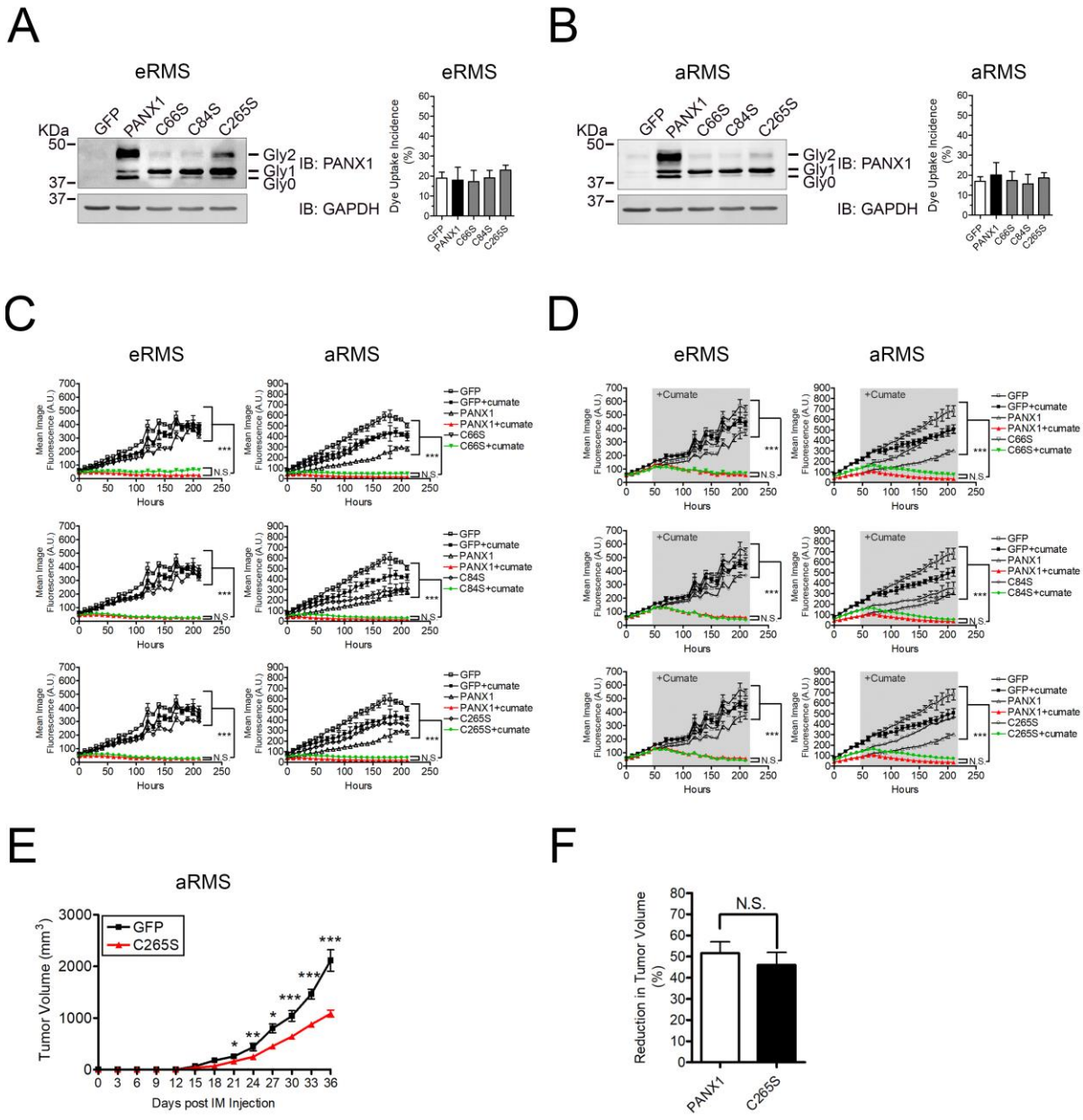
A
eRMS
KDa
GFP
PANX1
C66S
C84S
C265S
50
37
37
Gly2
Gly1
Gly0
IB: PANX1
IB: GAPDH
eRMS
Dye Uptake Incidence (%)
B
aRMS
aRMS
C
eRMS
aRMS
Mean Image Fluorescence (A.U.)
Hours
GFP
GFP+cumate
PANX1
PANX1+cumate
C66S
C66S+cumate
C84S
C84S+cumate
C265S
C265S+cumate
***
N.S
D
+Cumate
E
aRMS
Tumor Volume (mm3)
Days post IM Injection
F
Reduction in Tumor Volume (%)
N.S.
PANX1
C265S

Figure 2.8 Channel Defective PANX1 Mutants Reduce RMS Tumor Growth.

Western blot of C66S, C84S, and C265S PANX1 mutants compared to wild-type PANX1 in eRMS (Rh18) **(A)** and aRMS (Rh30) cells **(B)**. The Gly0, Gly1, and Gly2 species of PANX1 are indicated. GAPDH was used as a loading control. Similar to wild-type PANX1 expressing cells, no increase in dye uptake was observed when C66S, C84S, and C265S mutants were expressed in eRMS (Rh18) **(A)** and aRMS (Rh30) cells **(B)**. 3D spheroid formation **(C)** and regression **(D)** assays described previously were performed using inducible eRMS (Rh18) and aRMS (Rh30) stable cell lines expressing either the C66S, C84S, or C265S PANX1 mutant and compared to cells expressing wild-type PANX1, as well as to GFP control cells. In both eRMS and aRMS cells, expression of PANX1 mutants inhibited formation of 3D spheroids **(C)** and caused their regression **(D)** similar to wild-type PANX1. *** $P<0.001$ compared GFP; GFP treated with cumate; PANX1; and C66S or C84S or C265S mutant. N.S.: not significant. aRMS (Rh30) cells over-expressing the C265S mutant or the GFP control vector were injected orthotopically into the left and right gastrocnemius of the mice, respectively. Intraperitoneal injection of cumate was performed every 3 days. Expression of the C265S mutant significantly reduced aRMS xenograft growth rate **(E)**. Expression of PANX1 and the C265S mutant both resulted in a diminution of ~50% in tumor volume when compared to control xenografts **(F)**. N.S.: not significant. Day 0 denotes the day of intramuscular (IM) cell injection. * $P<0.05$, ** $P<0.01$, *** $P<0.001$ compared to GFP. Results are expressed as mean ± s.d.

2.6 DISCUSSION

Given that RMS arises from skeletal muscle progenitor cells lacking the ability to terminally differentiate, we demonstrate here, using a panel of patient-derived RMS cell lines and RMS tumor specimens, that PANX1 expression is down-regulated in eRMS and aRMS as compared to normal skeletal muscle cells and tissue. Our findings that PANX1 transcript and protein levels in RMS cells were comparable to that of proliferative and undifferentiated skeletal muscle myoblasts suggested that the down-regulation of PANX1 may be involved in the malignant phenotype of RMS. Our complementary data revealed that ectopic expression of PANX1 significantly reduced RMS malignant properties *in vitro* and *in* vivo. Importantly, this effect was consistent between eRMS and aRMS despite their heterogeneous background of genetic alterations. Altogether the data presented here constitute the first evidence of PANX1 tumor suppressive functions in human cancer and suggest that increasing PANX1 levels would be a novel therapeutic approach for RMS.

Surprisingly, ectopic PANX1 was incapable of dye uptake when expressed in eRMS (Rh18) and aRMS (Rh30) cells. While Panx1 is thought to form channels only on the plasma membrane (Chiu et al., 2018), Panx1 channels localized in the ER have been suggested to contribute to ER Ca^{2+} leakage (Vanden Abeele et al., 2006). However, no differences in intracellular Ca^{2+} concentration have been detected in Rh30 and Rh18 cells over-expressing PANX1 compared to control cells when assessed by flow cytometry using the Fura-2 calcium indicator (data not shown). Based on our current knowledge of PANX1 channels, these data suggest that ectopic PANX1 does not form functional channels in RMS. While the possibility remains that non-canonical PANX1 channel activity was not detected or that mechanical stimulation may not be an activator of PANX1 channels in these cells, treatment with CBX

and 10PANX failed to reverse or alter the PANX1-mediated reduction in eRMS and aRMS cell proliferation and migration. Furthermore, PANX1 mutations causing deficient channel function did not affect PANX1's ability to prevent the formation and growth of eRMS and aRMS 3D spheroids and induce their regression. Notably, the C265S PANX1 mutant also had the ability to reduce RMS tumor growth *in vivo*. Collectively, these complementary approaches suggest that PANX1 tumor suppressive function in RMS involves a mechanism independent of its canonical channel activity.

In skeletal muscle myoblasts, we have shown that PANX1 induces differentiation through a channel-dependent process given that myogenic fusion and differentiation were inhibited by probenecid and CBX (Langlois et al., 2014). It has been documented that myogenic differentiation involves the release of ATP, activation of purinergic receptors, and rise of intracellular Ca^{2+} levels (Araya et al., 2004; Ryten et al., 2004). Furthermore, Panx1 channels mediate the acquisition of myogenic commitment and increased MyoD levels in C_2C_{12} reserve cells through a mechanism that involves ATP release and purinergic receptor activation (Riquelme et al., 2015). Together, these data suggest that ATP released through PANX1 channels plays a pivotal role in its ability to promote myogenic differentiation. Consequently, the lack of channel activity at the cell surface exhibited by ectopic PANX1 in eRMS and aRMS may explain its inability to trigger their differentiation. Regardless, ectopic PANX1 had a potent inhibitory effect on several RMS malignant properties *in vitro*, which resulted in a significant reduction of tumor growth *in vivo.*

While Panx1 over-expression has been shown to reduce murine N2a cell proliferation *in vitro*, this process was reversed by probenecid (Wicki-Stordeur et al., 2012). Panx1 has also been shown to reduce the size of rat glioma aggregates. This process could be disrupted by CBX and rescued by exogenous ATP (Bao et al., 2012). Conversely, our data suggest that

PANX1 lacks its cell surface channel function in eRMS and aRMS cells and that its tumor-suppressive effects are mediated through a channel-independent mechanism. Thus, the non-canonical function by which PANX1 triggers inhibition of RMS proliferation, migration, and spheroid growth likely involves a novel molecular mechanism or signaling pathway. While the Panx1/PANX1 interactome has started to be tackled by several researchers and Panx1 protein interaction partners have been identified, the functional relevance of these interactions has either remained unknown or often linked to the modulation of Panx1 channel activity (examples: Panx2, P2X and P2X7 receptors, α-1D adrenergic receptor) (Wicki-Stordeur and Swayne, 2014). Of interest, some binding partners are involved in apoptosis such as caspase-1, caspase-11, and the inhibitor of apoptosis XIAP (X-linked inhibitor of apoptosis) (Penuela et al., 2013). In skeletal muscle cells, it has been demonstrated that Panx1 is part of a multiprotein complex that includes the dihydropyridine receptor (DHPR), P2Y2 receptor, as well as caveolin-3, and dystrophin (Arias-Calderón et al., 2016). Interestingly, deletions of the dystrophin gene (*DMD*) were found in RMS specimens and, similar to PANX1, dystrophin over-expression inhibited the invasiveness, migration, and anchorage-independent growth of the human metastatic eRMS cell line RMS176 *in vitro* (Wang et al., 2014).

Taken together, our results show that PANX1 is down-regulated in RMS and that restoration of its levels significantly reduced aRMS and eRMS malignant phenotypes *in vitro* and *in vivo*. Our findings also indicate that the tumor suppressive role of PANX1 does not require its canonical channel activity suggesting the existence of a novel, yet to be described, mechanism by which PANX1 functions. In order to understand the molecular mechanism by which PANX1 alleviates malignant properties in RMS, further analyses will be required to reveal the direct PANX1 interactors in these cells together with their downstream signaling pathways, which may also identify other potential new therapeutic targets. The comparison of

PANX1 direct interactors in RMS cells to that of skeletal muscle myoblasts may also enable a better understanding of the mechanisms activating and inhibiting PANX1 channels in physiologic and pathologic processes.

2.7 REFERENCES

Vanden Abeele, F., Bidaux, G., Gordienko, D., Beck, B., Panchin, Y. V., Baranova, A. V., Ivanov, D. V., Skryma, R., and Prevarskaya, N. (2006). Functional implications of calcium permeability of the channel formed by pannexin 1. J. Cell Biol. *174*, 535–546.

Araya, R., Riquelme, M.A., Brandan, E., and Sáez, J.C. (2004). The formation of skeletal muscle myotubes requires functional membrane receptors activated by extracellular ATP. Brain Res. Brain Res. Rev. *47*, 174–188.

Arias-Calderón, M., Almarza, G., Díaz-Vegas, A., Contreras-Ferrat, A., Valladares, D., Casas, M., Toledo, H., Jaimovich, E., and Buvinic, S. (2016). Characterization of a multiprotein complex involved in excitation-transcription coupling of skeletal muscle. Skelet. Muscle *6*, 15.

Aslam, M.I., Abraham, J., Mansoor, A., Druker, B.J., Tyner, J.W., and Keller, C. (2014). PDGFR-beta reverses EphB4 signaling in alveolar rhabdomyosarcoma. Proc. Natl. Acad. Sci. *111*, 6383–6388.

Bao, B.A., Lai, C.P., Naus, C.C., and Morgan, J.R. (2012). Pannexin1 drives multicellular aggregate compaction via a signaling cascade that remodels the actin cytoskeleton. J. Biol. Chem. *287*, 8407–8416.

Bao, L., Locovei, S., and Dahl, G. (2004). Pannexin membrane channels are mechanosensitive conduits for ATP. FEBS Lett. *572*, 65–68.

Boassa, D., Ambrosi, C., Qiu, F., Dahl, G., Gaietta, G., and Sosinsky, G. (2007). Pannexin1 channels contain a glycosylation site that targets the hexamer to the plasma membrane. J. Biol. Chem. *282*, 31733–31743.

Bunse, S., Schmidt, M., Hoffmann, S., Engelhardt, K., Zoidl, G., and Dermietzel, R. (2011). Single cysteines in the extracellular and transmembrane regions modulate Pannexin 1 channel function. J. Membr. Biol. *244*, 21–33.

Celetti, S.J., Cowan, K.N., Penuela, S., Shao, Q., Churko, J., and Laird, D.W. (2010). Implications of pannexin 1 and pannexin 3 for keratinocyte differentiation. J. Cell Sci. *123*, 1363–1372.

Chekeni, F.B., Elliott, M.R., Sandilos, J.K., Walk, S.F., Kinchen, J.M., Lazarowski, E.R., Armstrong, A.J., Penuela, S., Laird, D.W., Salvesen, G.S., et al. (2010). Pannexin 1 channels mediate 'find-me' signal release and membrane permeability during apoptosis. Nature *467*,

863–867.
Chiu, Y.H., Schappe, M.S., Desai, B.N., and Bayliss, D.A. (2018). Revisiting multimodal activation and channel properties of Pannexin 1. J. Gen. Physiol. *150*, 19–39.
Ciarapica, R., De Salvo, M., Carcarino, E., Bracaglia, G., Adesso, L., Leoncini, P.P., Dall'agnese, A., Walters, Z.S., Verginelli, F., De Sio, L., et al. (2014). The Polycomb group (PcG) protein EZH2 supports the survival of PAX3-FOXO1 alveolar rhabdomyosarcoma by repressing FBXO32 (Atrogin1/MAFbx). Oncogene *33*, 4173–4184.
Cowan, K.N., Langlois, S., Penuela, S., Cowan, B.J., and Laird, D.W. (2012). Pannexin1 and Pannexin3 exhibit distinct localization patterns in human skin appendages and are regulated during keratinocyte differentiation and carcinogenesis. Cell Commun. Adhes. *19*, 45–53.
Dobson, C.C., Langlois, S., Grynspan, D., and Cowan, K.N. (2016). Engaging Cell Death Pathways for the Treatment of Rhabdomyosarcoma. Crit. Rev. Oncog. *21*, 221–239.
Draganov, D., Gopalakrishna-Pillai, S., Chen, Y.-R., Zuckerman, N., Moeller, S., Wang, C., Ann, D., and Lee, P.P. (2015). Modulation of P2X4/P2X7/Pannexin-1 sensitivity to extracellular ATP via Ivermectin induces a non-apoptotic and inflammatory form of cancer cell death. Sci. Rep. *5*, 16222.
Egas-Bejar, D., and Huh, W.W. (2014). Rhabdomyosarcoma in adolescent and young adult patients: current perspectives. Adolesc. Health. Med. Ther. *5*, 115–125.
Furlow, P.W., Zhang, S., Soong, T.D., Halberg, N., Goodarzi, H., Mangrum, C., Wu, Y.G., Elemento, O., and Tavazoie, S.F. (2015). Mechanosensitive pannexin-1 channels mediate microvascular metastatic cell survival. Nat. Cell Biol. *7*, 943–952.
Hettmer, S., Li, Z., Billin, A.N., Barr, F.G., Cornelison, D.D.W., Ehrlich, A.R., Guttridge, D.C., Hayes-Jordan, A., Helman, L.J., Houghton, P.J., et al. (2014). Rhabdomyosarcoma: Current Challenges and Their Implications for Developing Therapies. Cold Spring Harb. Perspect. Med. *4*, a025650.
Keller, C., and Guttridge, D.C. (2013). Mechanisms of impaired differentiation in rhabdomyosarcoma. FEBS J. *280*, 4323–4334.
Lai, C.P.K., Bechberger, J.F., Thompson, R.J., MacVicar, B.A., Bruzzone, R., and Naus, C.C. (2007). Tumor-suppressive effects of pannexin 1 in C6 glioma cells. Cancer Res. *67*, 1545–1554.
Langlois, S., and Cowan, K.N. (2017). Regulation of Skeletal Muscle Myoblast

Differentiation and Proliferation by Pannexins. Adv. Exp. Med. Biol. *925*, 57–73.
Langlois, S., Cowan, K.N., Shao, Q., Cowan, B.J., and Laird, D.W. (2008). Caveolin-1 and -2 interact with connexin43 and regulate gap junctional intercellular communication in keratinocytes. Mol. Biol. Cell *19*, 912–928.
Langlois, S., Xiang, X., Young, K., Cowan, B.J., Penuela, S., and Cowan, K.N. (2014). Pannexin 1 and pannexin 3 channels regulate skeletal muscle myoblast proliferation and differentiation. J. Biol. Chem. *289*, 30717–30731.
Locovei, S., Wang, J., and Dahl, G. (2006a). Activation of pannexin 1 channels by ATP through P2Y receptors and by cytoplasmic calcium. FEBS Lett. *580*, 239–244.
Locovei, S., Bao, L., and Dahl, G. (2006b). Pannexin 1 in erythrocytes: function without a gap. Proc. Natl. Acad. Sci. U. S. A. *103*, 7655–7659.
Ma, H.L., Jiang, Q., Han, S., Wu, Y., Tomshine, J.C., Wang, D., Gan, Y., Zou, G., and Liang, X.J. (2012). Multicellular tumor spheroids as an in vivo-like tumor model for three-dimensional imaging of chemotherapeutic and nano material cellular penetration. Mol. Imaging *11*, 487–498.
Malempati, S., and Hawkins, D.S. (2012). Rhabdomyosarcoma: Review of the Children's Oncology Group (COG) soft-tissue Sarcoma committee experience and rationale for current COG studies. Pediatr. Blood Cancer *59*, 5–10.
Orellana, J.A., Velasquez, S., Williams, D.W., Saez, J.C., Berman, J.W., and Eugenin, E.A. (2013). Pannexin1 hemichannels are critical for HIV infection of human primary CD4+ T lymphocytes. J Leukoc Biol *94*, 399–407.
Paoletti, A., Raza, S.Q., Voisin, L., Law, F., Caillet, M., Martins, I., Deutsch, E., and Perfettini, J.L. (2013). Editorial: Pannexin-1--the hidden gatekeeper for HIV-1. J Leukoc Biol *94*, 390–392.
Parham, D.M., and Barr, F.G. (2013). Classification of rhabdomyosarcoma and its molecular basis. Adv. Anat. Pathol. *20*, 387–397.
Pelegrin, P., and Surprenant, A. (2006). Pannexin-1 mediates large pore formation and interleukin-1beta release by the ATP-gated P2X7 receptor. EMBO J. *25*, 5071–5082.
Penuela, S., Bhalla, R., Gong, X.Q., Cowan, K.N., Celetti, S.J., Cowan, B.J., Bai, D., Shao, Q., and Laird, D.W. (2007). Pannexin 1 and pannexin 3 are glycoproteins that exhibit many distinct characteristics from the connexin family of gap junction proteins. J. Cell Sci. *120*,

3772–3783.
Penuela, S., Bhalla, R., Nag, K., and Laird, D.W. (2009). Glycosylation regulates pannexin intermixing and cellular localization. Mol. Biol. Cell *20*, 4313–4323.
Penuela, S., Gyenis, L., Ablack, A., Churko, J.M., Berger, A.C., Litchfield, D.W., Lewis, J.D., and Laird, D.W. (2012). Loss of pannexin 1 attenuates melanoma progression by reversion to a melanocytic phenotype. J. Biol. Chem. *287*, 29184–29193.
Penuela, S., Gehi, R., and Laird, D.W. (2013). The biochemistry and function of pannexin channels. Biochim. Biophys. Acta - Biomembr. *1828*, 15–22.
Petricoin, E.F., Espina, V., Araujo, R.P., Midura, B., Yeung, C., Wan, X., Eichler, G.S., Johann, D.J., Qualman, S., Tsokos, M., et al. (2007). Phosphoprotein pathway mapping: Akt/mammalian target of rapamycin activation is negatively associated with childhood rhabdomyosarcoma survival. Cancer Res. *67*, 3431–3440.
Riquelme, M.A., Cea, L.A., Vega, J.L., Puebla, C., Vargas, A.A., Shoji, K.F., Subiabre, M., and Sáez, J.C. (2015). Pannexin channels mediate the acquisition of myogenic commitment in C2C12 reserve cells promoted by P2 receptor activation. Front. Cell Dev. Biol. *3*, 25.
Rudzinski, E.R., Teot, L.A., Anderson, J.R., Moore, J., Bridge, J.A., Barr, F.G., Gastier-Foster, J.M., Skapek, S.X., Hawkins, D.S., and Parham, D.M. (2013). Dense pattern of embryonal rhabdomyosarcoma, a lesion easily confused with alveolar rhabdomyosarcoma: a report from the Soft Tissue Sarcoma Committee of the Children's Oncology Group. Am. J. Clin. Pathol. *140*, 82–90.
Ryten, M., Yang, S., and Dunn, P. (2004). Purinoceptor expression in regenerating skeletal muscle in the mdx mouse model of muscular dystrophy and in satellite cell cultures. FASEB J. *34*, 1–34.
Sandilos, J.K., Chiu, Y.-H., Chekeni, F.B., Armstrong, A.J., Walk, S.F., Ravichandran, K.S., and Bayliss, D. a (2012). Pannexin 1, an ATP release channel, is activated by caspase cleavage of its pore-associated C-terminal autoinhibitory region. J. Biol. Chem. *287*, 11303–11311.
Séror, C., Melki, M.-T., Subra, F., Raza, S.Q., Bras, M., Saïdi, H., Nardacci, R., Voisin, L., Paoletti, A., Law, F., et al. (2011). Extracellular ATP acts on P2Y2 purinergic receptors to facilitate HIV-1 infection. J. Exp. Med. *208*, 1823–1834.
Silverman, W.R., de Rivero Vaccari, J.P., Locovei, S., Qiu, F., Carlsson, S.K., Scemes, E.,

Keane, R.W., and Dahl, G. (2009). The pannexin 1 channel activates the inflammasome in neurons and astrocytes. J. Biol. Chem. *284*, 18143–18151.

Stewart, M.K.G., Plante, I., Penuela, S., and Laird, D.W. (2016). Loss of Panx1 impairs mammary gland development at lactation: Implications for breast tumorigenesis. PLoS One *11*, 1–23.

Tapscott, S.J., Thayer, M.J., and Weintraub, H. (1993). Deficiency in rhabdomyosarcomas of a factor required for MyoD activity and myogenesis. Science *259*, 1450–1453.

Thompson, R.J., Jackson, M.F., Olah, M.E., Rungta, R.L., Hines, D.J., Beazely, M.A., Macdonald, J.F., and Macvicar, B.A. (2008). Activation of Pannexin-1 Hemichannels Augments Aberrant Bursting in the Hippocampus. Science (80-.). *319*, 1555–1559.

Wang, Y., Marino-Enriquez, A., Bennett, R.R., Zhu, M., Shen, Y., Eilers, G., Lee, J.C., Henze, J., Fletcher, B.S., Gu, Z., et al. (2014). Dystrophin is a tumor suppressor in human cancers with myogenic programs. Nat. Genet. *46*, 601–606.

Wicki-Stordeur, L.E., and Swayne, L.A. (2014). The emerging Pannexin 1 signalome: a new nexus revealed? Front. Cell. Neurosci. *7*, 287.

Wicki-Stordeur, L.E., Dzugalo, A.D., Swansburg, R.M., Suits, J.M., and Swayne, L.A. (2012). Pannexin 1 regulates postnatal neural stem and progenitor cell proliferation. Neural Dev. *7*, 11.

Wolf, S.J., Huynh, T., Bryce, N.S., Hambley, T.W., Wakelin, L.P.G., Stewart, B.W., and Catchpoole, D.R. (2011). Intracellular trafficking as a determinant of AS-DACA cytotoxicity in rhabdomyosarcoma cells. BMC Cell Biol. *12*, 36.

Yang, D., He, Y., Muñoz-Planillo, R., Liu, Q., and Núñez, G. (2015). Caspase-11 Requires the Pannexin-1 Channel and the Purinergic P2X7 Pore to Mediate Pyroptosis and Endotoxic Shock. Immunity *43*, 923–932.

3. CHAPTER THREE: IDENTIFICATION OF PANNEXIN 1 REGULATED GENES, INTERACTOME, AND PATHWAYS IN RHABDOMYOARCOMA AND ITS TUMOR INHIBITORY INTERACTION WITH AHNAK

Authors: Xiao Xiang, Stéphanie Langlois, Marie-Eve St-Pierre, Anna Blinder, Philippe Charron, Tyson E. Graber, Stephanie L. Fowler, Stephen D. Baird, Steffany A.L. Bennett, Tommy Alain, and Kyle N. Cowan

Status: In press

Oncogene

Accepted for publication on December 11, 2020

3.1 ACKNOWLEDGEMENTS

The majority of the experiments in this manuscript were performed by me under the supervision of Kyle N. Cowan. Stéphanie Langlois performed dye uptake assays using mechanical stimulation. Marie-Eve St-Pierre and Anna Blinder performed the Western blot presented in Figure 3.1O. Philippe Charron created the online databases. Tyson E. Graber helped me with analyzing RNA-seq data. Stephanie L. Fowler helped me with experiments related to subcellular fractionation. Tyson E. Graber and Tommy Alain provided critical review of the manuscript. This manuscript was written and revised by me with editorial help from Stéphanie Langlois and Kyle N. Cowan.

3.2 ABSTRACT

Rhabdomyosarcoma (RMS), the most common soft tissue sarcoma in children, is an aggressive cancer with a poor prognosis. Despite current management, the 5-year survival rate for patients with metastatic RMS is ~30%; underscoring the need to develop better treatment strategies. We have recently reported that pannexin 1 (PANX1) levels are down-regulated in RMS and that restoring its expression inhibits RMS progression. Here, we have surveyed and characterized the molecular changes induced by PANX1 re-expression in RMS. We catalogued transcriptomic changes in this context by RNA-sequencing. At the protein level, we unveiled PANX1 interactors using BioID, complemented by co-immunoprecipitation coupled to high-performance liquid chromatography/electrospray ionization tandem mass spectrometry performed in PANX1-enriched fractions. Using these data, we generated searchable public databases for the PANX1 interactome and changes to the RMS transcriptome occurring when PANX1 expression is restored. STRING network analyses revealed a PANX1 interactome involving plasma membrane and cytoskeleton-associated proteins including the previously undescribed interactor AHNAK. Indeed, AHNAK knockdown abrogated the PANX1-mediated reduction in RMS cell viability and migration. Using these unbiased approaches, we bring insight to the mechanisms by which PANX1 inhibits RMS progression, identifying the cell migration protein AHNAK as a key modifier of PANX1-mediated changes in RMS malignant properties.

Keywords: Cancer; Pannexin; PANX1; Rhabdomyosarcoma (RMS); RNA-sequencing; BioID; Transcriptomics; Proteomics; Interactome

3.3 INTRODUCTION

Rhabdomyosarcoma (RMS) is the most common soft tissue sarcoma in childhood (Chen et al., 2019). RMS tumors are typically associated with the skeletal muscle lineage, displaying 2 major subtypes: embryonal (eRMS) and alveolar (aRMS) (Dobson et al., 2016). While eRMS is generally associated with a favourable clinical outcome, aRMS is more aggressive and often metastatic (Parham and Barr, 2013). The 5-year survival of patients with metastatic RMS is below 30% and despite the use of invasive multimodal treatment regimens, their prognosis has not improved in the last 30 years (Chen et al., 2019; Malempati and Hawkins, 2012). The discovery of novel therapeutic strategies for RMS is thus of utmost importance.

RMS is thought to originate as a consequence of regulatory disruption of myogenic precursor cell differentiation (Keller and Guttridge, 2013; Langlois et al., 2014). We recently described a key role for pannexin 1 (PANX1) in skeletal myogenesis (Langlois and Cowan, 2017; Langlois et al., 2014). Pannexins (PANX1, PANX2, and PANX3) are single membrane channels that allow the release of small molecules such as nucleotides (Chiu et al., 2018). Our work has shown that PANX1 levels are low in undifferentiated skeletal muscle myoblasts and increase during myogenesis *in vitro* and *in vivo* (Langlois et al., 2014; Pham et al., 2018). Blocking PANX1 channel activity inhibited myoblast differentiation while PANX1 over-expression promoted this process (Langlois et al., 2014). Based on this, we explored whether PANX1 levels are altered in RMS and if so, whether restoration of its expression could reduce RMS malignant properties. We found that PANX1 expression is down-regulated in patient-derived RMS cell lines and tumor specimens when compared to differentiated skeletal muscle cells and tissue (Xiang et al., 2018). Increasing PANX1 levels abrogated the proliferative and

migratory potential of eRMS and aRMS cells, inhibited 3D tumor spheroid growth and induced regression of established spheroids through the induction of apoptosis (Xiang et al., 2018). Moreover, while control tumors grew rapidly in mice, PANX1 over-expression significantly reduced eRMS and aRMS growth (Xiang et al., 2018). As ectopic PANX1 effectively alleviates RMS tumor growth, deciphering its downstream signaling pathways would bring insight into the molecular mechanism by which PANX1 reduces RMS malignant properties while offering an opportunity to identify potential new therapeutic targets.

PANX1 is a type III multi-pass transmembrane glycoprotein with both the amino- and carboxyl-termini inside the lumen (Penuela et al., 2007). PANX1 channels have been implicated in various pathological conditions including ischemia (Bargiotas et al., 2011), stroke (Good et al., 2018), diabetes (Cui et al., 2016), epilepsy (Dossi et al., 2018) and hypertension (Good et al., 2017) as well as cancers such as glioma (Lai et al., 2007) and melanoma (Freeman et al., 2019; Penuela et al., 2012). While the underlying signaling mechanism of PANX1 under pathological conditions remains largely unknown, it has been primarily attributed to disrupted purinergic and/or adrenergic signaling via ATP or other nucleotides (Wicki-Stordeur and Swayne, 2014). However, PANX1 has been recently implicated in the Wnt/β-catenin signaling pathway in melanoma (Freeman et al., 2019). In addition, modulation of PANX1 expression has been shown to alter the expression of E-cadherin, vimentin, and matrix metalloproteinase-9 via the extracellular signal-regulated kinase 1/2 signaling pathway in testicular cancer cells (Liu et al., 2019). Although ATP release has been central in PANX1 research (Wicki-Stordeur and Swayne, 2014), it has become increasingly evident that the interaction of PANX1 with various signaling molecules mediates key cellular processes. For instance, the interaction of PANX1 with actin related proteins 2/3 has been proposed to regulate the actin-mediated mechanical force generation (Wicki-Stordeur

and Swayne, 2013), and the sequestration of collapsin response mediator protein-2 by Panx1 channels regulates microtubule remodeling (Xu et al., 2018). While the molecular mechanisms by which PANX1 functions have started to be unveiled in some contexts, the signaling pathways involved in PANX1-mediated inhibition of RMS progression had yet to be investigated.

In the present study, we show that PANX1 over-expression in RMS cells invoked transcriptomic changes in a number of biological processes such as apoptosis and cellular migration, as well as in the MAPK and Rap1 signaling pathways. Using BioID, we revealed the PANX1 interactome in Rh18 (eRMS) and Rh30 (aRMS) patient-derived cell lines. Common PANX1 interactors between the two RMS subtypes were associated with the plasma membrane and cytoskeleton. The BioID PANX1 interactome was further compared to and corroborated with a complementary set of PANX1 binding partners identified by HPLC-ESI-MS/MS analysis from PANX1-enriched subcellular fractions. We validated the novel interaction of PANX1 with AHNAK, which was identified here as the top PANX1 interactor. AHNAK is a large scaffolding protein that has been linked to migration and invasion in other cancers (Chen et al., 2017; Gentil et al., 2003; Silva et al., 2016; Sudo et al., 2014). Knockdown of AHNAK in PANX1-expressing Rh18 and Rh30 cells abrogated the PANX1-mediated reduction in cell viability, migration and increase in anoikis, suggesting that PANX1 regulation of RMS tumor malignant properties involves its interaction with AHNAK. Using data generated through these genome-wide unbiased approaches, we have also generated the first PANX1 transcriptomic and proteomic public searchable databases for easy access to our entire RNA-seq and BioID data, which may foster new research avenues identifying pathways regulating PANX1 and its functions, as well as potential clinical translation towards novel therapeutic strategies.

3.4 MATERIAL AND METHODS

Cells

Rh18 and Rh30 cell lines were from Dr. P. Houghton (St. Jude Children's Hospital, Memphis, TN). HEK293T cell line was from the American Type Culture Collection. See "Supplemental Material and Methods" for detailed information.

Subcloning, Transfection, and Stable Cell Lines Generation

pcDNA3.1-MCS-Bir*A(R118G)-HA was a gift from Kyle Roux (plasmid #36047, Addgene, Cambridge, MA) (Roux et al., 2012). *PANX1* cDNA (Origene, Rockville, MD) was subcloned into pcDNA3.1-MCS-BirA*(R118G)-HA. *PANX1-BirA*(R118G)-HA* and *Myc-PANX1* cDNA (Origene) were subcloned into the pCDH-CuO-MCS-EF1-GFP lentiviral vector (System Biosciences, CA). All constructs were verified by sequencing. See "Supplemental Material and Methods" for detailed information.

Transfections were performed using Lipofectamine 2000 Reagent (Thermo Scientific, Waltham, MA). SparQ^{TM} Cumate Switch Inducible System (System Bioscience) was used to generate stable cell lines (Xiang et al., 2018). Cumate (System Bioscience) was used at 30 µg/mL.

RT-qPCR

Stable Rh30 cells were treated and analyzed as described in the "Supplemental Material and Methods".

RNA Sequencing and Data Analysis

Stable Rh30 cells were treated with cumate for 48 hours. Total RNA was extracted using RNeasy Mini Kit (Qiagen, Germantown, MD) and submitted to Princess Margaret Genomics Centre (Toronto, ON, Canada) for RNA-seq analysis on an Illumina HiSeq2000 sequencing platform. See "Supplemental Material and Methods" for detailed information.

Western Blotting

Cell lysates were obtained and analyzed as previously described (Cowan et al., 2012; Langlois et al., 2014). See "Supplemental Material and Methods" for detailed information on antibodies and their dilutions.

Dye Uptake Assay

Sulforhodamine B dye uptake assay was performed as previously described (Xiang et al., 2018). See "Supplemental Material and Methods" for detailed information.

3D Tumor Spheroid Assay

3D tumor spheroid assay was performed as previously described (Xiang et al., 2018). See "Supplemental Material and Methods" for detailed information.

BioID

BioID was performed according to Roux *et al.* (2012). See "Supplemental Material and Methods" for detailed information.

co-IP using Enriched Subcellular Fractions

Subcellular fractionation from cells grown in five 15 cm dishes was performed according to Fowler *et al.* (Fowler et al., 2013) A total of 24 fractions were collected per sample. Myc-PANX1 enriched fractions were pooled and the buffer exchanged for IP lysis buffer (150 mM NaCl, 10 mM Tris-HCl, pH 7.4, 1 mM EDTA, 0.5% NP-40, and 1% Triton X-100) prior to performing the co-IP. See "Supplemental Material and Methods" for detailed information.

Mass Spectrometry and Proteomic Analysis

Mass spectrometry was carried out at the Ottawa Institute of System Biology. See "Supplemental Material and Methods" for detailed information.

co-IP using Whole Cell Lysates

Cells were lysed using IP lysis buffer, as described above. Pre-cleared lysates were incubated with 5-8 µg of antibodies for 16 hours, and then with 20 µL of freshly prepared protein A/G plus agarose beads (Thermo Fisher) for 60 minutes. Beads were washed, boiled in Laemmli buffer, and eluates submitted to Western blotting.

Confocal Laser Microscopy

Immunofluorescent labeling and acquisition of confocal images were described previously (Xiang et al., 2018). See "Supplemental Material and Methods" for detailed information.

Proliferation Assay

Cells were subjected to a BrdU cell proliferation assay as previously described (Xiang et al., 2018). See “Supplemental Material and Methods” for detailed information.

RNA Interference

Cells were transfected with 5 nM of Silencer® Select siRNA targeting *AHNAK* (Sense: CCAUCUACUUUGACAACCUtt; Anti-sense: AGGUUGUCAAAGUAGAUGGtg) or its non-targeting control (NTC), Silencer® Select Negative Control No. 1 (Life Technologies) for 72 hours prior to analysis by Western blotting for AHNAK levels or for 48 hours prior to be subjected to various functional assays.

shRNA (TRCN0000130911) targeting *AHNAK* (Forward 5’ – 3’: ctagcGCACTTGAAGATGCCCAAGATCTCGAGATCTTGGGCATCTTCAAGTGCTTTTTTG; Reverse 5’ – 3’: gCGTGAACTTCTACGGGTTCTAGAGCTCTAGAACCCGTAGAAGTTCACGAAAAACttaa) and or its NTC (Forward 5’ – 3’: ctagcGCGCGATAGCGCTAATAATTTCTCGAGAAATTATTAGCGCTATCGCGCTTTTTG; Reverse 5’ – 3’: gCGCGCTATCGCGATTATTAAAGAGCTCTTTAATAATCGCGATAGCGCGAAAAACttaa) were subcloned into EZ-Tet-pLKO-Hygro plasmid (a gift from Cindy Miranti, plasmid # 85972, Addgene), and packaged into lentiviruses using pMD2.G and psPAX2 packaging plasmids (gifts from Didier Trono, Addgene plasmids # 12259 and 12260) (Frank et al., 2017). Cumate-inducible Rh18 and Rh30 cells (Xiang et al., 2018) were used to generate the shRNA stable cells. Resulting cells were under cumate and doxycycline (50 ng/µL; Sigma-Aldridge) switch for PANX1 and shRNA expression, respectively.

Alamar Blue Viability Assay

Cells were incubated with 0.15 g/mL Alamar Blue (Sigma-Aldridge) for 2 hours and read on a Synergy HTX plate reader (BioTek, VT) equipped with excitation;emission filter set at 530/25; 590/25 nm. See "Supplemental Material and Methods" for detailed information.

Migration Assay

Migration assay was performed as previously described (Xiang et al., 2018). See "Supplemental Material and Methods" for detailed information.

Soft Agar Anoikis Assay

Cells were seeded on 1% Noble agar (BD Biosciences, San Jose, CA) and viable cells counted (Xiang et al., 2018). See "Supplemental Material and Methods" for detailed information.

Data Deposition

Raw fastq files from the RNA-seq used for bioinformatical analyses and the Shinny DE database can be accessed from Gene Expression Omnibus (GEO) database (GSE144102). RAW spectra files from BioID and the Shinny DE database are deposited in the Center for Computational Mass Spectrometry (MassIVE MSV000084867).

Statistics

Unpaired two-tailed Student's *t*-tests and analysis of variance (ANOVA) followed by Tukey's or Bonferroni *post hoc* tests were used. Results are given as mean ± s.d. Results with

$P < 0.05$ were considered significant. Each experiment was performed at least three times (n=3). The exact number of times each experiment was performed is indicated in the Figure legends. The individual data points are also displayed on the graphs.

3.5 RESULTS

Identification of the PANX1 Transcriptome in RMS using RNA-Seq

We have previously shown that PANX1 over-expression in RMS cells reduced their proliferation, migration, and inhibited tumor growth via induction of apoptosis (Xiang et al., 2018). As our first step towards understanding the PANX1 downstream signaling in RMS, Rh30 (aRMS) cells expressing ectopic PANX1 or control GFP (Fig. 3.1A) were subjected to RNA-seq. The subsequent differential expression (DE) analysis identified 1273 genes (5.2%) significantly changed in PANX1 over-expressing cells with a False Discovery Rate less than 0.05 ($q < 0.05$) (Fig. 3.1B). Amongst the 1273 significantly changed genes, 39 were down-regulated (Log2 Fold expression change < -1) and 898 were up-regulated (Log_2 Fold expression change > 1), which are shown in the upper left and right quadrants of the volcano plot, respectively (Fig. 3.1C). The significantly regulated genes were classified by gene ontology (GO) according to biological process (BP) using DAVID (Huang et al., 2009) (Fig. 3.1D), which revealed numerous highly enriched (Fisher's Exact P-Value < 0.05) GO_BP terms in accordance with our previous observations (Xiang et al., 2018), including regulation of apoptotic processes (Fig. 3.1E) and negative regulation of migration (Fig. 3.1F). Additionally, KEGG pathway analysis results (Fig. 3.1G) indicated that MAPK (Fig. 1H) and Rap1 (Fig. 1I) were amongst the most enriched (Fisher's Exact P-Value < 0.05) signaling

pathways in PANX1-expressing cells. To validate the RNA-seq results, we selected two up-regulated gene hits, matrix metalloprotease 2 (*MMP2*) and TNF receptor-associated factor 2 (*TRAF2*), and two down-regulated gene hits, apolipoprotein B mRNA-editing enzyme catalytic subunit 2 (*APOBEC2*) and myristoylated alanine rich C-kinase substrate (*MARCKS*), for RT-qPCR validation. Our results showed that *MMP2* (Fig. 3.1J) and *TRAF2* (Fig. 3.1K) were significantly up-regulated while *APOBEC2* (Fig. 3.1L) and *MARCKS* (Fig. 3.1M) were significantly down-regulated when PANX1 was expressed, which were all concordant with the RNA-seq results. The up-regulated *GJA1* gene (Fig. 3.1N) was further investigated as ectopic expression of its protein product connexin 43 (Cx43) in RMS cells was previously shown to elicit a tumor-suppressive phenotype (Proulx et al., 1997) similar to that of PANX1 (Xiang et al., 2018). Western blot analysis (Fig. 3.1O and P) showed a significant increase in Cx43 levels (unphosphorylated/poorly phosphorylated species (P_0)) in PANX1-expressing Rh30 cells compared to control cells while the 20 kDa variant of Cx43 (Cx43-20K) was not detected under these conditions (data not shown). Using this unbiased genome-wide approach, our transcriptomic analysis identified the genes that are regulated in PANX1-expressing RMS cells together with the key cellular processes in which they may be involved.

The BirA* tag does not Interfere with PANX1 Function

As many biological processes are mediated through protein-protein interactions (Vidal et al., 2011), and as transcriptomic data may not fully recapitulate the proteome of a cell, we next used BioID (Roux et al., 2012) to unveil PANX1 interacting proteins and gain further insight into the molecular mechanism by which PANX1 functions in RMS. The carboxyl terminus of PANX1 was fused with a promiscuous biotin ligase found in *E. coli*, BirA*, and expressed in RMS cells. With the addition of exogenous biotin, BirA* catalyzes the

biotinylation of the interacting partners in a distance-dependent manner. The biotin labeled proteins can be denatured and captured by streptavidin-mediated pull-down and subsequently identified by mass spectrometry. This method offers advantages such as capturing proteins with weak or transient interactions that could be missed by co-immunoprecipitation (Roux et al., 2012). BirA*-PANX1 showed a banding pattern similar to that of Myc-PANX1 by Western blotting (Fig. 3.2A). PANX1 is detected as multiple bands due to post-translational modifications (Boyce et al., 2018). As expected, Myc-PANX1 was detected as 3 main species with apparent molecular weights of ~43, 45, and 53 kDa, while BirA*-PANX1 was detected as ~69, 72, and 81 kDa bands, showing an average increase of ~4 kDa (Myc predicted: 3.3 kDa (Xiang et al., 2018) and ~31 kDa (BirA* predicted: 35 kDa (Roux et al., 2012)), respectively, relative to untagged wild-type PANX1 (detected at ~39, 40, and 49 kDa in these cells) (Xiang et al., 2018). To ensure that BirA* does not affect PANX1 function, we first performed a sulforhodamine B dye uptake assay in HEK293T cells, devoid of endogenous pannexins, transiently expressing PANX1, BirA*-PANX1, or the GFP control vector. PANX1 and BirA*-PANX1 induced similar levels of dye uptake, which were both significantly higher than that of cells expressing the control vector (Fig. 3.2B). We then generated stable Rh18 (eRMS) and Rh30 (aRMS) cell lines using our previously described cumate-inducible system (Xiang et al., 2018) to express BirA*-PANX1 and performed a 3D spheroid formation assay. As we previously reported, all cells express GFP constitutively under this expression system but express PANX1 or BirA*-PANX1 only in the presence of cumate (Xiang et al., 2018). In this spheroid assay, cumate was added at the time of cell seeding. Aggregation and compaction in GFP control, PANX1-, and BirA*-PANX1-expressing Rh18 (Fig. 3.2C) and Rh30 (Fig. 3.2D) cells were observed 48 hours after seeding. Using the constitutively expressed GFP to quantify spheroid size in all conditions, we show that the expression of both PANX1 and

BirA*-PANX1 prevented Rh18 (Fig. 3.2C) and Rh30 (Fig. 3.2D) 3D spheroid growth compared to their respective GFP control cells. Indeed, PANX1- and BirA*-PANX1-expressing cells gradually lost their constitutive GFP fluorescence likely due to cell death (Xiang et al., 2018). All together showing that the BirA* tag does not interfere with PANX1 functions.

BioID Analysis Identified Plasma Membrane and Cytoskeletal PANX1 Interacting Proteins in RMS cells

Following these validation steps, the banding patterns of the biotinylated proteins captured by streptavidin beads from BirA*-PANX1, compared to its BirA* and Myc-PANX1 negative controls, were examined by Western blotting. In both Rh18 and Rh30 cells, the BirA* biotin ligase activity was evident by the intense bands detected by fluorochrome conjugated streptavidin (Fig. 3.3A and B). Importantly, BirA*-PANX1 exhibited different banding patterns of biotinylated proteins compared to those biotinylated by BirA* alone (Fig. 3.3A and B). Rh18 and Rh30 cells were then treated with cumate to induce BirA*-PANX1 expression, or Myc-PANX1 as a background control, and exposed to biotin for 24 hours to allow proximity biotinylation by BirA*. Cells were lysed and biotinylated proteins were captured using streptavidin-conjugated beads. The captured proteins were digested on-bead and immediately submitted for HPLC-ESI-MS/MS. A total of 240 and 238 proteins labeled by BirA*-PANX1 were identified from Rh18 and Rh30 cells, respectively. Interactors were ranked by the unique peptide scores, which were calculated using Myc-PANX1 as the background control, indicating relative abundance of the peptides biotinylated by BirA*-PANX1. The top 50 interactors from Rh18 and Rh30 cells are shown in Fig. 3.3C and 3.3D, respectively. Most notably, 43 out of the top 50 candidate hits were shared between Rh18 and Rh30 cells,

suggesting a high degree of confidence in the targets identified (Fig. 3.3E). STRING Functional Protein Association Network analysis and gene ontology classification of the overlapped 43 protein hits presented a network of PANX1 interactors consisting of plasma membrane and cytoskeleton associated proteins in RMS (Fig. 3.3F). Further analysis of the 14 mutually exclusive proteins (7 from each cell line (Fig. 3.3E)) showed that they are phosphoproteins with localizations in the cytosol, cytoskeleton, and plasma membrane. Taken together, these data suggest that PANX1 primarily interacts with proteins with functions localized in or proximal to the plasma membrane of both eRMS and aRMS cells.

Online Databases for Searching the PANX1 Transcriptome and Interactome

To provide access to the information on the individual transcripts regulated in PANX1-expressing cells, as well as PANX1 interactors, we have generated user-friendly public online databases using RStudio equipped with the Shiny package. These databases can be freely accessed at http://bigbear.med.uottawa.ca:2000 and have been designed to toggle between the transcriptomic and proteomic data with a dropdown menu. The individual gene symbol and Ensemble gene ID or protein symbol in their respective databases can be freely searched. The gene hits are displayed with their Log_2 Fold Change, P- and Q-Values while the protein hits are displayed with their background-corrected scores (BirA*- or Myc-PANX1-expressing cells as negative controls), and these parameters can all be freely adjusted to meet individual specific search interests. When using our databases, kindly acknowledge the current manuscript.

Proteomic Analysis from Co-IP performed using PANX1-Enriched Membrane Fractions

Fowler *et al*. have previously developed and optimized a method to effectively isolate and enrich subcellular compartments containing integral membrane proteins using a sucrose density gradient prior to co-IP followed by LC-MS/MS analysis (Fowler et al., 2016, 2013). This complementary method was used here to isolate Myc-PANX1-enriched membrane microdomains from Rh18 and Rh30 cells prior to co-IP in an attempt to eliminate potential false positive interactors from BioID. Previously used in various contexts, the Myc tag showed no impact on PANX1 channel activity (Lai et al., 2007; Ma et al., 2009), trafficking (Boassa et al., 2007) and localization (Ma et al., 2012). Accordingly, transient expression of PANX1 and Myc-PANX1 inhibited Rh18 (Fig. 3.4A) and Rh30 (Fig. 3.4B) cell proliferation to a similar extent, as compared to their respective negative controls. In addition, transient expression of both PANX1 and Myc-PANX1 in HEK293T cells induced comparable levels of dye uptake, which were significantly higher than that of the GFP control (Fig. 3.4C). Following these verification steps, whole lysates of stable Rh18 (Fig. 3.4D) and Rh30 (Fig. 3.4E) cells expressing Myc-PANX1 or GFP under the control of the cumate-inducible system were separated on a sucrose gradient from which a total of 22 matching fractions were collected. Fractions with high levels of Myc-PANX1 (indicated by shaded area; Fig. 3.4F and 3.4G) were pooled and used for co-IP followed by HPLC-ESI-MS/MS analysis.

A total of 146 and 202 protein hits were identified by HPLC-ESI-MS/MS from Rh18 and Rh30 cells, respectively. These proteins were selected according to their scores, which were derived from the relative fold change of unique peptides from Myc-PANX1 samples to the GFP controls, and only proteins with scores above 1 were selected for the downstream analyses. The protein hits were cross-referenced with the PANX1 interactome identified from BioID and revealed 27 and 26 overlapped protein hits, where AHNAK, UTRN, and MYH9 were amongst the highest enriched hits, in both the BioID and co-IP approaches in Rh18 (Fig.

3.5A) and Rh30 (Fig. 3.5B) cells, respectively. These 27 and 26 PANX1 interactors in Rh18 (Fig. 3.5C) and Rh30 (Fig. 3.5D) cells are predicted in clusters of interacting proteins consisting of plasma membrane-, actin filaments- and microtubule-associated proteins.

PANX1 Tumor Inhibitory Function in RMS is Dependent on its Interaction with AHNAK

To start assessing the functional relevance of the PANX1 interactome discovered here, we first wanted to confirm the physical interaction of PANX1 with AHNAK; the highest ranked protein hit from BioID and detected by co-IP using enriched subcellular fractions. AHNAK is a large scaffold protein (Benaud et al., 2004; Gentil et al., 2003; Komuro et al., 2004) that has been shown to regulate the proliferation, migration and invasion of mesothelioma (Sudo et al., 2014), triple negative breast cancer (Chen et al., 2017) and pancreatic cancer cells (Zhang et al., 2019). However, the functional role of AHNAK in RMS and its interaction with PANX1 were unknown. Co-IP was performed using whole lysates of Rh18 and Rh30 cells expressing PANX1. ACTB was chosen as a positive control since PANX1 has been shown to interact with components of actin filaments (Wicki-Stordeur et al., 2013). ACTB was also identified as a PANX1 interactor from our BioID and subcellular fractionation/co-IP results. As expected, ACTB was co-immunoprecipitated with Myc-PANX1 in Rh18 (Fig. 3.6A) and Rh30 (Fig. 3.6B) cells. PANX1 was also pulled-down with endogenous AHNAK in both Rh18 (Fig. 3.6C) and Rh30 (Fig. 3.6D) cells and was not detected when lysates were incubated with beads alone; thereby further validating this novel PANX1 interactor.

PANX1 is localized both in intracellular compartments and at the plasma membrane in Rh18 and R30 cells (Xiang et al., 2018). As AHNAK has been reported in many subcellular localizations such as the nucleus (Shtivelman and Bishop, 1993; Shtivelman et al., 1992),

cytoplasm (Hashimoto et al., 1993, 1995; Huang et al., 2007; Nie et al., 2000), and plasma membrane (Gentil et al., 2005; Hashimoto et al., 1993; Huang et al., 2007; Komuro et al., 2004; Salim et al., 2009) including pseudopodia (Shankar et al., 2010), immunofluorescence confocal microscopy was performed to examine in which cellular compartment PANX1 and AHNAK may interact. Confocal microscopy images (Fig. 3.6E) of Rh18 and Rh30 transiently expressing PANX1 showed PANX1 and AHNAK mainly in intracellular compartments but also at, or associated with, the plasma membrane. Notably, a pool of PANX1 and AHNAK were found localized at the plasma membrane within structures resembling pseudopodia (Shankar et al., 2010) (arrowheads), suggesting that a population of PANX1 and AHNAK interact in specialized plasma membrane compartments.

To interrogate the functional role of this interaction, AHNAK was knocked down in PANX1-expressing Rh18 (Fig. 3.7A) and Rh30 (Fig. 3.7B) cells. As PANX1 reduces RMS cell proliferation and migration, and sensitizes RMS cells to anoikis (Xiang et al., 2018), we used assays reflective of each phenotype. Indeed, Rh18 and Rh30 transfected with AHNAK siRNA or the scramble non-targeting control (NTC) were treated with or without cumate to induce PANX1 expression (Xiang et al., 2018) prior to Alamar Blue viability, scratch wound migration, or soft agar anoikis assays. We found that AHNAK knockdown abrogated the PANX1-mediated reduction in Rh18 (Fig. 3.7C) and Rh30 (Fig. 3.7D) cell viability seen in their respective NTC siRNA counterparts. A partial reversal of the PANX1-mediated reduction in migration of PANX1-expressing Rh18 (Fig. 3.7E) and Rh30 (Fig. 3.7F) cells was observed when AHNAK expression was knocked down. Reduction of AHNAK expression completely reversed the PANX1-mediated sensitization to anoikis in Rh18 (Fig. 3.7G) cells, while a partial effect was observed in Rh30 (Fig. 3.7H) cells, compared to their respective controls. To further confirm our findings, we used shRNA as an alternative AHNAK knockdown strategy. Our

cumate-inducible stable Rh18 (Fig. 3.7I) and Rh30 (Fig. 3.7J) cells were further engineered to express either NTC or AHNAK-targeting shRNA under a doxycycline switch (Frank et al., 2017; Xiang et al., 2018). In accordance with our previous results, shRNA-mediated AHNAK knockdown in both Rh18 (Fig. 3.7K) and Rh30 (Fig. 3.7L) cells showed significant mitigation of PANX1-mediated reduction in cell viability. Altogether, these results indicate that the PANX1 tumor inhibitory function in RMS involves its interaction with AHNAK.

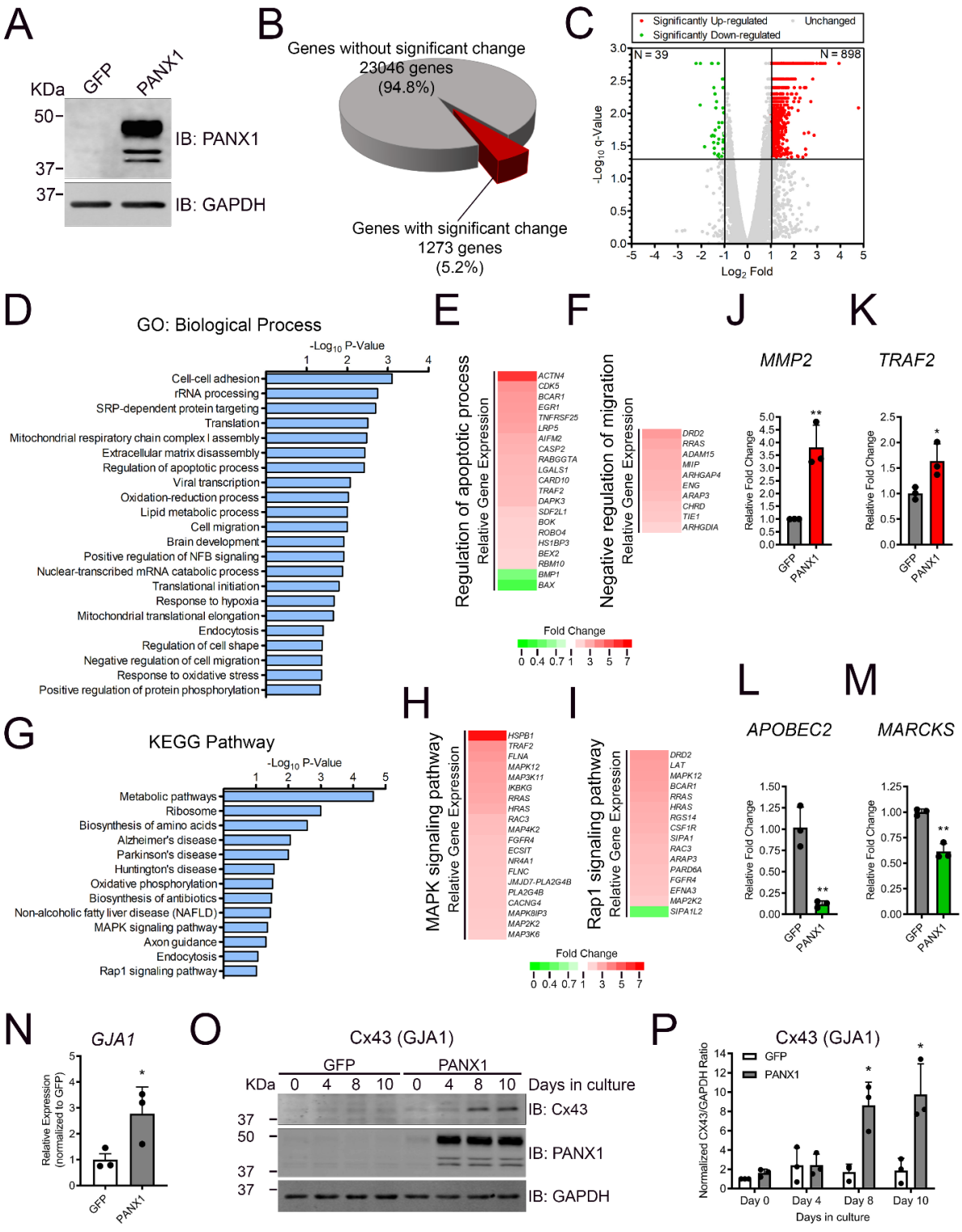
A
KDa
GFP
PANX1
50
37
37
IB: PANX1
IB: GAPDH
B
Genes without significant change
23046 genes
(94.8%)
Genes with significant change
1273 genes
(5.2%)
C
Significantly Up-regulated
Significantly Down-regulated
Unchanged
N = 39
N = 898
-Log10 q-Value
Log2 Fold
D
GO: Biological Process
-Log10 P-Value
Cell-cell adhesion
rRNA processing
SRP-dependent protein targeting
Translation
Mitochondrial respiratory chain complex I assembly
Extracellular matrix disassembly
Regulation of apoptotic process
Viral transcription
Oxidation-reduction process
Lipid metabolic process
Cell migration
Brain development
Positive regulation of NFB signaling
Nuclear-transcribed mRNA catabolic process
Translational initiation
Response to hypoxia
Mitochondrial translational elongation
Endocytosis
Regulation of cell shape
Negative regulation of cell migration
Response to oxidative stress
Positive regulation of protein phosphorylation
E
Regulation of apoptotic process
Relative Gene Expression
ACTN4
CDK5
BCAR1
EGR1
TNFRSF25
LRP5
AIFM2
CASP2
RABGGTA
LGALS1
CARD10
TRAF2
DAPK3
SDF2L1
BOK
ROBO4
HS1BP3
BEX2
RBM10
BMP1
BAX
F
Negative regulation of migration
Relative Gene Expression
DRD2
RRAS
ADAM15
MIIP
ARHGAP4
ENG
ARAP3
CHRD
TIE1
ARHGDIA
Fold Change
0 0.4 0.7 1 3 5 7
J
MMP2
Relative Fold Change
GFP
PANX1
K
TRAF2
Relative Fold Change
GFP
PANX1
G
KEGG Pathway
-Log10 P-Value
Metabolic pathways
Ribosome
Biosynthesis of amino acids
Alzheimer's disease
Parkinson's disease
Huntington's disease
Oxidative phosphorylation
Biosynthesis of antibiotics
Non-alcoholic fatty liver disease (NAFLD)
MAPK signaling pathway
Axon guidance
Endocytosis
Rap1 signaling pathway
H
MAPK signaling pathway
Relative Gene Expression
HSPB1
TRAF2
FLNA
MAPK12
MAP3K11
IKBKG
RRAS
HRAS
RAC3
MAP4K2
FGFR4
ECSIT
NR4A1
FLNC
JMJD7-PLA2G4B
PLA2G4B
CACNG4
MAPK8IP3
MAP2K2
MAP3K6
I
Rap1 signaling pathway
Relative Gene Expression
DRD2
LAT
MAPK12
BCAR1
RRAS
HRAS
RGS14
CSF1R
SIPA1
RAC3
ARAP3
PARD6A
FGFR4
EFNA3
MAP2K2
SIPA1L2
Fold Change
0 0.4 0.7 1 3 5 7
L
APOBEC2
Relative Fold Change
GFP
PANX1
M
MARCKS
Relative Fold Change
GFP
PANX1
N
GJA1
Relative Expression
(normalized to GFP)
GFP
PANX1
O
Cx43 (GJA1)
GFP
PANX1
KDa
0 4 8 10 0 4 8 10
Days in culture
37
50
37
37
IB: Cx43
IB: PANX1
IB: GAPDH
P
Cx43 (GJA1)
GFP
PANX1
Normalized CX43/GAPDH Ratio
Day 0
Day 4
Day 8
Day 10
Days in culture

Figure 3.1 RNA-Seq Analysis of PANX1-Expressing aRMS Cells.

RNA was extracted from stable Rh30 cells expressing PANX1 or the GFP control for RNA-seq analysis 48 hours post cumate induction. **(A)** Representative Western blots of stable Rh30 cells expressing PANX1 and its GFP control prior to RNA extraction. Western blots are representative of three independent experiments. **(B)** Pie chart highlighting the number of genes identified by RNA-seq (n=3). Genes with an FDR cut-off of $q < 0.05$ after differential expression test are considered significantly changed. **(C)** Volcano plot showing gene expression profiles. Up- (Log_2 Fold > 1) and down-regulated (Log_2 Fold < -1) genes are shown in red and green, respectively. The horizontal bar indicates the FDR cut-off ($q = 0.05$). **(D)** DAVID gene ontology (GO) analysis of the significantly up- and down-regulated genes. A list of enriched GO terms in biological processes is shown. The gene hits under GO: Regulation of apoptotic process **(E)** and GO: Negative regulation of migration **(F)** are shown along with their expression in cells expressing PANX1 relative to their respective GFP controls. **(G)** KEGG pathway analysis of the significantly up- and down-regulated genes, of which the relative expression of the genes implicated in MAPK signaling **(H)** and Rap1 signaling **(I)** pathways are shown. RT-qPCR validation of RNA-seq hits *MMP2* **(J)**, *TRAF2* **(K)**, *APOBEC2* **(L)**, and *MARCKS* **(M)**. Red and green bars indicate up- or down-regulation from RNA-seq. Results are expressed as mean ± s.d. of three independent experiments. * $P < 0.05$ and ** $P < 0.01$ compared to GFP. *GJA1*, which encodes Cx43, showing significantly increased transcript levels **(N)** from RNA-seq, and validation of its temporal increase in protein levels by Western blotting **(O)** and its quantification **(P)** in Rh30 cells expressing PANX1 compared to the GFP control. * $P < 0.05$ compared to GFP on Day 8 and Day 10 in **(O)**. Results are expressed as mean ± s.d. of three independent experiments.

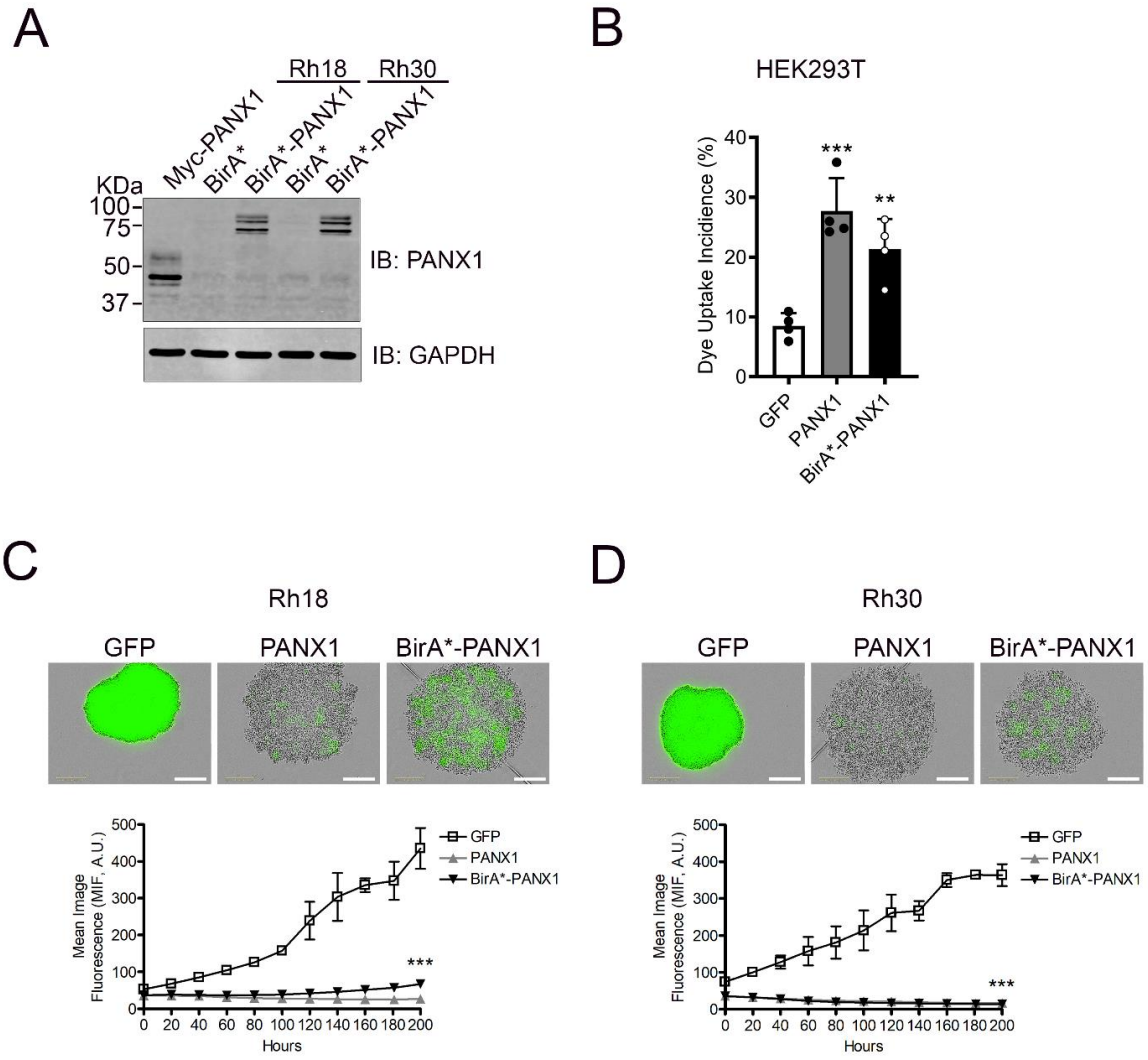
A
Rh18
Rh30
Myc-PANX1
BirA*
BirA*-PANX1
BirA*
BirA*-PANX1
KDa
100
75
50
37
IB: PANX1
IB: GAPDH
B
HEK293T
Dye Uptake Incidience (%)
40
30
20
10
0
***
**
GFP
PANX1
BirA*-PANX1
C
Rh18
GFP
PANX1
BirA*-PANX1
Mean Image Fluorescence (MIF, A.U.)
500
400
300
200
100
0
0 20 40 60 80 100 120 140 160 180 200
Hours
GFP
PANX1
BirA*-PANX1
***
D
Rh30
GFP
PANX1
BirA*-PANX1
Mean Image Fluorescence (MIF, A.U.)
500
400
300
200
100
0
0 20 40 60 80 100 120 140 160 180 200
Hours
GFP
PANX1
BirA*-PANX1
***

Figure 3.2 The BirA* Tag Does Not Affect PANX1 Function.

(A) Representative Western blot of BirA*-PANX1 and Myc-PANX1 expressed in Rh18 (eRMS) and Rh30 (aRMS) cells. Western blots are representative of three independent experiments. **(B)** Sulforhodamine B dye uptake induced by mechanical stimulation in HEK293T cells expressing GFP (control), PANX1, or BirA*-PANX1. Results are expressed as mean ± s.d. of four independent experiments. *** $P < 0.001$ and ** $P < 0.01$ compared to GFP. 3D spheroid formation using our stable cumate-inducible Rh18 and Rh30 cell lines was assessed in the presence of cumate to allow PANX1 or BirA*-PANX1 expression. Representative images of Rh18 **(C)** and Rh30 **(D)** cells taken at 200 hours are shown. As these cells express GFP constitutively, the changes in mean image fluorescence (MIF) over time, a measurement of spheroid size, were quantified for both Rh18 **(C)** and Rh30 **(D)** cells. Results are expressed as mean ± s.d. of three independent experiments. *** $P<0.001$ compared to GFP for both PANX1 and BirA*-PANX1. A.U.: arbitrary units. Bars = 300 μm.

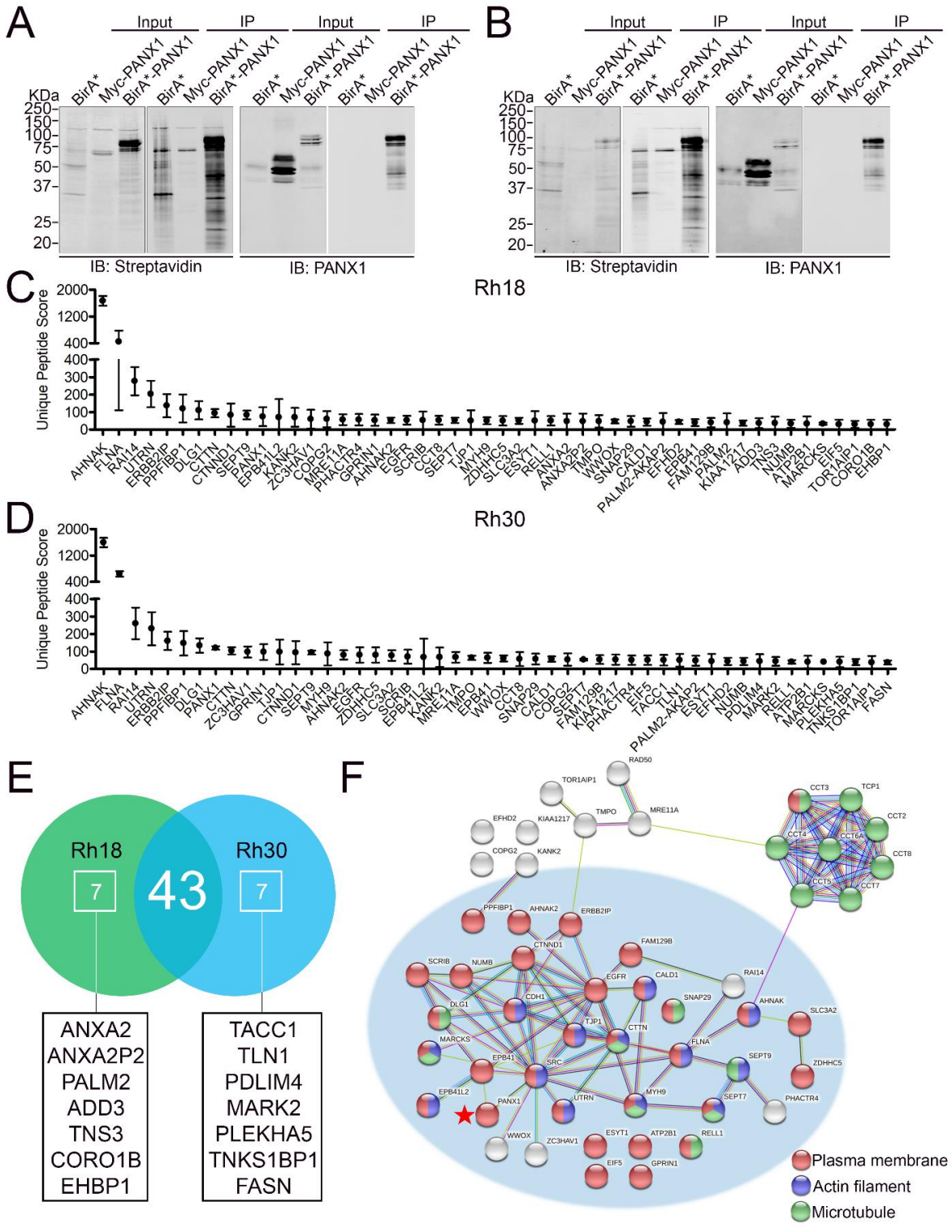
A
Input
IP
Input
IP
BirA*
Myc-PANX1
BirA*-PANX1
KDa
250
150
100
75
50
37
25
20
IB: Streptavidin
IB: PANX1
B
Rh18
C
Unique Peptide Score
2000
1200
400
300
200
100
0
AHNAK
FLNA
RAI14
UTRN
ERBB2IP
PPFIBP1
DLG1
CTTN
CTNND1
SEPT9
PANX1
EPB41L2
KANK2
ZC3HAV1
COPG2
MRE11A
PHACTR4
GPRIN1
AHNAK2
EGFR
SCRIB
CCT8
SEPT7
TJP1
MYH9
ZDHHC5
SLC3A2
ESYT1
RELL1
ANXA2
ANXA2P2
TMPO
WWOX
SNAP29
CALD1
PALM2-AKAP2
EFHD2
EPB41
FAM129B
PALM2
KIAA1217
ADD3
TNS3
NUMB
ATP2B1
MARCKS
EIF5
TOR1AIP1
CORO1B
EHBP1
D
Rh30
E
Rh18
7
43
Rh30
7
ANXA2
ANXA2P2
PALM2
ADD3
TNS3
CORO1B
EHBP1
TACC1
TLN1
PDLIM4
MARK2
PLEKHA5
TNKS1BP1
FASN
F
RAD50
TOR1AIP1
TMPO
MRE11A
EFHD2
KIAA1217
COPG2
KANK2
CCT3
TCP1
CCT2
CCT4
CCT6A
CCT8
CCT5
CCT7
PPFIBP1
AHNAK2
ERBB2IP
CTNND1
FAM129B
SCRIB
NUMB
EGFR
CALD1
RAI14
DLG1
CDH1
SNAP29
AHNAK
SLC3A2
TJP1
CTTN
MARCKS
FLNA
EPB41
SRC
SEPT9
ZDHHC5
EPB41L2
PANX1
UTRN
MYH9
SEPT7
PHACTR4
WWOX
ZC3HAV1
ESYT1
ATP2B1
RELL1
EIF5
GPRIN1
Plasma membrane
Actin filament
Microtubule

Figure 3.3 BioID Analysis of PANX1-interacting Proteins in RMS Cells.

Representative Western blots of biotinylated proteins captured by streptavidin and BirA*-PANX1 in Rh18 (eRMS) **(A)** and Rh30 (aRMS) **(B)** are shown. BirA* and Myc-PANX1 were used as background controls for biotinylation and HPLC-ESI-MS/MS, respectively. Western blots are representative of three independent experiments. Top 50 protein hits in Rh18 **(C)** and Rh30 **(D)** identified by BioID are displayed. Results are shown as mean ± s.d. of Unique Peptide Counts normalized to the Myc-PANX1 background controls from three independent experiments. **(E)** Venn diagram showing the overlapping top 50 hits between Rh18 and Rh30 cells. **(F)** STRING analysis of the 43 overlapping hits reveals a PANX1 (red star) interactome consisting of plasma membrane (red), actin microfilament (blue) and microtubule (green) associated proteins.

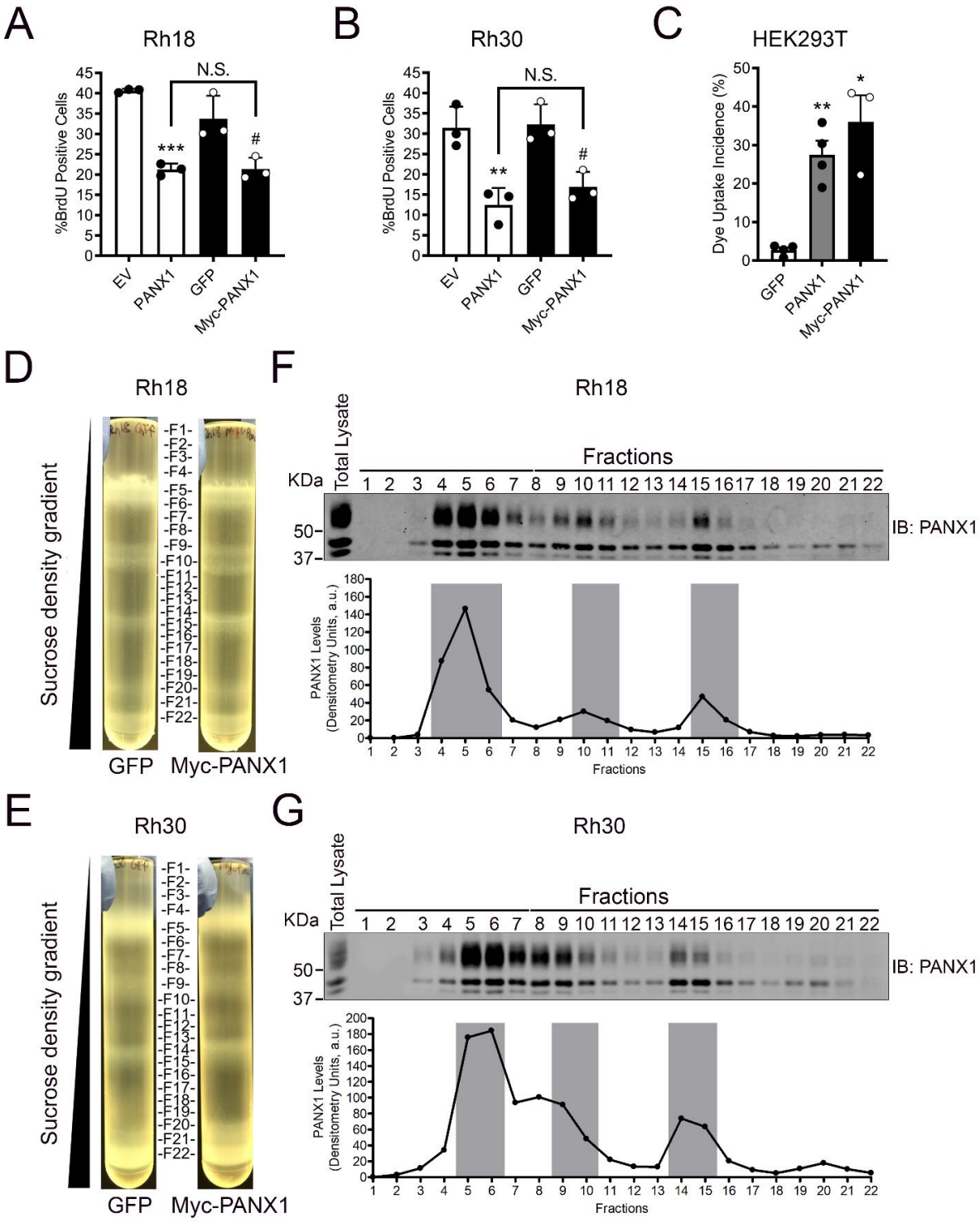
A
Rh18
%BrdU Positive Cells
N.S.
***
#
EV
PANX1
GFP
Myc-PANX1
B
Rh30
%BrdU Positive Cells
N.S.
**
#
EV
PANX1
GFP
Myc-PANX1
C
HEK293T
Dye Uptake Incidence (%)
**
*
GFP
PANX1
Myc-PANX1
D
Rh18
Sucrose density gradient
-F1-
-F2-
-F3-
-F4-
-F5-
-F6-
-F7-
-F8-
-F9-
-F10-
-F11-
-F12-
-F13-
-F14-
-F15-
-F16-
-F17-
-F18-
-F19-
-F20-
-F21-
-F22-
GFP
Myc-PANX1
E
Rh30
Sucrose density gradient
-F1-
-F2-
-F3-
-F4-
-F5-
-F6-
-F7-
-F8-
-F9-
-F10-
-F11-
-F12-
-F13-
-F14-
-F15-
-F16-
-F17-
-F18-
-F19-
-F20-
-F21-
-F22-
GFP
Myc-PANX1
F
Rh18
Total Lysate
Fractions
KDa
1 2 3 4 5 6 7 8 9 10 11 12 13 14 15 16 17 18 19 20 21 22
50
37
IB: PANX1
PANX1 Levels
(Densitometry Units, a.u.)
Fractions
G
Rh30
Total Lysate
Fractions
KDa
1 2 3 4 5 6 7 8 9 10 11 12 13 14 15 16 17 18 19 20 21 22
50
37
IB: PANX1
PANX1 Levels
(Densitometry Units, a.u.)
Fractions

Figure 3.4 Enrichment of PANX1 by Subcellular Fractionation.

BrdU incorporation of wild-type Rh18 (eRMS) **(A)** and Rh30 (aRMS) **(B)** cells expressing PANX1 or Myc-PANX1 and respective empty vector (EV) or GFP controls. Results are expressed as mean ± s.d. of three independent experiments. ** $P < 0.01$ and *** $P < 0.001$ compared to EV, # $P < 0.05$ compared to GFP. N.S.: Not Significant. **(C)** Sulforhodamine B dye uptake induced by mechanical stimulation with HEK293T cells transiently expressing GFP, PANX1, or Myc-PANX1. Results are expressed as mean ± s.d. of four independent experiments. * $P < 0.05$ and ** $P < 0.01$ compared to GFP. Stable Rh18 and Rh30 cells expressing Myc-PANX1 or its GFP control vector were homogenized and separated by a sucrose gradient by ultra-highspeed centrifugation to enrich Myc-PANX1-containing subcellular fractions. The Myc-PANX1 enriched fractions or their corresponding GFP control fractions were pooled and subjected to co-immunoprecipitation by anti-Myc antibodies. The co-IP'ed samples were further analyzed by HPLC-ESI-MS/MS. Representative images of Rh18 **(D)** and Rh30 **(E)** cell lysates separated by a sucrose density gradient. Subcellular fractions of Rh18 **(F)** and Rh30 **(G)** cell lysates containing Myc-PANX1 were analyzed by Western blotting and the quantification of Myc-PANX1 levels are shown below. The Myc-PANX1 enriched fractions, indicated by the shaded areas, and their corresponding GFP control fractions were combined separately for co-IP by anti-Myc antibodies and the subsequent HPLC-ESI-MS/MS analysis. Results are from two independent experiments.

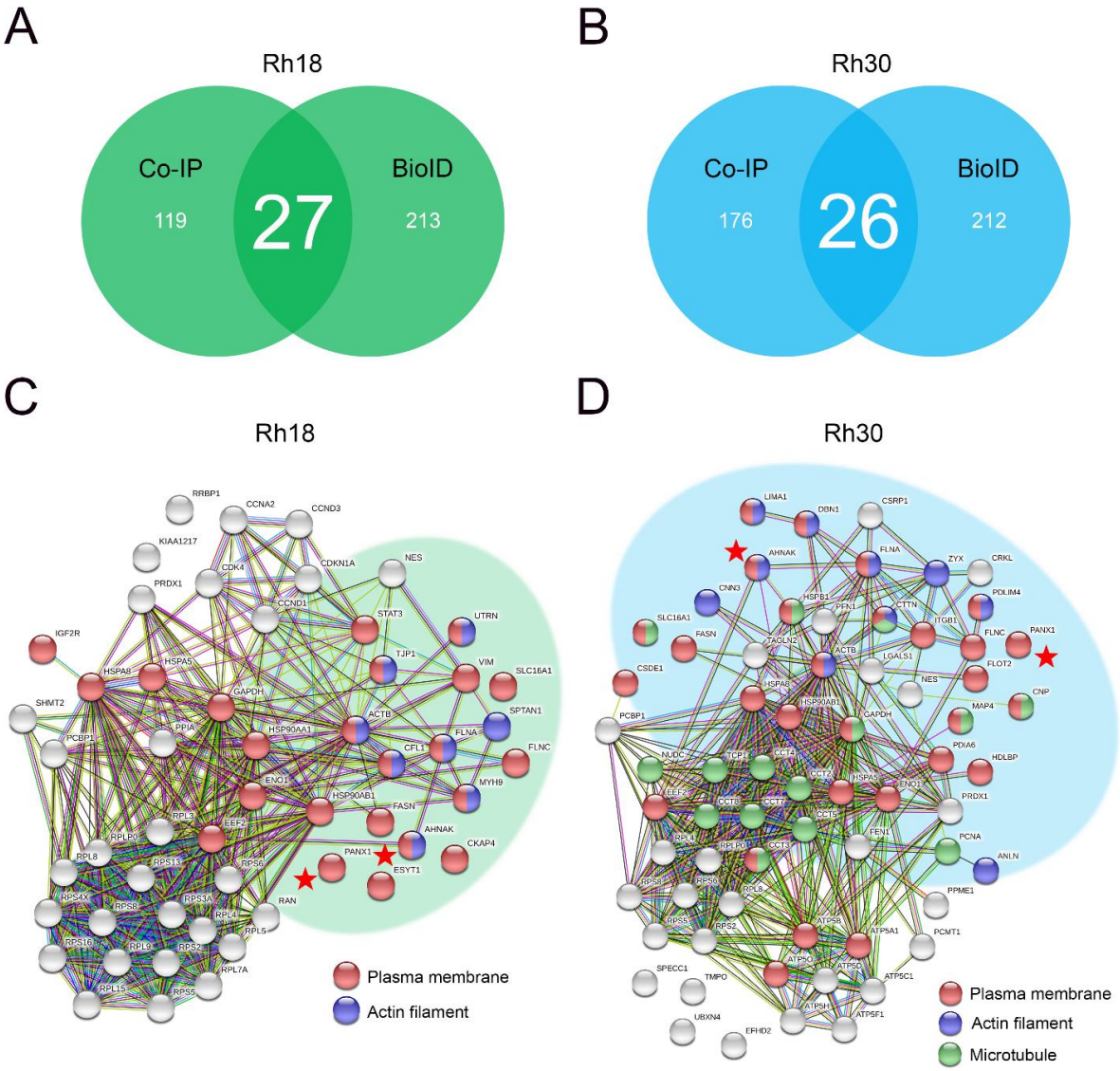
A
Rh18
Co-IP
119
27
BioID
213
B
Rh30
Co-IP
176
26
BioID
212
C
Rh18
Plasma membrane
Actin filament
D
Rh30
Plasma membrane
Actin filament
Microtubule

Figure 3.5 The Overlapping Hits Identified from BioID and Co-IP using PANX1-Enriched Subcellular Fractions Revealed an Interactome Consisting of Plasma Membrane-, Actin Filament-, and Microtubule-Associated Proteins.

The total protein hits in Rh18 (eRMS) and Rh30 (aRMS) cells identified by both BioID and co-IP using myc-PANX1 enriched fractions were analyzed. Venn diagrams show 27 and 26 overlapping protein hits between the two HPLC-ESI-MS/MS approaches with Rh18 **(A)** and Rh30 **(B)** cells, respectively. STRING protein interaction network analysis of the overlapping hits from Rh18 **(C)** and Rh30 **(D)** cells. The proteins in the network are labeled according to their respective cell component GO terms: plasma membrane (red), actin microfilament (blue) and microtubules (green). PANX1 and the top hit AHNAK are marked with a red star. The shaded areas show clusters of plasma membrane associated protein hits.

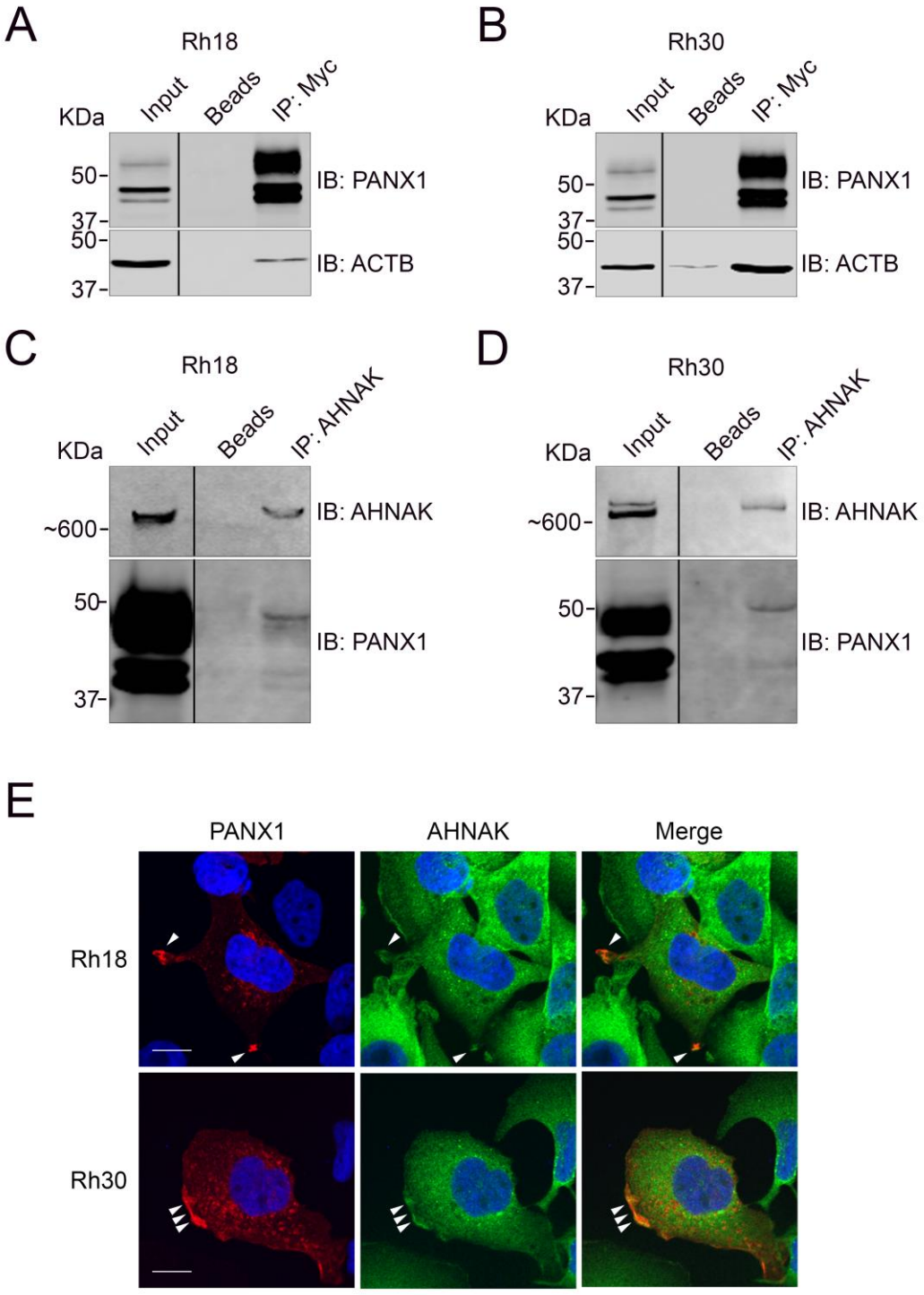
A
Rh18
Input
Beads
IP: Myc
KDa
50-
37-
50-
37-
IB: PANX1
IB: ACTB
B
Rh30
Input
Beads
IP: Myc
KDa
50-
37-
50-
37-
IB: PANX1
IB: ACTB
C
Rh18
Input
Beads
IP: AHNAK
KDa
~600-
50-
37-
IB: AHNAK
IB: PANX1
D
Rh30
Input
Beads
IP: AHNAK
KDa
~600-
50-
37-
IB: AHNAK
IB: PANX1
E
PANX1
AHNAK
Merge
Rh18
Rh30

Figure 3.6 PANX1 Interacts with ACTB and AHNAK.

Stable Rh18 (eRMS) and Rh30 (aRMS) cells were induced to express PANX1 or Myc-PANX1 for 48 hours and whole cell lysates were subjected to co-IP followed by Western blotting analyses. The known PANX1 binding partner, ACTB, was pull-downed with Myc-PANX1 in Rh18 **(A)** and Rh30 **(B)** lysates using anti-Myc antibodies. In addition, PANX1 was pull-downed with AHNAK in both Rh18 **(C)** and Rh30 **(D)** lysates using anti-AHNAK antibodies. All Western blots are representative of three independent experiments. **(E)** Immunofluorescence confocal laser microscopy showing colocalization (arrowheads) of transiently expressed PANX1 (red) and endogenous AHNAK (green) in Rh18 and Rh30 cells. DAPI-stained nuclei are shown in blue. Bar = 20 μm.

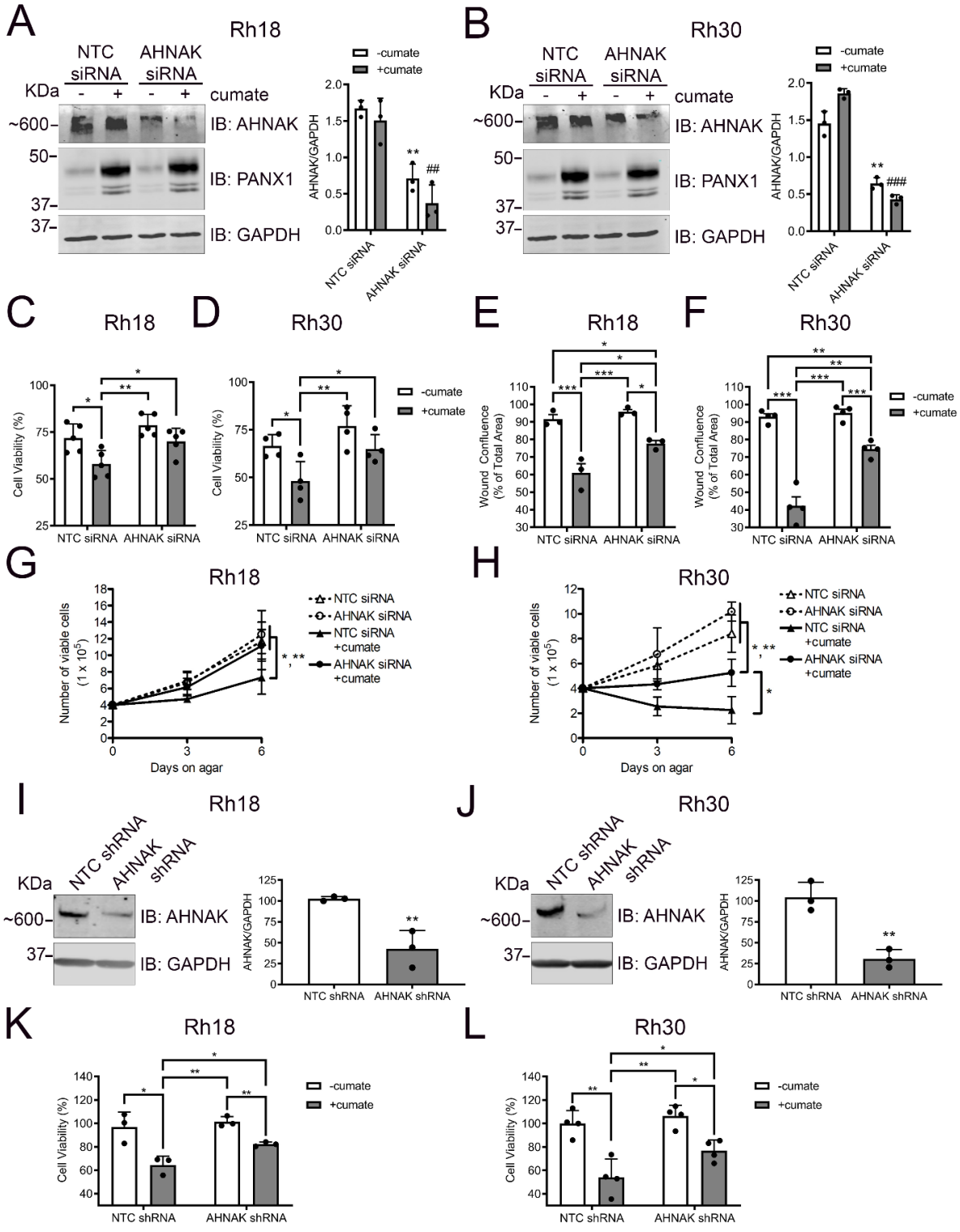
A
Rh18
NTC siRNA
AHNAK siRNA
KDa
cumate
~600
IB: AHNAK
50
IB: PANX1
37
37
IB: GAPDH
-cumate
+cumate
AHNAK/GAPDH
NTC siRNA
AHNAK siRNA
B
Rh30
C
Rh18
Cell Viability (%)
D
Rh30
E
Rh18
Wound Confluence (% of Total Area)
F
Rh30
G
Rh18
Number of viable cells (1 x 10^5)
Days on agar
NTC siRNA
AHNAK siRNA
NTC siRNA +cumate
AHNAK siRNA +cumate
H
Rh30
I
Rh18
NTC shRNA
AHNAK shRNA
J
Rh30
K
Rh18
L
Rh30

Figure 3.7 AHNAK Knockdown Significantly Reversed the PANX1-induced Suppression of Malignant Properties in RMS Cells.

Rh18 (eRMS) and Rh30 (aRMS) cells were transiently transfected with siRNA targeting AHNAK or a scrambled siRNA non-targeting control (NTC). Representative Western blots of Rh18 **(A)** and Rh30 **(B)** cells and their respective quantifications (n=3) of AHNAK levels 72 hours following siRNA-mediated knockdown (KD). GAPDH was used as a loading control. ** $P < 0.01$ compared to NTC siRNA (- cumate); ## $P < 0.01$ and ### $P < 0.001$ compared to NTC siRNA (+ cumate). PANX1 expression was induced with 30 µg/mL of cumate 48 hours post AHNAK KD and then subjected to Alamar blue viability, scratch wound migration, and soft agar anoikis assays. Alamar blue assay of Rh18 (n=5) **(C)** and Rh30 (n=4) **(D)** showing percent (%) cell viability normalized to NTC siRNA (-cumate) of the respective cell line. * $P < 0.05$ and ** $P < 0.01$. Wound closure of Rh18 (n=3) **(E)** and Rh30 (n=4) **(F)** cells, were monitored for 60 or 80 hours, respectively. The confluence of the wound area at the endpoint is shown as a percentage of the NTC siRNA (-cumate) from the respective cell line. * $P < 0.05$, ** $P < 0.01$ and *** $P < 0.001$. Rh18 (n=4) **(G)** and Rh30 (n=3) **(H)** cells were grown in suspension for 6 days and the number of viable cells counted by Trypan Blue dye exclusion assay on Days 0, 3 and 6 are shown. Day 0 denotes the time of cell seeding on soft agar. * $P < 0.05$ and ** $P < 0.01$. Stable Rh18 and Rh30 cells were treated with 50 ng/µL doxycycline for 96 hours to induce the expression of AHNAK shRNA or its NTC shRNA and then analyzed by Western blotting to assess AHNAK KD efficiency. Representative Western blots and their respective quantifications (n=3) of AHNAK levels in Rh18 **(I)** and Rh30 **(J)**. GAPDH was used as a loading control. ** $P < 0.01$ compared to NTC shRNA. For Alamar blue viability assay, stable Rh18 and Rh30 cells were treated with 30 µg/mL of cumate for 48 hours to allow

PANX1 expression post shRNA-mediated AHNAK KD. Results are expressed as percent (%) cell viability of NTC shRNA of either Rh18 (n=3) **(K)** or Rh30 (n=4) **(L)** cells in absence of PANX1 over-expression (-cumate). * $P < 0.05$ and ** $P < 0.01$. All results are expressed as mean ± s.d.

3.6 DISCUSSION

We had previously demonstrated that PANX1 alleviates RMS malignant properties (Xiang et al., 2018). However, the molecular mechanisms involved remained to be investigated. Here, we have taken a combination of unbiased genome-wide approaches to provide a comprehensive view of the PANX1 transcriptome and interactome in RMS. We found that PANX1 modulates the expression of genes involved in numerous biological processes characteristic of cancer including, in descending order of significance, cell-cell adhesion, extracellular matrix disassembly, regulation of apoptosis, migration, and cellular morphology. Notably, regulation of apoptosis and cell migration were reflective of our previously reported PANX1-mediated inhibition of RMS migratory capacity and induction of apoptosis (Xiang et al., 2018) and providing insights for potential responsible genes. For instance, the transcript of caspase 2, the most conserved caspase family member across species (Kumar et al., 1994; Yuan et al., 1993), is found to be significantly up-regulated in RMS cells expressing ectopic PANX1. Interestingly, PANX1 is a recognized target of caspase 3 and the cleavage of its c-terminal tail aids the progression of apoptosis (Chekeni et al., 2010). We also found MAPK and Rap1 signaling pathways being significantly implicated in PANX1-expressing RMS cells. Induction of p38 MAPK signaling by a constitutively active mutant form of MAPK kinase 6 promotes terminal differentiation of RMS cells (Puri et al., 2000) and PKCα-mediated activation of MAPK cascades results in RMS cell growth arrest and differentiation (Mauro et al., 2002). Moreover, the crosstalk between MAPK and Rap1 signaling pathways has been shown to regulate metastasis of numerous cancers (Zhang et al., 2017). Future research may unveil whether PANX1 acts through MAPK and Rap1 signal transduction to reduce the proliferation and migration capacities of RMS cells (Xiang et al.,

2018). To our surprise, the transcript and protein levels of Cx43 are increased by ectopic expression of PANX1 in RMS cells. As Cx43 over-expression in RMS has been shown to inhibit its proliferation and promote cellular fusion, an early step of myogenic differentiation (Proulx et al., 1997), PANX1 may work in synergy with Cx43 to suppress RMS malignant phenotypes.

Notably, 43 of the top 50 protein hits from BioID between eRMS and aRMS cells are identical, suggesting that PANX1 inhibits the RMS malignant phenotype through similar mechanisms in both histological subtypes. The majority of the proteins in the PANX1 interactome are associated with the plasma membrane where PANX1 is known to localize and function (Chiu et al., 2018). However, due to the long half-life of PANX1 (Penuela et al., 2007), plasma membrane bound proteins with weak or transient interactions with PANX1 may be over-represented by extensive biotinylation. Moreover, as the number and spatial accessibility of lysine residues correlate with the level of biotinylation (Minde et al., 2020; Roux et al., 2012), candidate proteins of large size may also be over-represented. Nonetheless, these proteins may still be genuine interactors of PANX1 thus warranting further confirmation by Co-IP. The diverse localization pattern of the 14 mutually exclusive proteins in the cytosolic, cytoskeletal, and plasma membrane compartments suggest that these phosphoproteins were likely biotinylated during the trafficking of BirA*-PANX1 to the plasma membrane or were signaling molecules that traversed between multiple cellular compartments in RMS. The physical interaction between PANX1 and the actin cytoskeleton scaffold has been proposed to be responsible for the mechanosensitive opening of PANX1 channels in several cell types (Bhalla-Gehi et al., 2010; Locovei et al., 2006; Richter et al., 2014; Seminario-Vidal et al., 2011). In addition, Panx1 has been suggested to regulate murine neurite migration and extension by remodeling their actin cytoskeleton through interaction

with an actin cytoskeleton modulating protein, actin-related protein 3 (Arp3) (Wicki-Stordeur and Swayne, 2013). We also found components of the actin cytoskeleton in our PANX1 interactome database, which together with our co-IP data of Myc-PANX1 and ACTB using whole cell lysates, further confirmed this interaction in RMS. However, the ARP family of proteins were not found in our PANX1 interactome suggesting alternative mechanisms for PANX1 to regulate RMS cell migration for which the interaction of PANX1 with AHNAK may shed clues. Our data suggest that PANX1 interacts with AHNAK in specialized plasma membrane compartments resembling pseudopodia, which are known to be associated with tumor cell migration and invasion (Chen et al., 2017; Lee et al., 2014; Shankar et al., 2010; Sheppard et al., 2016; Zhang et al., 2019). Interestingly, AHNAK has been implicated in the regulation of cell membrane cytoarchitecture, as well as pseudopod protrusion via interaction with Annexin A2, septin-9, and Ca^{2+}-dependent S100 proteins (Benaud et al., 2004; Shankar et al., 2010), which have both been shown to contribute to cancer metastasis (Chen et al., 2017; Peng et al., 2019; Shankar et al., 2010; Silva et al., 2016; Sudo et al., 2014). Both Annexin A2 and the pseudopodia specific protein septin-9 (Shankar et al., 2010) were found in the PANX1 interactome. Aside from migration, AHNAK has also been shown to regulate proliferation of several cancers (Chen et al., 2017; Lee et al., 2014) and enhances the PKCα signaling pathway in fibroblast (In et al., 2008) which coincides with our RNA-seq data.

Collectively, we provide the first comprehensive transcriptomic and proteomic databases for PANX1 and further demonstrate their usefulness for exploring novel signaling mechanisms such as the newly described interaction of PANX1 with AHNAK. The functional dependence of AHNAK in PANX1-mediated regulation of RMS cell proliferation, migration, and anoikis provides the first insights into the molecular mechanism by which PANX1 inhibits RMS malignant properties. We expect that our transcriptomic and proteomic databases will

foster new research and extend our current knowledge of the mechanism regulating PANX1, together with PANX1-mediated downstream signaling pathways in RMS and other cellular contexts.

3.7 REFERENCES

Bargiotas, P., Krenz, A., Hormuzdi, S.G., Ridder, D.A., Herb, A., Barakat, W., Penuela, S., von Engelhardt, J., Monyer, H., and Schwaninger, M. (2011). Pannexins in ischemia-induced neurodegeneration. Proc. Natl. Acad. Sci. U. S. A. *108*, 20772–20777.

Benaud, C., Gentil, B.J., Assard, N., Court, M., Garin, J., Delphin, C., and Baudier, J. (2004). AHNAK interaction with the annexin 2/S100A10 complex regulates cell membrane cytoarchitecture. J. Cell Biol. *164*, 133–144.

Bhalla-Gehi, R., Penuela, S., Churko, J.M., Shao, Q., and Laird, D.W. (2010). Pannexin1 and pannexin3 delivery, cell surface dynamics, and cytoskeletal interactions. J. Biol. Chem. *285*, 9147–9160.

Boassa, D., Ambrosi, C., Qiu, F., Dahl, G., Gaietta, G., and Sosinsky, G. (2007). Pannexin1 channels contain a glycosylation site that targets the hexamer to the plasma membrane. J. Biol. Chem. *282*, 31733–31743.

Boyce, A.K.J., Epp, A.L., Nagarajan, A., and Swayne, L.A. (2018). Transcriptional and post-translational regulation of pannexins. Biochim. Biophys. Acta - Biomembr. *1860*, 72–82.

Chekeni, F.B., Elliott, M.R., Sandilos, J.K., Walk, S.F., Kinchen, J.M., Lazarowski, E.R., Armstrong, A.J., Penuela, S., Laird, D.W., Salvesen, G.S., et al. (2010). Pannexin 1 channels mediate 'find-me' signal release and membrane permeability during apoptosis. Nature *467*, 863–867.

Chen, B., Wang, J., Dai, D., Zhou, Q., Guo, X., Tian, Z., Huang, X., Yang, L., Tang, H., and Xie, X. (2017). AHNAK suppresses tumour proliferation and invasion by targeting multiple pathways in triple-negative breast cancer. J. Exp. Clin. Cancer Res. *36*, 1–11.

Chen, C., Dorado Garcia, H., Scheer, M., and Henssen, A.G. (2019). Current and Future Treatment Strategies for Rhabdomyosarcoma. Front. Oncol. *9*, 1–18.

Chiu, Y.H., Schappe, M.S., Desai, B.N., and Bayliss, D.A. (2018). Revisiting multimodal activation and channel properties of Pannexin 1. J. Gen. Physiol. *150*, 19–39.

Cowan, K.N., Langlois, S., Penuela, S., Cowan, B.J., and Laird, D.W. (2012). Pannexin1 and Pannexin3 exhibit distinct localization patterns in human skin appendages and are regulated during keratinocyte differentiation and carcinogenesis. Cell Commun. Adhes. *19*, 45–53.

Cui, H., Liu, Y., Qin, L., Wang, L., and Huang, Y. (2016). Increased membrane localization of pannexin1 in human corneal synaptosomes causes enhanced stimulated ATP release in

chronic diabetes mellitus. Medicine (Baltimore). *95*, e5084.
Dobson, C.C., Langlois, S., Grynspan, D., and Cowan, K.N. (2016). Engaging Cell Death Pathways for the Treatment of Rhabdomyosarcoma. Crit. Rev. Oncog. *21*, 221–239.
Dossi, E., Blauwblomme, T., Moulard, J., Chever, O., Vasile, F., Guinard, E., Le Bert, M., Couillin, I., Pallud, J., Capelle, L., et al. (2018). Pannexin-1 channels contribute to seizure generation in human epileptic brain tissue and in a mouse model of epilepsy. Sci. Transl. Med. *10*, 1–14.
Fowler, S., Akins, M., and Bennett, S.A.L. (2016). Preparation of Gap Junctions in Membrane Microdomains for Immunoprecipitation and Mass Spectrometry Interactome Analysis. In Methods in Molecular Biology, pp. 9–14.
Fowler, S.L., Akins, M., Zhou, H., Figeys, D., and Bennett, S.A.L.L. (2013). The liver connexin32 interactome is a novel plasma membrane-mitochondrial signaling nexus. J. Proteome Res. *12*, 2597–2610.
Frank, S.B., Schulz, V. V., and Miranti, C.K. (2017). A streamlined method for the design and cloning of shRNAs into an optimized Dox-inducible lentiviral vector. BMC Biotechnol. *17*, 1–10.
Freeman, T.J., Sayedyahossein, S., Johnston, D., Sanchez-Pupo, R.E., O'Donnell, B., Huang, K., Lakhani, Z., Nouri-Nejad, D., Barr, K.J., Harland, L., et al. (2019). Inhibition of pannexin 1 reduces the tumorigenic properties of human melanoma cells. Cancers (Basel). *11*, 1–24.
Gentil, B.J., Delphin, C., Benaud, C., and Baudier, J. (2003). Expression of the giant protein AHNAK (desmoyokin) in muscle and lining epithelial cells. J. Histochem. Cytochem. *51*, 339–348.
Gentil, B.J., Benaud, C., Delphin, C., Remy, C., Berezowski, V., Cecchelli, R., Feraud, O., Vittet, D., and Baudier, J. (2005). Specific AHNAK expression in brain endothelial cells with barrier properties. J. Cell. Physiol. *203*, 362–371.
Good, M.E., Chiu, Y.-H., Poon, I.K., Medina, C.B., Butcher, J.T., Mendu, S.K., DeLalio, L.J., Lohman, A.W., Leitinger, N., Barrett, E.J., et al. (2017). Pannexin 1 Channels as an Unexpected New Target of the Anti-Hypertensive Drug Spironolactone. Circ. Res.
Good, M.E., Chiu, Y.-H.H., Poon, I.K.H., Medina, C.B., Butcher, J.T., Mendu, S.K., DeLalio, L.J., Lohman, A.W., Leitinger, N., Barrett, E.J., et al. (2018). Pannexin 1 channels as an unexpected new target of the anti-hypertensive drug spironolactone. Circ. Res. *122*,

606–615.
Hashimoto, T., Amagai, M., Parry, D.A.D., Dixon, T.W., Tsukita, S., Tsukita, S., Miki, K., Sakai, K., Inokuchi, Y., Kudoh, J., et al. (1993). Desmoyokin, a 680 kDa keratinocyte plasma membrane-associated protein, is homologous to the protein encoded by human gene AHNAK. J. Cell Sci. *105*, 275–286.
Hashimoto, T., Gamou, S., Shimizu, N., Kitajima, Y., and Nishikawa, T. (1995). Regulation of translocation of the desmoyokin/AHNAK protein to the plasma membrane in keratinocytes by protein kinase C. Exp. Cell Res. *217*, 258–266.
Huang, D.W., Sherman, B.T., and Lempicki, R.A. (2009). Systematic and integrative analysis of large gene lists using DAVID bioinformatics resources. Nat. Protoc. *4*, 44–57.
Huang, Y., Laval, S.H., van Remoortere, A., Baudier, J., Benaud, C., Anderson, L.V.B., Straub, V., Deelder, A., Frants, R.R., den Dunnen, J.T., et al. (2007). AHNAK, a novel component of the dysferlin protein complex, redistributes to the cytoplasm with dysferlin during skeletal muscle regeneration. FASEB J. *21*, 732–742.
In, H.L., Hee, J.L., Yoon, S., Je, K.S., Duk, S.B., Sue, G.R., and Yun, S.B. (2008). Ahnak protein activates protein kinase C (PKC) through dissociation of the PKC-protein phosphatase 2A complex. J. Biol. Chem. *283*, 6312–6320.
Keller, C., and Guttridge, D.C. (2013). Mechanisms of impaired differentiation in rhabdomyosarcoma. FEBS J. *280*, 4323–4334.
Komuro, A., Masuda, Y., Kobayashi, K., Babbitt, R., Gunel, M., Flavell, R.A., and Marchesi, V.T. (2004). The AHNAKs are a class of giant propeller-like proteins that associate with calcium channel proteins of cardiomyocytes and other cells. Proc. Natl. Acad. Sci. *101*, 4053–4058.
Kumar, S., Kinoshita, M., Noda, M., Copeland, N.G., and Jenkins, N.A. (1994). Induction of apoptosis by the mouse Nedd2 gene, which encodes a protein similar to the product of the Caenorhabditis elegans cell death gene ced-3 and the mammalian IL-1β-converting enzyme. Genes Dev. *8*, 1613–1626.
Lai, C.P.K., Bechberger, J.F., Thompson, R.J., MacVicar, B.A., Bruzzone, R., and Naus, C.C. (2007). Tumor-suppressive effects of pannexin 1 in C6 glioma cells. Cancer Res. *67*, 1545–1554.
Langlois, S., and Cowan, K.N. (2017). Regulation of Skeletal Muscle Myoblast

Differentiation and Proliferation by Pannexins. Adv. Exp. Med. Biol. *925*, 57–73.
Langlois, S., Xiang, X., Young, K., Cowan, B.J., Penuela, S., and Cowan, K.N. (2014). Pannexin 1 and pannexin 3 channels regulate skeletal muscle myoblast proliferation and differentiation. J. Biol. Chem. *289*, 30717–30731.
Lee, I.H., Sohn, M., Lim, H.J., Yoon, S., Oh, H., Shin, S., Shin, J.H., Oh, S.-H., Kim, J., Lee, D.K., et al. (2014). Ahnak functions as a tumor suppressor via modulation of TGFβ/Smad signaling pathway. Oncogene *33*, 4675–4684.
Liu, H., Yuan, M., Yao, Y., Wu, D., Dong, S., and Tong, X. (2019). In vitro effect of Pannexin 1 channel on the invasion and migration of I-10 testicular cancer cells via ERK1/2 signaling pathway. Biomed. Pharmacother. *117*, 109090.
Locovei, S., Wang, J., and Dahl, G. (2006). Activation of pannexin 1 channels by ATP through P2Y receptors and by cytoplasmic calcium. FEBS Lett. *580*, 239–244.
Ma, H.L., Jiang, Q., Han, S., Wu, Y., Tomshine, J.C., Wang, D., Gan, Y., Zou, G., and Liang, X.J. (2012). Multicellular tumor spheroids as an in vivo-like tumor model for three-dimensional imaging of chemotherapeutic and nano material cellular penetration. Mol. … *11*, 487–498.
Ma, W., Hui, H., Pelegrin, P., and Surprenant, A. (2009). Pharmacological characterization of pannexin-1 currents expressed in mammalian cells. J. Pharmacol. Exp. Ther. *328*, 409–418.
Malempati, S., and Hawkins, D.S. (2012). Rhabdomyosarcoma: Review of the Children's Oncology Group (COG) soft-tissue Sarcoma committee experience and rationale for current COG studies. Pediatr. Blood Cancer *59*, 5–10.
Mauro, A., Ciccarelli, C., Cesaris, P. De, Scoglio, A., Bouche, M., Molinaro, M., Aquino, A., and Zani, B.M. (2002). PKCalpha-mediated ERK, JNK and p38 activation regulates the myogenic program in human rhabdomyosarcoma cells. J. Cell Sci. *115*, 3587–3599.
Minde, D.P., Ramakrishna, M., and Lilley, K.S. (2020). Biotin proximity tagging favours unfolded proteins and enables the study of intrinsically disordered regions. Commun. Biol. *3*, 1–13.
Nie, Z., Ning, W., Amagai, M., and Hashimoto, T. (2000). C-terminus of desmoyokin/AHNAK protein is responsible for its translocation between the nucleus and cytoplasm. J. Invest. Dermatol. *114*, 1044–1049.

Parham, D.M., and Barr, F.G. (2013). Classification of rhabdomyosarcoma and its molecular basis. Adv. Anat. Pathol. *20*, 387–397.

Peng, R., Zhang, P.F., Yang, X., Wei, C.Y., Huang, X.Y., Cai, J. Bin, Lu, J.C., Gao, C., Sun, H.X., Gao, Q., et al. (2019). Overexpression of RNF38 facilitates TGF-β signaling by Ubiquitinating and degrading AHNAK in hepatocellular carcinoma. J. Exp. Clin. Cancer Res. *38*, 1–14.

Penuela, S., Bhalla, R., Gong, X.Q., Cowan, K.N., Celetti, S.J., Cowan, B.J., Bai, D., Shao, Q., and Laird, D.W. (2007). Pannexin 1 and pannexin 3 are glycoproteins that exhibit many distinct characteristics from the connexin family of gap junction proteins. J. Cell Sci. *120*, 3772–3783.

Penuela, S., Gyenis, L., Ablack, A., Churko, J.M., Berger, A.C., Litchfield, D.W., Lewis, J.D., and Laird, D.W. (2012). Loss of pannexin 1 attenuates melanoma progression by reversion to a melanocytic phenotype. J. Biol. Chem. *287*, 29184–29193.

Pham, T. Le, St-Pierre, M.E., Ravel-Chapuis, A., Parks, T.E.C., Langlois, S., Penuela, S., Jasmin, B.J., and Cowan, K.N. (2018). Expression of Pannexin 1 and Pannexin 3 during skeletal muscle development, regeneration, and Duchenne muscular dystrophy. J. Cell. Physiol. *233*, 7057–7070.

Proulx, A.A., Lin, Z.X., and Naus, C.C.G. (1997). Transfection of rhabdomyosarcoma cells with connexin43 induces myogenic differentiation. Cell Growth Differ. *8*, 533–540.

Puri, P.L., Wu, Z., Zhang, P., Wood, L.D., Bhakta, K.S., Han, J., Feramisco, J.R., Karin, M., and Wang, J.Y. (2000). Induction of terminal differentiation by constitutive activation of p38 MAP kinase in human rhabdomyosarcoma cells. Genes Dev. *14*, 574–584.

Richter, K., Kiefer, K.P., Grzesik, B.A., Clauss, W.G., and Fronius, M. (2014). Hydrostatic pressure activates ATP-sensitive K channels in lung epithelium by ATP release through pannexin and connexin hemichannels. FASEB J. *28*, 45–55.

Roux, K.J., Kim, D.I., Raida, M., and Burke, B. (2012). A promiscuous biotin ligase fusion protein identifies proximal and interacting proteins in mammalian cells. J. Cell Biol. *196*, 801–810.

Salim, C., Boxberg, Y. V., Alterio, J., Féréol, S., and Nothias, F. (2009). The giant protein AHNAK involved in morphogenesis and laminin substrate adhesion of myelinating Schwann cells. Glia *57*, 535–549.

Seminario-Vidal, L., Okada, S.F., Sesma, J.I., Kreda, S.M., van Heusden, C.A., Zhu, Y., Jones, L.C., O'Neal, W.K., Penuela, S., Laird, D.W., et al. (2011). Rho signaling regulates pannexin 1-mediated ATP release from airway epithelia. J. Biol. Chem. *286*, 26277–26286.

Shankar, J., Messenberg, A., Chan, J., Underhill, T.M., Foster, L.J., and Nabi, I.R. (2010). Pseudopodial actin dynamics control epithelial-mesenchymal transition in metastatic cancer cells. Cancer Res. *70*, 3780–3790.

Sheppard, H.M., Feisst, V., Chen, J., Print, C., and Dunbar, P.R. (2016). AHNAK is downregulated in melanoma, predicts poor outcome, and may be required for the expression of functional cadherin-1. Melanoma Res. *26*, 108–116.

Shtivelman, E., and Bishop, J.M. (1993). The human gene AHNAK encodes a large phosphoprotein located primarily in the nucleus. J. Cell Biol. *120*, 625–630.

Shtivelman, E., Cohen, F.E., and Bishop, J.M. (1992). A human gene (AHNAK) encoding an unusually large protein with a 1.2-μm polyionic rod structure. Proc. Natl. Acad. Sci. U. S. A. *89*, 5472–5476.

Silva, T.A., Smuczek, B., Valadão, I.C., Dzik, L.M., Iglesia, R.P., Cruz, M.C., Zelanis, A., de Siqueira, A.S., Serrano, S.M.T., Goldberg, G.S., et al. (2016). AHNAK enables mammary carcinoma cells to produce extracellular vesicles that increase neighboring fibroblast cell motility. Oncotarget *7*.

Sudo, H., Tsuji, A.B., Sugyo, A., Abe, M., Hino, O., and Saga, T. (2014). AHNAK is highly expressed and plays a key role in cell migration and invasion in mesothelioma. Int. J. Oncol. *44*, 530–538.

Vidal, M., Cusick, M.E., and Barabási, A.L. (2011). Interactome networks and human disease. Cell *144*, 986–998.

Wicki-Stordeur, L.E., and Swayne, L.A. (2013). Panx1 regulates neural stem and progenitor cell behaviours associated with cytoskeletal dynamics and interacts with multiple cytoskeletal elements. Cell Commun. Signal. *11*, 1–8.

Wicki-Stordeur, L.E., and Swayne, L.A. (2014). The emerging Pannexin 1 signalome: a new nexus revealed? Front. Cell. Neurosci. *7*, 287.

Wicki-Stordeur, L.E., Boyce, A.K.J., and Swayne, L.A. (2013). Analysis of a pannexin 2-pannexin 1 chimeric protein supports divergent roles for pannexin C-termini in cellular localization. Cell Commun. Adhes. *20*, 73–79.

Xiang, X., Langlois, S., St-Pierre, M.E., Barré, J.F., Grynspan, D., Purgina, B., and Cowan, K.N. (2018). Pannexin 1 inhibits rhabdomyosarcoma progression through a mechanism independent of its canonical channel function. Oncogenesis *7*.

Xu, X., Wicki-stordeur, L.E., Sanchez-arias, J.C., and Liu, M. (2018). Probenecid Disrupts a Novel Pannexin 1-Collapsin Response Mediator Protein 2 Interaction and Increases Microtubule Stability. Front. Cell. Neurosci. *12*, 1–13.

Yuan, J., Shaham, S., Ledoux, S., Ellis, H.M., and Horvitz, H.R. (1993). The C. elegans cell death gene ced-3 encodes a protein similar to mammalian interleukin-1β-converting enzyme. Cell *75*, 641–652.

Zhang, Y.L., Wang, R.C., Cheng, K., Ring, B.Z., and Su, L. (2017). Roles of Rap1 signaling in tumor cell migration and invasion. Cancer Biol. Med. *14*, 90–99.

Zhang, Z., Liu, X., Huang, R., Liu, X., Liang, Z., and Liu, T. (2019). Upregulation of nucleoprotein AHNAK is associated with poor outcome of pancreatic ductal adenocarcinoma prognosis via mediating epithelial-mesenchymal transition. J. Cancer *10*, 3860–3870.

3.8 SUPPLEMENTAL MATERIALS

Table 3.1 Complete list of all proteins identified by BioID

Complete list of all proteins identified by BioID. Proteins sharing identical peptides were placed in the same group in which the most abundant protein is presented with its protein and associated gene name. The unique peptides were only associated with their specific protein groups, which were used for downstream analysis.

This table can be accessed in the "Supplemental Materials" section of the online version of this manuscript.

3.8.1 Supplemental Material and Methods

Cell Lines and Culture Conditions

Patient-derived rhabdomyosarcoma cell lines Rh18 (eRMS) and Rh30 (aRMS) lines, representing each of the main RMS subtype, were obtained from Dr. P. Houghton (St. Jude Children's Hospital, Memphis, TN) whereas HEK293T cell line was purchased from the American Type Culture Collection. The parental Rh18 and Rh30 cell lines were cultured in RPMI-1640 media supplemented with 10% FBS and 1% penicillin/streptomycin. The doubling time of parental Rh18 and Rh30 cells are 34.0 ± 1.5 and 38.8 ± 5.6 hours, respectively. Stable Rh18 and Rh30 cell lines for GFP, PANX1, Myc-PANX1 and BirA*-PANX1 expression were cultured in the same RPMI-1640 media with additional 100 µg/mL geneticin and 2 µg/mL puromycin. Hygromycin was further added at 50 µg/mL for maintaining stable Rh18 and Rh30 cells lines for AHNAK or NTC shRNA expression. HEK293T cell line was cultured in Dulbecco's modified Eagle's Medium (DMEM) media supplemented with 10% FBS and 1% penicillin/streptomycin. All cell cultures were incubated at 37°C, 5% CO_2 and all tested negative for mycoplasma.

Subcloning, Transfection and Generation of Stable Cell Lines

BioID plasmid pcDNA3.1-MCS-BirA*(R118G)-HA was a gift from Kyle Roux (plasmid #36047, Addgene, Cambridge, MA)(Roux et al., 2012). *PANX1* cDNA (Origene, Rockville, MD) was subcloned into pcDNA3.1-MCS-BirA*(R118G)-HA. *Myc-PANX1* cDNA (Origene, Rockville, MD) and *PANX1-BirA*(R118G)-HA (BirA*-PANX1)* were then subcloned into the pCDH-CuO-MCS-EF1-GFP lentiviral vector (System Biosciences, Palo Alto, CA). Stable cell lines were generated using SparQ Cumate Switch Inducible System

(System Bioscience). Briefly, cells stably expressing CymR repressor (pCDH-EF1-CymR-T2A-Neo lentivector) were transduced with pCDH-CuO-Myc-PANX1-EF1-GFP (Myc-PANX1) and pCDH-CuO-BirA*-PANX1-EF1-GFP (BirA*-PANX1) and selected. Cumate-inducible cell lines for stable PANX1 expression or their empty plasmid control (GFP) were generated previously(Xiang et al., 2018). Stable expression of PANX1, Myc-PANX1, and BirA*-PANX1 was induced with 30 µg/mL cumate (System Bioscience).

Transient transfections were performed using Lipofectamine 2000 Reagent (Thermo Scientific, Waltham, MA).

RNA Sequencing and Data Analysis

Inducible stable Rh30 cells were treated with cumate for 48 hours. Total RNA was extracted using RNeasy Mini Kit (Qiagen, Germantown, MD) and submitted to Princess Margaret Genomics Centre (Toronto, ON, Canada) for RNA-seq analysis on an Illumina HiSeq2000 sequencing platform. The RNA Integrity Number (RIN) was 10 for all sequenced samples. Total purity filtered reads sequenced generated were 80,991,098, 93,328,541, and 156,294,622 for the biological replicates of GFP control samples, and 89,903,239, 102,149,600, and 105,348,940 for the matching replicates of PANX1-expressing samples. Overall read quality was checked using FASTQC v.0.11.2 RNA-SeQC (v1.1.7) software. Raw sequence data, in the form of FASTQ files, was aligned to the human genome (hg19, iGenome GTF definition file) using the BOWTIE/TOPHAT pipeline (BOWTIE v2.2.3, TOPHAT 2.0.13)(Trapnell et al., 2012). Accessory programs for the alignment stage included SAMTOOLS (v1.0) and CUTADAPT (v1.7.1). Transcript assembly, abundance estimation, and tests for differential regulation were done using CUFFLINKS (v2.2.1). Genes with a false discovery rate (q value) < 0.05 were considered significantly changed, and genes with a $\log_2$

fold change > 1 or < -1 were denoted as up- or down-regulated. Gene Ontology (GO) enrichment and Kyoto Encyclopedia of Genes and Genomes (KEGG) pathway analyses were performed using the Database for Annotation, Visualization and Integrated Discovery (DAVID) v6.8 (https://david.ncifcrf.gov/) against a background species of the *H. sapiens*(Huang et al., 2009). Enrichment of GO Biological Process (BP) terms and KEGG pathways were considered statistically significant when the Fisher's exact p-values were < 0.05.

RT-qPCR

Inducible stable Rh30 (aRMS) cells were treated with cumate for 48 hours prior to extraction of total RNA using RNeasy Mini Kit (Qiagen). Total RNA was DNase-treated with TURBO DNA-free^{TM} kit and reverse transcribed into cDNA using High-Capacity cDNA Reverse Transcription Kit (Thermo Fisher). qPCR was performed with SsoAdvanced SYBR Green^{TM} Super Mix using 50 ng cDNA with the following gene-specific validated primers (Origene): *MMP2*: forward 5'- AGCGAGTGGATGCCGCCTTTAA-3'; reverse 5'- CATTCCAGGCATCTGCGATGAG-3', *TRAF2*: forward 5'- GAGCAGAAGGTCTTGGAGATGG-3'; reverse 5'- GCAGACACATCTTGTAGCCGTAC-3', *APOBEC2*: forward 5'- AGAACCTGGACGACCCTGAGAA-3'; reverse 5'- CAACCACATAGCAGAGGAAGGTC-3', *MARCKS*: forward 5'- CTCCTCGACTTCTTCGCCCAAG-3'; reverse 5'- TCTTGAAGGAGAAGCCGCTCAG-3', *GAPDH*: forward 5'- GTCTCCTCTGACTTCAACAGCG-3'; reverse 5'- ACCACCCTGTTGCTGTAGCCAA-3'. Relative expression was determined using the comparative Ct method.

Western Blotting

Lysates were separated by SDS-PAGE, transferred to PVDF membranes, and probed with anti-Cx43 (1:2000; Sigma-Aldrich, Cat#: C6219), PANX1 (Sigma-Aldrich, Cat#: HPA016930), Myc (Cell Signaling Technologies, Danvers, MA, Cat#: 2276), ACTB (Santa Cruz, TX, Cat#: sc-47778), AHNAK (AVIVA Systems, San Diego, CA, Cat#: OAEE00010), or GAPDH (1:5000; Advanced ImmunoChemical, Long Beach, CA, Cat#: 2RGM2). Alexa 680- (Thermo Scientific, Cat#: A-31553) or infrared fluorescent-labeled secondary antibodies IRDye 800 (Rockland Immunochemicals, Pottstown, PA, Cat#: 610-132-121) were used. For detection of biotinylated proteins, Streptavidin-Alexa Fluor 790 (Jackson ImmunoResearch, PA, Cat#: 016-650-084) was utilized. Immunoblots were processed and quantified using the Odyssey infrared-imaging system (LI-COR Biosciences, Lincoln, NE). All primary antibodies were used at 1:1000 unless otherwise specified. All secondary antibodies were used at 1:5000.

Dye Uptake Assay

HEK293T cells were transiently transfected with GFP, PANX1, BirA*-PANX1, or Myc-PANX1 constructs in 35 mm collagen-coated dishes. At 48 hours post-transfection, cells were washed twice with sterile Dulbecco's-PBS (PBS plus 0.1 g/l $CaCl_2$ anhydrous and 0.1 g/l $MgCl_2.6\ H_2O$, pH 7.4) on ice and mechanically stimulated with a continuous drip of 800 µl of sulforhodamine B dye (2 mg/ml prepared in Dulbecco's-PBS) released from a height of 2.5 cm above the dish. The stimulation was repeated two times and cells were then incubated with the dye on ice for 5 minutes. The cells were washed 10 times with cold Dulbecco's-PBS prior to examining the dye uptake under a fluorescent microscope (Olympus IX51). Four fluorescent and their corresponding phase-contrast image fields were collected at the drip target site using a 20x objective. The % of dye uptake incidence was calculated as (the number

of cells that took the dye/the total number of cells) x 100 for each of the four field and then averaged for each experiment (n=4)(Xiang et al., 2018).

3D Tumor Spheroid Assay

3D spheroid assay was performed and quantified using IncuCyte ZOOM Live Cell Imaging System (Essen Bioscience) and its accompanying software as previously described(Xiang et al., 2018). Briefly, stable Rh18 and Rh30 cells expressing PANX1, BirA*-PANX1 or empty plasmid (GFP) were pre-treated with cumate for 16 hours and then seeded in ultralow adhesion (ULA) 96-well plates at 5,000 cells per well. Mean image fluorescence, a surrogate measurement of 3D tumor growth, was quantified using IncuCyte ZOOM Live Cell Imaging System every 2 hours for 200 hours.

BioID

BioID was performed according to Roux *et al.*(Roux, 2013). Briefly, stable Rh18 (eRMS) and Rh30 (aRMS) were treated with 30 µg/mL cumate for 24 hours to induce expression of BirA*, Myc-PANX1 and BirA*-PANX1, after which the cells were further incubated with 50 µM biotin for another 24 hours before harvesting. The cells were sonicated using a VCX 130 Sonic Vibra-Cell™ sonicator (Sonics & Materials, TC) set to 20% amplitude and 5 s/pulse till the lysate became clear. The biotinylated proteins were captured by incubating with Pierce™ NeutrAvidin™ Agarose (Thermo Scientific) beads for 18 hours at 4 ℃ on a rotator. To prepare for mass spectrometry, the beads were washed and re-suspended in 200 µL of 50 mM ammonium bicarbonate, incubated in 10 mM TCEP at 40 ℃ for 30 minutes and then reduced in 20 mM iodoacetamide for 30 minutes in the dark at 25 ℃. On-bead digestion was performed by adding 1/20 total sample volume of MS grade trypsin

protease (Thermo Scientific) and incubating for 16 hours at 37 ℃ on a rotator. The reaction was stopped by adding 2% v/v formic acid and the samples were immediately submitted for LC-MS/MS analysis.

co-IP using Enriched Subcellular Fractions

Subcellular fractionation was performed according to Fowler *et al.*(Fowler et al., 2013) with modifications to accommodate cells as starting analytes. Stable Rh18 (eRMS) and Rh30 (aRMS) cells were grown to 90% confluence in 15 cm dishes and then treated with 30 µg/mL cumate for 48 hours to induce Myc-PANX1 expression. Their respective GFP-expressing cells were grown and treated alongside as controls. The cells were collected using a cell scraper and each sample was pooled from five 15 cm dishes. The cells were transferred into a Dounce homogenizer (Sigma-Aldrich, MO) and 100 strokes were applied to complete the lysis. The nuclei and cellular debris were removed by centrifuging at 800x g for 5 minutes at 4 ℃. The post nuclear supernatants (PNS) were then concentrated down to 1.4 mL using Amicon Ultra-15 Centrifugal Filter Units with a 10 kDa molecular weight cut-off (Millipore, MA) by centrifuging at 4000x g for 90 minutes at 4 ℃. The concentrated PNS were mixed with OptiPrep™ Density Gradient Medium (OP) (Sigma-Aldrich) to reach a final OP concentration of 30%. The 30% OP/PNS solution was added into polyallomer centrifuge tubes (VWR, PA) on which a discontinuous gradient of 25%, 20%, 17.5% and 10% of OP were overlaid sequentially. The gradients were assembled into a SW41 Ti rotor (Beckman Coulter, IN) and centrifuged at 200,000x g for 16 hours at 4 ℃ (acceleration = 1, deceleration = 0). A total of 22 fractions were collected from each sample and the Myc-PANX1 enriched fractions and their corresponding fractions in the GFP controls were pooled according to the Western blotting results. The buffer of the pooled lysates was exchanged for IP lysis buffer by three

concentration and re-suspension cycles using the centrifugal devices and 2.5 mg of each pooled lysates were subject to co-IP. Each lysate was pre-cleared with 50 µL of beads, then added into 100 µL of agarose beads pre-adsorbed with 5 ug of anti-Myc antibodies and incubated on a rotator for 16 hours at 4 ℃. The beads were prepared for LC-MS/MS analysis as described above.

Mass Spectrometry and Proteomic Analysis

Mass spectrometry was carried out at the OISB (Ottawa Institute of System Biology). Briefly, the trypsin-digested peptides were desalted on Sep-Pak® C18 columns (Waters, MA), dried down in SpeedVac (Thermo Scientific) and reconstituted in 0.5% (v/v) formic acid before analysis by high-performance liquid chromatography/electrospray ionization tandem mass spectrometry (HPLC-ESI-MS/MS). The acquired MS/MS spectra were searched against the human International Protein Index (IPI) protein sequence database (v3.85) using Maxquant with the label free quantitation (LFQ) option and a biotin variable modification was added for BioID(Cox and Mann, 2008). The false discovery rate (FDR) was set to ≤ 1% on both protein and peptide level. Quantification was performed using normalized LFQ intensity. The number of unique peptides of each protein was further scored and ranked using the respective background controls; for BioID, the unique peptide number from BirA*-PANX1 was divided by those from Myc-PANX1 + 0.1 for each protein and ranked according to this ratio, and for subcellular fractionation combined with co-IP, the unique peptide number from Myc-PANX1 was divided by those from GPF + 0.1 for each matched protein. A cut-off unique peptide score of 1 was set for proteins found by either BioID or subcellular fractionation combined with co-IP. Overlapped protein hits were identified using Venny v2.1.0 (https://bioinfogp.cnb.csic.es/tools/venny/). Protein-protein interaction networks of the

overlapped hits were predicted by STRING v11.0 (https://string-db.org/) with the interaction score set to medium, the maximum interactors to be displayed in the 1st shell set to 10, and the network clustering set to 'no clustering'. GO (Cellular Component) terms plasma membrane (GO: 0005886), actin cytoskeleton (GO: 0015629) and microtubule cytoskeleton (GO: 0015630) were selected to highlight the interactors accordingly.

Confocal Laser Microscopy

Rh18 (eRMS) and Rh30 (aRMS) on glass coverslips were transfected with Myc-PANX1 for 48 hours prior to fixation in 3.7% PFA for 20 minutes at room temperature. The fixed cells were blocked and permeabilized in 2% BSA and 0.1% Triton X-100 for 45 minutes and then sequentially labeled with anti-PANX1 (1:200; Sigma-Aldrich, Cat#: HPA016930), Alexa Fluor 594 conjugated anti-rabbit IgG (1:500; Thermo Fisher, Cat#: A-11012), anti-AHNAK (1:50; AVIVA Systems, Cat#: OAEE00010), and Alexa Fluor 488 conjugated anti-mouse IgG (1:500; Thermo Fisher, Cat#: A-11001) for 45 minutes each with PBS washes in between. The cells were then mounted with DAPI-Fluoromount G™ (Thermo Fisher) and viewed with an Olympus Fluoview FV-1000 Laser Confocal Microscope equipped with a 60X oil objective. Image acquisition was performed with the Fluoview software. All settings were kept constant during image acquisition.

Proliferation Assay

Rh18 (eRMS) and Rh30 (aRMS) cells were transfected with either PANX1 or Myc-PANX1 and their respective empty vector (EV) or GFP controls. Twenty four hours post-transfection, cells were incubated with 10 µM BrdU (Sigma-Aldrich) for either 3 hours (Rh18) or 1 hour (Rh30) and processed for immunohistochemistry(Xiang et al., 2018). Briefly, the

cells were fixed on glass coverslips for 20 minutes at room temperature in 3.7% PFA, washed with PBS. The fixed cells were blocked with 2% BSA with 0.1% Trinton X-100 for 45 minutes, and then incubated in 2N HCl for 20 minutes to nature the nuclear DNA. The cells were labeled sequentially with anti-BrdU (1:200; Thermo Fisher, Cat#: B35128), Alexa Fluor 594 conjugated anti-mouse IgG (1:500, Thermo Fisher, Cat#: A-11032), anti-PANX1 (1:200; Sigma-Aldrich, Cat#: HPA016930) and Alexa Fluor 488 conjugated anti-rabbit IgG (1:500, Thermo Fisher, Cat#: A-11008) with PBS washes in between. The labeled cells were then mounted using DAPI Fluoromount-G^{TM} (Thermo Fisher). Ten random field images per sample were taken using a fluorescent microscope equipped with a 20X objective and the number of BrdU positive nuclei from total transfected cells (positive for GFP- or Myc-staining) were counted and quantified.

Alamar Blue Viability Assay

For siRNA-based knockdown, stable Rh18 (eRMS) and Rh30 (aRMS) cells were seeded in 96 well plates at 10,000 cells per well. The cells were transfected with AHNAK siRNA or NTC for 24 hours and then treated with cumate for another 48 hours before analysis. For shRNA-based knockdown, the shRNA-stable Rh18 and Rh30 cells were incubated in 50 ng/mL doxycycline (Sigma-Aldridge) for 72 hours, then seeded in 96 well plates at 20,000 cells per well. The cells were treated with and without cumate for 48 hours before analysis. Doxycycline and cumate were refreshed daily. In both knockdown approaches, the cells were incubated in culture media with 0.15 g/mL Alamar Blue (Sigma-Aldridge) for 2 hours, then the plates were read on a Synergy HTX plate reader (BioTek, VT) equipped with excitation;emission filter set at 530/25; 590/25 nm.

Migration Assay

Stable Rh18 and Rh30 cell lines were transfected with AHNAK siRNA or the NTC in the presence of cumate of its vehicle control (H_2O) for 48 hours before a uniform scratch was made using the 96-well WoundMaker device (Essen Bioscience). The cells were monitored using the IncuCyte ZOOM Live Cell Imaging System (Essen Bioscience) and the green fluorescence from constitutively expressed GFP was used to measure the % of wound confluence over the period of 60 (Rh18) or 80 (Rh30) hours by its accompanying software.

Soft Agar Anoikis Assay

Stable Rh18 and Rh30 cell lines were transfected with AHNAK siRNA or the NTC for 24 hours and then seeded on top of 1% Noble agar (BD Biosciences, San Jose, CA) at 400,000 cells/well with and without cumate(Wolf et al., 2011). The cells were counted on Days 0 (day of cell seeding on agar), 3 and 6 by Trypan Blue (Thermo Scientific) dye exclusion using the Countess^{TM} Automated Cell Counter (Life Technologies) following the manufacturer's instructions.

3.8.2 References

Cox, J., and Mann, M. (2008). MaxQuant enables high peptide identification rates, individualized p.p.b.-range mass accuracies and proteome-wide protein quantification. Nat. Biotechnol. *26*, 1367–1372.

Fowler, S.L., Akins, M., Zhou, H., Figeys, D., and Bennett, S.A.L.L. (2013). The liver connexin32 interactome is a novel plasma membrane-mitochondrial signaling nexus. J. Proteome Res. *12*, 2597–2610.

Huang, D.W., Sherman, B.T., and Lempicki, R.A. (2009). Systematic and integrative analysis of large gene lists using DAVID bioinformatics resources. Nat. Protoc. *4*, 44–57.

Roux, K.J. (2013). Marked by association: Techniques for proximity-dependent labeling of proteins in eukaryotic cells. Cell. Mol. Life Sci. *70*, 3657–3664.

Roux, K.J., Kim, D.I., Raida, M., and Burke, B. (2012). A promiscuous biotin ligase fusion protein identifies proximal and interacting proteins in mammalian cells. J. Cell Biol. *196*, 801–810.

Trapnell, C., Roberts, A., Goff, L., Pertea, G., Kim, D., Kelley, D.R., Pimentel, H., Salzberg, S.L., Rinn, J.L., and Pachter, L. (2012). Differential gene and transcript expression analysis of RNA-seq experiments with TopHat and Cufflinks. Nat. Protoc. *7*, 562–578.

Wolf, S.J., Huynh, T., Bryce, N.S., Hambley, T.W., Wakelin, L.P.G., Stewart, B.W., and Catchpoole, D.R. (2011). Intracellular trafficking as a determinant of AS-DACA cytotoxicity in rhabdomyosarcoma cells. BMC Cell Biol. *12*, 36.

Xiang, X., Langlois, S., St-Pierre, M.E., Barré, J.F., Grynspan, D., Purgina, B., and Cowan, K.N. (2018). Pannexin 1 inhibits rhabdomyosarcoma progression through a mechanism independent of its canonical channel function. Oncogenesis *7*.

4. CHAPTER FOUR: QUERCETIN INDUCES PANNEXIN 1 EXPRESSION VIA AN ALTERNATIVE TRANSCRIPT WITH A TRANSLATIONALLY ACTIVE 5' LEADER IN RHABDOMYOSARCOMA

Authors: Xiao Xiang[§], Huy-Dung Hoang[§], Victoria Gilchrist, Stéphanie Langlois, Tommy Alain and Kyle N. Cowan

[§]These authors contributed equally

Status: Under final preparation for submission in January 2021

4.1 ACKNOWLEDGEMENTS

The experiments in this manuscript were designed and executed by me and Huy-Dung Hoang under the supervision of Tommy Alain and Kyle N. Cowan. Huy-Dung Hoang performed the experiments and/or data analysis that constituted Figure 4.1A and B, Figure 4.2C – H, and Figure 4.3A, E – G. Victoria Gilchrist helped with RT-qPCR analysis for Figure 4.2C and 4.3A and made the graphical illustration. This manuscript was written by me and Huy-Dung Hoang with editorial help from Stéphanie Langlois, Tommy Alain, and Kyle N. Cowan. We thank Stéphanie Langlois, Tommy Alain, and Kyle N. Cowan who provided critical review of this manuscript.

4.2 ABSTRACT

Rhabdomyosarcoma (RMS) is a deadly childhood neoplasm of presumed skeletal muscle origin. We have shown that the expression of the ion channel Pannexin 1 (PANX1) is strongly repressed in RMS cells, and that its upregulation dramatically inhibits tumor progression. PANX1 is dynamically expressed during the development of various tissues including skeletal muscle, but the underlining mechanisms by which PANX1 protein levels are controlled, especially in RMS, remain largely unknown. Here we show that both RMS and normal skeletal muscle express comparable amount of *PANX1* mRNAs, but surprisingly the canonical 5' untranslated region (5'UTR) or 5'leader of the transcript is completely lost in RMS cells. We uncover that quercetin, a natural plant flavonoid, increases PANX1 protein levels by inducing re-expression of a 5'leader-containing *PANX1* transcript variant that is efficiently translated. Mechanistically, abolishing CREB and ETV4 transcription factor binding sites in the *PANX1* promoter significantly reduced the luciferase reporter activities and *PANX1* 5'UTR levels, and we show that quercetin enriched the binding of ETV4, but not CREB, to its consensus element in the *PANX1* promoter. Furthermore, quercetin treatment promoted partial myogenic differentiation of RMS cells and both prevented RMS 3D *in vitro* tumor formation while inducing complete regression of established *in vitro* tumors. Collectively, our results demonstrate the tumor-suppressive effects of quercetin in RMS and present a hitherto undescribed mechanism of PANX1 regulation via ETV4-mediated transcription of a translationally-functional 5'leader-containing *PANX1* mRNA.

Keywords: Pannexin; Rhabdomyosarcoma; Quercetin; 5' untranslated region; RNA sequencing; Polysome profiling; Transcription; Alternative transcription; Translation

4.3 INTRODUCTION

Pannexin 1 (PANX1; known as Panx1 in rodents) is a ubiquitous transmembrane glycoprotein that oligomerizes to form single membrane channels (Deng et al., 2020; Jin et al., 2020; Michalski et al., 2020; Ruan et al., 2020). PANX1 channels allow the passage of ions, metabolites, and small molecules up to 1 kDa in size, and are considered major conduits for ATP release from various cell types (Bao et al., 2004). We have previously shown that PANX1 levels are highly upregulated in differentiating primary human skeletal muscle myoblasts (HSMM) (Langlois et al., 2014). Notably, ectopic expression of PANX1 in undifferentiated HSMM promoted their myogenic differentiation while blockade of PANX1 channels using pharmacological agents inhibited this process (Langlois et al., 2014). A similar upregulation of Panx1 levels was measured during their development and regeneration following injury in mice (Pham et al., 2018). Together, our results established PANX1 as an important regulator of skeletal muscle myogenic differentiation (Langlois and Cowan, 2017), which also prompted us to investigate the role of PANX1 in rhabdomyosarcoma (RMS), a childhood neoplasm thought to arise from muscle progenitors due to impaired myogenic differentiation (Charytonowicz et al., 2009; Lav et al., 2015; Monti and Fanzani, 2015). Interestingly, we detected low levels of PANX1 in RMS tissue specimens and patient-derived cell lines and showed that re-introduction of PANX1 in RMS cells dramatically suppressed their malignant properties *in vitro* and *in vivo* (Xiang et al., 2018). Subsequently, our study of the PANX1 transcriptome and interactome in RMS further implicated PANX1 in the regulation of genes involved in various key cellular processes, such as migration and apoptosis, and uncovered its tumor-inhibitory interaction with the neuroblast differentiation-associated protein AHNAK, respectively (Xiang et al., 2020).

RMS is the most common soft tissue sarcoma in children and adolescents with two major histological subtypes, termed embryonal RMS (eRMS) and alveolar RMS (aRMS), which together make up more than 80% of all RMS (Amer et al., 2019). eRMS, the most common subtype, has a more favorable prognosis whereas aRMS is more aggressive and often leads to a poor clinical outcome

(Amer et al., 2019; Oberlin et al., 2008; Punyko et al., 2005). While the molecular pathogenesis of eRMS and aRMS remains unclear, cytogenetic studies have revealed recurrent loss of heterozygosity at the 11p15 locus in eRMS and chromosomal translocations of t(2;13)(q35;q14) or t(1;13)(p36;q14) in aRMS resulting in paired homeobox (PAX)-forkhead box protein O1 (FOXO1) oncoproteins, PAX3- or PAX7-FOXO1 (Dobson et al., 2016; Shern et al., 2014). These genetic alterations have been associated with dysregulation of transcriptional, epigenetic, and molecular signalling mechanisms in many cellular processes, including proliferation and myogenic differentiation, in RMS (Shern et al., 2014). Despite aggressive treatment modalities, the overall survival rate of patients with metastatic or relapsed RMS has remained below 30% for over 30 years, underlining the urgency for better clinical management (Hettmer et al., 2014; Oberlin et al., 2008). Thus far, our findings strongly suggest that upregulating PANX1 is a promising therapeutic strategy for RMS (Xiang et al., 2018). As PANX1 levels are low in RMS compared to normal skeletal muscle, understanding the regulation or deregulation of *PANX1* transcriptional and translational control in RMS may reveal novel therapeutic targets.

PANX1/Panx1 levels are dynamically regulated during development and in pathologic states. In murine cortex, cerebellum, and retina, Panx1 levels peaked at embryonic day 18 and dramatically decreased upon birth and continued to decline into adulthood (Ray et al., 2005). This gradual decline in Panx1 levels was also reported in the rat brain (Vogt et al., 2005) and observed during differentiation of neural crest-like cells (Ray et al., 2005) *in vitro*. On the contrary, Panx1 levels increased in primary adipose-derived stromal cells upon induction into an adipogenic lineage (Lee et al., 2018). Under pathological conditions, Panx1 levels were down-regulated in C6 glioma cells as compared to normal astrocytes, and its ectopic expression reduced glioma tumor growth *in vivo* (Lai et al., 2007). By contrast, upregulation of PANX1/Panx1 levels was positively associated with both human and murine melanoma progression while shRNA-mediated knockdown of PANX1/Panx1 levels led to attenuation of the disease (Freeman et al., 2019; Penuela et al., 2012). This dynamic variation of PANX1 levels

across different tissue types or pathological conditions suggests tissue- or disease-dependent transcriptional or translational regulation (Boyce et al., 2018), however, studies demonstrating the mechanisms by which this regulation occurs have not been. Thus far, *Panx1* transcriptional regulation has only been comprehensively studied in the rat epididymis, where *Panx1* was shown to have an evolutionarily conserved promoter located in CpG islands under the control of methylation and the transcription factors CREB and ETV4 (Dufresne and Cyr, 2014).

Recently, a genome-wide drug screen in murine neuronal cells revealed quercetin, a naturally occurring flavonoid present in vegetables and fruits (Tang et al., 2020), as an up-regulator of *Panx1* mRNA levels (Hadwen et al., 2018). Thus, provided a pharmacological agent that could facilitate the investigation into the molecular mechanism of *PANX1* regulation in RMS. In the current study, using patient-derived Rh18 (eRMS) and Rh30 (aRMS) cell lines (Hinson et al., 2013), we show that *PANX1* transcripts in RMS cells are devoid of their putative 5'UTR (untranslated region) as compared to skeletal muscle tissue and differentiated HSMM, and that the presence of the *PANX1* 5'UTR corresponds to its protein expression in RMS cells and HSMM. After confirming that quercetin upregulates PANX1 protein expression in RMS cells, we reveal that this occurs through the restoration of transcription of a translationally functional *PANX1* mRNA containing a 5'leader. We further demonstrate that the transcription of this *PANX1* mRNA variant in RMS cells is dependent upon the binding of transcription factor ETV4 to the *PANX1* promoter. Collectively, our results show for the first time the involvement of *PANX1* 5'UTR in regulating its mRNA translation.

4.4 MATERIALS AND METHODS

Cell Culture, Drug Treatment and Transfection

Human rhabdomyosarcoma cell lines Rh18 (eRMS) and Rh30 (aRMS) lines were obtained from Dr. P. Houghton (St. Jude Children's Hospital, Memphis, TN). Stable Rh18 and Rh30 cell lines were generated using the SparQ Cumate Switch Inducible System (System Biosciences, CA) as described previously (Xiang et al., 2018). All RMS cell lines were maintained in RPMI-1640 medium supplemented with 10% FBS and 1% penicillin/streptomycin while the stable RMS cell lines were supplemented additionally with 100 µg/mL geneticin (Life Technologies, CA), and 2 µg/mL puromycin (Corning, NY). Primary human skeletal muscle myoblasts (HSMM) (Lonza, Walkersville, MD) were maintained in Clonetics SkGM™ medium supplemented with the SkGM™ SingleQuots™ kit (Lonza) as specified by the supplier. The HSMM were differentiated by switching to DMEM medium with 2% horse serum (Langlois et al., 2014). Quercetin was purchased from Sigma-Aldrich (St. Louis, MO) and prepared in DMSO. Quercetin was refreshed in culture medium every 24 hours. All transfections were performed with Lipofectamine 2000 Reagent (Thermo Scientific, Waltham, MA).

Western Blotting

Cells were lysed in IP lysis buffer (150 mM NaCl, 10 mM Tris-HCl, pH 7.4, 1 mM EDTA, 0.5% NP-40, and 1% Triton X-100) as previously described (Cowan et al., 2012). The lysates were separated in 10% SDS-PAGE and transferred to PVDF membranes. The proteins were immunoblotted with anti-PANX1 (1:2000, Sigma-Aldrich, Cat#: HPA016930), anti-MYOD (1:1000, Santa Cruz, TX, Cat#: sc-377460), anti-MYOG (1:1000, Santa Cruz, Cat#: sc-12732), anti-MHC (1:2000, R&D Systems, Minneapolis, MN, Cat#: MAB4470), anti-CREB (1:1000, Cell Signaling Technology, Danvers, MA, Cat#: 4820S), anti-pCREB (1:1000, Cell Signaling Technology, Cat#: 9198S) or anti-

GAPDH (1:5000, Advanced ImmunoChemical, Long Beach, CA, Cat#: 2RGM2) and then with Alexa 680- (1:5000, Thermo Scientific) or infrared fluorescent-labeled secondary antibodies IRDye 800 (1:5000, Rockland Immunochemicals, Pottstown, PA). The membranes were scanned on a LI-COR infrared-imaging system (LI-COR Biosciences, Lincoln, NE) and the densitometric units of the unsaturated images was quantified with the accompanying Odyssey V3.0 software.

RNA Sequencing and Data Analysis

Total RNA was extracted from Rh30 cells using RNeasy Mini Kit (Qiagen, Germantown, MD) and submitted to Princess Margaret Genomics Centre (Toronto, ON, Canada) for RNA-seq analysis on an Illumina HiSeq2000 sequencing platform as previously described (Xiang et al., 2020). The RNA Integrity Number (RIN) was 10 for all sequenced samples. Total purity filtered reads sequenced generated were 80,991,098, 93,328,541, and 156,294,622 for the biological replicates. Overall read quality was checked using FASTQC v.0.11.2 RNA-SeQC (v1.1.7) software. Raw sequence data, in the form of FASTQ files, was aligned to the human genome (hg19, iGenome GTF definition file) using the BOWTIE/TOPHAT pipeline (BOWTIE v2.2.3, TOPHAT 2.0.13) (Trapnell et al., 2012). Accessory programs for the alignment stage included SAMTOOLS (v1.0) and CUTADAPT (v1.7.1).

Polysome profiling

Polysome profiling was performed as previously described (Gandin et al., 2014). Briefly, cells were treated with cycloheximide (CHX) (Bioshop, Canada) at 100 µg/ml for 5 minutes to fix translating ribosome. Cells were washed three times with ice cold PBS containing CHX, then lysed using hypotonic buffer (5 mM Tris pH 7.5, 2.5 mM $MgCl_2$, 1.5 mM KCl, 2.5 mM DTT, 100U RNAsin nuclease inhibitor (Promega), 0.5% Triton X-100, 0.5% sodium deoxycholate). Cell debris was pelleted by centrifugation at 17,000 g, 10 minutes at 4^{o}C and supernatant was transferred to a new tube.

An equivalent of 10 OD at 260 nm of supernatant was then added on top of a continuous 10-50% sucrose gradient and centrifuged at 221,000 g (36,000 rpm) for 2 hours at 4°C. Fractions were then collected using a BR-188 Density Gradient Fractionation System (Brandel) and RNA was extracted using Trizol (Thermo Fisher) according to the manufacturer protocol.

RT-qPCR

Total RNA was extracted using RNeasy Mini kit (Qiagen, Germantown, MD), DNase-treated with TURBO DNA-*free*™ kit (Thermo Scientific) and reverse transcribed into cDNA using High-Capacity cDNA Reverse Transcription kit (Thermo Scientific). Quantitative PCR of the synthesized cDNA was performed on a CFX96 Touch Real-Time PCR Detection System (Bio-Rad, Hercules, CA) using SsoAdvanced™ Universal SYBR® Green Supermix (Bio-Rad). All primers were validated to have an amplification efficiency of 90 – 100% when used at 500 nM (see Supplemental Table S1 for primer sequences) with their respective qPCR program. All qPCR assays were performed using the following program unless otherwise specified: 95 ℃ for 3 min followed by 45 cycles of 95 ℃ for 10 sec, 58 ℃ for 15 sec and 72 ℃ for 50 sec). Relative expression was determined using the comparative Ct method.

5' Rapid Amplification of cDNA End (RACE)

Rh30 (aRMS) cells were treated with 10 µM quercetin or DMSO for 24 hours. Total RNA was collected and DNase-treated as described previously. Reverse transcription of 5' capped poly (A) RNA was performed with TELO™ PRIME Full-Length cDNA Amplification V2 kit following manufacturer's instructions. Briefly, 2 µg of DNase-treated total RNA was first reverse transcribed using an OligodT primer to form a cDNA/RNA hybrid strand. A double-stranded adapter with a 5' C overhang was then ligated to the 5' end of the capped cDNA/RNA by base pairing to the 5' G in the

cap structure while leaving all 5' uncapped cDNA/RNA unmodified. Full double-strand cDNA was then synthesized from the 5' capped RNA using a primer containing the 5' adapter sequence. Endpoint PCR using a forward primer with the 5' adaptor sequence and a reverse primer specific to exon 2 of *PANX1* (Supplemental Table S1) were used to amplified full length *PANX1* cDNA for 21 PCR cycles without allowing the amplification to reach saturation (determined by a separate qPCR analysis under identical conditions). The PCR products were resolved on a 2% agarose gel with GelRed™ (Biotium, Fremont, CA) and visualized on a Gel Doc XR+ Documentation System (Bio-Rad). All PCR programs were set up according to the manufacturer's instructions.

CAT Translation Reporter Assay

CAT translation reporter assay was performed as previously described (Graber et al., 2010). Briefly, cells were seeded at 75% confluency in a 6-well plate, then transfected with 1 µg each of pBGal (expressing β-galactosidase, a generous gift from Dr. Martin Holcik at Carleton University) and the pMCpA plasmid expressing the CAT open reading frame under the CMV promoter followed by the 5'UTR of interest using Lipofectamine 2000 (Thermo Fisher). 24 hours post transfection, CAT expression in transfected cells was measured using the CAT ELISA kit (Roche) according to the manufacturer's instruction, while β-galactosidase activity was measured by the ortho-Nitrophenyl-β-galactoside (ONPG) colorimetric assay. CAT expression was then normalized to β-galactosidase to control for transfection efficiency.

PANX1 Promoter Cloning, Plasmid Construction and Site-directed Mutagenesis

Total genomic DNA was extracted from primary HSMM cells using QIAamp DNA Mini kit (Qiagen). Two segments of *PANX1* promoter from positions -2697 to -1642 and -1616 to +37 as well as their deletion mutants from positions -926, -581 and -475 to +37 (relative to its ATG start codon)

were PCR amplified (95 ℃ for 3 min followed by 32 cycles of 95 ℃ for 15 sec, 60 ℃ for 15 sec and 72 ℃ for 90) using PCR Master Mix (Promega, Madison, WI), purified with QIAquick PCR Purification kit (Qiagen), and subcloned into the KpnI-XhoI sites in pGL3-Basic vector (Promega). Mutations at the CREB and ETV4 consensus sites on *PANX1* promoter (-581 to +37) in pGL3 vector were introduced using the Quick-Change Site-directed Mutagenesis kit (Agilent Technologies, Santa Clara, CA) following the manufacturer's instructions. All plasmid constructs were verified by Sanger sequencing. All restriction enzymes were purchased from New England Biolabs (Ipswich, MA). See Supplemental Table S1 for primer sequences.

Immunofluorescence Microscopy

Rh30 cells on glass coverslips were treated with 10 μM quercetin or DMSO for 24 hours and then fixed with 3.7% paraformaldehyde for 20 min at room temperature. The fixed cells were washed with PBS, and then blocked and permeabilized in 2% BSA with 0.1% Triton X-100 for 1 hour at room temperature. The cells were labeled with previously described primary antibodies against PANX1 (1:200) and ETV4 (1:50) at 4 ℃ overnight and then with Alexa 488 or 594 conjugated secondary antibodies (1:500) at room temperature for 1 hour. The coverslips were mounted with DAPI Fluoromount-G (Southern Biotech, Birmingham, AL) and visualized using EVOS Cell Imaging System (Thermo Fisher) with a 20X objective.

Dual-luciferase Reporter Assay

Rh18 (eRMS) and Rh30 (aRMS) cells were transfected in 96-well plates with 100 ng pGL3-*PANX1* promoter constructs or a promoterless pGL3-Basic negative and 100 ng pRL-TK (Promega) for 48 hours and analyzed using Dual-Glo® Luciferase Assay System (Promega) on a Synergy HTX plate reader (BioTek Instruments, Winooski, VT). Rh18 and Rh30 cells were also transfected in parallel

with 1 µg pGL3 constructs and 1 µg pRL-TK in 6-well plates for 48 hours before subjected to total RNA extraction for qPCR analyses of *Firefly Luciferase* and *PANX1* 5' UTR transcript levels (95 ℃ for 3 min followed by 45 cycles of 95 ℃ for 3 sec and 60 ℃ for 30 sec) with primers described in Supplemental Table S1.

Chromatin Immunoprecipitation

Rh30 (aRMS) cells were treated with 10 µM quercetin or DMSO for 24 hours and subjected to chromatin immunoprecipitation using EZ-ChIP kit (Millipore, Billerica, MA) according to manufacturer's instructions. Briefly, the cells were fixed with 1% formaldehyde for 10 minutes at room temperature and quenched with 125 mM glycine. The cells were pelleted, and then lysed at 1×10^7 cells/mL of SDS lysis buffer (1% SDS, 10 mM EDTA, and 50 mM Tris, pH 8.1) containing protease inhibitors. The cell lysates were sonicated by a VCX 130 sonicator (Sonics & Materials, Newtown, CT) mounted with a 2 mm tip for 15 sets of 10 s pulses at 30% of maximum power (50 Watts) to shear the crosslinked chromatin into 200 – 1000 bp fragments. Each immunoprecipitation was performed with 100 µL of sonicated chromatin, which was equivalent to 1×10^6 cells. The chromatin was diluted to 1 mL with the dilution buffer and precleared with 60 µL of protein G agarose beads for 1 hour at 4 ℃. A 20 µL aliquot of precleared chromatin was removed and set aside to be used as input in subsequent analysis. The precleared chromatin was then incubated with 1 µg anti-RNA Polymerase II (positive control), 1 µg mouse IgG (negative control), 10 µg anti-ETV4 (Santa Cruz; Cat#: sc-113X) or 10 µg anti-CREB (Santa Cruz; Cat#: sc-377154X) overnight at 4 ℃ on a rotator. The chromatin/DNA immunocomplexes were captured with 60 µL of protein G agarose beads for 1 hour at 4 ℃. The protein G agarose beads were washed, and the captured chromatin was eluted and purified for subsequent qPCR analysis (95 ℃ for 3 min followed by 45 cycles of 95 ℃ for 3 sec and 60 ℃ for 30 sec) using primers described in Supplemental Table S1.

3D Spheroid Assay

3D spheroid formation and regression assays were performed and quantified using IncuCyte ZOOM™ Live Cell Imaging System (Essen Bioscience, MI) and its accompanying software as previously described (Xiang et al., 2018)

Statistics

The data were analyzed for statistical significance using unpaired two-tailed Student's *t*-tests, multiple unpaired Student's *t*-test with Holm-Sidak correction, and analysis of variance (ANOVA) followed by Tukey's post-hoc tests.

4.5 RESULTS

PANX1 5'UTR and Protein Levels are Positively Correlated in RMS and HSMM

We have previously detected *PANX1* transcript and protein in undifferentiated HSMM and patient-derived RMS cell lines, but their levels are significantly lower than those in differentiated HSMM (Langlois et al., 2014; Xiang et al., 2018). Since re-introduction of PANX1 in RMS cells vastly reduced their malignant properties (Xiang et al., 2018), we performed RNA-sequencing (RNA-seq) to further study the transcriptomic changes elicited by PANX1 in Rh30 (aRMS) cells as this subtype of RMS remains particularly challenging to treat (Hettmer et al., 2014). To our surprise, the RNA-seq result from wild-type Rh30 cells revealed an abundance of endogenous *PANX1* transcripts which mapped to all five exons with the exception of the 5'UTR region (Fig. 4.1A). Further analyses of RNA-seq data on adult skeletal muscle tissue specimens deposited in the Gene Expression Omnibus (GEO) database, however, showed a clear mapping of *PANX1* transcripts onto its 5'UTR region (Fig. 1A). When normalized to the total RNA-seq reads of the *PANX1* coding sequence (CDS), the 5'UTR reads in differentiated HSMM were comparable to the CDS reads, while no 5'UTR read was detected in RNA samples from Rh30 cells, suggesting that *PANX1* mRNAs in Rh30 cells do not contain a 5'leader region (Fig. 4.1B). Using *PANX1* 5' UTR specific primers and a series of *PANX1* exon-exon junction primers, qPCR analyses corroborated the previous RNA-seq results showing that the difference in *PANX1* transcript levels between Rh18 (eRMS), or Rh30 cells, and differentiated HSMM was the most dramatic in the 5'UTR region, and this difference gradually diminished from exon 1 to 5 (Fig. 1C). Moreover, Western blotting analysis in parallel showed significantly higher PANX1 protein levels in differentiated HSMM as compared to that of Rh18 and Rh30 cells as well as its undifferentiated counterparts (Fig. 4.1D and E). An immunoreactive band around 65 kDa was recognized by our anti-PANX1 antibodies in all but differentiated HSMM (Fig. 4.1D, arrowhead). However, further Western blotting analysis indicated that it corresponded to a non-specific immunoreactive species, as siRNA targeting PANX1 induced a clear knockdown of PANX1 (normally identified between ~39.5 to ~49.9

kDa as a result of various post-translational modifications such as glycosylation and phosphorylation (Penuela et al., 2014)) in Rh30 cells while no change in the levels of the 65 kDa immunoreactive band was observed (Fig. 4.1F). Taken together, our data show that as compared to HSMM, the *PANX1* transcripts expressed in RMS cells are devoid of a 5'leader region and this correlates with protein expression. Thus, the 5'UTR region of the *PANX1* transcript may be important for its regulation in tissues.

Quercetin Enhances PANX1 mRNA Translation in RMS Cells

A recent screen using a pool of clinically approved drugs identified quercetin as an up-regulator of *Panx1* transcript levels in murine neuronal cells (Hadwen et al., 2018), which provided a potential tool to modulate PANX1 expression in RMS. As a proof of principle experiment, we treated Rh18 and Rh30 cells with increasing dosages of quercetin and subjected them to Western blotting analyses. Interestingly, quercetin treatment induced a dosage-dependent increase in PANX1 protein levels in Rh18 cells in which 50 µM of quercetin induced a statistically significant and maximal increase of PANX1 (Fig. 4.2A). In Rh30 cells, 10 µM of quercetin was able to elicit maximal induction of PANX1 expression (Fig. 4.2B). Thus, 50 µM and 10 µM were chosen as quercetin concentrations for treating Rh18 and Rh30 cells in the downstream experiments, respectively. We assessed the change in *PANX1* transcript levels using both primers specific to exon 1. Remarkably, quercetin treatment in both Rh18 and Rh30 cells did not lead to a significant increase in *PANX1* transcript levels as measured at exon region 1 (Fig. 4.2C). This prompted us to investigate whether quercetin treatment could instead modulate *PANX1* mRNA translation. Using polysome fractionation (Gandin et al., 2014), ribosome-associated mRNA from Rh30 cells with and without quercetin treatment was resolved on a continuous sucrose gradient where polysome-bound mRNA sedimented according to their density, which increases with the number of bound ribosomes and correlates with their translation rate (Fig. 4.2D). While there was no discernable change of the global translation profiles in Rh30 cells with or without quercetin

(Fig. 4.2D), the distribution of *PANX1* transcripts with quercetin treatment shifted towards the polysome fractions 5 – 8 when analyzed by qPCR (Fig. 4.2E). We further grouped the fractions into translationally inactive subpolysomes (fractions 1 – 4) and translationally active polysomes (fractions 5 – 8) for comparison. As expected, quercetin treatment induced a significant increase of the proportion of *PANX1* transcripts in the polysome fraction and a significant corresponding decrease of those in the subpolysome fraction (Fig. 4.2F). In contrast, the distribution of *GAPDH* transcripts across polysome fractions (Fig. 4.2G) and when comparing their proportions between subpolysome and polysome fractions (Fig. 4.2H), both showed no change upon quercetin treatment. Collectively, our data indicate that quercetin induced PANX1 expression in Rh30 cells by enhancing its translation.

Quercetin Induced Transcription of a Translationally-efficient PANX1 5' Leader-containing Transcript Variant

As the 5'UTR is an important regulator of translation of the downstream gene (Araujo et al., 2012; Hinnebusch et al., 2016), we thus performed qPCR analyses of Rh18 and Rh30 cells to determine whether quercetin treatment in these cells could restore the expression of 5'leader-containing *PANX1* transcripts. By analyzing the overall ratio of PANX1 in these cells, we found that the presence of transcripts containing the 5'UTR of *PANX1* significantly increased in both quercetin-treated Rh18 and Rh30 as compared to their respective DMSO vehicle controls (Fig. 4.3A). To further investigate the quercetin-induction of 5'leader *PANX1* transcripts, we performed 5'RACE (Rapid Amplification of cDNA Ends) using Rh30 cells with and without quercetin treatment. To this end, we first ligated a universal 5'adapter sequence to the 5'capped mature RNA and then reverse transcribed the full-length mRNA into cDNA sequentially using a polyA reverse primer followed by a forward primer that recognized the 5' universal adapter (Fig. 4.3B). Next, we PCR amplified the *PANX1* 5'leader using the universal adapter forward primer and a reverse primer that was designed to anneal to a position 305 bp downstream of the start codon on *PANX1* cDNA (Fig. 4.3B). Intriguingly, agarose gel electrophoresis

analysis showed multiple bands of PCR products, which suggests that *PANX1* mRNAs in Rh30 possess multiple alternative 5'UTRs of distinct lengths (Fig 4.3C). Notably, we did not detect any discernable band at the size corresponding to the annotated *PANX1* full-length 5'UTR (approximately 780 bp). Instead, most amplicons from both DMSO and quercetin treated Rh30 cells were detected between 260 and 300 bp, suggesting that the majority of *PANX1* transcripts in Rh30 cells are truncated at the 5'end of their open reading frame (ORF) (Fig. 4.3C). This was consistent with the lack of 5'UTR reads in our RNAseq data shown previously. We termed these bands collectively as *PANX1b* (Fig. 4.3C). Interestingly, quercetin-treated Rh30 cells also showed two additional bands: one at approximately 350 bp (*PANX1a*) and the other at slightly higher than 200 bp (*PANX1c*) (Fig. 4.3C), indicating that hitherto undescribed 5'UTR-containing *PANX1* transcript variants emerge upon quercetin treatment (Fig. 4.3D). This observation was also consistent with the increase in *PANX1* 5'UTR levels detected earlier in Rh30 cells following quercetin treatment (Fig. 4.3A). Next, we explored whether the various *PANX1* 5'leaders had a differential effect on the translation of *PANX1* mRNA. Using the public TSS database defined by CAGE/nanoCAGE (FANTOM Consortium and the RIKEN PMI and CLST [DGT] 2014), we found 6 other putative alternative transcription start sites (aTSS) from the annotated TSS for the *PANX1* gene locust that generated sequentially shorter 5'UTRs, which we numbered as aTSS1-6 (Fig. 4.3E). Intriguingly, the aTSS6, which initiated transcription 43 bp upstream of the start codon and yielded the shortest 5'UTR, corresponded to the 5'UTR of the *PANX1a* transcript that we had detected previously from our 5'RACE analysis in Rh30 cells after quercetin treatment. This further supports the existence of a novel *PANX1* transcript variant. Next, we cloned the full-length as well as the alternative 5'UTRs of *PANX1* from the public 5'CAGE database into a translation reporter assay system, which used chloramphenicol acetyl transferase as the reporter gene (Graber et al., 2010). Unexpectedly, the full length *PANX1* 5'UTR from the canonical TSS showed a strong repression on chloramphenicol acetyltransferase (CAT) reporter expression as compared to a 5'UTR-less construct. Furthermore, the shorter alternative 5'UTRs showed no improvement in CAT reporter activity until reaching the aTSS6 with the 43 bp-5'UTR upstream of the start codon which dramatically increased CAT reporter activities

in both Rh18 (Fig. 4.3F) and Rh30 (Fig. 4.3G) cells. Taken together, our data suggest that quercetin enhances *PANX1* translation by inducing the expression of an alternative *PANX1* transcript with a 43 bp long 5'UTR.

CREB and ETV4 Binding Sites Within the PANX1 Promoter Regulate its 5'UTR Expression

As the first step towards understanding the mechanism of *PANX1* alternative transcription, we turned our attention to the evolutionarily conserved *PANX1* promoter sequence. Due to its length, the *PANX1* promoter was separated into two sections (-2697 – -1642 and -1616 – +38) and cloned into the pGL3-basic vector. Our results from dual luciferase reporter assays showed no change in luciferase activities from the *PANX1* promoter section -2697 to -1642 (Fig. 4.4A). However, sequential removal of nucleotides at the 5' end of *PANX1* promoter section -1616 to +38 caused a gradual increase in luciferase activity that peaked at position -581, which was almost completely abolished by a further removal of 106 bp to position -475 in both Rh18 and Rh30 cells (Fig. 4.4A). Interestingly, embedded in this 106 bp sequence were putative binding sites for CREB and ETV4 which were previously shown to regulate *Panx1* transcription in rat epididymal tissue (Dufresne and Cyr, 2014). Therefore, constructs containing the *PANX1* promoter sequence from positions -581 (CREB-ETV4) and -475 (delCREB-delETV4) were chosen for further analyses (Fig. 4.4A). Subsequent dual luciferase reporter assays and qPCR analyses in parallel showed that delCREB-delETV4 caused a dramatic reduction of luciferase activities in Rh18 and Rh30 cells as compared to those containing CREB-ETV4 (Fig. 4.4B), while both *PANX1* promoter constructs produced comparable levels of *Firefly Luciferase* transcripts in Rh18 and Rh30 cells (Fig. 4.4C), suggesting a reduction at the translational level. As we previously showed that the *PANX1* 5'UTR regulated the translation of the downstream gene, we further compared its expression levels from both *PANX1* promoter constructs in Rh18 and Rh30 cells. Interestingly, we observed a significant reduction in the *PANX1* 5'UTR levels measured at positions -309, -257, -156 and -113 relative to the ATG in the absence of CREB and ETV4 sites as compared to their counterparts

(Fig. 4.4D). Collectively, our data indicate that a 106 bp portion of the *PANX1* promoter containing consensus sites for the transcription factors CREB and ETV4 is important for *PANX1* 5'UTR expression, which allows translation of the downstream coding sequence.

PANX1 Expression in RMS Requires CREB and ETV4 Consensus Sites

Next, we sought to further verify the importance of CREB and ETV4 consensus sites in regulating *PANX1* 5'UTR transcription and its translation. To this end, we performed site-directed mutagenesis to disrupt the putative consensus nucleotide sequences in the CREB binding site alone (mutCREB-ETV4) or the ETV4 binding site alone (CREB-mutETV4) or both CREB and ETV4 binding sites (mutCREB-mutETV4) from the CREB-ETV4 *PANX1* promoter construct in pGL3 vector. Using the newly generated site-mutant constructs, and CREB-ETV4 and delCREB-delETV4 as positive and negative controls, we subjected Rh18 and Rh30 cells to a dual luciferase reporter assay. As observed previously, delCREB-delETV4 *PANX1* promoter construct dramatically reduced the luciferase activities in both Rh18 (Fig. 4.5A) and Rh30 (Fig. 4.5B) cells as compared to those from CREB-ETV4. Interestingly, while the CREB site mutation alone did not change luciferase activities, the ETV4 site mutation alone (CREB-mutETV4) and the CREB-ETV4 dual site mutation (mutCREB-mutETV4) both induced similar yet significant reductions in luciferase activities as compared to the positive controls in Rh18 (Fig. 4.5A) and Rh30 (Fig. 4.5B). Similar to previous findings, none of the *PANX1* promoter site-mutation or deletion constructs significantly changed the levels of *Firefly Luciferase* reporter gene transcript in both Rh18 (Fig. 4.5C) and Rh30 (Fig. 4.5D) cells. However, it is worth noting that mutation of the CREB binding site showed a trend towards an increase in *Firefly Luciferase* transcripts, which was more evident in Rh18 (Fig. 4.5C) than in Rh30 (Fig. 4.5D) cells. Moreover, dual CREB-ETV4 site mutation also significantly reduced the 5' portion of the *Firefly Luciferase* reporter gene transcript that contained the *PANX1* 5'UTR in Rh18 (Fig. 4.5E) and Rh30 (Fig. 4.5F) cells. As we have shown here that quercetin upregulates *PANX1* 5'UTR containing

transcript levels leading to enhanced *PANX1* translation, we next tested if quercetin could also increase *PANX1* promoter activity. Our further dual luciferase reporter assays showed a trend towards a moderate increase in luciferase activities in all *PANX1* promoter constructs used after quercetin treatment in Rh18 cells (Fig. 4.5G). However, we observed a significant increase in luciferase activities following quercetin treatment with CREB-ETV4 and mutCREB-ETV4 constructs in Rh30 cells (Fig. 4.5H). This increase was no longer statistically significant when the ETV4 site was mutated or CREB and ETV4 sites were both deleted (Fig. 4.5H). Altogether, these results further suggest the involvement of transcription factors CREB and ETV4 in regulating the transcription of *PANX1* from its 5'UTR which controls its translation.

ETV4 Binding to its Consensus Site in the PANX1 Promoter is Enhanced in Quercetin-treated Rh30 cells and During Skeletal Muscle Myogenic Differentiation

In order to confirm that the transcription factors CREB and ETV4 are activated by quercetin and are part of the signalling mechanism to upregulate PANX1 expression in RMS cells, we selected Rh30 cells for further analysis. Both total CREB and phosphorylated CREB (ser133) were detected in Rh30 cells (Fig. 4.6A), but phosphorylated CREB levels following quercetin treatment were similar to the control (Fig. 4.6B). Immunofluorescence labeling showed ETV4 (red) in the nuclei of Rh30 cells treated with either DMSO (Fig. 4.6C) or quercetin (Fig. 4.6D). However, only quercetin-treated Rh30 cells showed clear co-labeling of PANX1 (green) and ETV4 (Fig. 4.6D), which was not observed in the DMSO-treated control cells (Fig. 4.6C). More importantly, although subsequent chromatin immunoprecipitation (ChIP) assays showed no change in CREB binding to its consensus site on the *PANX1* promoter in quercetin-treated Rh30 cells as compared to their DMSO controls (Fig. 4.6E, left panel), ETV4 binding was significantly enriched by quercetin (Fig. 4.6E, right panel). As PANX1 levels were highly upregulated during HSMM differentiation (Langlois et al., 2014), we suspected that ETV4 binding on the *PANX1* promoter would also be enriched during this process. We thus

differentiated HSMM for 6 days and subjected them, as well as their undifferentiated counterparts, to a ChIP assay. Indeed, the ChIP assay results showed a clear enrichment of ETV4 binding to the *PANX1* promoter in differentiated HSMM as compared to undifferentiated cells (Fig. 4.6F). Collectively, these data suggest that the mechanism by which quercetin upregulates *PANX1* translation in RMS cells involves the binding of ETV4 to its promoter region and the transcription of a translation-efficient 5'leader-containing *PANX1* mRNA.

Quercetin Induces Partial Myogenic Differentiation of RMS Cells, and Prevents Formation and Induces Regression of Established 3D In Vitro Tumors

Since quercetin has been shown to suppress various malignancies (Cossarizza et al., 2011; Rauf et al., 2018; Reyes-Farias and Carrasco-Pozo, 2019; Shafabakhsh and Asemi, 2019), we next wanted to determine whether quercetin could also induce tumor-suppression in RMS cells. Given its ability to upregulate PANX1, which was previously shown to induce partial myogenic differentiation and inhibit the progression of 3D spheroids in RMS cells (Xiang et al., 2018), we subjected Rh18 and Rh30 cells to similar tests after quercetin treatment. Following 24-hour exposure to quercetin, both Rh18 (Fig. 7A) and Rh30 (Fig. 7B) cells became elongated as compared to their respective DMSO-treated controls, which is indicative of myogenic differentiation (Langlois and Cowan, 2017). Consistent with this, subsequent Western blotting analyses and their corresponding quantification further showed a significant upregulation of MyoD levels and a trend towards an increase in MYOG after treatment with quercetin at 10 μM in both Rh18 and Rh30 cells (Fig. 4.7A and 4.7B). However, this increase in MyoD and MYOG was not observed in either cell line treated with higher concentrations of quercetin, which was likely the result of concurrently occurring apoptosis (data not shown). Next, we assessed the effect of quercetin in Rh18 and Rh30 3D spheroid formation and regression. To enable the accurate quantification of spheroid size, stable Rh18 and Rh30 cells engineered to constitutively express GFP were used, a previously described (Xiang et al., 2018). In order to assess the effect of quercetin in

spheroid formation and growth, stable Rh18 and Rh30 cells were treated with quercetin for 24 hours prior to induction of spheroid formation. Quercetin treatment induced a dose-dependent inhibitory effect on Rh18 (Fig. 4.7C) and Rh30 (Fig. 4.7D) spheroid formation and growth, completely abolishing their formation at the 50-100 μM range. Similarly, when Rh18 (Fig. 4.7E) and Rh30 (Fig. 4.7F) cells were exposed to quercetin after having been allowed to develop into established spheroids, a dramatic dose-dependent regression was observed. Notably, treatment of 100 μM of quercetin, a well tolerated dosage in normal human cells (Matsuo et al., 2005), completely obliterated both Rh18 (Fig. 4.7E) and Rh30 (Fig. 4.7F) spheroids. Together, these data demonstrate the tumour-suppressive effects of quercetin in RMS and further support its potential use as a therapeutic agent for this childhood malignancy.

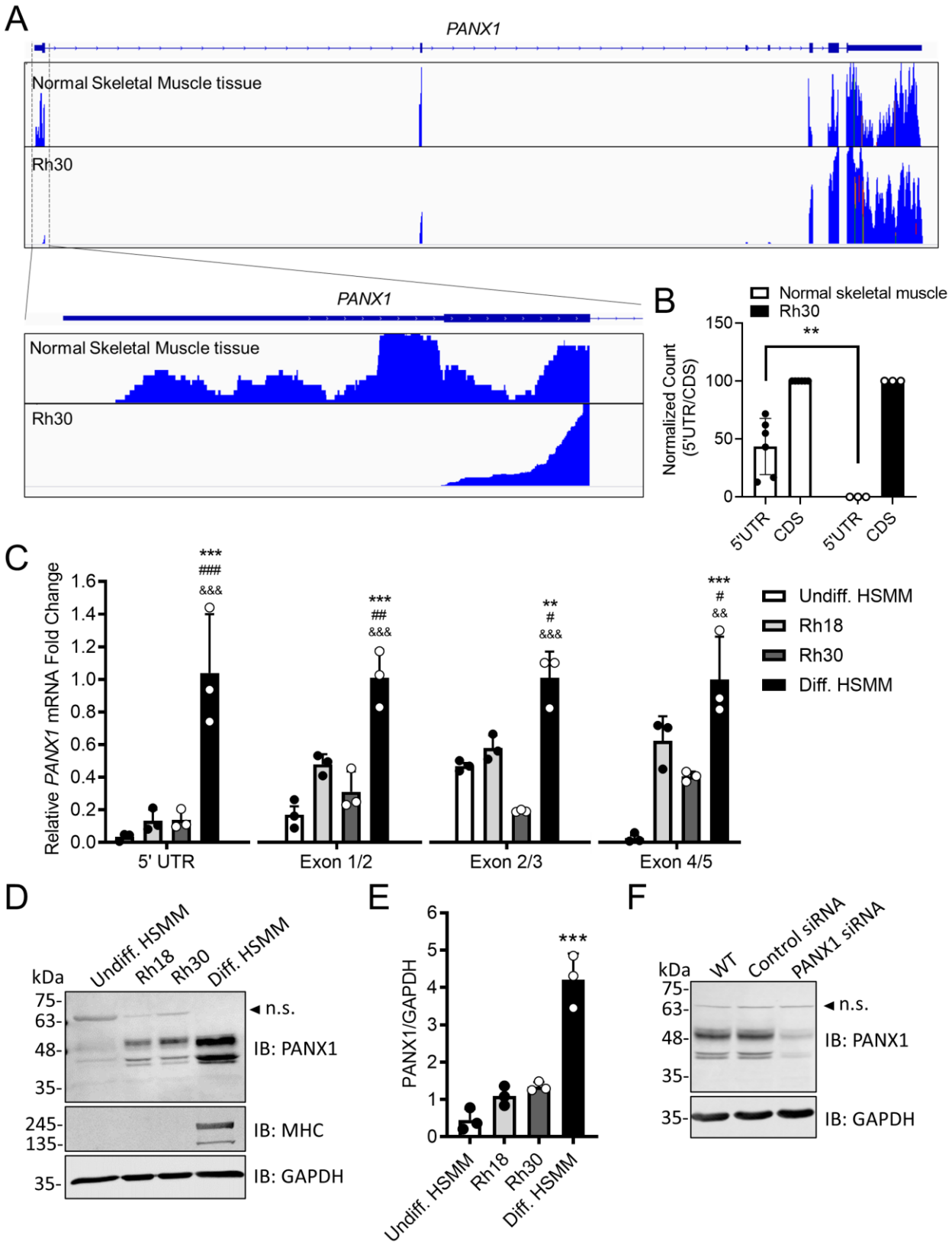
A
PANX1
Normal Skeletal Muscle tissue
Rh30
PANX1
Normal Skeletal Muscle tissue
Rh30
B
Normal skeletal muscle
Rh30
**
Normalized Count (5'UTR/CDS)
150
100
50
0
5'UTR
CDS
5'UTR
CDS
C
Relative PANX1 mRNA Fold Change
1.6
1.4
1.2
1.0
0.8
0.6
0.4
0.2
0.0
***
###
&&&
***
##
&&&
**
#
&&&
***
#
&&
5' UTR
Exon 1/2
Exon 2/3
Exon 4/5
Undiff. HSMM
Rh18
Rh30
Diff. HSMM
D
kDa
Undiff. HSMM
Rh18
Rh30
Diff. HSMM
75-
63-
48-
35-
n.s.
IB: PANX1
245-
135-
IB: MHC
35-
IB: GAPDH
E
PANX1/GAPDH
6
5
4
3
2
1
0
***
Undiff. HSMM
Rh18
Rh30
Diff. HSMM
F
kDa
WT
Control siRNA
PANX1 siRNA
75-
63-
48-
35-
n.s.
IB: PANX1
35-
IB: GAPDH

Figure 4.1 PANX1 5' UTR Expression Correlates with its Protein Abundance.

(A) RNA-seq reads mapped to the 5'UTR and exon 1 regions of *PANX1* from representative RNA libraries prepared from three biological replicates of Rh30 (aRMS) cells and as compared to representative RNA libraries from six normal human skeletal muscle tissue samples retrieved from Ryan et al., *JCI Insight* 2018. **(B)** Ratio of normalized counts of RNA-seq reads mapped to the 5'UTR region over the CDS region of *PANX1*. Note that there is no read mapped to the 5'UTR region of *PANX1* in Rh30 RNA samples. All normal skeletal muscle RNA-seq reads were retrieved from Ryan et al., *JCI Insight* 2018. **(C)** RT-qPCR of *PANX1* from Rh18 (eRMS) (n=3) and Rh30 cells (n=3) using primers specific to its 5' UTR (-276 to +1 relative to the *PANX1* ATG start codon) and exon-exon junctions. Undifferentiated (n=3) and differentiated (n=3) human skeletal muscle myoblasts (HSMM) were used as controls. Results from each amplified region was normalized independently to their differentiated (Diff. HSMM) HSMM controls in the respective *PANX1* mRNA regions. ** $P < 0.01$ and *** $P < 0.001$ compared to Undiff. HSMM; # $P < 0.05$, ## $P < 0.01$ and ### $P < 0.001$ compared to Rh18; && $P < 0.01$ and &&& $P < 0.001$ compared to Rh30. **(D)** Representative Western blots and their quantification (n=3) **(E)** showing levels of myosin heavy chain (MHC), a marker for terminal myogenic differentiation of HSMM, and PANX1. GAPDH was used as loading control. Arrowhead indicates a non-specific immunoreactive band (n.s.), which was further confirmed by **(F)** Western blotting analysis (n=3) of Rh30 cells 72 hours post siRNA-mediated knockdown of PANX1. Both wildtype Rh30 cells (WT) and Rh30 cells transfected with a scrambled siRNA sequence (Control siRNA) were used as controls. GAPDH was used as loading control. Arrowhead highlights the non-specific immunoreactive band (n.s.) also seen in **(D)**. *** $P < 0.001$ compared to Undiff. HSMM, Rh18 and Rh30. Results are expressed as mean ± s.d.

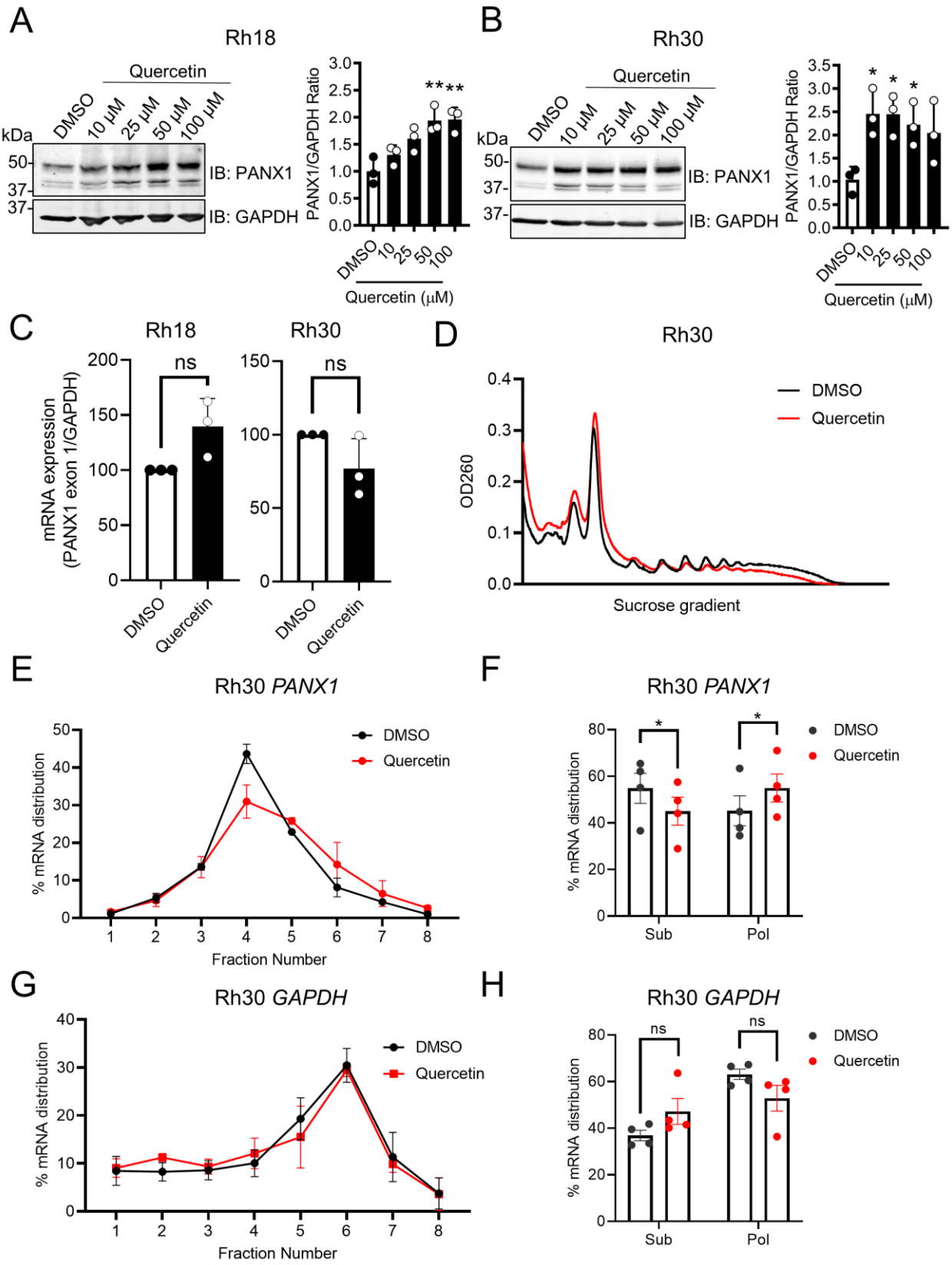
A
Rh18
Quercetin
DMSO
10 μM
25 μM
50 μM
100 μM
kDa
50-
37-
37-
IB: PANX1
IB: GAPDH
PANX1/GAPDH Ratio
****
DMSO
10
25
50
100
Quercetin (μM)
B
Rh30
Quercetin
DMSO
10 μM
25 μM
50 μM
100 μM
kDa
50-
37-
37-
IB: PANX1
IB: GAPDH
PANX1/GAPDH Ratio
*
*
*
DMSO
10
25
50
100
Quercetin (μM)
C
Rh18
Rh30
mRNA expression
(PANX1 exon 1/GAPDH)
ns
ns
DMSO
Quercetin
DMSO
Quercetin
D
Rh30
DMSO
Quercetin
OD260
Sucrose gradient
E
Rh30 PANX1
DMSO
Quercetin
% mRNA distribution
Fraction Number
F
Rh30 PANX1
*
*
DMSO
Quercetin
% mRNA distribution
Sub
Pol
G
Rh30 GAPDH
DMSO
Quercetin
% mRNA distribution
Fraction Number
H
Rh30 GAPDH
ns
ns
DMSO
Quercetin
% mRNA distribution
Sub
Pol

Figure 4.2 Quercetin Upregulates the Translation of PANX1 mRNA in RMS cells.

Rh18 (eRMS) and Rh30 (aRMS) cells were treated with increasing dosages of quercetin or its vehicle control (DMSO) for 24 hours. DMSO concentration corresponded to the highest dosage of quercetin. Representative Western blots and quantification for PANX1 in Rh18 (n=3) **(A)** and Rh30 (n=3) **(B)** cells are shown. * $P < 0.05$ and ** $P < 0.01$ compared to DMSO. GAPDH was used as loading control. **(C)** RT-qPCR analysis of *PANX1* transcript levels in Rh18 (n=3) and Rh30 (n=3) using primers specific to its exon 1 region. Results are relative to *GAPDH* transcript levels. ns: not significant. qPCR program: 95 ℃ for 3 min followed by 40 cycles of 95 ℃ for 15 sec, 60 ℃ for 30 sec. **(D)** Representative polysome traces of Rh30 cells treated with quercetin or DMSO. RT-qPCR analysis (n=4) showing **(E)** distribution of *PANX1* mRNA levels in polysome fractions and **(F)** their proportions in subpolysomes (fractions 1 – 4) and polysomes (fractions 5 – 8) fractions from DMSO- or quercetin-treated Rh30 cells. Results are expressed as the percentage of total *PANX1* mRNA. * $P < 0.05$. RT-qPCR analysis (n=4) showing **(G)** distribution of *GAPDH* mRNA levels in polysome fractions and **(H)** their proportions in combined subpolysomes (fractions 1 – 4) (translationally inactive) and polysomes (fractions 5 – 8) (translationally active) fractions from the DMSO- or quercetin-treated Rh30 cells in **(E)** and **(F)**. Results are expressed as the percentage of total *GAPDH* mRNA. Results are expressed as mean ± s.d. ns: not significant.

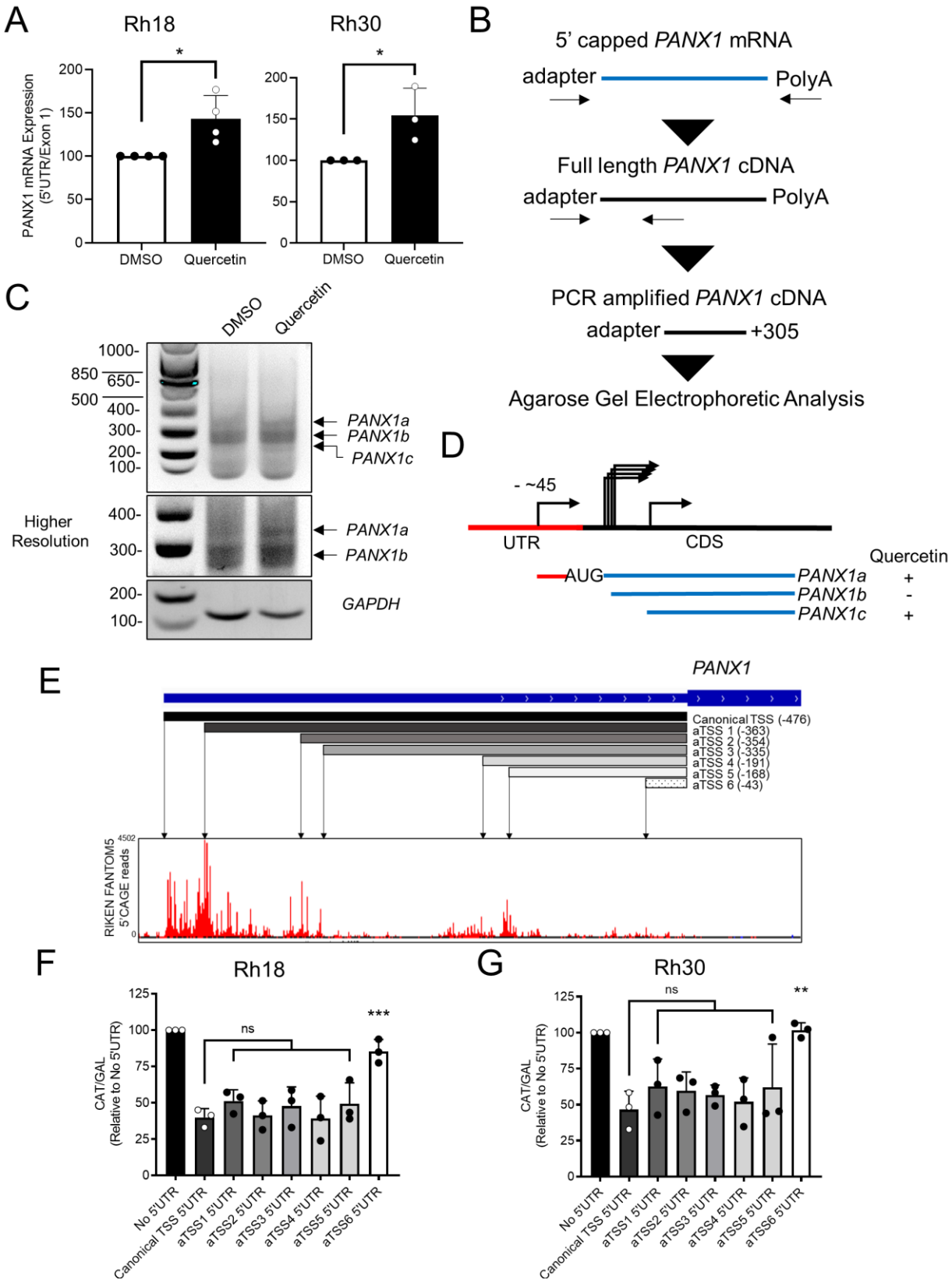
A
Rh18
Rh30
PANX1 mRNA Expression (5'UTR/Exon 1)
DMSO
Quercetin
B
5' capped PANX1 mRNA
adapter
PolyA
Full length PANX1 cDNA
PCR amplified PANX1 cDNA
+305
Agarose Gel Electrophoretic Analysis
C
Higher Resolution
PANX1a
PANX1b
PANX1c
GAPDH
D
- ~45
UTR
CDS
AUG
Quercetin
E
PANX1
Canonical TSS (-476)
aTSS 1 (-363)
aTSS 2 (-354)
aTSS 3 (-335)
aTSS 4 (-191)
aTSS 5 (-168)
aTSS 6 (-43)
RIKEN FANTOM5 5'CAGE reads
F
Rh18
CAT/GAL (Relative to No 5'UTR)
ns
***
No 5'UTR
Canonical TSS 5'UTR
aTSS1 5'UTR
aTSS2 5'UTR
aTSS3 5'UTR
aTSS4 5'UTR
aTSS5 5'UTR
aTSS6 5'UTR
G
Rh30
ns
**

Figure 4.3 Quercetin Induces the Transcription of a Translation-Competent Variant of 5' UTR Containing *PANX1* mRNA in RMS cells.

(A) RT-qPCR analysis (n=3) of *PANX1* transcript levels using primers specific to its 5' UTR region from DMSO- or quercetin-treated Rh18 (eRMS) and Rh30 (aRMS) cells. Results are relative to *GAPDH* transcript levels. * $P < 0.05$ compared to DMSO. qPCR program: 95 ℃ for 3 min followed by 40 cycles of 95 ℃ for 15 sec, 60 ℃ for 30 sec. **(B)** Schematic representation of the RACE workflow and regions amplified by PCR. A PCR product of 305 bps was expected for an intact *PANX1* cDNA from its ATG start codon. **(C)** Agarose gel electrophoresis analysis (n=2 technical replicates) of the RACE products from Rh30 cells 24 hours post quercetin treatment or its DMSO control. A higher resolution of the agarose gel image highlighting the 5' UTR containing *PANX1* mRNA variant (*PANX1a*) is shown below. GAPDH was used as control. **(D)** Schematic interpretation of the RACE products from **(C)** in which the 5' UTR containing *PANX1* cDNA (*PANX1a*), and a truncated transcript variant (*PANX1c*) induced by quercetin treatment are shown in addition to the quercetin-independent transcript variants collectively named *PANX1b*. **(E)** Aggregated CAGE reads mapped to the 5'UTR region of *PANX1* showing the canonical as well as six alternative transcription start sites (TSS). Data were retrieved from Riken FANTOM 5 track hub on hg38 genome and reviewed in UCSC genome browser. Translation reporter assay in Rh18 (n=3) **(F)** and Rh30 (n=3) **(G)** cells showing the translational activity of indicated *PANX1* putative 5'UTRs. Plasmids encoding the indicated 5'UTRs fused to a CAT CDS were co-transfected with β-galactosidase (GAL) to control transfection efficiency. CAT expression was measured by CAT ELISA kit, then normalized to the expression of a CAT mRNA without 5'UTR. ** $P<0.01$, *** $P<0.001$ compared to the canonical TSS 5' UTR. Results are expressed as mean ± s.d. ns: not significant.

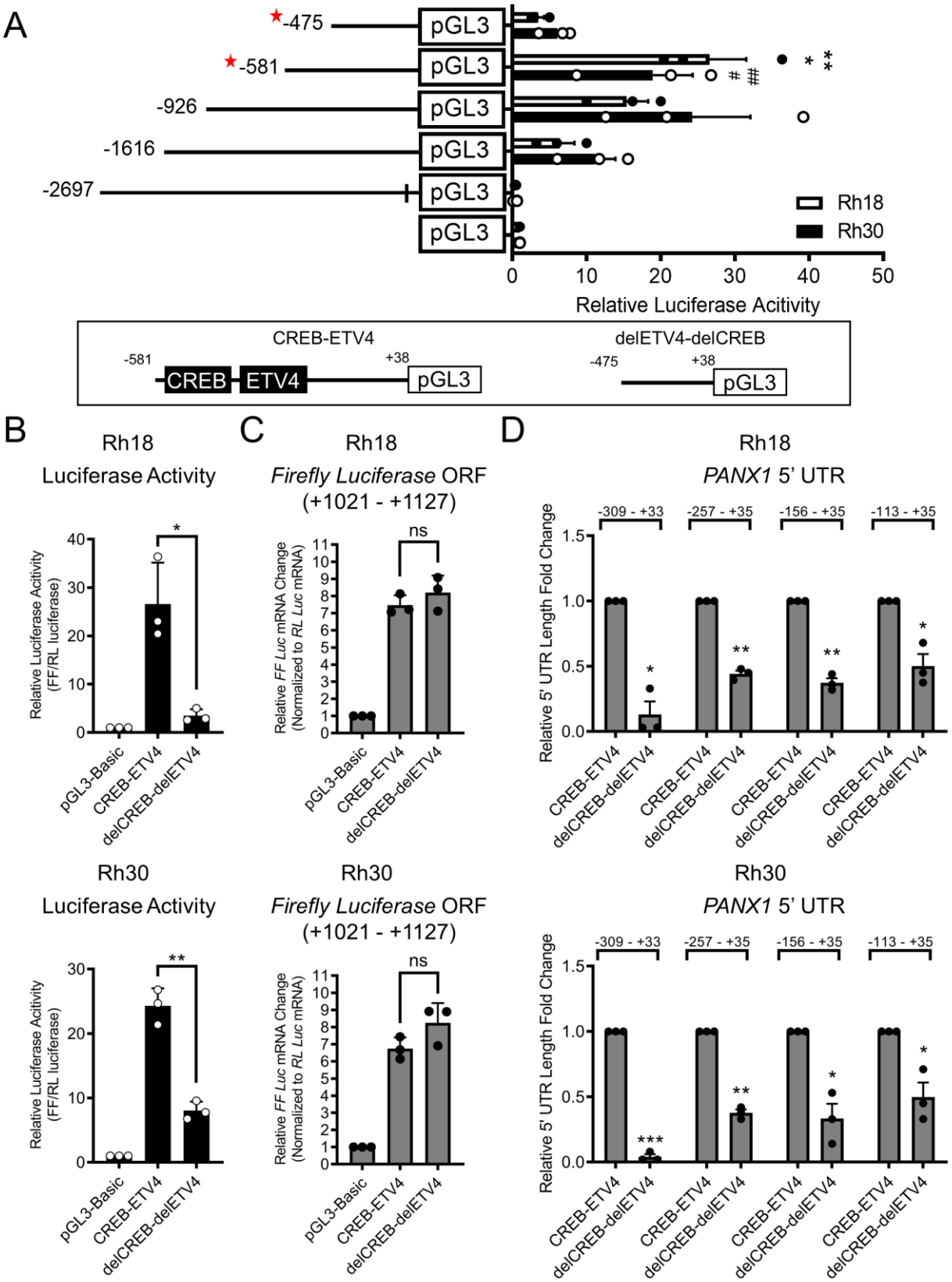
A
-475
-581
-926
-1616
-2697
pGL3
Rh18
Rh30
0
10
20
30
40
50
Relative Luciferase Acitivity
CREB-ETV4
-581
CREB
ETV4
+38
pGL3
delETV4-delCREB
-475
+38
pGL3
B
Rh18
Luciferase Activity
Relative Luciferase Acitivity (FF/RL luciferase)
pGL3-Basic
CREB-ETV4
delCREB-delETV4
C
Rh18
Firefly Luciferase ORF
(+1021 - +1127)
Relative FF Luc mRNA Change (Normalized to RL Luc mRNA)
ns
D
Rh18
PANX1 5' UTR
-309 - +33
-257 - +35
-156 - +35
-113 - +35
Relative 5' UTR Length Fold Change
Rh30
Luciferase Activity
Firefly Luciferase ORF
(+1021 - +1127)
PANX1 5' UTR

Figure 4.4 A Region of the *PANX1* Promoter Containing CREB and ETV4 Consensus Sites Regulates Transcription of its 5' UTR.

PANX1 promoter fragment from -2697 to -1642 as well as promoter fragments from -1616, -926, -581 and -475 to +38 relative to the ATG start codon were PCR amplified from primary HSMM cells and subcloned into the pGL3-basic plasmid. The pGL3 plasmids with *PANX1* promoter fragments were then co-transfected with pRL-TK into Rh18 (eRMS) and Rh30 (aRMS) for 48 hours prior to downstream assays. **(A)** Luciferase activities from pGL3 carrying various portions of the *PANX1* promoter in Rh18 (n=3) and Rh30 (n=3) cells relative to pRL-TK. Red stars highlight the two *PANX1* promoter clones shown in the schematic diagrams below which were selected for further analyses. *, # $P < 0.05$ compared to -1616 - + 38 and **, ## $P < 0.01$ compared to -475 - + 38. The pGL3-Basic or pGL3 carrying *PANX1* promoter fragments from -581 - + 38 (CREB-ETV4) or -475 - + 38 (delETV4-delCREB) were co-transfected with pRL-TK into Rh18 and Rh30 cells for 48 hours and subjected to dual luciferase reporter assay (n=3) **(B)** and RT-qPCR analyses (n=3) for **(C)** *Firefly Luciferase* (*FF*) mRNA and **(D)** *PANX1* 5'UTR levels. * $P < 0.05$ and ** $P < 0.01$ in **(B)**. ns indicates not significant in **(C)**. Each indicated amplified region was normalized separately to CREB-ETV4 in **(D)** where * $P < 0.05$, ** $P < 0.01$ and *** $P < 0.001$ compared to their respective ETV4-CREB controls. Results are expressed as mean ± s.d.

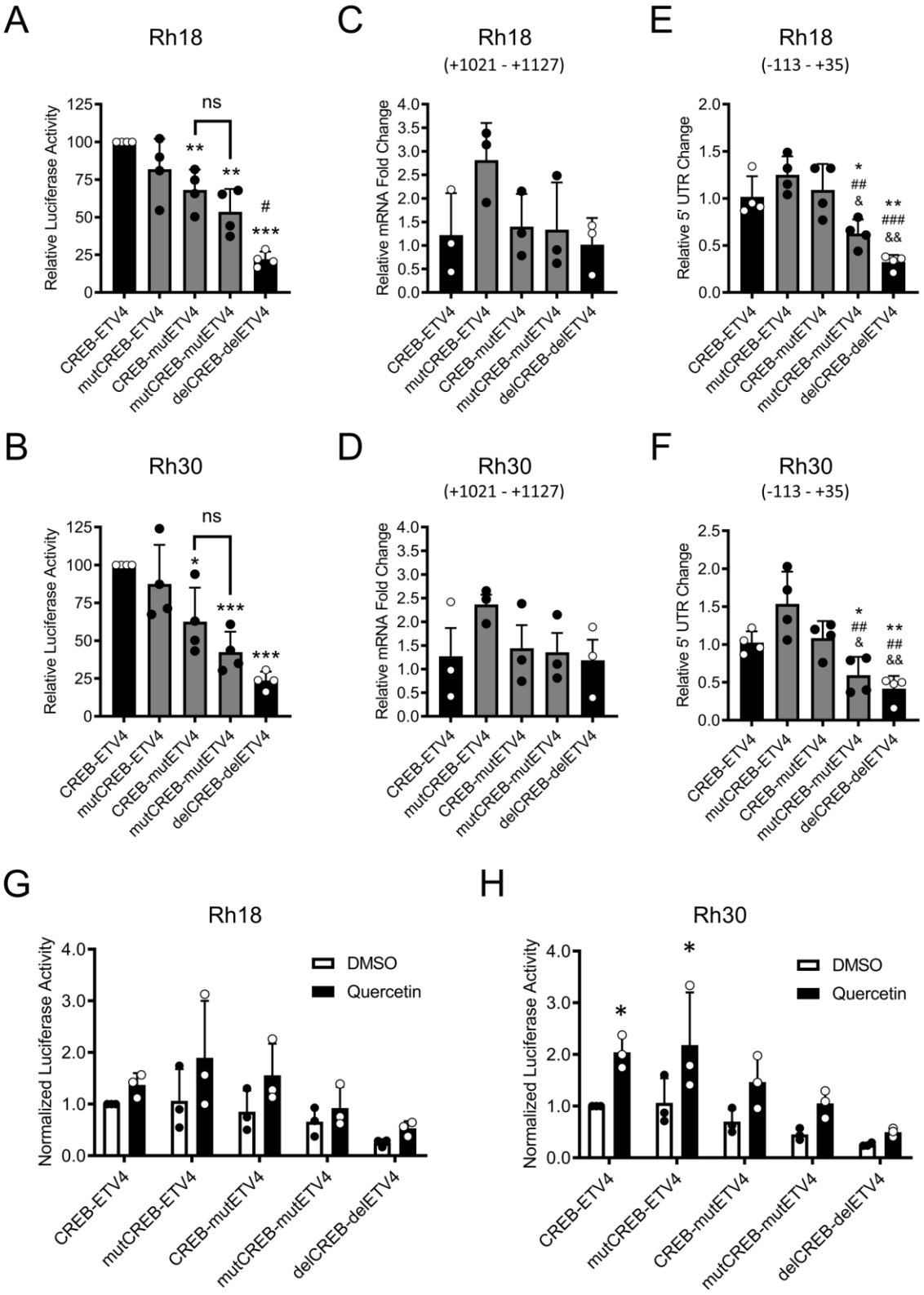
A
Rh18
Relative Luciferase Activity
ns
**
**
#
***
CREB-ETV4
mutCREB-ETV4
CREB-mutETV4
mutCREB-mutETV4
delCREB-delETV4
C
Rh18
(+1021 - +1127)
Relative mRNA Fold Change
E
Rh18
(-113 - +35)
Relative 5' UTR Change
*
##
&
**
###
&&
B
Rh30
Relative Luciferase Activity
ns
*
***
***
D
Rh30
(+1021 - +1127)
Relative mRNA Fold Change
F
Rh30
(-113 - +35)
Relative 5' UTR Change
*
##
&
**
##
&&
G
Rh18
Normalized Luciferase Activity
DMSO
Quercetin
H
Rh30
Normalized Luciferase Activity
*
*
DMSO
Quercetin

Figure 4.5 CREB and ETV4 Consensus Sites in the *PANX1* Promoter Regulate PANX1 Expression in RMS cells.

Rh18 (eRMS) and Rh30 (aRMS) cells were co-transfected with pRL-TK and pGL3 vectors containing one of the following constructs: the wildtype *PANX1* promoter (CREB-ETV4) or the *PANX1* promoter with point mutations in CREB (mutCREB-ETV4), ETV4 (CREB-mutETV4), or both sites (mutCREB-mutETV4). The pGL3 vector containing *PANX1* promoter with dual site deletion (delCREB-delETV4) was also included as a negative control. After 48 hours, cells were analyzed by dual luciferase reporter assays (n=4) **(A and B)** and then with RT-qPCR (n=4) for *FF* (amplified at +1021 - +1127 from *FF* ATG start codon) **(C and D)** or *PANX1* 5'UTR (amplified at -113 - +35 from *PANX1* ATG start codon) **(E and F)**. Dual luciferase reporter assays (n=3) were also performed in cells 48 hours post co-transfection following 24-hour DMSO or quercetin treatment prior to analysis **(G and H)**. In **(A)** and **(B)**, * $P < 0.05$, ** $P < 0.01$ and *** $P < 0.001$ compared to CREB-ETV4; # $P < 0.05$ compared to mutCREB-mutEVT4; ns = not significant. In **(E)** and **(F)**, * $P < 0.05$ and ** $P < 0.01$ compared to CREB-ETV4; ## $P < 0.01$ and ### $P < 0.001$ compared to mutCREB-ETV4; & $P < 0.05$ and && $P < 0.01$ compared to CREB-mutETV4. In **(H)**, * $P < 0.05$ compared to DMSO. pRL-TK was used as an internal normalizer in all results shown. Results are expressed as mean ± s.d.

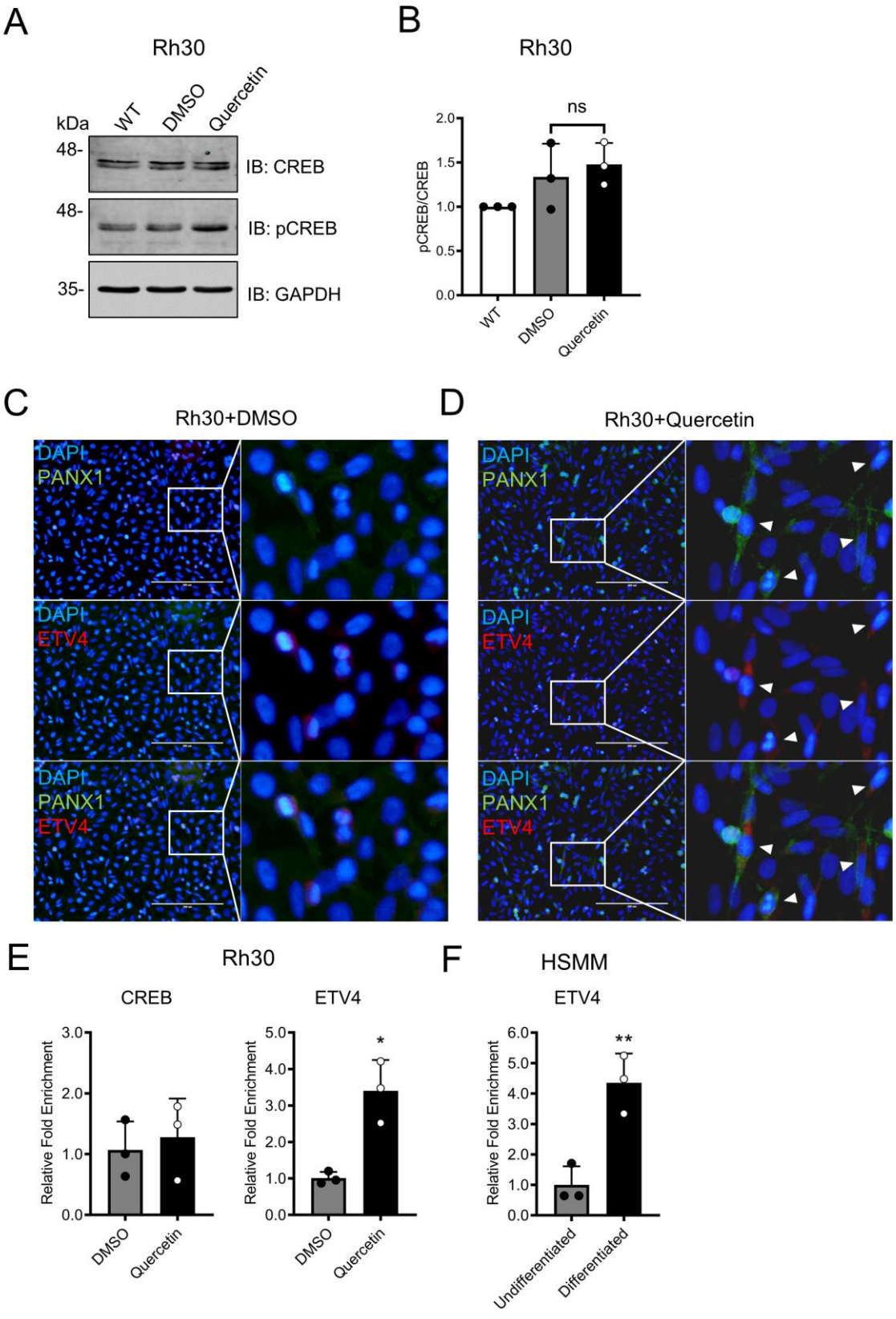
A
Rh30
kDa
WT
DMSO
Quercetin
48-
IB: CREB
48-
IB: pCREB
35-
IB: GAPDH
B
Rh30
ns
pCREB/CREB
2.0
1.5
1.0
0.5
0.0
WT
DMSO
Quercetin
C
Rh30+DMSO
DAPI
PANX1
DAPI
ETV4
DAPI
PANX1
ETV4
D
Rh30+Quercetin
DAPI
PANX1
DAPI
ETV4
DAPI
PANX1
ETV4
E
Rh30
CREB
ETV4
Relative Fold Enrichment
3.0
2.0
1.0
0.0
DMSO
Quercetin
*
5.0
4.0
3.0
2.0
1.0
0.0
DMSO
Quercetin
F
HSMM
ETV4
**
6.0
5.0
4.0
3.0
2.0
1.0
0.0
Undifferentiated
Differentiated

Figure 4.6 Quercetin Enhances the Binding of ETV4 to its Consensus Site in the *PANX1* Promoter.

Rh30 (aRMS) cells were treated with quercetin or DMSO for 24 hours and then subjected to various analyses. **(A)** Representative Western blot for CREB and pCREB. GAPDH was used as a loading control. **(B)** Quantification (n=3) of pCREB levels (relative to CREB) from **(A)**. Results were normalized to untreated Rh30 cells (WT: wild-type). N.S. = not significant. **(C and D)** Representative immunofluorescence (IF) images showing DAPI (blue), PANX1 (green) and ETV4 (red). Images were taken with a 20X objective. Arrowheads indicate PANX1 and ETV4 dual-positive Rh30 cells. Bar = 200 μm. **(E)** Chromatin Immunoprecipitation (ChIP) of CREB and ETV4 in Rh30 cells (n=3) showing enrichment of transcriptional factor binding to their respective consensus site in the *PANX1* promoter. * $P < 0.05$ compared to DMSO. **(F)** ChIP assay results (n=3) of undifferentiated and differentiated HSMM. HSMM cells were induced to differentiate by serum-withdrawal for 6 days prior to analysis. ** $P < 0.01$ compared to Undifferentiated. Results are expressed as mean ± s.d.

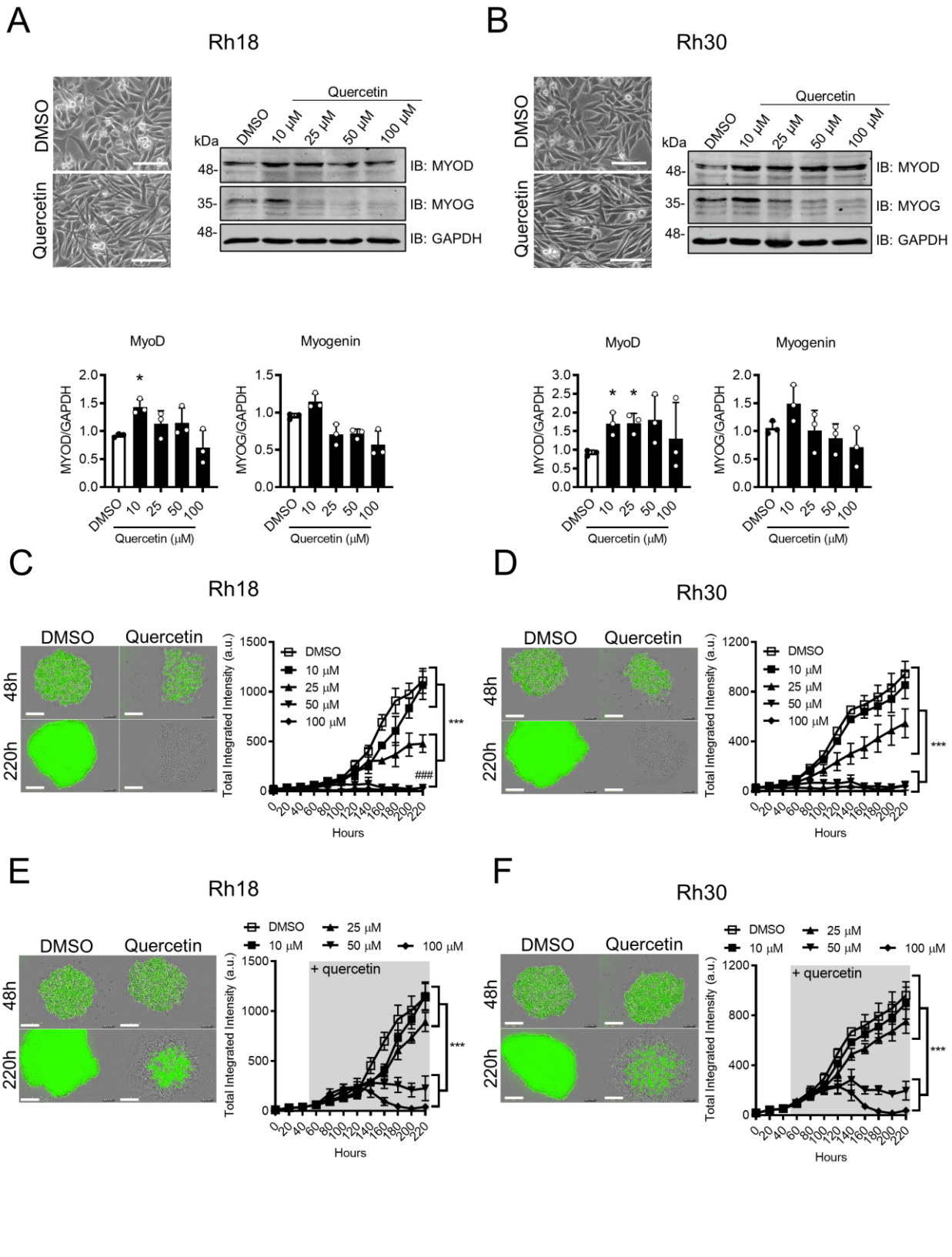
A
Rh18
DMSO
Quercetin
kDa
Quercetin
DMSO
10 μM
25 μM
50 μM
100 μM
48-
35-
48-
IB: MYOD
IB: MYOG
IB: GAPDH
B
Rh30
MyoD
Myogenin
MYOD/GAPDH
MYOG/GAPDH
Quercetin (μM)
C
Rh18
D
Rh30
48h
220h
Total Integrated Intensity (a.u.)
Hours
***
###
E
Rh18
F
Rh30
+ quercetin

Figure 4.7 Quercetin Induces Partial Differentiation of RMS Cells, and Both Inhibits Formation of and Induces Regression of their Established 3D *In Vitro* Tumors.

Representative images, Western blots, and their quantifications for myogenic markers, MYOD and MYOG, from Rh18 (eRMS) (n=3) **(A)** and Rh30 (aRMS) (n=3) **(B)** cells 24 h post quercetin treatment. DMSO was used as vehicle control. Bar = 100 μm. GAPDH was used as a loading control. * $P < 0.05$ compared to DMSO. Rh18 and Rh30 cells stably expressing GFP were subjected to 3D spheroid formation and regression assays. The GFP fluorescence, a surrogate measurement of spheroid size, was monitored over 220 h. In 3D spheroid formation and growth assay, Rh18 and Rh30 cells were pre-treated with quercetin or DMSO for 24 h. Representative images of Rh18 and Rh30 cells treated with 50 μM quercetin at 48 and 220 h are shown. The changes in total integrated intensities for Rh18 (n=3) **(C)** and Rh30 (n=3) **(D)** spheroids treated with the indicated dosages of quercetin are summarized to the right. In 3D spheroid regression assays, Rh18 and Rh30 cells were treated with quercetin 48 h post spheroid formation. Representative images of Rh18 **(E)** and Rh30 **(F)** cells treated with 50 μM of quercetin at 48 h (the time of treatment initiation) and 220 h are shown. Changes in total integrated intensities of Rh18 (n=3) **(E)** and Rh30 (n=3) **(F)** spheroids treated with the indicated dosages of quercetin are summarized to the right. *** $P < 0.001$ between indicated groups. ### $P < 0.001$ compared to 25 μM. Bar = 300 μm. Results are expressed as mean + or ± s.d.

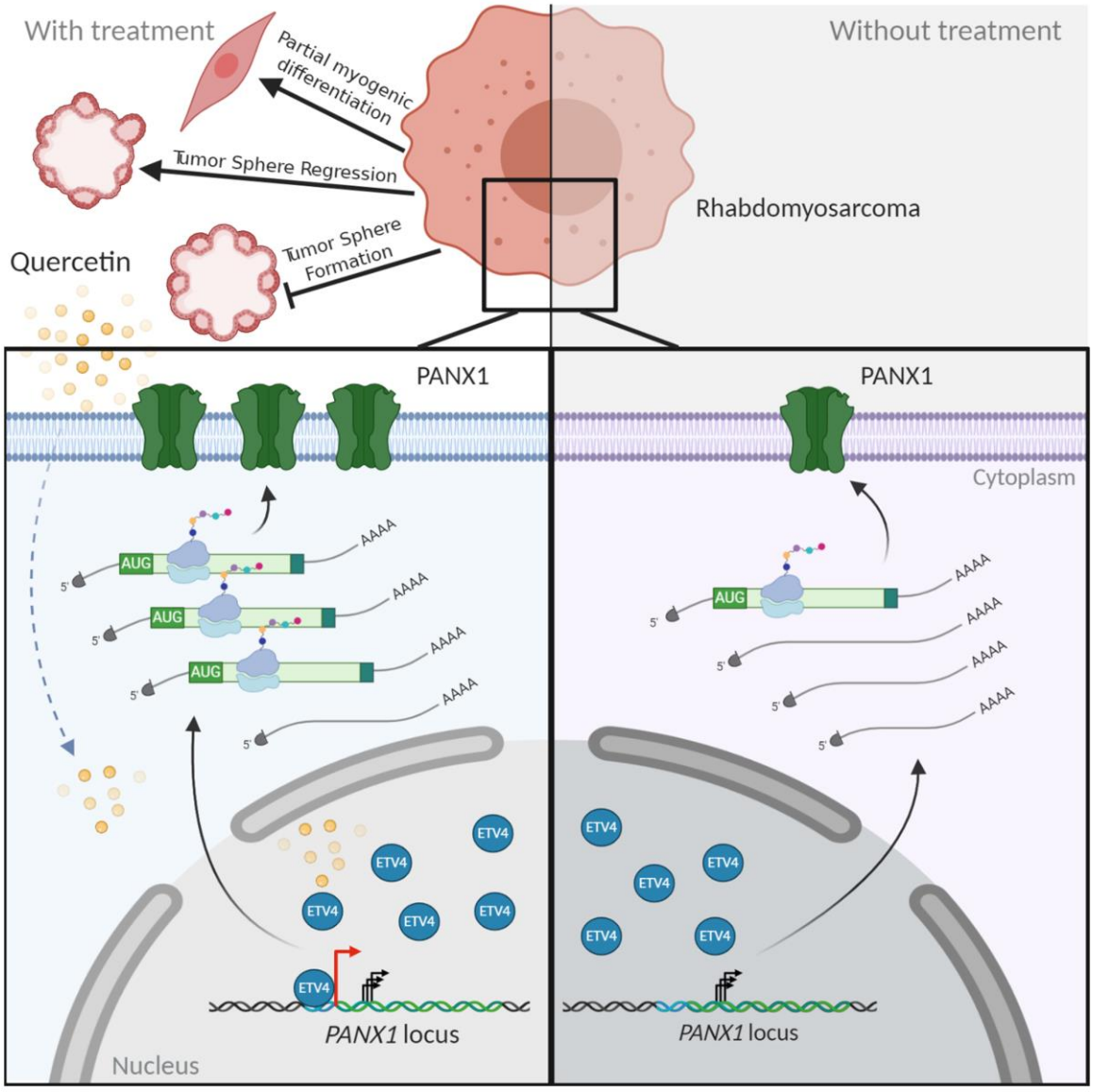
With treatment
Without treatment
Partial myogenic differentiation
Tumor Sphere Regression
Tumor Sphere Formation
Quercetin
Rhabdomyosarcoma
PANX1
PANX1
Cytoplasm
AUG
AAAA
5'
ETV4
PANX1 locus
PANX1 locus
Nucleus

Figure 4.8 Quercetin-Induced Transcriptional and Translational Control of *PANX1* in RMS.

Under normal culture conditions, the majority of basal *PANX1* transcription starts after the ATG start codon generating truncated mRNA of varying lengths that are not readily translated into PANX1 protein. Quercetin treatment enhances the binding of ETV4 to its consensus site in *PANX1* promoter, which allows the transcription of a variant of the *PANX1* transcript containing a short (~43 bp) fragment of its putative 5' UTR. This 5' UTR containing variant of the full length *PANX1* transcript can be readily bound by ribosomes resulting in an enhancement in its translation. This results in an increase in PANX1 levels and alleviation of RMS malignant properties, which suggests that repurposing of quercetin for RMS may constitute a potential new therapeutic strategy for this neoplasm. Moreover, the switch in *PANX1* transcription from producing various translationally incompetent mRNA to a more translatable 5' UTR containing variant of mRNA may have implications in the rapid modulation of PANX1 levels observed during tissue development and homeostasis, and by contrast, the dysregulation of which may lead to pathological conditions.

4.6 DISCUSSION

Despite the last five decades of research, clinical outcomes for patients with metastatic RMS remains unacceptably poor in the vulnerable patient population (Hettmer et al., 2014; Oberlin et al., 2008; Yohe et al., 2019). A major obstacle is the current limitation of therapeutic options, with treatment chemotherapy remaining largely the same having had only minor modifications in dosage, duration, and route of administration (Chen et al., 2019). Previous work from our laboratory has revealed that PANX1 is down-regulated in RMS and established upregulation of PANX1 as a potential new therapeutic approach (Xiang et al., 2018). In this study, we investigated the transcriptional and translational regulation of *PANX1* in RMS using quercetin as a pharmacological up-regulator of PANX1 expression. We present here a correlation between the levels of 5'UTR containing *PANX1* transcripts and PANX1 protein in skeletal muscle and RMS. We show that quercetin increases PANX1 levels in RMS cells by enriching the binding of the transcription factor ETV4 to the *PANX1* promoter, which induces the expression of an alternative *PANX1* mRNA transcript variant containing a translationally competent 5'leader. Moreover, we also demonstrate the tumor-suppressive effects of quercetin in RMS and the possibility for future clinic translation.

Our initial RNA-seq and RT-qPCR data revealed a unique transcriptional profile of *PANX1* in RMS where the majority of transcription starts sporadically around the ATG start codon without a defined TSS. The *PANX1*/*Panx1* promoters have been shown to reside in CpG islands and lack core promoter elements (Dufresne and Cyr, 2014). Such promoters generally have dispersed transcription initiation (Butler and Kadonaga, 2002; Zhang et al., 2013). Our data also suggest a considerable basal level of *PANX1* transcription in RMS cells. However, due to the lack of the *PANX1* 5'UTR, or in most cases the ATG start codon, they are deficient in the necessary message for translation into functional full-length PANX1 protein. Indeed, PANX1 levels in RMS are significantly lower than those of differentiated HSMM. Skeletal muscle differentiation is an intricately regulated process which involves precise temporal regulation of genes including *PANX1* (Langlois and Cowan, 2017; Langlois et al.,

2014). Thus, it is not surprising to see such aberrant transcription of *PANX1* in RMS as their myogenic differentiation program is largely impaired (Keller and Guttridge, 2013). Our observation adds to a growing body of literature that has identified the dynamic regulation of transcript variants, not just transcript abundance, to play an important role in eukaryotic gene expression via altering the translational output of each transcript (Cheng et al., 2018; Floor and Doudna, 2016). It also raises the intriguing question as to whether dynamic 5'UTR regulation might contribute to PANX1 protein expression during muscle development.

Recently, RNA-seq data from Hadwen et al. (2018) showed that quercetin induced *Panx1* mRNA levels in murine primary cerebral cultures. We further substantiate this data here by showing that quercetin induces PANX1 protein expression in RMS. However, as opposed to an induction of *PANX1* mRNA levels, quercetin-induced PANX1 expression at the translational level. This was supported by a shift in *PANX1* mRNA towards more translationally active polysome fractions upon treatment with quercetin. While total PANX1 mRNA levels stayed unchanged, we detected an increase of transcripts containing a 5'leader region, suggesting possible alternative transcription of *PANX1*. Thus, we performed 5'RACE to reveal potential aTSSs. Our results from 5'RACE of *PANX1* in Rh30 (aRMS) cells are also in accordance with our alignment of RNA-seq reads which reveal a broad band between ~260 to 300 bp indicative of *PANX1* transcripts with 5' truncation. However, we also identified two additional distinct bands following quercetin treatment that are ~350 bp (*PANX1a*) and ~230 bp (*PANX1c*) long. While *PANX1b* and *PANX1c* are truncated beyond the first ATG start codon, *PANX1a* represents a potentially translatable full-length mRNA. Notably, our survey of various *PANX1* 5'UTR lengths (between position -476 and -43 relative to the ATG start codon), which represent multiple potential alternative TSSs based on aggregated CAGE data, shows that the 5'UTR from *PANX1a* (43 bp) is the most translationally active. Alternative transcription of *Panx1* have been reported in rat epididymis which leads to three different *Panx1* mRNA transcript variants with 393 bp-, 429 bp- and 443 bp-long 5'UTR, respectively (Dufresne and Cyr, 2014). Although the translational

activities of these *Panx1* 5'UTRs were not studied in rat epididymis, their protein product Panx1 has been detected in the same tissue (Turmel et al., 2011) suggesting that they are translationally active. These data indicate potential tissue-dependent translational activity of the *PANX1* 5'UTR resulting in dynamic regulation of PANX1 expression (Langlois et al., 2014; Lee et al., 2018; Ray et al., 2005; Vogt et al., 2005).

The *PANX1* promoter is evolutionarily conserved between human and rodents especially in the region containing consensus sites for CREB and ETV4 (Dufresne and Cyr, 2014). Interestingly, we find that quercetin upregulates PANX1 in RMS through a mechanism of alternative transcription of *PANX1* involving ETV4. ETV4 (ETS variant 4), also known as PEA3, is a member of PEA3 (polyomavirus enhancer activator 3) subfamily of ETS transcription factors (Xin et al., 1992; Higashino et al., 1993). ETV4 has been detected in skeletal muscle and shown to be critically involved in myogenic differentiation (Taylor et al., 1997). The transactivity of ETV4 is enhanced by MEF2 and, more importantly, over-expression of ETV4 accelerates myogenic differentiation and blocking ETV4 function inhibits this process (Taylor et al., 1997). The functional role of ETV4 thus closely resembles that of PANX1 in skeletal muscle (Langlois et al., 2014). Similar to PANX1, ETV4 expression in RMS is generally low (Le Guellec et al., 2016). This correlation between ETV4 and PANX1 levels also remains in breast cancer (Qin et al., 2008; Wu et al., 2016), prostate cancer (Vanden Abeele et al., 2006; Tomlins et al., 2006), and melanoma (Freeman et al., 2019; Li et al., 2013), which further broadens the contextual implications of ETV4 for PANX1 expression. Our data also suggests the involvement of other transcription factors as abolishing the ETV4 binding site does not completely prevent the increase in reporter activity by quercetin. One potential candidate is interferon response factor 2 (IRF-2), an important regulator of skeletal myogenesis (Jesse and LaChance, 1998), as removal of its consensus site in the *PANX1* promoter significantly reduced reporter gene transcript levels and activities (data not shown). Thus, future efforts will be directed to deciphering the role of IRF-2 or other potential TFs on *PANX1* promoter regulation.

Moreover, our findings further expand the current functional implications of quercetin by suggesting that it may constitute a potential new therapeutic agent for diseases such as RMS (Xiang et al., 2018), glioma (Lai et al., 2007), and hearing loss (Zhao et al., 2015) where upregulation of PANX1 has been shown to be potentially beneficial. Quercetin is widely studied owing to its anti-oxidant, anti-inflammatory, anti-cancer, and chemopreventive properties (Cossarizza et al., 2011; Escribano-Ferrer et al., 2019; Rauf et al., 2018; Reyes-Farias and Carrasco-Pozo, 2019). As a polyphenol, quercetin can readily cross the nuclear envelope and modulate gene expression by altering the structure of transcription factors or directly interacting with the *cis* elements on DNA (Arif et al., 2015; Giuliani et al., 2008; Srivastava and Srivastava, 2019; Srivastava et al., 2016). Notably, quercetin has various protective roles in skeletal muscle (Ekinci Akdemir et al., 2016; Le et al., 2014; Spaulding et al., 2016). It has been recently shown to upregulate myocyte enhancer factor 2C (*MEF2C*) (Atrahimovich et al., 2019), an important myogenic factor in skeletal muscle differentiation (Potthoff et al., 2007) that is dysregulated in RMS (Ignatius et al., 2017; Zhang et al., 2015).

Interestingly, we also observed that quercetin treated RMS cells became elongated which was accompanied by upregulation of both myogenic markers, MyoD and MYOG, suggesting partial myogenic differentiation (Lukasiewicz and Miekus, 2009; Xiang et al., 2018). An earlier study also reported a dose-dependent inhibition of proliferation and morphological changes in RD cells, an eRMS cell line, after 48 hours in the presence of 30 - 130 μM of quercetin (Jagadeeswaran et al., 2000). However, it was unclear if the morphological changes in RD cells resembled myogenic differentiation (Jagadeeswaran et al., 2000). Notably, the quercetin-induced partial myogenic differentiation of RMS cells was only observed in low concentrations, and counter intuitively, treatment with higher concentrations of quercetin did not further change MyoD or MYOG levels in either Rh18 or Rh30 cells. This may be due to the biphasic effect of quercetin. Indeed, multiple reports have shown that low dosages of quercetin elicit changes in various biochemical pathways while higher concentrations induce cytotoxicity and cell death (Gibellini et al., 2010). More importantly, quercetin treatment

resulted in a dose-dependent growth inhibition and regression of Rh18 and Rh30 3D tumor spheroids. Remarkably, quercetin inhibited tumor RMS spheroid growth and induced complete regression of established RMS tumor spheroids when used at concentrations well tolerated by normal human cells (Matsuo et al., 2005), which suggest that quercetin treatment engaged a mechanism of tumor-suppression specific to RMS cells. As PANX1 expression alone promptly inhibited 3D spheroid formation and induced their regression in both Rh18 and Rh30 cells (Xiang et al., 2018), our results suggest a possible quercetin tumor-suppressive mechanism involving PANX1. However, further investigation is needed to establish the functional link between quercetin and PANX1. In addition, our results also warrant future studies to further assess the tumor-suppressive effects of quercetin in RMS with *in vivo* mouse models. Results from these studies will facilitate the process of drug repurposing of quercetin for treatment of RMS and accelerate its potential clinical translation.

Taken together, we present a mechanism of quercetin-induced PANX1 expression in RMS leading to induction of RMS differentiation, inhibition of 3D tumor spheroid growth, and regression of established *in vitro* tumors (Fig. 4.8). We have found that the majority of *PANX1* transcripts in RMS are truncated at their 5' ends thus lacking the putative 5'UTR leading to low PANX1 levels. Quercetin treatment enhances the binding of ETV4 to the PANX1 promoter, which induces the transcription of a *PANX1* mRNA transcript variant that contains a translationally active 5'UTR leading to an increase in PANX1 levels. To our knowledge, our results constitute the first evidence for upregulation of PANX1 by a pharmacological agent in human disease as well as the first report of a mechanism of PANX1 regulation via alternative transcription and 5'UTR usage. Collectively, our findings further establish quercetin as a potential therapeutic agent for treatment of RMS.

4.7 REFERENCES

Vanden Abeele, F., Bidaux, G., Gordienko, D., Beck, B., Panchin, Y. V., Baranova, A. V., Ivanov, D. V., Skryma, R., and Prevarskaya, N. (2006). Functional implications of calcium permeability of the channel formed by pannexin 1. J. Cell Biol. *174*, 535–546.

Amer, K.M., Thomson, J.E., Congiusta, D., Dobitsch, A., Chaudhry, A., Li, M., Chaudhry, A., Bozzo, A., Siracuse, B., Aytekin, M.N., et al. (2019). Epidemiology, Incidence, and Survival of Rhabdomyosarcoma Subtypes: SEER and ICES Database Analysis. J. Orthop. Res. *37*, 2226–2230.

Araujo, P.R., Yoon, K., Ko, D., Smith, A.D., Qiao, M., Suresh, U., Burns, S.C., and Penalva, L.O.F. (2012). Before It Gets Started: Regulating Translation at the 5' UTR. Comp. Funct. Genomics *2012*, 475731.

Arif, H., Rehmani, N., Farhan, M., Ahmad, A., and Hadi, S.M. (2015). Mobilization of copper ions by flavonoids in human peripheral lymphocytes leads to oxidative DNA breakage: A structure activity study. Int. J. Mol. Sci. *16*, 26754–26769.

Atrahimovich, D., Samson, A.O., Barsheshet, Y., Vaya, J., Khatib, S., and Reuveni, E. (2019). Genome-wide localization of the polyphenol quercetin in human monocytes. BMC Genomics *20*, 1–9.

Bao, L., Locovei, S., and Dahl, G. (2004). Pannexin membrane channels are mechanosensitive conduits for ATP. FEBS Lett. *572*, 65–68.

Boyce, A.K.J., Epp, A.L., Nagarajan, A., and Swayne, L.A. (2018). Transcriptional and post-translational regulation of pannexins. Biochim. Biophys. Acta - Biomembr. *1860*, 72–82.

Butler, J.E.F., and Kadonaga, J.T. (2002). The RNA polymerase II core promoter: A key component in the regulation of gene expression. Genes Dev. *16*, 2583–2592.

Charytonowicz, E., Cordon-Cardo, C., Matushansky, I., and Ziman, M. (2009). Alveolar rhabdomyosarcoma: Is the cell of origin a mesenchymal stem cell? Cancer Lett. *279*, 126–136.

Chen, C., Dorado Garcia, H., Scheer, M., and Henssen, A.G. (2019). Current and Future Treatment Strategies for Rhabdomyosarcoma. Front. Oncol. *9*, 1–18.

Cheng, Z., Otto, G.M., Powers, E.N., Keskin, A., Mertins, P., Carr, S.A., Jovanovic, M., and Brar, G.A. (2018). Pervasive, Coordinated Protein-Level Changes Driven by Transcript Isoform Switching during Meiosis. Cell *172*, 910-923.e16.

Cossarizza, A., Gibellini, L., Pinti, M., Nasi, M., Montagna, J.P., De Biasi, S., Roat, E., Bertoncelli, L., and Cooper, E.L. (2011). Quercetin and cancer chemoprevention. Evidence-Based Complement. Altern. Med. *2011*.

Cowan, K.N., Langlois, S., Penuela, S., Cowan, B.J., and Laird, D.W. (2012). Pannexin1 and Pannexin3 exhibit distinct localization patterns in human skin appendages and are regulated during keratinocyte differentiation and carcinogenesis. Cell Commun. Adhes. *19*, 45–53.

Deng, Z., He, Z., Maksaev, G., Bitter, R.M., Rau, M., Fitzpatrick, J.A.J., and Yuan, P. (2020). Cryo-EM structures of the ATP release channel pannexin 1. Nat. Struct. Mol. Biol. *27*, 373–381.

Dobson, C.C., Langlois, S., Grynspan, D., and Cowan, K.N. (2016). Engaging Cell Death Pathways for the Treatment of Rhabdomyosarcoma. Crit. Rev. Oncog. *21*, 221–239.

Dufresne, J., and Cyr, D.G. (2014). Regulation of the Pannexin-1 Promoter in the Rat Epididymis. Biol. Reprod. *91*, 143–143.

Ekinci Akdemir, F.N., Gülçin, İ., Karagöz, B., and Soslu, R. (2016). Quercetin protects rat skeletal muscle from ischemia reperfusion injury. J. Enzyme Inhib. Med. Chem. *31*, 162–166.

Escribano-Ferrer, E., Queralt Regué, J., Garcia-Sala, X., Boix Montanés, A., and Lamuela-Raventos, R.M. (2019). In vivo anti-inflammatory and antiallergic activity of pure naringenin, naringenin

chalcone, and quercetin in Mice. J. Nat. Prod. *82*, 177–182.

Floor, S.N., and Doudna, J.A. (2016). Tunable protein synthesis by transcript isoforms in human cells. Elife *5*, 1–25.

Freeman, T.J., Sayedyahossein, S., Johnston, D., Sanchez-Pupo, R.E., O'Donnell, B., Huang, K., Lakhani, Z., Nouri-Nejad, D., Barr, K.J., Harland, L., et al. (2019). Inhibition of pannexin 1 reduces the tumorigenic properties of human melanoma cells. Cancers (Basel). *11*, 1–24.

Gandin, V., Sikström, K., Alain, T., Morita, M., McLaughlan, S., Larsson, O., and Topisirovic, I. (2014). Polysome fractionation and analysis of mammalian translatomes on a genome-wide scale. J. Vis. Exp. 1–9.

Gibellini, L., Pinti, M., Nasi, M., de Biasi, S., Roat, E., Bertoncelli, L., and Cossarizza, A. (2010). Interfering with ROS metabolism in cancer cells: The potential role of quercetin. Cancers (Basel). *2*, 1288–1311.

Giuliani, C., Noguchi, Y., Harii, N., Napolitano, G., Tatone, D., Bucci, I., Piantelli, M., Monaco, F., and Kohn, L.D. (2008). The flavonoid quercetin regulates growth and gene expression in rat FRTL-5 thyroid cells. Endocrinology *149*, 84–92.

Graber, T.E., Baird, S.D., Kao, P.N., Mathews, M.B., and Holcik, M. (2010). NF45 functions as an IRES transacting factor that is required for translation of cIAP1 during the unfolded protein response. Cell Death Differ. *17*, 719–729.

Le Guellec, S., Velasco, V., Pérot, G., Watson, S., Tirode, F., and Coindre, J.M. (2016). ETV4 is a useful marker for the diagnosis of CIC-rearranged undifferentiated round-cell sarcomas: A study of 127 cases including mimicking lesions. Mod. Pathol. *29*, 1523–1531.

Hadwen, J., Schock, S., Mears, A., Yang, R., Charron, P., Zhang, L., Xi, H.S., and MacKenzie, A. (2018). Transcriptomic RNAseq drug screen in cerebrocortical cultures: toward novel neurogenetic

disease therapies. Hum. Mol. Genet. *27*, 3206–3217.

Hettmer, S., Li, Z., Billin, A.N., Barr, F.G., Cornelison, D.D.W., Ehrlich, A.R., Guttridge, D.C., Hayes-Jordan, A., Helman, L.J., Houghton, P.J., et al. (2014). Rhabdomyosarcoma: Current Challenges and Their Implications for Developing Therapies. Cold Spring Harb. Perspect. Med. *4*, a025650.

Hinnebusch, A.G., Ivanov, I.P., and Sonenberg, N. (2016). Translational control by 5'-untranslated regions of eukaryotic mRNAs. Science (80-.). *352*, 1413–1416.

Hinson, A.R.P., Jones, R., Crose, L.E.S., Belyea, B.C., Barr, F.G., and Linardic, C.M. (2013). Human rhabdomyosarcoma cell lines for rhabdomyosarcoma research: utility and pitfalls. Front. Oncol. *3*, 183.

Ignatius, M.S., Hayes, M.N., Lobbardi, R., Chen, E.Y., McCarthy, K.M., Sreenivas, P., Motala, Z., Durbin, A.D., Molodtsov, A., Reeder, S., et al. (2017). The NOTCH1/SNAIL1/MEF2C Pathway Regulates Growth and Self-Renewal in Embryonal Rhabdomyosarcoma. Cell Rep. *19*, 2304–2318.

Jagadeeswaran, R., Thirunavukkarasu, C., Gunasekaran, P., Ramamurty, N., and Sakthisekaran, D. (2000). In vitro studies on the selective cytotoxic effect of crocetin and quercetin. Fitoterapia *71*, 395–399.

Jesse, T., and LaChance, R. (1998). Interferon regulatory factor-2 is a transcriptional activator in muscle where it regulates expression of vascular cell adhesion molecule-1. J. Cell … *140*, 1265–1276.

Jin, Q., Zhang, B., Zheng, X., Li, N., Xu, L., Xie, Y., Song, F., Bhat, E.A., Chen, Y., Gao, N., et al. (2020). Cryo-EM structures of human pannexin 1 channel. Cell Res. *30*, 449–451.

Keller, C., and Guttridge, D.C. (2013). Mechanisms of impaired differentiation in rhabdomyosarcoma. FEBS J. *280*, 4323–4334.

Lai, C.P.K., Bechberger, J.F., Thompson, R.J., MacVicar, B.A., Bruzzone, R., and Naus, C.C. (2007). Tumor-suppressive effects of pannexin 1 in C6 glioma cells. Cancer Res. *67*, 1545–1554.

Langlois, S., and Cowan, K.N. (2017). Regulation of Skeletal Muscle Myoblast Differentiation and Proliferation by Pannexins. Adv. Exp. Med. Biol. *925*, 57–73.

Langlois, S., Xiang, X., Young, K., Cowan, B.J., Penuela, S., and Cowan, K.N. (2014). Pannexin 1 and pannexin 3 channels regulate skeletal muscle myoblast proliferation and differentiation. J. Biol. Chem. *289*, 30717–30731.

Lav, R., Heera, R., and Cherian, L.M. (2015). Decoding the 'embryonic' nature of embryonal rhabdomyosarcoma. J. Dev. Orig. Health Dis. 1–6.

Le, N.H., Kim, C.S., Park, T., Park, J.H.Y., Sung, M.K., Lee, D.G., Hong, S.M., Choe, S.Y., Goto, T., Kawada, T., et al. (2014). Quercetin protects against obesity-induced skeletal muscle inflammation and atrophy. Mediators Inflamm. *2014*.

Lee, V., Barr, K., Kelly, J., Johnston, D., Brown, C., Robb, K., Gros, R., Flynn, L., and Penuela, S. (2018). Pannexin 1 regulates adipose stromal cell differentiation and fat accumulation. Sci. Rep. 1–14.

Li, S., Huang, X., Zhang, D., Huang, Q., Pei, G., Wang, L., Jiang, W., Hu, Q., Tan, R., and Hua, Z.C. (2013). Requirement of PEA3 for transcriptional activation of FAK gene in tumor metastasis. PLoS One *8*, 1–13.

Lukasiewicz, E., and Miekus, K. (2009). Inhibition of rhabdomyosarcoma's metastatic behavior through downregulation of MET receptor signaling. Folia Histochem. … *47*, 485–489.

Matsuo, M., Sasaki, N., Saga, K., and Kaneko, T. (2005). Cytotoxicity of flavonoids toward cultured normal human cells. Biol. Pharm. Bull. *28*, 253–259.

Michalski, K., Syrjanen, J.L., Henze, E., Kumpf, J., Furukawa, H., and Kawate, T. (2020). The Cryo-

EM structure of a pannexin 1 reveals unique motifs for ion selection and inhibition. Elife *9*, 9–11.

Monti, E., and Fanzani, A. (2015). Uncovering metabolism in rhabdomyosarcoma. Cell Cycle *4101*, 00–00.

Oberlin, O., Rey, A., Lyden, E., Bisogno, G., Stevens, M.C.G.G., Meyer, W.H., Carli, M., and Anderson, J.R. (2008). Prognostic factors in metastatic rhabdomyosarcomas: results of a pooled analysis from United States and European cooperative groups. J. Clin. Oncol. *26*, 2384–2389.

Penuela, S., Gyenis, L., Ablack, A., Churko, J.M., Berger, A.C., Litchfield, D.W., Lewis, J.D., and Laird, D.W. (2012). Loss of pannexin 1 attenuates melanoma progression by reversion to a melanocytic phenotype. J. Biol. Chem. *287*, 29184–29193.

Penuela, S., Lohman, A.W., Lai, W., Gyenis, L., Litchfield, D.W., Isakson, B.E., and Laird, D.W. (2014). Diverse post-translational modifications of the pannexin family of channel-forming proteins. Channels (Austin). *8*, 124–130.

Pham, T. Le, St-Pierre, M.E., Ravel-Chapuis, A., Parks, T.E.C., Langlois, S., Penuela, S., Jasmin, B.J., and Cowan, K.N. (2018). Expression of Pannexin 1 and Pannexin 3 during skeletal muscle development, regeneration, and Duchenne muscular dystrophy. J. Cell. Physiol. *233*, 7057–7070.

Potthoff, M.J., Arnold, M.A., McAnally, J., Richardson, J.A., Bassel-Duby, R., and Olson, E.N. (2007). Regulation of Skeletal Muscle Sarcomere Integrity and Postnatal Muscle Function by Mef2c. Mol. Cell. Biol. *27*, 8143–8151.

Punyko, J. a, Mertens, A.C., Baker, K.S., Ness, K.K., Robison, L.L., and Gurney, J.G. (2005). Long-term survival probabilities for childhood rhabdomyosarcoma. A population-based evaluation. Cancer *103*, 1475–1483.

Qin, L., Liao, L., Redmond, A., Young, L., Yuan, Y., Chen, H., O'Malley, B.W., and Xu, J. (2008). The AIB1 Oncogene Promotes Breast Cancer Metastasis by Activation of PEA3-Mediated Matrix

Metalloproteinase 2 (MMP2) and MMP9 Expression. Mol. Cell. Biol. *28*, 5937–5950.

Rauf, A., Imran, M., Khan, I.A., ur-Rehman, M., Gilani, S.A., Mehmood, Z., and Mubarak, M.S. (2018). Anticancer potential of quercetin: A comprehensive review. Phyther. Res. *32*, 2109–2130.

Ray, A., Zoidl, G., Weickert, S., Wahle, P., and Dermietzel, R. (2005). Site-specific and developmental expression of pannexin1 in the mouse nervous system. Eur. J. Neurosci. *21*, 3277–3290.

Reyes-Farias, M., and Carrasco-Pozo, C. (2019). The anti-cancer effect of quercetin: Molecular implications in cancer metabolism. Int. J. Mol. Sci. *20*, 1–19.

Ruan, Z., Orozco, I.J., Du, J., and Lü, W. (2020). Structures of human pannexin 1 reveal ion pathways and mechanism of gating. Nature.

Shafabakhsh, R., and Asemi, Z. (2019). Quercetin: A natural compound for ovarian cancer treatment. J. Ovarian Res. *12*, 1–9.

Shern, J.F., Chen, L., Chmielecki, J., Wei, J.S., Patidar, R., Rosenberg, M., Ambrogio, L., Auclair, D., Wang, J., Song, Y.K., et al. (2014). Comprehensive genomic analysis of rhabdomyosarcoma reveals a landscape of alterations affecting a common genetic axis in fusion-positive and fusion-negative tumors. Cancer Discov. *4*, 216–231.

Spaulding, H.R., Ballmann, C.G., Quindry, J.C., and Selsby, J.T. (2016). Long-Term quercetin dietary enrichment partially protects dystrophic skeletal muscle. PLoS One *11*, 1–18.

Srivastava, N.S., and Srivastava, R.A.K. (2019). Curcumin and quercetin synergistically inhibit cancer cell proliferation in multiple cancer cells and modulate Wnt/β-catenin signaling and apoptotic pathways in A375 cells. Phytomedicine *52*, 117–128.

Srivastava, S., Somasagara, R.R., Hegde, M., Nishana, M., Tadi, S.K., Srivastava, M., Choudhary, B., and Raghavan, S.C. (2016). Quercetin, a natural flavonoid interacts with DNA, arrests cell cycle

and causes tumor regression by activating mitochondrial pathway of apoptosis. Sci. Rep. *6*, 1–13.

Tang, S.M., Deng, X.T., Zhou, J., Li, Q.P., Ge, X.X., and Miao, L. (2020). Pharmacological basis and new insights of quercetin action in respect to its anti-cancer effects. Biomed. Pharmacother. *121*, 109604.

Taylor, J.M., Dupont-Versteegden, E.E., Davies, J.D., Hassell, J.A., Houlé, J.D., Gurley, C.M., and Peterson, C.A. (1997). A role for the ETS domain transcription factor PEA3 in myogenic differentiation. Mol. Cell. Biol. *17*, 5550–5558.

Tomlins, S.A., Mehra, R., Rhodes, D.R., Smith, L.R., Roulston, D., Helgeson, B.E., Cao, X., Wei, J.T., Rubin, M.A., Shah, R.B., et al. (2006). TMPRSS2:ETV4 gene fusions define a third molecular subtype of prostate cancer. Cancer Res. *66*, 3396–3400.

Trapnell, C., Roberts, A., Goff, L., Pertea, G., Kim, D., Kelley, D.R., Pimentel, H., Salzberg, S.L., Rinn, J.L., and Pachter, L. (2012). Differential gene and transcript expression analysis of RNA-seq experiments with TopHat and Cufflinks. Nat. Protoc. *7*, 562–578.

Turmel, P., Dufresne, J., Hermo, L., Smith, C.E., Penuela, S., Laird, D.W., and Cyr, D.G. (2011). Characterization of pannexin1 and pannexin3 and their regulation by androgens in the male reproductive tract of the adult rat. Mol. Reprod. Dev. *78*, 124–138.

Vogt, A., Hormuzdi, S.G., and Monyer, H. (2005). Pannexin1 and Pannexin2 expression in the developing and mature rat brain. Mol. Brain Res. *141*, 113–120.

Wu, D., Li, L., and Chen, L. (2016). A new perspective of mechanosensitive pannexin-1 channels in cancer metastasis: clues for the treatment of other stress-induced diseases. Acta Biochim. Biophys. Sin. (Shanghai). gmw018.

Xiang, X., Langlois, S., St-Pierre, M.E., Barré, J.F., Grynspan, D., Purgina, B., and Cowan, K.N. (2018). Pannexin 1 inhibits rhabdomyosarcoma progression through a mechanism independent of its

canonical channel function. Oncogenesis *7*.

Yohe, M.E., Heske, C.M., Stewart, E., Adamson, P.C., Ahmed, N., Antonescu, C.R., Chen, E., Collins, N., Ehrlich, A., Galindo, R.L., et al. (2019). Insights into pediatric rhabdomyosarcoma research: Challenges and goals. Pediatr. Blood Cancer 1–10.

Zhang, L., Yu, H., Wang, P., Ding, Q., and Wang, Z. (2013). Screening of transcription factors with transcriptional initiation activity. Gene *531*, 64–70.

Zhang, M., Zhu, B., and Davie, J. (2015). Alternative splicing of MEF2C pre-mRNA controls its activity in normal myogenesis and promotes tumorigenicity in rhabdomyosarcoma cells. J. Biol. Chem. *290*, 310–324.

Zhao, H.-B., Zhu, Y., Liang, C., and Chen, J. (2015). Pannexin 1 deficiency can induce hearing loss. Biochem. Biophys. Res. Commun. 1–5.

4.8 SUPPLEMENTAL MATERIAL

Table 4.1 List of Primers Used

Assay	Primer Name	Sequence (5' to 3')
PANX1 Promoter Cloning	-1616PANX1pmt-Fwd	CCCAAGGAGCCCTCATGTTT
	-926PANX1pmt-Fwd	AAGAGAAACGGGACCAGCAG
	-581PANX1pmt-Fwd	CGCTCAGTGGGAAAATCCCT
	-475PANX1pmt-Fwd	TGGGTACTTGGTTTCCCCG
	+38PANX1pmt-Rev	GAGAACACGTACTCCGTGGC
	-2679PANX1pmt-Fwd	CCTACCCTCAAGAAGCCGAT
	-1642PANX1pmt-Rev	CTTGGCTCCCTTCTCTGTGG
PANX1 5' UTR Cloning		
qPCR	5'UTRPANX1-Fwd	GGACTTGCACGGGCG
	5'UTRPANX1-Rev	GTACCAATCGAGATCTCCTG
	PANX1Exon1/2-Fwd	CACGATGGTCACGTGCATTG
	PANX1Exon1/2-Rev	GTACCAATCGAGATCTCCTG
	PANX1Exon2/3-Fwd	GCTGTTCAGCAGAAGAACTCAC
	PANX1Exon2/3-Rev	TCTGAGCAAATATGAGGAGCAG
	PANX1Exon4/5-Fwd	AAGTGTACGAAATCCTCCCC
	PANX1Exon4/5-Rev	GTTCATACCTTGGAGCTCTGC
	FireflyLuc-Fwd	CTCACTGAGACTACATCAGC
	FireflyLuc-Rev	TCCAGATCCACAACCTTCGC
	RenillaLuc-Fwd	GGAATTATAATGCTTATCTACGTGC
	RenillaLuc-Rev	CTTGCGAAAAATGAAGACCTTTTAC
	5'UTRPANX1(-309)-Fwd	GAGGCGCGAATCCGAGTG
	5'UTRPANX1(-309)-Rev	CGGGCCTTTCTTTATGTTTTTGG

	5'UTRPANX1(-257)-Fwd	GGGTGGAACCGCAGGAAG
	5'UTRPANX1(-257)-Rev	GCCGGGCCTTTCTTTATGTTTTT
	5'UTRPANX1(-156)-Fwd	CTGAGGCACCGAGACACAAA
	5'UTRPANX1(-156)-Rev	GCCGGGCCTTTCTTTATGTTTTT
	5'UTRPANX1(-113)-Fwd	CAAAGGGAAAGCGAAAGCCG
	5'UTRPANX1(-113)-Rev	GCCGGGCCTTTCTTTATGTTTTT
	5'UTRPANX1()-Fwd	CCATGGCCATCGCTCAACT
	5'UTRPANX1()-Rev	GCCGGGCCTTTCTTTATGTTTTT *Continue on next page*
	GAPDH-Fwd	GTCTCCTCTGACTTCAACAGCG
	GAPDH-Rev	ACCACCCTGTTGCTGTAGCCAA
Mutagenesis	mutCREB-Fwd	CGCCCACCCCGC**CCCTTACCA**CCGCGTCTTCCGG
	mutCREB-Rev	CCGGAAGACGCGG**TGGTAAGGG**GCGGGGTGGGCG
	mutETV4-Fwd	CCCGCGTCACCGCG**TCCCAAGG**AAGCTCCACGC
	mutETV4-Rev	GCGTGGAGC**TTCCTTGGGA**CGCGGTGACGCGGG
	mutCREBmutETV4-Fwd	GC**CCCTTACCA**CCGCG**TCCCAAGG**AAGCTCCA
	mutCREBmutETV4-Rev	TGGAGCTT**CCTTGGGA**CGCGG**TGGTAAGGG**GC
ChIP	CREB-Fwd	CGCTCAGTGGGAAAATCCCT
	CREB-Rev	GGGGAAACCAAGTACCCAGG
	ETV4-Fwd	GCCAGGACGTGAGGAGAATC
	ETV4-Rev	CCATGCGGGGAAACCAAGTA
	GAPDH_ChIP-Fwd	TACTAGCGGTTTTACGGGCG
	GAPDH_ChIP-Rev	TCGAACAGGAGGAGCAGAGAGCGA
5' RACE	TeloFwd	TGGATTGATATGTAATACGACTCACTATAG
	TeloRev	TCTCAGGCGTTTTTTTTTTTTTTTTT
	PANX1Exon2-Rev	GGGAGGTTTCCAGACTCGC

Bold letters indicate the predicted DNA sequence of TF consensus site. Underlined letters indicate the bases changed by directed mutagenesis.

5. CHAPTER FIVE: GENERAL DISCUSSION

In the series of studies presented in this thesis, we established PANX1 as a therapeutic target for RMS by demonstrating, for the first time, its tumour-inhibitory effects *in vitro* and *in vivo* (Chapter 2). Notably, our findings suggest that PANX1 alleviates RMS malignant properties through a mechanism that is independent of its canonical channel function (Chapter 2). In order to elucidate the mechanism of this previously undescribed PANX1 function, we performed unbiased transcriptomic and proteomic analyses in PANX1-expressing RMS cells. In doing so, we recorded the expression changes of various genes involved in cellular processes and signaling pathways related to tumour-suppression and demonstrated up-regulation of Cx43 by PANX1 in aRMS cells (Chapter 3). We also identified a previously unknown PANX1 interactor, AHNAK, through which PANX1 mediates its tumour-inhibitory effects in RMS (Chapter 3). In addition, we constructed the first PANX1 transcriptomic and proteomic databases that provide open access to our entire RNA-seq and BioID data in a user-friendly fashion (Chapter 3). We then looked for strategies to up-regulate PANX1 in RMS that could be potentially clinically translatable. To this end, we found that quercetin increased PANX1 expression in RMS cells and subsequently elucidated the mechanism of *PANX1* regulation at the transcriptional and, for the first time, translational levels in RMS cells (Chapter 4). We further documented the tumour-suppressive effects of quercetin in RMS cells, which demonstrated the potential for future clinical translation (Chapter 4).

By evaluating PANX1 expression in human eRMS and aRMS tumour specimens and patient-derived cell lines, we found that PANX1 levels were down-regulated across all specimens and cell lines to a level that resembled those expressed in fetal skeletal muscle tissue and undifferentiated human skeletal muscle myoblasts (HSMM), respectively. Since the

transformation event for RMS could happen in mesenchymal cells prior to their commitment into the myogenic lineage or in skeletal muscle myoblasts and mature muscle fibres (Charytonowicz et al., 2009; Hettmer and Wagers, 2010; Lav et al., 2015), the down-regulated PANX1 levels observed in eRMS and aRMS cells was likely a result of two different mechanisms. While the exact origin of eRMS cells remains unclear, current evidence suggests that the transformation of eRMS likely takes place in committed skeletal muscle progenitors such as myoblasts (Linardic et al., 2005; Wagers and Conboy, 2005). Since skeletal muscle myoblasts do not express PANX1 prior to the initiation of myogenic differentiation (Langlois et al., 2014), the low levels of PANX1 in eRMS might be a result of tumour transformation events that happen before the developmental stage in which PANX1 expression was naturally induced. On the other hand, tumour transformation into the aRMS subtype has been observed with expression of the PAX3/7-FOXO1 oncoproteins in mature skeletal muscle tissues, leading to the hypothesis that aRMS tumourigenesis requires de-differentiation of maturing skeletal muscles (Keller and Capecchi, 2005). Previous results from our laboratory indicates that ectopic PANX1 expression in undifferentiated HSMM promotes their differentiation and reduces their proliferative potential (Langlois et al., 2014), thus down-regulation of PANX1 during the de-differentiation process may be needed for the cells to re-engage cellular proliferation (Keller and Capecchi, 2005). Moreover, aRMS have also been recapitulated in mesenchymal stem cells with simultaneous expression of PAX-FOXO1 and inactivation of p53 (Ren et al., 2008), suggesting a possible mesenchymal origin (Charytonowicz et al., 2009; Hettmer and Wagers, 2010; Ren et al., 2008). Expression of PAX3/7-FOXO1 fusion oncoproteins induce aberrant transcription of genes including *MyoD* and *Myog* involved in myogenic differentiation (Khan et al., 1999; Ren et al., 2008), which may thus predispose

mesenchymal stem cells to develop into an immature skeletal muscle lineage that express low levels of PANX1 (Langlois et al., 2014; Pham et al., 2018).

While *PANX1* mRNA in eRMS and aRMS cells was significantly lower compared to that in differentiated HSMM by RT-qPCR, a considerable amount was detected by RNA-seq. Similarly, *PANX1* mRNA in HEK293T and HeLa cells can be detected by RT-qPCR using primers specific to exons 4 and 5 near the 3' end of its ORF while both cells lines are not known to express endogenous PANX1 protein (Vanden Abeele et al., 2006; Negoro et al., 2014). Interestingly, our subsequent alignment analysis of *PANX1* mRNA reads from RNA-seq revealed a lack of reads mapped to the 5' end of its open reading frame (ORF) indicating that majority of mRNAs were truncated beyond the first ATG start codon. Without the first ATG start codon, these *PANX1* mRNAs were unlikely to be translated into the full-length protein they originally encoded. Nevertheless, there are also two other ATG codons in the 5' end of *PANX1* ORF in the Kozak consensus sequences which can potentially act as translation initiation sites (TIS) to produce two PANX1 isoforms of shorter lengths (Baranova et al., 2004). However, we did not observe any immunoreactive species of PANX1 that corresponded to these shorter isoforms by Western blotting, suggesting a lack of translation of the 5' end truncated *PANX1* mRNAs, lack of degradation of any N-terminus truncated protein products, or both. However, future experiments involving inhibition of the lysosomal degradation pathway, which has been implicated in Panx1 clearance (Boyce and Swayne, 2017; Boyce et al., 2015; Sagdullaev et al., 2017), or the proteasomal pathway (unpublished data from our laboratory), should unveil if the N-terminus truncated PANX1 is subjected to degradation in these cells. Collectively, these results not only provided a plausible explanation to the low

levels of PANX1 detected in RMS cells but also suggested for the first time that the 5' end modification of *PANX1*/*Panx1* mRNA might uniquely regulate its translation.

In accordance with our observations, *Panx1* expression is down-regulated in C6 glioma cells at the transcript level which has been speculated to contribute to gliomagenesis (Lai et al., 2007). In addition, PANX1 is also down-regulated in gallbladder adenocarcinoma and was inversely correlated with disease progression (Schalper et al., 2014). However, PANX1/Panx1 levels were found to be up-regulated in other cancers such as melanoma (Freeman et al., 2019; Penuela et al., 2012), breast cancer (Furlow et al., 2015), testicular cancer (Liu et al., 2019), and hepatocellular carcinoma (Shi et al., 2019) promoting cancer aggression. This may suggest that the expression of PANX1 during cancer progression is highly dependent on the type and, as in the case of RMS, the tissue context of neoplastic transformation. Furthermore, as PANX1/Panx1 is ubiquitously expressed and its levels are dynamically regulated during development, such as in the brain (Ray et al., 2005; Vogt et al., 2005), eye (Ray et al., 2005), skeletal muscle (Pham et al., 2018), and adipose tissue (Lee et al., 2018), it can be speculated that PANX1 expression is under strict temporal (Pham et al., 2018; Ray et al., 2005; Vogt et al., 2005), spatial (Wicki-Stordeur et al., 2016), and state-dependent regulation (Jiang et al., 2012; Meems et al., 2016; Zhang et al., 2015). Therefore, while the function of PANX1 in cancer remains paradoxical (Penuela et al., 2014b), dysregulation of these stringent regulatory controls, such as during the process of tumourigenic transformation, may lead to aberrant PANX1 expression.

Thus far, regulation of PANX1/Panx1 expression has been shown to take place at epigenetic, such as methylation (Jiang et al., 2012; Meems et al., 2016) and histone modification (Zhang et al., 2015), and transcriptional (Dufresne and Cyr, 2014) levels in

response to state-dependent stimuli. Here we provide the first evidence for regulation of PANX1 at the translational level through the 5'UTR of its mRNA. While *PANX1* transcripts from RMS were truncated at the 5' end of the ORF, *PANX1* transcripts from human skeletal muscle contained various lengths of 5'UTR (Baranova et al., 2004; Ryan et al., 2018), and the levels of *PANX1* 5'UTR mRNA, not the total *PANX1* mRNA levels, correlated with the levels of the encoded protein. *PANX1* 5'UTRs that were likely translationally active in HSMM were translationally repressive when cloned into a CAT reporter plasmid and expressed in eRMS and aRMS cells. While their effect on translational regulation remains to be elucidated, *Panx1* in rat epididymis contains alternative TSSs that produce mRNAs with different lengths of 5'UTR (Dufresne and Cyr, 2014), suggesting that an alternative transcription of *PANX1* may take place in various tissue types. Taken together, these results suggest the possibility that *PANX1* translation, like many other genes, could be under tissue or state-specific control by its 5'UTR leading to dynamic protein expression (Cheng et al., 2018; Floor and Doudna, 2016). Despite these exciting findings, it is still unclear whether this type of PANX1 regulation takes place in other tissue types or disease contexts. To address this, one could survey the existing GEO and CAGE databases looking for changes in *PANX1* mRNA read coverage and TSSs, respectively, between cell, tissue, and disease types. In addition, one could assess the translational activity of putative *PANX1* 5'UTRs in a form CAT reporter assay across cell lines and compare their abilities to initiate translation in each setting (Kawaji et al., 2006). This could be further coupled with polysome profiling and pulse-chase with radiolabeled ^{35}S-methionine to confirm the changes of *PANX1* mRNA translation by different 5'UTRs.

As RMS cells are deficient in PANX1, we attempted to restore its levels in both eRMS (Rh18) and aRMS (Rh30) cells. While ectopic expression of PANX1 failed to overcome the

inability of both eRMS and aRMS cells to reach terminal differentiation, it markedly reduced cell proliferation, motility, and anchorage-independent growth and prevented the formation of 3D tumour spheroids and induced their regression through induction of apoptosis. Moreover, PANX1 expression also significantly inhibited eRMS and aRMS tumour growth *in vivo*. Since Panx1 expression in C6 glioma cells induced tumour-suppressive effects (Lai et al., 2007), which could be reversed by inhibition of its channel activity (Bao et al., 2012), we sought to investigate whether PANX1 channel functions were also involved in suppressing the malignant properties of RMS. Unexpectedly, PANX1 did not form functional channels in the plasma membrane of eRMS and aRMS cells that could be activated by mechanical stimulation. Using a combination of PANX1 channel inhibitors and channel-deficient PANX1 mutants, we further demonstrated that the PANX1-mediated tumour-inhibition in eRMS and aRMS did not require a functional channel. Thus, our results suggested a non-canonical mechanism of PANX1 by which it mediated tumour-suppression in RMS.

As a first step toward delineating the molecular mechanism by which PANX1 reduces RMS malignant properties, we took an unbiased approach by performing RNA-seq based whole genome transcriptomic and BioID-based whole cell proteomic analyses in RMS cells. In doing so, we also created the first searchable PANX1 transcriptomic and proteomic databases and made them available to the scientific community.

Notably, PANX1 expression alone in aRMS cells induced significant change in the expression of over 1200 genes which were implicated in various key cellular responses, such as cell motility, apoptosis, and myogenic differentiation, that were consistent with the observed tumour-suppressive effects induced by PANX1 (Gredinger et al., 1998; Proulx et al., 1997; Zhang et al., 2017). While we demonstrated our PANX1 transcriptome as a valuable source of

information by further confirming the expression change of several gene hits at the transcriptional level, and, in the case of Cx43, the corresponding change at the protein level, we could not at this point pursue the entire lists of genes from the relevant biological processes and signaling pathways due to their quantity. Thus, the future effort will be directed at validation of the expression of these gene candidates and further investigation of their functional roles in the PANX1-mediated tumour suppression using RNA interference or over-expression plasmids as potential research strategies. High throughput functional screening using commercially available siRNA libraries coupled with Opera Phenix high-content screening system could also facilitate the testing of a large number of gene candidates in an unbiased manner.

Prior to these studies, co-immunoprecipitation (Co-IP) using whole cell lysates has been the predominant method to identify PANX1 interactors. However, one of the shortcomings of traditional Co-IP is the loss of protein candidates due to weak or transient interactions (Roux, 2013; Roux et al., 2012). Instead BioID offers the advantage of capturing protein-protein interactions as well as these weak and transient interactors under natural conditions in live cells (Roux, 2013; Roux et al., 2012). Given that some PANX1 interactors may be subject to cellular state-dependent regulation which alters the interaction between them (Weilinger et al., 2012; Weilinger et al., 2016; DeLalio et al., 2018; DeLalio et al., 2019), BioID would thus be ideal to enable capturing these transient interactions. Moreover, since PANX1 interactions often involve specialized cellular machinery such as the purinergic receptors (Pelegrin and Surprenant, 2006), inflammasome (Silverman et al., 2009), and DHPR/RYR complex (Arias-Calderón et al., 2016) that act as central hubs that mediate

downstream signaling transduction, BioID may help reveal these transient secondary interactions that are characteristic of them thus providing further supportive information.

While BioID offers the above-mentioned advantages, the result often contains a large list of protein candidates that require further validation (Kim et al., 2016). Thus, we complemented BioID by traditional Co-IP coupled to tandem mass spectrometry to facilitate high-throughput validation of our identified protein hits from BioID. We revealed that the PANX1 interactome in RMS cells consists of largely plasma membrane-bound and cytoskeletal proteins, which are consistent with previous reports (Bao et al., 2012; Bhalla-Gehi et al., 2010; Wicki-Stordeur and Swayne, 2013). In addition, we further related the tumour-inhibitory function of PANX1, in large part, to its interaction with AHNAK.

The interaction between Panx1 and the actin cytoskeleton has been implicated in its plasma membrane trafficking and stability (Bhalla-Gehi et al., 2010), mechanosensitive channel activation (Bhalla-Gehi et al., 2010; Boyce et al., 2014; Locovei et al., 2006a; Wicki-Stordeur and Swayne, 2013), and alteration of cellular behaviour by actin remodeling (Bao et al., 2012; Lai et al., 2007; Wicki-Stordeur and Swayne, 2013). Recently, Panx1 channels have been shown to regulate microtubule stability by physically sequestering collapsin response mediator protein 2 (crmp2) (Xu et al., 2018). Interestingly, Panx1/crmp2 interaction can be disrupted by binding of probenecid to the first extracellular loop which causes an allosteric change in the channel structure (Xu et al., 2018). Perhaps the reverse can also happen. Interaction between PANX1 and surrounding multiprotein complexes may restrict its pore structure such that it prevents mechanosensitive channel activation. AHNAK is a multifaceted structural protein that contains a large interface for protein-protein interaction (Benaud et al., 2004; Hashimoto et al., 1995; Huang et al., 2007; Lee et al., 2004). In RMS cells, PANX1

colocalizes with AHNAK in specialized areas of the plasma membrane and being embedded in this super structural element may render the channels insensitive to mechanical stimulus. Future dye uptake assays in PANX1-expressing RMS cells with and without AHNAK KD could help to shed light on this hypothesis.

However, other possibilities also exist. RMS cells may lack the necessary mechanism to allow PANX1 channel activation (Chiu et al., 2018). Endogenous PANX1 in RMS cells may be truncated in the N-terminus which is an essential structural domain for channel activation (Michalski et al., 2018). These defective PANX1 protomers may intermix with their full-length counterparts and act in a dominant negative manner to suppress channel activation (Li et al., 2011a). It was found recently that mechanosensitive activation of ectopic Panx1 channels could be inhibited by phosphorylation at T302 and S328 by protein kinase A (PKA) in HeLa cells (López et al., 2020). Thus, it would be of interest to verify whether such a mechanism of regulation existed in RMS by site-directed mutagenesis at the corresponding residues in human PANX1 and then evaluating their ability to be activated by mechanical stimulation-mediated dye uptake assays (Xiang et al., 2018). Interestingly, we found that PANX1 channels in a different eRMS cell line, RD cells, could be activated by mechanical stimuli (data not shown). As we have identified the PANX1 interactome in RD cells using BioID (data not shown), the comparison of the PANX1 interactomes between RD and Rh18 or Rh30 cells may reveal potential unique candidate interactors that impede or allow channel activation.

More importantly, since AHNAK is implicated in many signaling pathways such as AKT/MAPK (Chen et al., 2017), Wnt/β-catenin (Chen et al., 2017), and transforming growth factor beta (TGF-β) /Smad pathways (Lee et al., 2014), our findings provide a potential

molecular mechanism for PANX1 to initiate signal transduction from the plasma membrane to other cellular compartments, such as the nucleus, to regulate cellular behaviours and gene expression. Future efforts should be directed towards evaluating the protein expression change, phosphorylation, and subcellular localization of the aforementioned pathway mediators. In the event one or more pathway mediators are potentially implicated, functional assays with RNAi-mediated KD or transient over-expression of these pathway mediators in PANX1-expressing RMS cells should further confirm their involvement in tumour-suppression.

In addition to AHNAK, the identification of Annexin A2 (ANXA2) in both our BioID and Co-IP assays using PANX1-enriched fractions suggests the presence of PANX1 in the putative AHNAK-ANXA2-S100A10 signaling complex (Benaud et al., 2004; Ozorowski et al., 2013; Rezvanpour et al., 2011). S100A10 is a plasminogen receptor that localizes in the plasma membrane with ANXA2 which has been shown to promote migration and invasion of several types of cancer (Noye et al., 2018; Shang et al., 2013; Wang et al., 2019; Yang et al., 2011). Interestingly, disruption of S100A10-ANXA2 interaction by competitive binding of the Rho GTPase-activating protein, DLC1, induces ubiquitin-mediated degradation of S100A10 and leads to inhibition of cell migration, invasion, and anchorage-independent growth of lung cancer cells (Yang et al., 2011). Similarly, PANX1 may also mediate tumour-suppression by displacing S100A10 from ANXA2 and inducing its subsequent degradation in RMS cells. Therefore, future Western blotting analysis could reveal a change in S100A10 levels in RMS cells with and without PANX1. Additional Co-IP assays would confirm whether ANXA2 is part of the AHNAK-PANX1 immunocomplex, and over-expression of ANXA2 in PANX1-expressing RMS cells could reveal its functional relevance in the PANX1-mediated inhibition of RMS progression. Electrophoretic mobility shift assays with purified PANX1, ANXA2, and

S100A10 using radiolabelled antibodies would reveal the potential competitive binding between PANX1 and S100A10 with ANXA2. Moreover, as the PANX1 C-terminus has been suggested as the primary interface for protein-protein interaction, expression of the PANX1 C-terminal domain alone should further confirm the site of PANX1-ANXA2 interaction (Xu et al., 2018).

Although PANX1 expression in eRMS and aRMS cells did not induce terminal differentiation, we documented an increase in the proportion of multi-nucleated aRMS cells with PANX1 expression suggesting partial differentiation. When compared to their mononucleated counterparts, more multi-nucleated aRMS cells showed expression of myogenin, which is characteristic of myogenic differentiation. However, these observations were not made with eRMS cells. While we could not explain why PANX1-mediated partial myogenic differentiation was only seen in aRMS, it is possible that, as eRMS and aRMS are vastly different in their mutational background (Shern et al., 2014), some products of genetic alterations such as the PAX-FKHR fusion protein, although advantageous for aRMS survival, may be more susceptible to inhibition by PANX1 thus allowing engagement of early myogenic differentiation. While the absence of terminal differentiation in eRMS and aRMS cells may be attributable to a lack of PANX1 channel function that would otherwise provide the cells with extracellular ATP required for myogenic differentiation (Araya et al., 2004), the possibility exists that a different pathway is regulated by PANX1 to induce partial myogenic differentiation in aRMS cells. Recently, PANX1/Panx1 have been shown to regulate Wnt/β-catenin signaling pathway in melanoma cells (Freeman et al., 2019; Penuela et al., 2012). Wnt/β-catenin signaling has been shown to play an important role in the development of skeletal muscle such as promoting fusion and differentiation of myoblasts (Cisternas et al.,

2014; Cui et al., 2019). In RMS, activation of the Wnt/β-catenin pathway by treatment with human recombinant Wnt3a induces an elongated cellular morphology, expression of Myf5 and reduces proliferation of aRMS cells (Annavarapu et al., 2013). Similar to our observations, these effects are also absent in eRMS cells (Annavarapu et al., 2013) and suggest the possibility that PANX1-induced partial differentiation of aRMS cells is mediated through regulation of Wnt/β-catenin pathway. While key mediators of Wnt/β-catenin pathway were not enriched in our PANX1 interactome, it remains possible that the regulation is not by direct protein-protein interaction. Thus, Western blotting analysis of β-catenin, glycogen synthase kinase 3 β (GSK3β), Akt and their respective phosphorylated counter parts in aRMS cells with and without PANX1 expression should help reveal whether Wnt/β-catenin pathway is involved (Wu and Pan, 2010).

Furthermore, while it is currently unknown whether this also occurs in eRMS cells, expression of PANX1 in aRMS cells induced a significant increase in the levels of *GJA1* mRNA after 48 hours and its encoding protein, Cx43, after 96 hours. Since Cx43 expression in RMS cells has been shown to increase their myogenic differentiation leading to alleviation of malignancies (Proulx et al., 1997), PANX1 could thus mediate myogenic differentiation independent of its channel activity through up-regulation of Cx43. The establishment of gap junctional intercellular communication should be assessed via microinjection of lucifer yellow dye in PANX1-expressing RMS cells (Frank et al., 2006). In addition, Cx43 is a well-known regulator of Wnt/β-catenin signaling pathway (Hou et al., 2019; López et al., 2019; Spagnol et al., 2018), thus providing further support for its involvement in aRMS myogenic differentiation. Future experiments using a combination of shRNA-mediated KD and

inhibitory drugs such as CBX should help elucidate the role of Cx43 in myogenic differentiation and tumour-suppression of RMS cells.

Collectively our results demonstrated a tumour-suppressive role of PANX1 and established it as a therapeutic target for both eRMS and aRMS. We thus sought out a strategy to up-regulate PANX1 expression that could potentially be translated into the clinic setting. Over the past two decades, a considerable list of molecules and peptides that can selectively inhibit PANX1 channel activity has been described (Willebrords et al., 2017). However, pharmacological up-regulation of PANX1 expression was rarely, if ever, reported or investigated. Such drugs may hold great promise to be applied in the clinical setting for the treatment of diseases in which induction of PANX1/Panx1 has been shown to be beneficial (Lai et al., 2007; Zhao et al., 2015). In these studies, we identified the FDA- and Health Canada-approved drug quercetin as an up-regulator of PANX1 in RMS cells. To our surprise, while treatment with therapeutic dosages of quercetin led to significant increase of PANX1 expression in both eRMS and aRMS cells, it failed to change the total *PANX1* mRNA levels in either cell line. Using 5'RACE and CAT reporter assays, we subsequently related this up-regulation of PANX1 to the transcription of *PANX1* from an alternative TSS which generated an mRNA variant with a specific 5'UTR that was translationally active in RMS cells. These results demonstrate for the first time that up-regulation of PANX1 can be achieved through the use of a pharmacologic agent and provide additional evidence for the regulation of PANX1 at the translational level.

In addition, we further elucidated the mechanism for this quercetin-induced alternative transcription of *PANX1* by showing an enrichment of ETV4 to its consensus site in the *PANX1* promoter after quercetin treatment. Indeed, abolishing this site resulted in a significant

reduction in *PANX1* 5'UTR-containing mRNA levels. ETV4 has been shown to regulate *Panx1* expression in rat epididymal tissue (Dufresne and Cyr, 2014), and, while it also has been shown to regulate skeletal muscle in a similar fashion as Panx1 (Taylor et al., 1997), its link to PANX1/Panx1 up-regulation needs to be further elucidated. These reports suggest that this form of regulation of PANX1 may be applicable in different tissue types. In addition, expression of ETV4/Etv4 and PANX1/Panx1 are directly correlated in several cancers (Vanden Abeele et al., 2006; Freeman et al., 2019; Li et al., 2013; Penuela et al., 2012; Qin et al., 2008; Tomlins et al., 2006; Wu et al., 2016) including RMS (Le Guellec et al., 2016; Xiang et al., 2018). Since targeting PANX1/Panx1 in these cancers have led to a beneficial outcome (Vanden Abeele et al., 2006; Freeman et al., 2019; Penuela et al., 2012; Wu et al., 2016; Xiang et al., 2018), the synergistic effects of PANX1/Panx1 modulators and small molecule drugs that target the ETS family of TFs such as YK-4-279 (Erkizan et al., 2009) in these cancers could be explored.

However, the mechanistic role of quercetin in *PANX1* regulation remains an intriguing research topic which needs to be further pursued; an important question is: can quercetin ameliorate the neoplastic properties of RMS and serve as a potential therapeutic agent? To address this, we treated RMS cells with various therapeutic dosages of quercetin and subjected them to 3D spheroid formation and regression assays (Xiang et al., 2018). Our results showed a clear dosage-dependent inhibition of tumour spheroid growth and regression of established spheroids. Moreover, quercetin treated RMS cells exhibited an elongated morphology similar to that of differentiating myoblasts, and subsequent Western blotting analyses in these cells revealed an increase of MyoD and myogenin, indicating that quercetin treatment induced partial myogenic differentiation, an effect similar to that induced by PANX1 expression

(Langlois et al., 2014; Xiang et al., 2018). With these encouraging preliminary results, our future research will be directed at uncovering whether quercetin-induced tumour-suppression is linked to increase in PANX1 levels. Moreover, we will also compare the effects of quercetin to the current chemotherapy backbone for RMS, which consists of vincristine, actinomycin D, and cyclophosphamide (Crist et al., 1995; Maurer et al., 1993; Walterhouse et al., 2014) as well as any possible synergistic effects in various combinations of them in *in vitro* and *in vivo*. Next, we will also include patient tumour-derived primary RMS cells in assessing the effectiveness of quercetin to further confirm our findings. In doing so, we will establish quercetin as a potential new therapeutic agent for RMS. *De novo* drug synthesis takes an average of 13.5 years from initial experimentation to completion of vigorous regulatory reviews (Paul et al., 2010), which is unable to meet the urgent need for novel therapeutic options to treat patients with high-grade metastatic or recurrent RMS (Hettmer et al., 2014; Miwa et al., 2020; Yohe et al., 2019). Therefore, repurposing drugs previously approved for other indications, such as quercetin, can greatly accelerate their use for RMS treatment (Pantziarka et al., 2014; Pushpakom et al., 2018; Sleire et al., 2017). To this end, using our established 3D spheroid system, we can perform high throughput screens of other therapeutic agents that have been shown to increase PANX1 levels on patient-derived RMS cell lines to facilitate drug repurposing (Hadwen et al., 2018; Xiang et al., 2018) (Fig. 5.1). By including primary cells derived from patient tumour biopsies in the screening process, we can further confirm the drug efficacies and construct a potential personalized treatment strategy for RMS (Fig. 5.1). Together, these experiments will help expand the current arsenal of therapeutic agents for RMS, and in turn, improve the clinical outcome for patients.

5.1 CONCLUSION

Our discovery of PANX1 down-regulation in RMS ultimately led us to a potential clinic-translatable therapeutic strategy for its treatment. Altogether, these findings have demonstrated a critical role of PANX1 in suppressing RMS progression and provided a potential therapeutic option that may improve its clinical outcome. In addition, the results presented here have significantly advanced our understanding of PANX1 channels by showing for the first time the PANX1 transcriptome and interactome in RMS, its tumour-inhibitory interaction with AHNAK, and its mechanism of translational control.

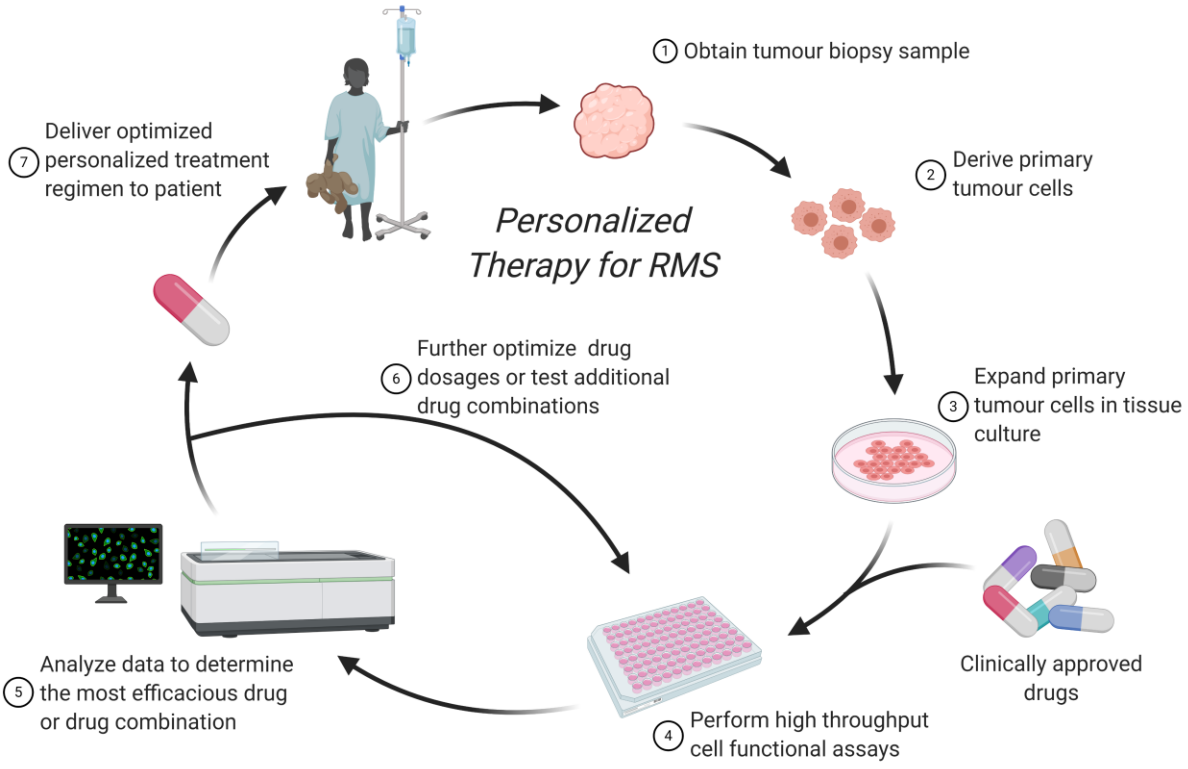
1 Obtain tumour biopsy sample
2 Derive primary tumour cells
3 Expand primary tumour cells in tissue culture
Clinically approved drugs
4 Perform high throughput cell functional assays
5 Analyze data to determine the most efficacious drug or drug combination
6 Further optimize drug dosages or test additional drug combinations
7 Deliver optimized personalized treatment regimen to patient
Personalized Therapy for RMS

Figure 5.1 A Proposed High-throughput Screening Model for Drug Repurposing and Personalized Treatment of RMS.

Our proposed procedure begins with derivation of patient-specific primary cell cultures from biopsy tissue specimens of RMS. The primary cells are then induced to grow into 3D spheroids for high-throughput drug screening. The drug responses are closely monitored by automated cell imaging systems for the duration of the treatment. The drug responses can either be analyzed during the treatment or at its end by specialized image analysis software which generates a list of candidate drugs. The candidate drugs can then be potentially integrated into a new personalized treatment regimen for patients with RMS or other malignancies.

5.2 REFERENCES

Vanden Abeele, F., Bidaux, G., Gordienko, D., Beck, B., Panchin, Y. V., Baranova, A. V., Ivanov, D. V., Skryma, R., and Prevarskaya, N. (2006). Functional implications of calcium permeability of the channel formed by pannexin 1. J. Cell Biol. *174*, 535–546.

Annavarapu, S.R., Cialfi, S., Dominici, C., Kokai, G.K., Uccini, S., Ceccarelli, S., McDowell, H.P., and Hellxxiwell, T.R. (2013). Characterization of Wnt/β-catenin signaling in rhabdomyosarcoma. Lab. Investig. *93*, 1090–1099.

Araya, R., Riquelme, M.A., Brandan, E., and Sáez, J.C. (2004). The formation of skeletal muscle myotubes requires functional membrane receptors activated by extracellular ATP. Brain Res. Brain Res. Rev. *47*, 174–188.

Arias-Calderón, M., Almarza, G., Díaz-Vegas, A., Contreras-Ferrat, A., Valladares, D., Casas, M., Toledo, H., Jaimovich, E., and Buvinic, S. (2016). Characterization of a multiprotein complex involved in excitation-transcription coupling of skeletal muscle. Skelet. Muscle *6*, 15.

Bao, B.A., Lai, C.P., Naus, C.C., and Morgan, J.R. (2012). Pannexin1 drives multicellular aggregate compaction via a signaling cascade that remodels the actin cytoskeleton. J. Biol. Chem. *287*, 8407–8416.

Baranova, A., Ivanov, D., Petrash, N., Pestova, A., Skoblov, M., Kelmanson, I., Shagin, D., Nazarenko, S., Geraymovych, E., Litvin, O., et al. (2004). The mammalian pannexin family is homologous to the invertebrate innexin gap junction proteins. Genomics *83*, 706–716.

Benaud, C., Gentil, B.J., Assard, N., Court, M., Garin, J., Delphin, C., and Baudier, J. (2004). AHNAK interaction with the annexin 2/S100A10 complex regulates cell membrane cytoarchitecture. J. Cell Biol. *164*, 133–144.

Bhalla-Gehi, R., Penuela, S., Churko, J.M., Shao, Q., and Laird, D.W. (2010). Pannexin1 and pannexin3 delivery, cell surface dynamics, and cytoskeletal interactions. J. Biol. Chem. *285*, 9147–9160.

Boyce, A.K.J., and Swayne, L.A. (2017). P2X7 receptor cross-talk regulates ATP-induced pannexin 1 internalization. Biochem. J. *474*, 2133–2144.

Boyce, A.K.J., Wicki-Stordeur, L.E., and Swayne, L.A. (2014). Powerful partnership: crosstalk between pannexin 1 and the cytoskeleton. Front. Physiol. *5*, 27.

Boyce, A.K.J., Kim, M.S., Wicki-Stordeur, L.E., and Swayne, L.A. (2015). ATP stimulates Pannexin 1 internalisation to endosomal compartments. Biochem. J. 319–330.

Charytonowicz, E., Cordon-Cardo, C., Matushansky, I., and Ziman, M. (2009). Alveolar rhabdomyosarcoma: Is the cell of origin a mesenchymal stem cell? Cancer Lett. *279*, 126–136.

Chen, B., Wang, J., Dai, D., Zhou, Q., Guo, X., Tian, Z., Huang, X., Yang, L., Tang, H., and Xie, X. (2017). AHNAK suppresses tumour proliferation and invasion by targeting multiple pathways in triple-negative breast cancer. J. Exp. Clin. Cancer Res. *36*, 1–11.

Cheng, Z., Otto, G.M., Powers, E.N., Keskin, A., Mertins, P., Carr, S.A., Jovanovic, M., and Brar, G.A. (2018). Pervasive, Coordinated Protein-Level Changes Driven by Transcript Isoform Switching during Meiosis. Cell *172*, 910-923.e16.

Chiu, Y.H., Schappe, M.S., Desai, B.N., and Bayliss, D.A. (2018). Revisiting multimodal activation and channel properties of Pannexin 1. J. Gen. Physiol. *150*, 19–39.

Cisternas, P., Henriquez, J.P., Brandan, E., and Inestrosa, N.C. (2014). Wnt Signaling in Skeletal Muscle Dynamics: Myogenesis, Neuromuscular Synapse and Fibrosis. Mol. Neurobiol. *49*, 574–589.

Crist, W., Gehan, E.A., Ragab, A.H., Dickman, P.S., Donaldson, S.S., Fryer, C., Hammond, D., Hays, D.M., Herrmann, J., Heyn, R., et al. (1995). The Third Intergroup Rhabdomyosarcoma Study. J. Clin. Oncol. *13*, 610–630.

Cui, S., Li, L., Yu, R.T., Downes, M., Evans, R.M., Hulin, J.-A., Makarenkova, H.P., and Meech, R. (2019). β-Catenin is essential for differentiation of primary myoblasts via cooperation with MyoD and α-catenin. Development *146*, dev167080.

Dufresne, J., and Cyr, D.G. (2014). Regulation of the Pannexin-1 Promoter in the Rat Epididymis. Biol. Reprod. *91*, 143–143.

Erkizan, H. V, Kong, Y., Merchant, M., Schlottmann, S., Barber-Rotenberg, J.S., Yuan, L.,

Abaan, O.D., Chou, T., Dakshanamurthy, S., Brown, M.L., et al. (2009). A small molecule blocking oncogenic protein EWS-FLI1 interaction with RNA helicase A inhibits growth of Ewing's sarcoma. Nat. Med. *15*, 750–756.

Floor, S.N., and Doudna, J.A. (2016). Tunable protein synthesis by transcript isoforms in human cells. Elife *5*, 1–25.

Frank, D.K., Szymkowiak, B., and Hughes, C.A. (2006). Connexin expression and gap junctional intercellular communication in human squamous cell carcinoma of the head and neck. Otolaryngol. Neck Surg. *135*, 736–743.

Freeman, T.J., Sayedyahossein, S., Johnston, D., Sanchez-Pupo, R.E., O'Donnell, B., Huang, K., Lakhani, Z., Nouri-Nejad, D., Barr, K.J., Harland, L., et al. (2019). Inhibition of pannexin 1 reduces the tumorigenic properties of human melanoma cells. Cancers (Basel). *11*, 1–24.

Furlow, P.W., Zhang, S., Soong, T.D., Halberg, N., Goodarzi, H., Mangrum, C., Wu, Y.G., Elemento, O., and Tavazoie, S.F. (2015). Mechanosensitive pannexin-1 channels mediate microvascular metastatic cell survival. Nat. Cell Biol. *7*, 943–952.

Gredinger, E., Gerber, A.N., Tamir, Y., Tapscott, S.J., and Bengal, E. (1998). Mitogen-activated protein kinase pathway is involved in the differentiation of muscle cells. J. Biol. Chem. *273*, 10436–10444.

Le Guellec, S., Velasco, V., Pérot, G., Watson, S., Tirode, F., and Coindre, J.M. (2016). ETV4 is a useful marker for the diagnosis of CIC-rearranged undifferentiated round-cell sarcomas: A study of 127 cases including mimicking lesions. Mod. Pathol. *29*, 1523–1531.

Hadwen, J., Schock, S., Mears, A., Yang, R., Charron, P., Zhang, L., Xi, H.S., and MacKenzie, A. (2018). Transcriptomic RNAseq drug screen in cerebrocortical cultures: toward novel neurogenetic disease therapies. Hum. Mol. Genet. *27*, 3206–3217.

Hashimoto, T., Gamou, S., Shimizu, N., Kitajima, Y., and Nishikawa, T. (1995). Regulation of translocation of the desmoyokin/AHNAK protein to the plasma membrane in keratinocytes by protein kinase C. Exp. Cell Res. *217*, 258–266.

Hettmer, S., and Wagers, A.J. (2010). Muscling in: Uncovering the origins of rhabdomyosarcoma. Nat. Med. *16*, 171–173.

Hettmer, S., Li, Z., Billin, A.N., Barr, F.G., Cornelison, D.D.W., Ehrlich, A.R., Guttridge, D.C., Hayes-Jordan, A., Helman, L.J., Houghton, P.J., et al. (2014). Rhabdomyosarcoma: Current Challenges and Their Implications for Developing Therapies. Cold Spring Harb. Perspect. Med. *4*, a025650.

Hou, X., Khan, M.R.A., Turmaine, M., Thrasivoulou, C., Becker, D.L., and Ahmed, A. (2019). Wnt signaling regulates cytosolic translocation of connexin 43. Am. J. Physiol. Integr. Comp. Physiol. *317*, R248–R261.

Huang, Y., Laval, S.H., van Remoortere, A., Baudier, J., Benaud, C., Anderson, L.V.B., Straub, V., Deelder, A., Frants, R.R., den Dunnen, J.T., et al. (2007). AHNAK, a novel component of the dysferlin protein complex, redistributes to the cytoplasm with dysferlin during skeletal muscle regeneration. FASEB J. *21*, 732–742.

Jiang, T., Xu, R.X., Zhang, A.W., Di, W., Xiao, Z.J., Miao, J.Y., Luo, N., and Fang, Y.N. (2012). Effects of transcranial direct current stimulation on hemichannel pannexin-1 and neural plasticity in rat model of cerebral infarction. Neuroscience *226*, 421–426.

Kawaji, H., Kasukawa, T., Fukuda, S., Katayama, S., Kai, C., Kawai, J., Carninci, P., and Hayashizaki, Y. (2006). CAGE Basic/Analysis Databases: the CAGE resource for comprehensive promoter analysis. Nucleic Acids Res. *34*, 632–636.

Keller, C., and Capecchi, M.R. (2005). New genetic tactics to model alveolar rhabdomyosarcoma in the mouse. Cancer Res. *65*, 7530–7532.

Khan, J., Bittner, M.L., Saal, L.H., Teichmann, U., Azorsa, D.O., Gooden, G.C., Pavan, W.J., Trent, J.M., and Meltzer, P.S. (1999). cDNA microarrays detect activation of a myogenic transcription program by the PAX3-FKHR fusion oncogene. Proc. Natl. Acad. Sci. U. S. A. *96*, 13264–13269.

Kim, D.I., Jensen, S.C., and Roux, K.J. (2016). Identifying Protein-Protein Associations at the Nuclear Envelope with BioID. Methods Mol Biol 133–146.

Lai, C.P.K., Bechberger, J.F., Thompson, R.J., MacVicar, B.A., Bruzzone, R., and Naus, C.C. (2007). Tumor-suppressive effects of pannexin 1 in C6 glioma cells. Cancer Res. *67*, 1545–1554.

Langlois, S., Xiang, X., Young, K., Cowan, B.J., Penuela, S., and Cowan, K.N. (2014). Pannexin 1 and pannexin 3 channels regulate skeletal muscle myoblast proliferation and differentiation. J. Biol. Chem. *289*, 30717–30731.

Lav, R., Heera, R., and Cherian, L.M. (2015). Decoding the 'embryonic' nature of embryonal rhabdomyosarcoma. J. Dev. Orig. Health Dis. 1–6.

Lee, I.H., You, J.O., Ha, K.S., Bae, D.S., Suh, P.G., Rhee, S.G., and Bae, Y.S. (2004). AHNAK-mediated activation of phospholipase C-γ1 through protein kinase C. J. Biol. Chem. *279*, 26645–26653.

Lee, I.H., Sohn, M., Lim, H.J., Yoon, S., Oh, H., Shin, S., Shin, J.H., Oh, S.-H., Kim, J., Lee, D.K., et al. (2014). Ahnak functions as a tumor suppressor via modulation of TGFβ/Smad signaling pathway. Oncogene *33*, 4675–4684.

Lee, V., Barr, K., Kelly, J., Johnston, D., Brown, C., Robb, K., Gros, R., Flynn, L., and Penuela, S. (2018). Pannexin 1 regulates adipose stromal cell differentiation and fat accumulation. Sci. Rep. 1–14.

Li, S., Tomić, M., and Stojilkovic, S.S. (2011). Characterization of novel Pannexin 1 isoforms from rat pituitary cells and their association with ATP-gated P2X channels. Gen. Comp. Endocrinol. *174*, 202–210.

Li, S., Huang, X., Zhang, D., Huang, Q., Pei, G., Wang, L., Jiang, W., Hu, Q., Tan, R., and Hua, Z.C. (2013). Requirement of PEA3 for transcriptional activation of FAK gene in tumor metastasis. PLoS One *8*, 1–13.

Linardic, C., Downie, D., and Qualman, S. (2005). Genetic modeling of human rhabdomyosarcoma. Cancer Res. 4490–4495.

Liu, H., Yuan, M., Yao, Y., Wu, D., Dong, S., and Tong, X. (2019). In vitro effect of Pannexin 1 channel on the invasion and migration of I-10 testicular cancer cells via ERK1/2 signaling pathway. Biomed. Pharmacother. *117*, 109090.

Locovei, S., Bao, L., and Dahl, G. (2006). Pannexin 1 in erythrocytes: function without a gap. Proc. Natl. Acad. Sci. U. S. A. *103*, 7655–7659.

López, C., Aguilar, R., Nardocci, G., Cereceda, K., Vander Stelt, K., Slebe, J.C., Montecino, M., and Concha, I.I. (2019). Wnt/β-catenin signaling enhances transcription of the CX43 gene in murine Sertoli cells. J. Cell. Biochem. *120*, 6753–6762.

López, X., Escamilla, R., Fernández, P., Duarte, Y., González-Nilo, F., Palacios-Prado, N., Martinez, A.D., and Sáez, J.C. (2020). Stretch-Induced Activation of Pannexin 1 Channels Can Be Prevented by PKA-Dependent Phosphorylation. Int. J. Mol. Sci. *21*, E9180.

Maurer, H.M., Gehan, E.A., Beltangady, M., Crist, W., Dickman, P.S., Donaldson, S.S., Fryer, C., Hammond, D., Hays, D.M., Herrmann, J., et al. (1993). The intergroup rhabdomyosarcoma study-II. Cancer *71*, 1904–1922.

Meems, L.M.G., Mahmud, H., Buikema, H., Tost, J., Michel, S., Takens, J., Verkaik-Schakel, R.N., Vreeswijk-Baudoin, I., Mateo-Leach, I. V., Plosch, T., et al. (2016). Parental vitamin D deficiency during pregnancy is associated with increased blood pressure in offspring via Panx1 hypermethylation. Am. J. Physiol. - Hear. Circ. Physiol. ajpheart.00141.2016.

Michalski, K., Henze, E., Nguyen, P., Lynch, P., and Kawate, T. (2018). The weak voltage dependence of pannexin 1 channels can be tuned by N-terminal modifications. J. Gen. Physiol. 1–11.

Miwa, S., Yamamoto, N., Hayashi, K., Takeuchi, A., Igarashi, K., and Tsuchiya, H. (2020). Recent advances and challenges in the treatment of rhabdomyosarcoma. Cancers (Basel). *12*, 1–18.

Negoro, H., Urban-Maldonado, M., Liou, L.S., Spray, D.C., Thi, M.M., and Suadicani, S.O. (2014). Pannexin 1 channels play essential roles in urothelial mechanotransduction and intercellular signaling. PLoS One *9*, e106269.

Noye, T.M., Lokman, N.A., Oehler, M.K., and Ricciardelli, C. (2018). S100A10 and cancer hallmarks: Structure, functions, and its emerging role in Ovarian cancer. Int. J. Mol. Sci. *19*.

Ozorowski, G., Milton, S., and Luecke, H. (2013). Structure of a C-terminal AHNAK peptide in a 1:2:2 complex with S100A10 and an acetylated N-terminal peptide of annexin A2. Acta Crystallogr. Sect. D Biol. Crystallogr. *69*, 92–104.

Pantziarka, P., Bouche, G., Meheus, L., Sukhatme, V., and Sukhatme, V.P. (2014). The Repurposing Drugs in Oncology (ReDO) Project. Ecancermedicalscience *8*, 1–13.

Paul, S.M., Mytelka, D.S., Dunwiddie, C.T., Persinger, C.C., Munos, B.H., Lindborg, S.R., and Schacht, A.L. (2010). How to improve RD productivity: The pharmaceutical industry's grand challenge. Nat. Rev. Drug Discov. *9*, 203–214.

Pelegrin, P., and Surprenant, A. (2006). Pannexin-1 mediates large pore formation and interleukin-1β release by the ATP-gated P2X7 receptor. EMBO J. *25*, 5071–5082.

Penuela, S., Gyenis, L., Ablack, A., Churko, J.M., Berger, A.C., Litchfield, D.W., Lewis, J.D., and Laird, D.W. (2012). Loss of pannexin 1 attenuates melanoma progression by reversion to a melanocytic phenotype. J. Biol. Chem. *287*, 29184–29193.

Penuela, S., Harland, L., Simek, J., and Laird, D.W. (2014). Pannexin channels and their links to human disease. Biochem. J. *461*, 371–381.

Pham, T. Le, St-Pierre, M.E., Ravel-Chapuis, A., Parks, T.E.C., Langlois, S., Penuela, S., Jasmin, B.J., and Cowan, K.N. (2018). Expression of Pannexin 1 and Pannexin 3 during skeletal muscle development, regeneration, and Duchenne muscular dystrophy. J. Cell. Physiol. *233*, 7057–7070.

Proulx, A.A., Lin, Z.X., and Naus, C.C.G. (1997). Transfection of rhabdomyosarcoma cells with connexin43 induces myogenic differentiation. Cell Growth Differ. *8*, 533–540.

Pushpakom, S., Iorio, F., Eyers, P.A., Escott, K.J., Hopper, S., Wells, A., Doig, A., Guilliams, T., Latimer, J., McNamee, C., et al. (2018). Drug repurposing: Progress, challenges and recommendations. Nat. Rev. Drug Discov. *18*, 41–58.

Qin, L., Liao, L., Redmond, A., Young, L., Yuan, Y., Chen, H., O'Malley, B.W., and Xu, J. (2008). The AIB1 Oncogene Promotes Breast Cancer Metastasis by Activation of PEA3-Mediated Matrix Metalloproteinase 2 (MMP2) and MMP9 Expression. Mol. Cell. Biol. *28*, 5937–5950.

Ray, A., Zoidl, G., Weickert, S., Wahle, P., and Dermietzel, R. (2005). Site-specific and developmental expression of pannexin1 in the mouse nervous system. Eur. J. Neurosci. *21*, 3277–3290.

Ren, Y.X., Finckenstein, F.G., Abdueva, D. a., Shahbazian, V., Chung, B., Weinberg, K.I., Triche, T.J., Shimada, H., and Anderson, M.J. (2008). Mouse mesenchymal stem cells expressing PAX-FKHR form alveolar rhabdomyosarcomas by cooperating with secondary mutations. Cancer Res. *68*, 6587–6597.

Rezvanpour, A., Santamaria-Kisiel, L., and Shaw, G.S. (2011). The S100A10-annexin A2 complex provides a novel asymmetric platform for membrane repair. J. Biol. Chem. *286*, 40174–40183.

Roux, K.J. (2013). Marked by association: Techniques for proximity-dependent labeling of proteins in eukaryotic cells. Cell. Mol. Life Sci. *70*, 3657–3664.

Roux, K.J., Kim, D.I., Raida, M., and Burke, B. (2012). A promiscuous biotin ligase fusion protein identifies proximal and interacting proteins in mammalian cells. J. Cell Biol. *196*, 801–810.

Ryan, T.E., Yamaguchi, D.J., Schmidt, C.A., Zeczycki, T.N., Shaikh, S.R., Brophy, P., Green, T.D., Tarpey, M.D., Karnekar, R., Goldberg, E.J., et al. (2018). Extensive skeletal muscle cell mitochondriopathy distinguishes critical limb ischemia patients from claudicants. JCI Insight *3*.

Sagdullaev, B.T., Penuela, S., Fabbretti, E., Swayne, L.A., and Boyce, A.K.J. (2017). Regulation of Pannexin 1 Surface Expression by Extracellular ATP: Potential Implications for Nervous System Function in Health and Disease. *11*, 1–11.

Schalper, K.A., Carvajal-Hausdorf, D., and Oyarzo, M.P. (2014). Possible role of hemichannels in cancer. Front. Physiol. *5 JUN*, 1–18.

Shang, J., Zhang, Z., Song, W., Zhou, B., Zhang, Y., Li, G., and Qiu, S. (2013). S100A10 as a novel biomarker in colorectal cancer. Tumor Biol. *34*, 3785–3790.

Shern, J.F., Chen, L., Chmielecki, J., Wei, J.S., Patidar, R., Rosenberg, M., Ambrogio, L., Auclair, D., Wang, J., Song, Y.K., et al. (2014). Comprehensive genomic analysis of rhabdomyosarcoma reveals a landscape of alterations affecting a common genetic axis in fusion-positive and fusion-negative tumors. Cancer Discov. *4*, 216–231.

Shi, G., Liu, C., Yang, Y., Song, L., Liu, X., Wang, C., Peng, Z., Li, H., and Zhong, L.

(2019). Panx1 promotes invasion-metastasis cascade in hepatocellular carcinoma. J. Cancer *10*, 5681–5688.

Silverman, W.R., de Rivero Vaccari, J.P., Locovei, S., Qiu, F., Carlsson, S.K., Scemes, E., Keane, R.W., and Dahl, G. (2009). The pannexin 1 channel activates the inflammasome in neurons and astrocytes. J. Biol. Chem. *284*, 18143–18151.

Sleire, L., Førde-Tislevoll, H.E., Netland, I.A., Leiss, L., Skeie, B.S., and Enger, P.Ø. (2017). Drug repurposing in cancer. Pharmacol. Res. *124*, 74–91.

Spagnol, G., Trease, A., Zheng, L., Gutierrez, M., Basu, I., Sarmiento, C., Moore, G., Cervantes, M., and Sorgen, P. (2018). Connexin43 Carboxyl-Terminal Domain Directly Interacts with β-Catenin. Int. J. Mol. Sci. *19*, 1562.

Taylor, J.M., Dupont-Versteegden, E.E., Davies, J.D., Hassell, J.A., Houlé, J.D., Gurley, C.M., and Peterson, C.A. (1997). A role for the ETS domain transcription factor PEA3 in myogenic differentiation. Mol. Cell. Biol. *17*, 5550–5558.

Tomlins, S.A., Mehra, R., Rhodes, D.R., Smith, L.R., Roulston, D., Helgeson, B.E., Cao, X., Wei, J.T., Rubin, M.A., Shah, R.B., et al. (2006). TMPRSS2:ETV4 gene fusions define a third molecular subtype of prostate cancer. Cancer Res. *66*, 3396–3400.

Vogt, A., Hormuzdi, S.G., and Monyer, H. (2005). Pannexin1 and Pannexin2 expression in the developing and mature rat brain. Mol. Brain Res. *141*, 113–120.

Wagers, A.J., and Conboy, I.M. (2005). Cellular and molecular signatures of muscle regeneration: Current concepts and controversies in adult myogenesis. Cell *122*, 659–667.

Walterhouse, D.O., Pappo, A.S., Meza, J.L., Breneman, J.C., Hayes-Jordan, A.A., Parham, D.M., Cripe, T.P., Anderson, J.R., Meyer, W.H., and Hawkins, D.S. (2014). Shorter-duration therapy using vincristine, dactinomycin, and lower-dose cyclophosphamide with or without radiotherapy for patients with newly diagnosed low-risk rhabdomyosarcoma: A report from the soft tissue sarcoma committee of the Children's Oncology . J. Clin. Oncol. *32*, 3547–3552.

Wang, C., Zhang, C., Li, X., Shen, J., Xu, Y., Shi, H., Mu, X., Pan, J., Zhao, T., Li, M., et al. (2019). CPT1A-mediated succinylation of S100A10 increases human gastric cancer

invasion. J. Cell. Mol. Med. *23*, 293–305.

Wicki-Stordeur, L.E., and Swayne, L.A. (2013). Panx1 regulates neural stem and progenitor cell behaviours associated with cytoskeletal dynamics and interacts with multiple cytoskeletal elements. Cell Commun. Signal. *11*, 1–8.

Wicki-Stordeur, L.E., Sanchez-Arias, J.C., Dhaliwal, J., Carmona-Wagner, E.O., Shestopalov, V.I., Lagace, D.C., and Swayne, L.A. (2016). Pannexin 1 Differentially Affects Neural Precursor Cell Maintenance in the Ventricular Zone and Peri-Infarct Cortex. J. Neurosci. *36*, 1203–1210.

Willebrords, J., Maes, M., Crespo Yanguas, S., and Vinken, M. (2017). Inhibitors of connexin and pannexin channels as potential therapeutics. Pharmacol. Ther.

Wu, D., and Pan, W. (2010). GSK3: a multifaceted kinase in Wnt signaling. Trends Biochem. Sci. *35*, 161–168.

Wu, D., Li, L., and Chen, L. (2016). A new perspective of mechanosensitive pannexin-1 channels in cancer metastasis: clues for the treatment of other stress-induced diseases. Acta Biochim. Biophys. Sin. (Shanghai). gmw018.

Xiang, X., Langlois, S., St-Pierre, M.E., Barré, J.F., Grynspan, D., Purgina, B., and Cowan, K.N. (2018). Pannexin 1 inhibits rhabdomyosarcoma progression through a mechanism independent of its canonical channel function. Oncogenesis *7*.

Xu, X., Wicki-stordeur, L.E., Sanchez-arias, J.C., and Liu, M. (2018). Probenecid Disrupts a Novel Pannexin 1-Collapsin Response Mediator Protein 2 Interaction and Increases Microtubule Stability. Front. Cell. Neurosci. *12*, 1–13.

Yang, X., Popescu, N.C., and Zimonjic, D.B. (2011). DLC1 interaction with S100A10 mediates inhibition of in vitro cell invasion and tumorigenicity of lung cancer cells through a rhogap-independent mechanism. Cancer Res. *71*, 2916–2925.

Yohe, M.E., Heske, C.M., Stewart, E., Adamson, P.C., Ahmed, N., Antonescu, C.R., Chen, E., Collins, N., Ehrlich, A., Galindo, R.L., et al. (2019). Insights into pediatric rhabdomyosarcoma research: Challenges and goals. Pediatr. Blood Cancer 1–10.

Zhang, Y., Laumet, G., Chen, S.-R., Hittelman, W.N., and Pan, H.-L. (2015). Pannexin-1 Up-regulation in the Dorsal Root Ganglion Contributes to Neuropathic Pain Development. J. Biol. Chem. *290*, 14647–14655.

Zhang, Y.L., Wang, R.C., Cheng, K., Ring, B.Z., and Su, L. (2017). Roles of Rap1 signaling in tumor cell migration and invasion. Cancer Biol. Med. *14*, 90–99.

Zhao, H.-B., Zhu, Y., Liang, C., and Chen, J. (2015). Pannexin 1 deficiency can induce hearing loss. Biochem. Biophys. Res. Commun. 1–5.

Appendix A: Curriculum Vitae

Xiao Xiang

Language Skills

Language	Read	Write	Speak	Understand
English	Yes	Yes	Yes	Yes
Mandarin Chinese	Yes	Yes	Yes	Yes

Degrees

2015/1 (2021/6) Doctorate, Doctor of Philosophy, Cellular and Molecular Medicine, University of OttawaDegree Status: In Progress
Thesis Title: **Tumour-suppressive Effects of Pannexin 1 and its Mechanism of Actionand Regulation in Rhabdomyosarcoma**
Transferred to PhD without

completing Masters?: Yes

Supervisors: Kyle N. Cowan,

2015/1 -

Research Disciplines: Cell Biology, Biochemistry

Areas of Research: Cancer of the Musculoskeletal System

Fields of Application: Pathogenesis and Treatment of Diseases, Biomedical Aspects ofHuman Health

2008/9 - 2013/5 Bachelor's Honours, Honours Bachelor of Science, Biochemistry, University of OttawaDegree Status: Completed
Thesis Title: **PERIPHERAL BLOOD LYMPHOCYTE PHENOTYPING INPATIENTS WITHFAILED HIP IMPLANTS**

Credentials

2013/5 Honourary Bachelor of Science, University of Ottawa

Recognitions

2018/9 - 2019/9 Queen Elizabeth II Graduate Scholarships in Science and Technology - 15,000 (Canadiandollar)

2018/9 - 2019/1 University of Ottawa Excellence Scholarship - 2,358 (Canadian dollar)

	University of Ottawa Distinction
2017/9 - 2018/9	Ontario Graduate Scholarship - 15,000 (Canadian dollar)
	University of Ottawa Distinction
2017/9 - 2018/9	University of Ottawa Excellence Scholarship - 7,074 (Canadian dollar)
	University of Ottawa Distinction
2017/9 - 2018/9	Queen Elizabeth II Graduate Scholarships in Science and Technology - 15,000 (Canadiandollar) This scholarship has been rejected due to the acceptance of OGS in the same year
2016/9 - 2017/9	Ontario Graduate Scholarship - 15,000 (Canadian dollar)
	University of Ottawa Distinction
2016/9	Best Presentation in CAPS Annual Meeting 2016 (2nd place) - 0 (Canadian dollar)
	Canadian Association of Paediatric Surgeons Prize / Award
2016/4 - 2016/4	Taichman Award - 100 (Canadian dollar)
2015/9 - 2016/9	University of Ottawa Excellence Scholarship - 7,074 (Canadian dollar)
	University of Ottawa Distinction
	Research Disciplines: Cell Biology
2015/9 - 2016/9	Destination 2020 Faculty of Medicine Domestic Graduate Scholarship - 10,000 (Canadiandollar)
	Research Disciplines: Cell Biology
2015/9 - 2016/9	Ontario Graduate Scholarship - 15,000 (Canadian dollar)
	University of Ottawa Distinction
	Research Disciplines: Cell Biology
2015/1 - 2015/1	Faculty of Graduate and Postdoctoral Studies Dean's

	Scholarship - 1,500 (Canadiandollar) For successfully transferring from Msc. to PhD. program well within the allowed time
2015/1 - 2017/4	Ph.D. Admission Scholarship - 9,000 (Canadian dollar) University of Ottawa Distinction
2013/9 - 2014/12	Master's Admission Scholarship - 7,500 (Canadian dollar) University of Ottawa Distinction
2013/4	Dean's Honour List University of Ottawa Distinction
2011/9 - 2012/1	Industrial Undergraduate Student Research Award - 4,500 (Canadian dollar) Natural Sciences and Engineering Research Council of Canada (NSERC) Distinction
2008/9 - 2009/4	Renewable Admission Scholarship - 2,500 (Canadian dollar) University of Ottawa Distinction
2008/9 - 2009/4	Registrar's Special Scholarship - 1,000 (Canadian dollar) University of Ottawa Distinction
2008/9 - 2009/4	Education Bursary - 1,000 (Canadian dollar) University of Ottawa Distinction

User Profile

Research Specialization Keywords:

Rhabdomyosarcoma, PannexinsDisciplines

Trained In: Cell Biology, Biochemistry

Research Disciplines: Cell Biology, Molecular Biology

Areas of Research: Cell Signaling and

Cancer, Cellular DifferentiationFields of

Application: Biomedical Aspects of Human

Health

Employment

2012/9 - 2013/4 Honour's Student
Metal-on-metal (MM) hip implants have been considered as an alternative to conventionalmetal-on-polyethylene (MPE) implants because of their lower volumetric wear. However, reports of adverse tissue reactions (e.g. hypersensitivity) leading to premature implant failure are a growing cause for concern. Unfortunately, the exact origin and mechanisms of these reactions remain largely unknown. We hypothesize that larger percentages of memory T-cells and type 1 T-helper (Th1) cells (expressing IFN-?) will be observed in patients with failed MM implants if a type-IV hypersensitivity reaction is prevalent in these patients. The objective of this ongoing study is to compare the proportions of lymphocyte subsets in the peripheral blood of patients with failed implants (MM and MPE) and healthyvolunteers without implants (HC).

2012/5 - 2012/8 Research Assistant (Co-op Student)
Children's
Hospital of
Eastern
Ontario
Full-time
Studied the post-translational modifications of Pannexin 3 in human skeletal muscle andpediatric rhabdomyosarcoma cell lines, and the results found were incorporated into a peer-reviewed journal publication (J Biol Chem. 2014 Oct 31;289(44):30717-31. doi: 10.1074/jbc.M114.572131. Epub 2014 Sep 19).

2011/9 - 2011/12 Research
Assistant
(Co-op Student)
Health Canada
Full-time
Participated in the development and optimization of in vitro diagnostic genetic testing reagents in preparation for FDA approval. Developed and tested a method for an externalcontrol

system for DNA probe specificity in the genetic testing reagents.

2011/1 - 2011/8 Scientific
Evaluator
(Co-op Student)
Health Canada
Full-time
Evaluated the toxicity of the food-packaging materials and participated in developing andreviewing of toxicology reports

Affiliations

The primary affiliation is denoted by (*)

(*) 2013/9 Graduate student, Children's Hospital of Eastern Ontario

Staff Supervision

Number of

Scientific and

Technical Staff: 1

Number of

Employees: 5

Community and Volunteer Activities

2016/9 International Student Advisor, University of Ottawa
Meet with international students and help them make a smooth transition to the newenvironment and the study.

Other Memberships

2016/4 - 2016/12 Associate Member, American

Association for Cancer Research2013/9 - 2015/9 Member,

Royal Astronomical Society of Canada

Presentations

1. (2019). Deciphering Pannexin 1 Translational Regulation: Towards a Novel Therapeutic Strategy for Rhabdomyosarcoma. Children's Hospital of Eastern Ontario Department of Surgery Annual ResearchSymposium, Ottawa,

Canada

2. (2019). BioID as a Novel Tool for Studying the Pannexin 1 Interactome. International Gap JunctionConference, Victoria, Canada
3. (2017). Pannexin 1 is Down-regulated in Rhabdomyosarcomas and its Reintroduction Inhibits Tumor Growth: a Potential Novel Therapeutic Target. International Gap Junction Conference, Glasgow, UnitedKingdom
4. (2017). Regulation of Pannexin 1 and Pannexin 3 levels during Skeletal Muscle Development, Regeneration, and Duchenne's Dystrophy. International Gap Junction Conference, Glasgow, UnitedKingdom
5. (2017). Delineating the Molecular Pathway Induced by Pannexin 1 in Rhabdomyosarcoma to Identify NovelTherapeutic Targets. Children's Hospital of Eastern Ontario Department of Surgery Annual Symposium, Ottawa, Canada
6. (2016). Pannexin 1 regulates the malignant properties of rhabdomyosarcoma: novel therapeuticimplications. Canadian Association of Paediatric Surgeons, Vancouver, Canada
7. (2015). Pannexin 1 is a Novel Therapeutic Target for Rhabdomyosarcoma. Children's Hospital of EasternOntario Department of Surgery Annual Symposium, Ottawa, Canada
8. (2014). Dysregulation of Pannexin1 in Rhabdomyosarcoma and Suppression of its Neoplastic Potential byPannexin1 Overexpression. Children's Hospital of Eastern Ontario Research Day, Ottawa, Canada
9. (2014). Pannexin 1 as a Potential Novel Therapeutic Target for Rhabdomyosarcoma. Children's Hospital ofEastern Ontario Department of Surgery Annual Symposium, Ottawa, Canada

Publications

Journal Articles

1. Xiang X*, Langlois S, St-Pierre ME, Blinder A, Charron P, Graber TE, Fowler SL, Baird SD, Bennett SAL,Alain T and Cowan KN. (2020). **Identification of Pannexin 1 Regulated Genes, Interactome, and Pathways in Rhabdomyosarcoma and its TumorInhibitory Interaction with AHNAK** . Oncogene. First Listed Author
2. Hoang HD*, Graber TE, Jia JJ, Vaidya N*, Gilchrist VH*, Xiang X*, Li WC, Cowan KN, Gkogkas GG, Jaramillo M, Jafarnejad SM and Alain T. (2019). **Induction of an Alternative mRNA 5' Leader EnhancesTranslation of the Ciliopathy Gene Inpp5e and Resistance to Oncolytic Virus Infection**. Cell Reports.49(12): 4010-4023.
3. Xiang X*, Langlois S, St-Pierre ME, Barré J, Grynspan D, Purgina B and Cowan KN. (2018). **Pannexin1 Inhibits Rhabdomyosarcoma Progression through a Mechanism Independent of its CanonicalChannel Function**. Oncogenesis.

7(11): 89.

4. Faye MD*, Beug ST, Graber TE, Earl N, Xiang X*, Wild B*, Langlois S, Michaud J, Cowan KN, KornelukRG, Holcik M. (2015). **IGF2BP1 controls cell death and drug resistance in rhabdomyosarcomas byregulating translation of cIAP1**. Oncogene. 34(12): 1532-1541.

5. Langlois L, Xiang X*, Young K*, Cowan BJ, Penuela S, Cowan KN. (2014). **Pannexin 1 and Pannexin 3 Regulate Skeletal Muscle Myoblasts Proliferation and Differentiation**. Journal of Biological Chemistry.289(44): 30717-30731.

Working Papers

1. First Listed Author. (Xiang X*, Hoang HD, Gilchrist V, Langlois S, Alain T and Cowan KN). (2020). Quercetin Induces Pannexin 1 Expression via an Alternative Transcript with a Translationally Active 5'Leader in Rhabdomyosarcoma.

2. First Listed Author. (Xiang X*, Langlois S and Cowan KN). (2020). Drug Screening in Three- dimensional Patient-derived Tumour Spheroids Identifies Quercetin as a Potential Therapeutic Agent forRhabdomyosarcoma.

Conference Publications

1. Xiang X, Freeman E, Karami S, Langlois S, Cowan KN. (2020). **Targeted Drug Repurposing to Treat Rhabdomyosarcoma**. Conference Book of Abstracts. American Pediatric Surgical Association (APSA), ,Conference Date: 2020/5

2. Xiang X*, Langlois S, Cowan KN. (2019). **BioID as a Novel Tool for Studying the Pannexin 1 Interactome**. Conference Book of Abstracts. International Gap Junction Conference, Victoria, Canada,Canada

3. Xiang X*, Langlois S, St-Pierre ME, Barré J, Grynspan D, Purgina B, and Cowan KN. (2017). **Pannexin1 is Down-regulated in Rhabdomyosarcomas and its ReintroductionInhibits Tumor Growth: a Potential NovelTherapeutic Target**. Conference Book of Abstracts. International Gap JunctionConference, Glasgow, United Kingdom,

4. Pham TL*, Ravel-Chapuis A, Crawford Parks TE, Lunde JA, Xiang X*, Langlois S, Penuela S, Jasmin BJ, and Cowan KN. (2017). **Regulationof Pannexin 1 and Pannexin 3 levels during Skeletal Muscle Development,Regeneration, and Duchenne's Dystrophy** . Conference Book of Abstrats. International Gap Junction Conference, Glasgow, United Kingdom,

5. Xiang X*, St-Pierre ME, Langlois S, Barré J, Pham TL*, Cowan KN. (2016). **Pannexin 1 regulates the malignant properties of rhabdomyosarcoma: novel therapeutic implications**. Canadian Association of Paediatric Surgeons, Vancouver, Canada

6. Xiang X*, Langlois S, St-Pierre ME, Barré J, Pham TL*, and Cowan NK. (2016).

Pannexin 1 Regulates RhabdomyosarcomaTumor Growth: a Potential Novel Therapeutic Target . Conference Proceedings.American Association for Cancer Research, New Orleans, United States (325). American Association for Cancer Research, United States

7. Xiang X*, Langlois S, Barré J, St-Pierre ME, Pham TL*, Cowan KN. (2016). **Pannexin 1 is down- regulatedin rhabdomyosarcoma and negatively regulatestumor growth** . American Society of CellBiology (ASCB), San Diego, United States,

8. Xiang X*, Guira E*, Hurda I*, Lehoux EA, Lemay MO*, Baskey SJ*, Beaulé PE, Catelas I. (2014). **Comparison of peripheral blood lymphocyte phenotypes in patients with failed metal-on-metal hipimplants with and without a pseudotumor**. AOA/COA Combined Meeting, Montreal, Canada

9. Lehoux EA, Xiang X*, Lemay MO*, Guira E*, Hurda I*, Baskey SJ*, Beaulé PE, Catelas I. (2014). **Immunophenotypic Analysis of Peripheral Blood Lymphocytes in Patients with Failed Metal-on-Metal Hip Implants Associated with a Pseudotumor**. Hip Arthroplasty. Orthopedic Research SocietyAnnual Meeting, New Orleans, United States

10. Guira E*, Xiang X*, Hurda I*, Lehoux EA, Beaulé PE, Baskey SJ*, Catelas I. (2013). **Analysis of Peripheral Blood Lymphocyte Phenotypes in Patientswith Failed Metal-on-Metal Hip Implants**. 30thAnnual Meeting of the Canadian Biomaterials Society, Ottawa, Canada,

Intellectual Property

Patents

1. Full-automatic medical fluorescence PCR (Polymerase Chain Reaction) analysis system based on POCT(Point-of-care Testing) mode. China. CN107513490A. 2017/09/29.
   Patent Status: Pending
   The invention relates to the technical field of biomedicines and in particular relates to a full-automatic medical fluorescence PCR (Polymerase Chain Reaction) analysis system based on a POCT (Point-of-care Testing) mode. The system comprises a PCR instrument and a client, wherein the PCR instrument is used for amplifying DNA through a PCR reaction; the PCR instrument is further used for performing fluorescencedetection on the DNA, generating fluorescence images and transmitting the images to the client; and the client is used for analyzing the fluorescence images and generating analysis results. According to the full-automatic medical fluorescence PCR analysis system based on the POCT mode provided by the invention,the defects that the traditional gene detection process is complicated, the cost is high and the waiting cycle is long can be overcome.

2. Primer, molecular beacon, kit and detection method for rapidly detecting polymorphism of MTHFR-A1298Cgene. China. CN107299140A. 2017/07/25.

Patent Status: Pending
The invention discloses a kit for rapidly detecting the polymorphism of an MTHFR-A1298C gene and an RS1801131 gene. The kit comprises a PCR reaction liquid, a specific primer, a molecular beacon, 0.04-0.1U/muL of DNA polymerase, 0.1-0.5mM of dNTPs, 0.5-1.5X of a PCR buffer solution, 1-2.5mM of MgCl2, 0.0005-0.015% (w/v) of lauryl sodium sulfate and 0.001-0.03% (w/v) of polyethylene glycol octylphenol ether; the specific primer comprises an upstream primer and a downstream primer, and the final concentration is 0.2-0.7muM; the molecular beacon comprises a mutant molecular beacon and a wild molecular beacon, and the final concentration is 0.2-0.7muM; and the kit is used for detecting a cell sample.The invention aims at solving the technical problem of providing a primer, a molecular beacon, a kit and a detection method, which are simple in operation and fast in detection and are capable of avoiding pollution, for rapidly detecting the polymorphism of the MTHFR-A1298C gene.

3. Primer, molecular beacon and kit for rapidly detecting CYP2C9*3 gene polymorphism and detectionmethod of CYP2C9*3 gene polymorphism. China. CN107227371A. 2017/07/25.
Patent Status: Pending
The invention discloses a kit for rapidly detecting CYP2C9*3 gene polymorphism. The kit comprises a PCR (Polymerase Chain Reaction) reaction mixing solution which comprises the following raw materials by final concentration: 0.05-0.12 U/microliter of DNA polymerase, 0.2 mM of dNTPs, 1 X of 5 X PCR buffering solution, 1.5-3.5 mM of MgCl2, 0.0005-0.015% (w/v) of lauryl sodium sulfate, 0.001-0.03% (w/v) of polyethylene glycol octylphenol ether, 0.5-1 micron of a forward primer, 0.5-1 micron of a reverse primer,0.5-1 micron of a mutant molecular beacon, and 0.5-1 micron of a wild type molecular beacon; and the PCR reaction mixing solution is used for detecting cell samples. The primer, a Taqman-MGB probe and the kit for rapidly detecting the CYP2C9*3 gene polymorphism and the detection method of the CYP2C9*3 gene polymorphism are simple to operate, free from pollution, and rapid to detect.

4. Primer, molecular beacon and kit of MTRR gene polymorphism rapid test and testing method thereof.China. CN107245527A. 2017/07/25.
Patent Status: Pending
The invention discloses a kit of MTRR gene polymorphism rapid test. The kit comprises PCR reaction liquid; the PCR reaction liquid is prepared from 0.04-0.09 U/microliter of DNA polymerase, 0.1-0.5 mM ofdNTPS, 0.5-1.5 X of 5X PCR buffer solution, 1-2.5 mM of MgCl2, 0.0005-0.015%(w/v) of lauryl sodium sulfate, 0.001-0.03%(w/v) of polyethylene glycol octylphenol ether, 0.2-1.0 muM of upstream primer, 0.2-1.0 muM of downstream primer, 0.3-0.5 muM of mutant molecular beacon and 0.3-0.7 muM of wild molecular beacon, and is used for testing cell samples. The technical problem to be solved is to provide a primer, molecular beacon and

kit of MTRR gene polymorphism rapid test and a testing method thereof through which sampling can be conducted in the painless environment and which are simple in operation,low in cost, rapid in test, short in time and high in success rate, and accordingly guidance is provided for individualization folic acid use, and the fetal anomaly risk is reduced.

5. Primer, molecular beacon, kit of VKORC1 gene polymorphism rapid testing and test method thereof. China.CN107354212A. 2017/07/25.
Patent Status: Pending
The invention discloses a kit of VKORC1 gene polymorphism rapid testing. The kit comprises a PCR reaction mixed solution prepared from 0.04-0.1 U/microliter of DNA polymerase, 0.1-0.5 mM of dNTPs,0.5-1.5 X of PCR buffer liquid, 1.5-3.5 mM of MgCl2, 0.0005-0.015%(w/v) of lauryl sodium sulfate, 0.001-0.03%(w/v) of polyethylene glycol octylphenol ether, 0.2-1.0 micrometer of forward primers,
0.2-1.0 micrometer of reverse primers, 0.2-1.0 micrometer of mutant type molecular beacons and 0.2-1.0micrometer of wild type molecular beacons. The kit is used for testing buccal mucosal cell samples.
Through a primer and molecular beacon and the kit related to VKORC1 gene polymorphism rapid testingand a test method thereof, the operation is simple, pollution is avoided, and testing is rapid.

6. Sampling means for buccal cells. China.
CN205359515 U. 2016/01/21.Patent Status:
Granted/Issued
Year Issued: 2016

7. Gene single nucleotide polymorphisms rapid detection kit. China.
CN205368373 U. 2016/01/21.Patent Status: Granted/Issued
Year Issued: 2016